

MHD Turbulence: A Biased Review

Alexander A. Schekochihin[†]

Rudolf Peierls Centre for Theoretical Physics, University of Oxford,
Clarendon Laboratory, Parks Road, Oxford OX1 3PU, UK
Merton College, Oxford OX1 4JD, UK

(compiled on 21 July 2022)

This (self-contained and aspiring to pedagogy) review of scaling theories of MHD turbulence aims to put the developments of the last few years in the context of the canonical time line (from Kolmogorov to Iroshnikov–Kraichnan to Goldreich–Sridhar to Boldyrev). It is argued that Beresnyak’s (valid) objection that Boldyrev’s alignment theory, at least in its original form, violates the RMHD rescaling symmetry can be reconciled with alignment if the latter is understood as an intermittency effect. Boldyrev’s scalings, a version of which is recovered in this interpretation, and the concept of dynamic alignment (equivalently, local 3D anisotropy) are thus an example of a qualitative, physical theory of intermittency in a turbulent system. The emergence of aligned structures naturally brings into play reconnection physics and thus the theory of MHD turbulence becomes intertwined with the physics of tearing, current-sheet disruption and plasmoid formation. Recent work on these subjects by Loureiro, Mallet et al. is reviewed and it is argued that we may, as a result, finally have a reasonably complete picture of the MHD turbulent cascade (forced, balanced, and in the presence of a strong mean field) all the way to the dissipation scale. This picture appears to reconcile Beresnyak’s advocacy of the Kolmogorov scaling of the dissipation cutoff (as $\text{Re}^{3/4}$) with Boldyrev’s aligned cascade. It turns out also that these ideas open the door to some progress in understanding MHD turbulence without a mean field—MHD dynamo—whose saturated state is argued to be controlled by reconnection and to contain, at small scales, a tearing-mediated cascade very similar to its strong-mean-field counterpart (this is a new result). On the margins of this core narrative, standard weak-MHD-turbulence theory is argued to require some adjustment—and a new scheme for such an adjustment is proposed—to take account of the determining part that a spontaneously emergent 2D condensate plays in mediating the Alfvén-wave cascade from a weakly-interacting state to a strongly turbulent (critically balanced) one. This completes the picture of the MHD cascade at large scales. A number of outstanding issues are surveyed, most of them concerning variants of MHD turbulence featuring various imbalances: between the two Elsasser fields (“cross-helicity”) or between velocity and magnetic field (“residual energy”); subviscous and decaying regimes of MHD turbulence (where there has been dramatic progress recently and reconnection again turns out to feature prominently) are also reviewed under this heading. Some new, if often tentative, ideas about these regimes are proposed along the way (a new theory of imbalanced turbulence amongst them). Finally, it is argued that the natural direction of research is now away from the fluid MHD theory and into kinetic territory—and then, possibly, back again. The review lays no claim to objectivity or completeness, focusing on topics and views that the author finds most appealing at the present moment.

[†] Email: alex.schekochihin@physics.ox.ac.uk

CONTENTS

1. Introduction	5
PART I. A LONG ROAD TO KOLMOGOROV	8
2. K41, IK and GS95	8
2.1. K41	8
2.2. IK	9
2.3. GS95	10
3. Reduced MHD	12
4. Weak MHD Turbulence	15
4.1. WT is Irrelevant	15
4.2. A Sketch of WT Theory	16
4.3. Imbalanced WT	17
4.4. 2D Condensate	19
5. Critical Balance, Parallel Cascade, and Anisotropy	21
5.1. Critical Balance	21
5.2. Parallel Cascade	21
5.3. Local, Scale-Dependent Anisotropy	23
6. Dynamic Alignment, Perpendicular Cascade, and Intermittency	25
6.1. Alignment and Anisotropy in the Perpendicular Plane	26
6.2. Boldyrev's Alignment Conjecture	28
6.3. Plot Thickens	29
6.4. Revised Model of Aligned MHD Turbulence	31
6.4.1. Dimensional and RMHD-Symmetry Constraints	31
6.4.2. Intermittency Matters!	33
6.5. 3D Anisotropy	36
6.6. Higher-Order Statistics	38
7. MHD Turbulence Meets Reconnection	39
7.1. Disruption by Tearing	41
7.1.1. Some Reservations and Limitations	41
7.1.2. Debris of Disruption	42
7.2. Tearing-Mediated Turbulence	43
7.2.1. Mini-cascades and the Spectrum of Tearing-Mediated Turbulence	44
7.2.2. Restoration of Kolmogorov Cutoff	46
7.2.3. Alignment in the Tearing-Mediated Range	47
7.2.4. Parallel Cascade in the Tearing-Mediated Range	47
7.3. Is This a Falsifiable Theory?	49
7.4. Tearing Disruption, Plasmoid Chains, Fast Reconnection, and Reconnection-Driven Turbulence	49
7.4.1. Nature of Tearing Disruption	50
7.4.2. Onset of Fast Reconnection	51
7.4.3. Reconnection-Driven Turbulence	53
8. Halfway Summary	54
8.1. Is This the End of the Road?	54
8.2. What Can Go Wrong?	54
8.3. What Is Lost in Translation?	55
8.3.1. Waves vs. Structures	55
8.3.2. Cellularisation of Turbulence	55
8.3.3. Stochastic Reconnection	56

PART II. IMBALANCES AND LOOSE ENDS	57
9. Imbalanced MHD Turbulence	58
9.1. Imbalance Global and Local	58
9.2. Numerical and Observational Evidence	60
9.3. <i>Lithwick et al.</i> (2007)	63
9.4. <i>Perez & Boldyrev</i> (2009)	64
9.5. Parallel Scales and Two Flavours of CB	65
9.6. Towards a New Theory of Imbalanced MHD Turbulence	66
9.6.1. Two Semi-Local Cascades	66
9.6.2. Perpendicular Spectra	68
9.6.3. Parallel Spectra	69
9.6.4. Pinning	69
9.6.5. Alignment, Intermittency, Reconnection	70
10. Residual Energy in MHD Turbulence	70
10.1. Observational and Numerical Evidence	70
10.2. Old Theories	72
10.3. New Theories: Residual Energy in Weak MHD Turbulence	73
10.4. New Theories: Residual Energy in Strong MHD Turbulence	74
10.5. Summary	75
11. Subviscous MHD Turbulence	76
11.1. Viscous Cutoff	76
11.2. Magnetic Fields at Subviscous Scales	76
11.3. Velocity Field at Subviscous Scales	78
11.4. Disruption by Tearing	79
12. Decaying MHD Turbulence	80
12.1. Selective Decay	81
12.1.1. Decay of 2D MHD Turbulence	81
12.1.2. Decay of Helical MHD Turbulence	82
12.2. Reconnection Takes Over	83
12.2.1. Reconnection-Controlled Decay of 2D MHD Turbulence	83
12.2.2. Reconnection-Controlled Decay of Helical MHD Turbulence	85
12.2.3. Lack of Rescaling Symmetry for Dissipation Coefficients	86
12.3. Decay of Non-helical MHD Turbulence: Simulations and Theories	87
12.4. Selective Decay Constrained by Saffman Invariants	88
12.4.1. Generalised Saffman Invariants	89
12.4.2. Decay of Magnetically Dominated Non-helical MHD Turbulence	91
12.4.3. Selective Decay Constrained by Saffman Cross-Helicity Invariant	92
12.5. Permanence of Large Scales vs. Inverse Transfer	94
12.5.1. Scalings for Inverse Transfer of Magnetic Energy	95
12.5.2. Self-Similar Spectra and Inverse Energy Transfer	95
12.6. Decay of Magnetically Dominated RMHD Turbulence	96
12.6.1. Saffman Cross-Helicity Invariant in RMHD	97
12.6.2. Self-Similar Decay in RMHD	98
12.7. Decay of Imbalanced MHD Turbulence: Towards Elsasser States	99
12.8. Inertial-Range Spectra of Decaying MHD Turbulence: Numerical Evidence	100
12.9. Summary	100
13. MHD Dynamo Meets Reconnection	101
13.1. Old Arguments About Saturated Dynamo at Large Pm	102
13.2. Numerical Evidence: Reconnection Strikes Again	103

13.3. Towards a New Theory of Reconnection-Limited Dynamo	107
13.3.1. Kinematic Dynamo and Onset of Tearing	107
13.3.2. Self-Similar Dynamo	108
13.3.3. Tearing-Limited Dynamo: Universality Regained	108
13.3.4. Outstanding Question	111
13.4. Saturation Scenarios	112
13.4.1. Multiscale Folds?	112
13.4.2. Spectra Above the Reversal Scale	113
13.4.3. Magnetoelastic Turbulence?	114
13.4.4. Fast-Reconnection-Limited Dynamo?	117
13.4.5. Xu & Lazarian (2016)	117
13.4.6. Subramanian (1999)	119
13.4.7. Inverse Magnetic-Energy Transfer via Sporadic Decay?	120
13.4.8. Local Shear Dynamo?	121
14. The Frontier: Kinetic Turbulence	122
14.1. Sundry Microphysics at Low Collisionality	122
14.2. Cascade Fragility	124
14.3. Phase-Space Turbulence	125
14.4. Statistical Thermodynamics of Collisionless Plasma	127
14.5. Macro- and Microphysical Consequences of Pressure Anisotropy	128
15. Conclusion	130
 APPENDICES	131
Appendix A. Splendours and Miseries of WT Theory	131
A.1. RMHD in Scalar Form	131
A.2. Classic WT Calculation	132
A.3. Solution of WT Equation	133
A.4. Case of Broad-Band Forcing: Spectral Continuity	134
A.5. Residual Energy in WT	136
A.6. Imbalanced WT	139
Appendix B. Alignment, Imbalance, and Reduction of Nonlinearity	139
B.1. Geometry and Types of Alignment	139
B.2. Alignment and Reduction of Nonlinearity	141
Appendix C. 2D Spectra of RMHD Turbulence	143
C.1. Determining δ : Long Parallel Wavelengths	143
C.2. Determining γ : Short Perpendicular Wavelengths	144
C.3. Determining β : Long Perpendicular Wavelengths	144
C.3.1. Kinematics	144
C.3.2. Thermodynamics	145
C.3.3. Dynamics	145
C.4. Determining α : Short Parallel Wavelengths	146
C.5. 2D Spectrum of WT	148
Appendix D. A Reconnection Primer	148
D.1. Tearing Instability	149
D.1.1. Outer Solution	149
D.1.2. Scaling of Δ'	150
D.1.3. Inner Solution	151
D.1.4. Peak Growth Rate and Wavenumber	152
D.1.5. Case of Arbitrary Scaling of Δ'	154
D.2. Onset of Nonlinearity	155

D.3. What Happens Next?	156
D.4. Sweet–Parker Sheet	156
D.4.1. Sweet–Parker Reconnection	156
D.4.2. Plasmoid Instability	158
D.5. Formation and Disruption of Sheets	159
D.5.1. “Ideal Tearing”	162
D.5.2. Recursive Tearing	163
D.6. Fast MHD Reconnection	167
D.6.1. Plasmoid Flux and Width Distribution	170
D.6.2. Spectrum of Plasmoid Chain	170
D.6.3. Reconnection-Driven Turbulence	171
D.7. Stochastic Reconnection and MHD Turbulence	173
D.7.1. Stochastic Reconnection Mediated by Strong Turbulence	175
D.7.2. Stochastic Reconnection Mediated by Weak Turbulence	176
D.7.3. Stochastic Reconnection in GS95 Turbulence	178
D.7.4. Stochastic Reconnection in Aligned Turbulence	178

... Oft turning others' leaves, to see if thence would flow
 Some fresh and fruitful showers upon my sunburn'd brain.
 But words came halting forth, wanting invention's stay;
 Invention, Nature's child, fled step-dame Study's blows;
 And others' feet still seemed but strangers in my way.
 Thus great with child to speak and helpless in my throes,
 Biting my truant pen, beating myself for spite,
 “Fool,” said my Muse to me, “look in thy heart, and write.”

Sir Philip Sidney, *Astrophil and Stella*

Nothing is more usual and more natural for those, who pretend to discover any thing new to the world in philosophy and sciences, than to insinuate the praises of their own systems, by decrying all those, which have been advanced before them.

David Hume, *A Treatise of Human Nature*

1. Introduction

At times during the last two decades, watching furious debates about the theory of MHD turbulence raging over increasingly technical and/or unfalsifiable issues, or working hard on minute refinements to existing results, one might have been forgiven for gradually losing interest. Is MHD turbulence to follow hydrodynamic (isotropic, homogeneous, Kolmogorov) turbulence and become a boutique field, ever more disconnected from the excitements of “real” physics? This perhaps is the fate of any successful theory (what more is there to be done?) or indeed of one that stalls for too long after initial breakthroughs (all the low-hanging fruit already picked?).

Most of the reasons for which I have found myself writing this piece with a degree of renewed enthusiasm emerged or crystallised in and since 2017. Enough has happened in these recent years for this text to be entirely different than it would have been had it been written before 2017; I do not think that the same could have been said during any of the 5, perhaps 10, years before that. The last significant conceptual breakthrough

predating 2017 was the dynamic-alignment theory of Boldyrev (2006) (see § 6.2), which updated the previous decade’s paradigm-changing theory of Goldreich & Sridhar (1995) (§ 5) and was followed by a flurry of numerical activity, sustaining the field for nearly 10 years. Some of the furious debates alluded to above had to do with the validity of this work—but in the absence of a new idea as to what might be going on dynamically, the insistence in a series of papers by Beresnyak (2011, 2012a, 2014b) that Boldyrev’s theory failed at small scales (meeting with casual dismissal from Beresnyak’s opponents and with amused indifference from the rest of the community) appeared doomed to be kicked into the long grass, waiting for ever bigger computers.¹

Simultaneously, the community has been showing increasing interest and investing increasing resources into studying the dissipation mechanisms in MHD turbulence—in particular, the role of spontaneously formed current sheets and associated local reconnection processes (this was pioneered a long time ago by Matthaeus & Lamkin 1986 and Politano *et al.* 1989, but has only recently bloomed into an active field: see references in § 7). The most intriguing question (which, however, remained mostly unasked—in print—until 2017) surely had to be this: if Boldyrev’s MHD turbulence consisted of structures that were ever more aligned and so ever more sheet-like at small scales, was a scale eventually to be reached, given a broad enough inertial range, where these sheets would become too thin to stay stable and the reconnection processes known to disrupt such sheets would kick in?

Like Boldyrev’s theory, the full/quantitative realisation that large-aspect-ratio current sheets cannot survive also dates back to the first decade of the century, if one accepts that the trigger was the paper by Loureiro *et al.* (2007) on the plasmoid instability (see appendix D.4.2; as always, in retrospect, one can identify early precursors, notably Bulanov *et al.* 1978, 1979, Biskamp 1982, 1986 and Tajima & Shibata 1997). This, however, did not translate into a clear understanding of the disruption of *dynamically forming* sheets until the papers by Pucci & Velli (2014) and Uzdensky & Loureiro (2016) (which, in fact, had been around in preprint form since 2014, while PRL was undertaking its characteristically thorough deliberations on the potential impact of publishing it). Once this result was out, it did not take long (even so, it took surprisingly long) to apply it to Boldyrev’s aligning structures—it is this calculation (see § 7), published in the twin papers by Mallet *et al.* (2017b) and Loureiro & Boldyrev (2017b), that, in my view, pushed the theory of MHD turbulence forward far enough that it is now both closer to a modicum of logical completeness and ripe for a review. The outcome appears to be that the Beresnyak vs. Boldyrev controversy is resolved (both are right, in a sense: see § 7.2.2), Kolmogorov’s dissipation scale is back, in a somewhat peculiar way, reconnection and turbulence have joined hands, and the modellers hunting for current sheets have been vindicated and offered further scope for their modelling.

While emphasising this development as conceptually the most exciting amongst the recent ones, I will also take the opportunity presented by this review to discuss, in § 4 and appendix A, my reservations about the standard version of weak Alfvén-wave turbulence theory and some ideas for how to fix (or interpret) it; to summarise, in § 6.4, what I view as a set of rather pretty new ideas on the intrinsically intermittent nature of aligned

¹Beresnyak (2011) did put forward an unassailable, if formal, theoretical objection, discussed in § 6.3, to Boldyrev’s original interpretation of dynamic alignment as an angular uncertainty associated with field-line wandering. This interpretation is not, however, essential for the dynamic alignment itself to remain a feasible feature of the turbulent cascade (Chandran *et al.* 2015; Mallet & Schekochihin 2017). I will put Beresnyak’s objection to good use in a slightly revised model of the aligned cascade in § 6.4.

turbulence (Mallet *et al.* 2015, 2016; Chandran *et al.* 2015; Mallet & Schekochihin 2017); to explore some old ideas, and propose some new ones, on various imbalanced regimes of MHD turbulence (with cross-helicity, with residual magnetic energy, subviscous, decaying: see §§ 9–12—in the case of decaying turbulence, reconnection has stolen the limelight again and some very neat new ideas have recently emerged); to offer an updated, if tentative, perspective on the saturated state of MHD dynamo—i.e., MHD turbulence with no mean field, which turns out also to be intertwined with reconnection (§ 13); and to advocate (in § 14) a number of lines of further investigation focusing on plasma effects—some of which have started emerging in a particularly intriguing way during the last few years. That over a half of this review is taken up by these sections, treating of open questions, old confusions, new speculative schemes, and promising directions for further forays into the unknown, should alert my reader to a very heavy caveat attaching to my earlier claim about the “logical completeness” of our current picture of MHD turbulence: this claim in fact only applies to forced, balanced, inertial-range turbulence, with collisional dissipation and in the presence of a strong mean field. To many disappointed readers, this will seem to be a rarefied version of MHD turbulence falling short of anything useful in any global context or indeed of appearing anywhere in reality. This is true, but only a few years ago, we did not even have a grip on that!

Because the subject of this review, if not exactly young, is still an active one and no one narrative has been settled as definitive, my exposition will be chronological, rather than logical, viz., I will discuss ideas that have proved to be wrong or incomplete before getting to those that as yet have not—not least because the latter were strongly influenced by, and would not have emerged without, the former. One day, there will be a much shorter story told in textbooks, with all intermediate steps forgotten. The erudites who already know this history, are uninterested in my prose and just want to skim the essential points and check out the new bits can start by reading §§ 6.4, 7.1–7.3, 9.6, 10.4, 11, 12.4, 13.3, and appendices A.4, C, D.5.2, D.6.2–D.6.3, and D.7. In § 8, there is a summary and discussion of the main takeaways from the material covered up to that point.

Before proceeding, I would like, by way of a disclaimer, to stress the point that is already made in the title of this piece: this is a thoroughly biased review. Rather than merely recycling the truism that there is no such thing as an unbiased review of anything, I am apologising here for this one drawing particularly heavily on published papers in which I myself participated. I hope that I might nonetheless be forgiven on the grounds that the lion’s share of the credit for those contributions in fact belongs to my co-authors. Leaving to more disengaged spectators the task of assigning to these works their true measure of (in)significance, perhaps as minor flecks of colour on the vast canvas of MHD turbulence theory, I will instead present this subject as I see it at the moment, with those flecks in the foreground.

PART I

A Long Road to Kolmogorov

Omnis autem, quae in rerum natura contingunt, mutationes ita sunt comparatae, ut si quid alicui rei accedit, id alteri derogetur. [...] Quae naturae lex cum sit universalis, ideo etiam ad regulas motus extenditur...

M. V. Lomonosov, *Letter to L. Euler, 5 July 1748*²

2. K41, IK and GS95

The basic starting point for this discussion is to imagine a static, homogeneous plasma or, more generally, a conducting continuous medium, threaded by a uniform magnetic field. One can think of this situation as describing some local patch of a larger system, in which the magnetic field and other equilibrium parameters (density, pressure, flow velocity) are large-scale and structured in some system-dependent way. I am not going to be concerned (except much later, in §§ 12 and 13) with the question of what this large-scale structure is or how it is brought about—locally, it always looks like our homogeneous patch. Within this patch, I shall consider perturbations whose time and length scales are short compared to any length scales associated with that large-scale structure. Of course, such a local approximation is not entirely universal: I am putting aside the cases of strong shear, various stratified or rotating systems, etc.—or, to be precise, I am excluding from consideration perturbations that are sufficiently extended in space and/or time to “feel” these background gradients. Arguably, in an ideal asymptotic world inhabited by theoretical physicists, one can always go to scales small enough for this restriction to be justified, without hitting dissipation/microphysical scales first (in a real world, this is, regrettably, not always true, but let us understand the asymptotically idealised reality first). The only large-scale feature that does not thus go away at small scales is the magnetic field. This is what makes MHD turbulence *a priori* different from, for example, rotating or stratified turbulence, which, at small enough scales, always reverts to the universal Kolmogorov state (see, e.g., [Nazarenko & Schekochihin 2011](#)).

2.1. K41

Let us recall with maximum brevity what this Kolmogorov state is. Assume that energy is being pumped into the system at large scales and at some fixed rate ε . Then, in the inertial range (i.e., at small enough scales so the system is locally homogeneous but not small enough for viscosity or any other microphysics to matter yet), this same ε is the constant energy flux from scale to scale. Assuming that the cascade (i.e., the passing of energy from scale to scale) is local, the energy spectrum is, by dimensional analysis,

$$E(k) \sim \varepsilon^{2/3} k^{-5/3}, \quad (2.1)$$

the famous Kolmogorov spectrum ([Kolmogorov 1941b](#); henceforth K41), or, in terms of typical velocity increments between points separated by a distance λ :

$$\delta u_\lambda \sim (\varepsilon \lambda)^{1/3}. \quad (2.2)$$

²“All changes in nature occur in such a way that if anything is added anywhere, the same amount is subtracted from somewhere else. [...] As this is a universal law of nature, it extends to the laws of motion...”—[Lomonosov \(1748\)](#).

This is all obvious because the dimensions of the quantities involved are

$$[\varepsilon] = \frac{U^3}{L}, \quad \left[\int dk E(k) \right] = [\delta u_\lambda^2] = U^2, \quad [k] = [\lambda^{-1}] = L^{-1}, \quad (2.3)$$

where U is a unit of velocity and L of length. As we will be dealing with an incompressible medium (which is always achievable by going to small enough scales and so to sufficiently subsonic motions), its density is an irrelevant constant.³

2.2. IK

It was Kraichnan (1965) who appears to have been the first to realise clearly the point made above about the irreducibility of the magnetic field. He therefore argued that, if the background uniform magnetic field \mathbf{B}_0 , which in velocity units is called the Alfvén speed,

$$v_A = \frac{B_0}{\sqrt{4\pi\rho_0}} \quad (2.4)$$

(ρ_0 is the mass density of the conducting medium), was to have a persistent (at small scales) role in the energy transfer from scale to scale, then the energy spectrum in the inertial range must be, again by dimensional analysis,

$$E(k) \sim (\varepsilon v_A)^{1/2} k^{-3/2} \Leftrightarrow \delta u_\lambda \sim (\varepsilon v_A \lambda)^{1/4}. \quad (2.5)$$

This is known as the Iroshnikov–Kraichnan spectrum (henceforth IK; figure 1).⁴ The scaling exponent was fixed by the requirement, put forward with the trademark combination of deep insight and slightly murky argumentation that one often finds in Kraichnan’s papers, that the Alfvén time $\tau_A \sim 1/kv_A$ was the typical time during which interactions would occur (before build-up of correlations was arrested by perturbations propagating away from each other), so the energy flux had to be proportional to τ_A and, therefore, to $1/v_A$ —thus requiring them to enter in the combination εv_A .⁵

Kraichnan’s prediction was viewed as self-evidently correct for 30 years, then wrong for 10 years (§ 5), then correct again (in a different sense) for another 10 years (§ 6), then had to be revised again, at small enough scales (§ 7). His own interpretation of it (which was also Iroshnikov’s, arrived at independently) was certainly wrong, as it was based on the assumption—natural for a true Kolmogorovian susceptible to the great man’s universalist

³In what follows, the considerations leading to scaling laws such as (2.1) or (2.2), will require dynamical reasoning involving “cascade times”—thus, (2.2) is obtained by assuming a constant, scale-local energy flux $\delta u_\lambda^2/\tau_c \sim \varepsilon$ with the cascade time $\tau_c \sim \lambda/\delta u_\lambda$ [same as (2.9)]. I am, however, starting here with a purely dimensional derivation to emphasise that K41 does not, in fact, require us to have any dynamical insight into what is going on in the inertial range, and the need for such an insight will arise only once dimensional analysis fails to give us a unique answer.

⁴Iroshnikov (1963) got the same result slightly earlier, by what one might view as an early weak-turbulence calculation (before weak turbulence was properly invented), involving treatment of Alfvén waves as quasiparticles, opportune closure assumptions and, in the end, dimensional analysis. No one seems to have noticed his paper at the time and he disappeared into Soviet obscurity. In later years, he worked at the Institute of Oceanology and died in 1991, aged 54.

⁵Another, much better known and now standard, argument for the IK spectrum, perhaps less cryptic (but still wrong), is to posit constant flux, $\delta u_\lambda^2/\tau_c \sim \varepsilon$, where the cascade time is $\tau_c \sim \tau_{nl}^2/\tau_A$ as in (4.5), but, assuming isotropy, $\tau_{nl} \sim \lambda/\delta u_\lambda$, $\tau_A \sim \lambda/v_A$, so $\tau_c \sim \lambda v_A/\delta u_\lambda^2$ and (2.5) follows. Thus, the IK theory follows from the heuristic theory of WT (§ 4.2) for MHD plus the isotropy assumption $k_{\parallel} \sim \lambda^{-1}$ (which, however, is inconsistent with weak three-wave interactions: see § 4.1).



R. S. Iroshnikov (1937-1991)



R. H. Kraichnan (1928-2008)



P. Goldreich



S. Sridhar

FIGURE 1. IK and GS (photo of R. S. Iroshnikov courtesy of N. Lipunova and K. Bychkov, Sternberg Astronomical Institute; photo of R. H. Kraichnan courtesy of the AIP Emilio Segrè Visual Archives).

notion of “restoration of symmetries” at small scales, but, in retrospect, illogical in the context of proclaiming the unwaning importance of \mathbf{B}_0 at those same small scales—that turbulence sufficiently deep in the inertial range would be isotropic, i.e., that there is only one k to be used in the dimensional analysis. In fact, one both can and should argue that, *a priori*, there is a k_{\parallel} and a k_{\perp} , which represent the variation of the turbulent fields along and across \mathbf{B}_0 and need not be the same. The presence of the dimensionless ratio k_{\parallel}/k_{\perp} undermines the dimensional inevitability of (2.5) and opens up space for much theorising, inspired or otherwise.

2.3. GS95

Intuitively, in a strong magnetic field, perturbations with $k_{\parallel} \ll k_{\perp}$ should be more natural than isotropic ones, as the field is frozen into the motions but hard to bend. It turns out that MHD turbulence is indeed anisotropic in this way, at all scales, however small. This was realised quite early on, when the first, very tentative, experimental and numerical evidence started to be looked at (Robinson & Rusbridge 1971; Montgomery & Turner 1981; Shebalin *et al.* 1983), but, interestingly, it took more than a decade after that for the IK theory to be properly revised.

Dynamically, the parallel variation (on scale $l_{\parallel} \sim k_{\parallel}^{-1}$) is associated with the propaga-

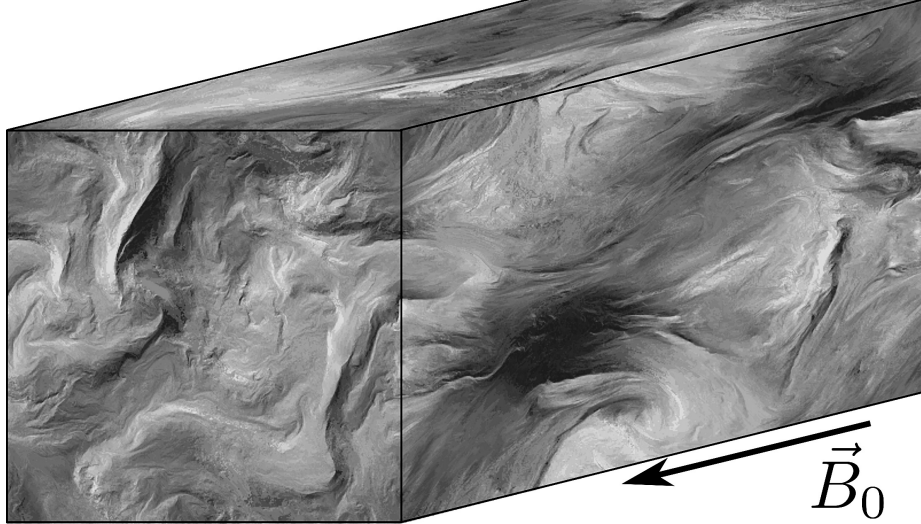


FIGURE 2. A visualisation of numerical RMHD turbulence, courtesy of A. Beresnyak (run R5 from [Beresnyak 2012a](#), 1536³). The shades of grey represent the absolute value of $\mathbf{Z}_\perp^+ = \mathbf{u}_\perp + \mathbf{b}_\perp$ (see §3).

tion of [Alfvén \(1942\)](#) waves, the wave period (or “propagation time”) being

$$\tau_A \sim \frac{l_{\parallel}}{v_A}, \quad (2.6)$$

and the perpendicular variation (on scale $\lambda \sim k_\perp^{-1}$) with nonlinear interactions, whose characteristic time is naively equal to the “eddy-turnover time”:

$$\tau_{nl} \sim \frac{\lambda}{\delta u_{\lambda}} \quad (2.7)$$

(we shall see in §6 why this is naïve). Here and below, δu_{λ} is used to represent the turbulent field on the grounds that, in Alfvénic perturbations, $\delta u_{\lambda} \sim \delta b_{\lambda}$, where δb is the magnetic perturbation in velocity units (see §3 for a discussion with equations). Declaring the two times comparable at all scales was an inspired conjecture by [Goldreich & Sridhar \(1995, 1997\)](#) (henceforth GS95; figure 1),⁶ which has come to be known as the *critical balance* (CB). I shall discuss the physical reasons for it properly in §§4 and 5, but here let me just postulate it. Then, naturally, the “cascade time” (i.e., the typical time to transfer energy from one perpendicular scale λ to the next) must be of the same order as either of the two other times:

$$\tau_c \sim \tau_A \sim \tau_{nl}. \quad (2.8)$$

If (2.7) is used for τ_{nl} , then (2.8) obviates the magnetic field and returns us to the K41 scaling (2.2), viz.,

$$\frac{\delta u_{\lambda}^2}{\tau_c} \sim \varepsilon, \quad \tau_c \sim \tau_{nl} \sim \frac{\lambda}{\delta u_{\lambda}} \quad \Rightarrow \quad \delta u_{\lambda} \sim (\varepsilon \lambda)^{1/3} \quad \Leftrightarrow \quad E(k_{\perp}) \sim \varepsilon^{2/3} k_{\perp}^{-5/3}. \quad (2.9)$$

This anisotropic version of K41 is known as the Goldreich–Sridhar (or GS95) spectrum.

⁶Anticipated, in fact, by [Higdon \(1984\)](#), who did not quite connect the dots, but, in retrospect, deserves more credit than he is getting.

Simultaneously, *along* the field,⁷ the velocity increments must satisfy

$$\frac{\delta u_{l\parallel}^2}{\tau_c} \sim \varepsilon, \quad \tau_c \sim \tau_A \sim \frac{l\parallel}{v_A} \quad \Rightarrow \quad \delta u_{l\parallel} \sim \left(\frac{\varepsilon l\parallel}{v_A} \right)^{1/2}. \quad (2.10)$$

Thus, \mathbf{B}_0 's influence does persist, but its size enters only the parallel scaling relations, not the perpendicular ones. Formally speaking, (2.9) is just the K41 dimensional argument for the perpendicular scale λ , with the CB conjecture used to justify not including v_A and $l\parallel$ amongst the local governing parameters. The assumption is that the sole role of \mathbf{B}_0 is to set the value of $l\parallel$ for any given λ : comparing (2.9) and (2.10), we get

$$l\parallel \sim v_A \varepsilon^{-1/3} \lambda^{2/3}. \quad (2.11)$$

Physically, this $l\parallel$ is the distance that an Alfvénic pulse travels along the field, at speed v_A , over the time τ_{nl} , given by (2.7), that it takes a turbulent perturbation of size λ to break up nonlinearly. It is natural to argue, by causality, that this is the maximum distance over which any perturbation can remain correlated (Boldyrev 2005; Nazarenko & Schekochihin 2011).

This narrative arc brings us approximately to the state of affairs in mid-1990s, although the GS95 theory did not really become mainstream until the early years of this century—and soon had to be revised. Before I move on to discussing this revision (§ 6) and the modern state of the subject, I would like to put the discussion of what happens dynamically and how CB is achieved on a slightly less hand-waving basis than I have done so far. Indeed, why critical balance? *Pace* the causality argument, which sets the maximum $l\parallel$, why can $l\parallel$ not be shorter? Is the nonlinear-time estimate (2.7), crucial for the scaling (2.9), justified? What happens dynamically?

From this point on, my exposition will be more sequential, I will avoid jumping ahead to the highlights and adopt a more systematic style, rederiving carefully some of the results reviewed in this section (an already well educated—or impatient—reader is welcome to skip or skim forward at her own pace).

3. Reduced MHD

The theoretical assumption (or numerical/observational evidence) that MHD turbulence consists of perturbations that have $k_\perp \gg k\parallel$ but that their Alfvénic propagation remains important (so as to allow CB should the system want to be in it) leads to the following set of equations for these perturbations:

$$\partial_t \mathbf{Z}_\perp^\pm \mp v_A \nabla_\parallel \mathbf{Z}_\perp^\pm + \mathbf{Z}_\perp^\mp \cdot \nabla_\perp \mathbf{Z}_\perp^\pm = -\nabla_\perp p + \eta \nabla_\perp^2 \mathbf{Z}_\perp^\pm + \mathbf{f}^\pm. \quad (3.1)$$

These are evolution equations for the Elsasser (1950) fields $\mathbf{Z}_\perp^\pm = \mathbf{u}_\perp \pm \mathbf{b}_\perp$, where \mathbf{u}_\perp is the fluid velocity perpendicular to the equilibrium field \mathbf{B}_0 , and \mathbf{b}_\perp is the magnetic-field perturbation, also perpendicular to \mathbf{B}_0 and expressed in velocity units, i.e., scaled to $\sqrt{4\pi\rho_0}$. The total pressure p (which includes the magnetic pressure) is determined by the condition that $\nabla_\perp \cdot \mathbf{Z}_\perp^\pm = 0$, enforcing the solenoidality of the magnetic field and the incompressibility of the motions, the latter achieved at small enough scales by small enough perturbations. Namely, p is the solution of

$$\nabla_\perp^2 p = -\nabla_\perp \nabla_\perp : \mathbf{Z}_\perp^+ \mathbf{Z}_\perp^-, \quad (3.2)$$

⁷It turns out that this has to be along the exact, perturbed field rather than the mean field (Cho & Vishniac 2000; Maron & Goldreich 2001)—see § 5.3.

which amounts to multiplying the nonlinear term on the left-hand side of (3.1) by a projection operator in Fourier space. I have, for simplicity, taken the kinematic viscosity and magnetic diffusivity η to be the same (but will relax this assumption from § 6.4 onwards). The last term in equation (3.1), the body force \mathbf{f}^\pm , stands in for any energy-injection mechanism that this small-scale approximation might inherit from the non-universal large scales.

The *Reduced MHD equations* (3.1–3.2) (RMHD, first proposed by Strauss 1976, but, as often happened in those days, also found independently by the Soviets, Kadomtsev & Pogutse 1974), which also have a compact scalar form (see appendix A.1), can be derived from the standard compressible MHD equations by ordering all perturbations of the equilibrium to be comparable to the Mach number and to $k_{\parallel}/k_{\perp} \ll 1$ and the rate of change of these perturbations to the Alfvén frequency $k_{\parallel}v_A$ (see Schekochihin & Cowley 2007 or Schekochihin 2022; a number of similar, if ever so subtly different, schemes exist: see review by Oughton *et al.* 2017 and references therein). These equations, apart from the visco-resistive terms, are, in fact, more general than the collisional MHD approximation and apply also to low-frequency, long-wavelength collisionless perturbations near a gyrotropic equilibrium (Schekochihin *et al.* 2009; Kunz *et al.* 2015),⁸ which makes them applicable to the solar wind (notable for being thoroughly measurable) and many other, more remote, astrophysical plasmas (only measurable with difficulty, but endlessly fascinating to large numbers of curious researchers in gainful employment).

While, like any nonlinear equations of serious consequence, they are impossible to solve except in almost-trivial special cases, the RMHD equations possess a number of remarkable properties that form the basis for all theories of their turbulent solutions.

(i) The perturbations described by them, known as *Alfvénic*, are nonlinear versions of (packets of) Alfvén waves: perturbations of velocity and magnetic field transverse to \mathbf{B}_0 and propagating at speed v_A along it (\mathbf{Z}_{\perp}^+ in the \mathbf{B}_0 direction, \mathbf{Z}_{\perp}^- in the $-\mathbf{B}_0$ direction). They are entirely decoupled from all other perturbations (compressive in the case of fluid MHD, kinetic for a collisionless plasma; see Schekochihin *et al.* 2009 and Kunz *et al.* 2015) and can be considered in isolation from them. If evolved via full compressible MHD equations, these Alfvénic perturbations do not generate motions or fields that violate the $k_{\parallel} \ll k_{\perp}$ assumption (e.g., higher-frequency fast MHD waves), so RMHD appears to be well posed in the sense that it does not break the assumptions that it is based on (this was checked numerically by Cho & Lazarian 2002, 2003, who trod in the footsteps of Matthaeus *et al.* 1996).

(ii) Only counterpropagating fields interact, so the nonlinearity vanishes if either $\mathbf{Z}_{\perp}^+ = 0$ or $\mathbf{Z}_{\perp}^- = 0$, giving rise to the so-called Elsasser states ($\mathbf{u}_{\perp} = \mp \mathbf{b}_{\perp}$), exact nonlinear solutions that are arbitrary-amplitude, arbitrary-shape pulses travelling along \mathbf{B}_0 at the velocity $\mp v_A$.

(iii) The energies of the two Elsasser fields are conserved individually (apart from any injection and dissipation terms), viz.,

$$\frac{\partial}{\partial t} \frac{\langle |\mathbf{Z}_{\perp}^{\pm}|^2 \rangle}{2} = \varepsilon^{\pm} - \eta \langle |\nabla_{\perp} \mathbf{Z}_{\perp}^{\pm}|^2 \rangle. \quad (3.3)$$

The energy fluxes $\varepsilon^{\pm} = \langle \mathbf{Z}_{\perp}^{\pm} \cdot \mathbf{f}^{\pm} \rangle$ need not be the same and their ratio $\varepsilon^+/\varepsilon^-$ is, in

⁸At high β , the amplitudes of these perturbations have to be small enough in order not to run afoul of some rather interesting and only recently appreciated spoiler physics (Squire *et al.* 2016, 2017b,*a*, 2019; Tenerani *et al.* 2017; Tenerani & Velli 2018), which I will discuss very briefly in § 14.5.

general, a parameter of the problem—when it is different from unity, the turbulence is called *imbalanced* (§ 9). Another way of framing (3.3) is by stating that RMHD has two invariants, the *total energy* and the *cross-helicity*:

$$\frac{\langle |\mathbf{u}_\perp|^2 + |\mathbf{b}_\perp|^2 \rangle}{2} = \frac{\langle |\mathbf{Z}_\perp^+|^2 + |\mathbf{Z}_\perp^-|^2 \rangle}{4}, \quad \langle \mathbf{u}_\perp \cdot \mathbf{b}_\perp \rangle = \frac{\langle |\mathbf{Z}_\perp^+|^2 - |\mathbf{Z}_\perp^-|^2 \rangle}{4}, \quad (3.4)$$

respectively (so imbalanced turbulence is turbulence with non-zero cross-helicity). The name of the second invariant has topological origins, alluding, in incompressible 3D MHD, to conservation of linkages between flux tubes and vortex tubes; in the context of small Alfvénic perturbations of a strong uniform mean field \mathbf{B}_0 , this does not appear to be a useful interpretation.

(iv) The amplitudes \mathbf{Z}_\perp^\pm , time and the gradients can be arbitrarily but simultaneously rescaled: $\forall \epsilon$ and a ,

$$\mathbf{Z}_\perp^\pm \rightarrow \epsilon \mathbf{Z}_\perp^\pm, \quad \mathbf{f}^\pm \rightarrow \frac{\epsilon^2}{a} \mathbf{f}^\pm, \quad \nabla_\perp \rightarrow \frac{1}{a} \nabla_\perp, \quad \nabla_\parallel \rightarrow \frac{\epsilon}{a} \nabla_\parallel, \quad t \rightarrow \frac{a}{\epsilon} t, \quad \eta \rightarrow \epsilon a \eta. \quad (3.5)$$

This means that \mathbf{Z}_\perp^\pm and ∇_\parallel are, formally speaking, infinitesimal compared to v_A and ∇_\perp , respectively (perpendicular and parallel distances in RMHD are measured “in different units,” as are the Alfvén speed and \mathbf{Z}_\perp^\pm). Any statistical scalings or heuristic theories must respect this symmetry (Beresnyak 2011, 2012a)—this requirement will feature prominently in § 6.4. Note that this symmetry implies that the parallel-to-perpendicular aspect ratio of the numerical box in simulations of RMHD is an arbitrary parameter.

(v) Defining field increments

$$\delta \mathbf{Z}_\lambda^\pm = \mathbf{Z}_\perp^\pm(\mathbf{r} + \boldsymbol{\lambda}) - \mathbf{Z}_\perp^\pm(\mathbf{r}), \quad (3.6)$$

where $\boldsymbol{\lambda}$ is a point-separation vector in the perpendicular plane, assuming statistical isotropy in this plane and considering separations $\lambda = |\boldsymbol{\lambda}|$ belonging to the inertial range (i.e., smaller than the energy-injection scale but greater than the viscous/resistive scale), one finds, in a statistical steady state,⁹

$$\langle \delta Z_L^\mp | \delta \mathbf{Z}_\lambda^\pm |^2 \rangle = -2\varepsilon^\pm \lambda, \quad (3.7)$$

where $\delta Z_L^\mp = \delta \mathbf{Z}_\lambda^\mp \cdot \boldsymbol{\lambda}/\lambda$ is the “longitudinal” increment. These exact laws are the RMHD version of the exact third-order laws that one always gets for turbulent systems with a convective nonlinearity, resembling the Kolmogorov (1941a) 4/5 law of hydrodynamic turbulence or (in fact, more closely) the Yaglom (1949) 4/3 law for a passive field (because in RMHD, \mathbf{Z}_\perp^+ advects \mathbf{Z}_\perp^- and vice versa). They were derived for incompressible MHD by Politano & Pouquet (1998a,b) assuming spatial isotropy and, isotropy having become untenable, adjusted to their RMHD form (3.7) by Boldyrev *et al.* (2009). They provide a useful (although not as restrictive as one might have hoped) analytical benchmark for any aspiring scaling theory of RMHD turbulence, weak or strong.

Everything in this review concerns turbulence that can be described by RMHD equations, with the following exceptions: parts of § 12, concerned with various types of decaying MHD turbulence, where energy-containing scales are the main object of study;

⁹Write an evolution equation for $\delta \mathbf{Z}_\lambda^\pm$ following directly from (3.1), take its scalar product with $\delta \mathbf{Z}_\lambda^\pm$, average to get an evolution equation for the second-order structure function $\langle |\delta \mathbf{Z}_\lambda^\pm|^2 \rangle$, then throw out the viscous/resistive terms, assume steady state ($\partial_t = 0$), spatial homogeneity (correlation functions depend on $\boldsymbol{\lambda}$ but not on \mathbf{r}) and isotropy in the perpendicular plane (scalar averaged quantities depend on $\lambda = |\boldsymbol{\lambda}|$ only), and, finally, integrate once with respect to λ .

§ 13, which deals with turbulent dynamo—a situation in which \mathbf{b}_\perp is emphatically not small compared to \mathbf{B}_0 (there is no \mathbf{B}_0) and so full MHD equations are needed; and § 14, where the limitations of the fluid description and the importance of kinetic effects are discussed.

4. Weak MHD Turbulence

Most theory in physics is perturbation theory. In turbulence, the available perturbation theory is the “weak-turbulence” (WT) approximation for wave-carrying systems. Its attraction is that it features a systematic derivation, an appealing interpretation of the turbulent system as a gas of weakly interacting quasiparticles, or “quantised” waves, and quantitative predictions for spectra, or occupation numbers, of these waves (see textbooks by [Zakharov et al. 1992](#), [Nazarenko 2011](#), [Schekochihin 2022](#), or, for a quick recap, appendix A.2). Putting aside the question of whether the conditions necessary for it to hold are commonly (or ever) satisfied by natural turbulent systems, it is still interesting—and, arguably, also a matter of due diligence—to inquire whether such a regime, and such a theory, are relevant for our RMHD system. “Such a regime” means small amplitudes—small enough for the nonlinear interactions to occur very slowly compared to wave motion. One can certainly imagine, at least in principle, driving an RMHD system in a WT way, very gently.

4.1. WT is Irrelevant

On a broad-brush qualitative level, one can deal with this possibility as follows. Assume that in the energy-injection range, represented by some perpendicular scale L_\perp and some parallel scale $L_\parallel = 2\pi/k_\parallel$, Alfvén waves are generated with amplitudes Z^\pm so small that

$$\omega_{\mathbf{k}}^\pm = \pm k_\parallel v_A = \frac{1}{\tau_A} \gg \frac{1}{\tau_{nl}^\pm} \sim \frac{Z^\mp}{L_\perp}. \quad (4.1)$$

If they are viewed as interacting quasiparticles (“+” can only interact with “−”, and vice versa), the momentum and energy conservation in a three-wave interaction require

$$\left. \begin{aligned} \mathbf{p} + \mathbf{q} &= \mathbf{k}, \\ \omega_{\mathbf{p}}^\mp + \omega_{\mathbf{q}}^\pm &= \omega_{\mathbf{k}}^\pm \end{aligned} \right\} \Rightarrow -p_\parallel + q_\parallel = k_\parallel \quad \Rightarrow \quad q_\parallel = k_\parallel, \quad p_\parallel = 0. \quad (4.2)$$

Thus, three-wave interaction in fact involves a wave (\mathbf{q}) scattering off a 2D perturbation ($p_\parallel = 0$, not a wave) and becoming a wave (\mathbf{k}) with the same frequency (because $k_\parallel = q_\parallel$) and a different perpendicular wavenumber ($\mathbf{k}_\perp = \mathbf{p}_\perp + \mathbf{q}_\perp$). Intuitively, there will be a cascade of the waves to higher k_\perp . If the amplitude of the waves does not fall off with k_\perp faster than k_\perp^{-1} , which is equivalent to their energy spectrum being less steep than k_\perp^{-3} , then the nonlinear-interaction time will become ever shorter with larger k_\perp , even as the waves’ k_\parallel and, therefore, their frequency stay the same. Eventually, at some perpendicular scale, which I shall call λ_{CB} , the condition $\tau_{nl} \gg \tau_A$ will be broken, so we end up with $\tau_{nl} \sim \tau_A$ and can return to considerations of the strong-turbulence regime, critical balance, etc. Numerically, this transition was first captured quite recently, by [Meyrand et al. \(2016\)](#), whose result is shown in figure 3.

The transition scale λ_{CB} is easy to estimate without the need for a specific WT theory. In view of (4.2), weak interactions cannot increase the characteristic parallel scale of the perturbations, which therefore remains L_\parallel . Then λ_{CB} is the perpendicular scale

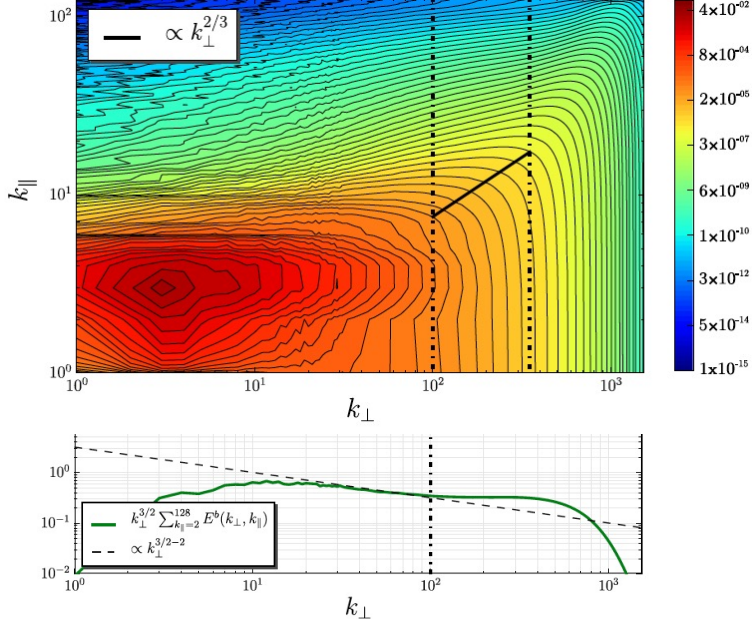


FIGURE 3. (Decaying) MHD simulation of transition from weak to strong turbulence by Meyrand *et al.* (2016): the upper panel shows the magnetic spectrum vs. k_{\parallel} and k_{\perp} (where k_{\parallel} is along the global mean field), the lower one the same integrated over k_{\parallel} and normalised by $k_{\perp}^{3/2}$ (see § 6 for why $k_{\perp}^{-3/2}$ rather than $k_{\perp}^{-5/3}$). A transition manifestly occurs from a k_{\perp}^{-2} to a $k_{\perp}^{-3/2}$ spectrum and, simultaneously, from a state with no k_{\parallel} cascade (and a relatively narrow-band parallel spectrum) to one consistent with a CB cascade (2D spectra of CB turbulence are worked out in appendix C). [Reprinted with permission from Meyrand *et al.* (2016), copyright (2016) by the American Physical Society.]

corresponding to $l_{\parallel} = L_{\parallel}$ in (2.11), viz.,

$$\lambda_{\text{CB}} \sim \varepsilon^{1/2} \left(\frac{L_{\parallel}}{v_A} \right)^{3/2}. \quad (4.3)$$

In fact, one does not even need to invoke the GS95 CB curve (2.11), because (4.3) is the only dimensionally correct possibility if one asks for a scale that depends on ε and $\tau_A \sim L_{\parallel}/v_A$ only; that L_{\parallel} and v_A must enter in this combination follows from the fact that ∇_{\parallel} and v_A only enter multiplying each other in the RMHD equations (3.1).

A reader who is both convinced by this argument and regards it as grounds for dismissing the WT regime as asymptotically irrelevant, can at this point skip to § 5. The rest of this section is for those restless souls who insist on worrying about what happens in weakly forced systems at $\lambda \gg \lambda_{\text{CB}}$.

4.2. A Sketch of WT Theory

A very simple heuristic WT calculation (Ng & Bhattacharjee 1997; Goldreich & Sridhar 1997)—a useful and physically transparent shortcut, and a good starting point for discussion—goes as follows.

Imagine two counterpropagating Alfvénic structures of perpendicular size λ and parallel coherence length L_{\parallel} (which cannot change in WT, as per the argument in § 4.1) passing through each other and interacting weakly. Their transit time through each other

is $\tau_A \sim L_{\parallel}/v_A$ and the change in their amplitudes during this time is

$$\Delta(\delta Z_{\lambda}^{\pm}) \sim \delta Z_{\lambda}^{\pm} \frac{\tau_A}{\tau_{\text{nl}}^{\pm}} \sim \frac{\delta Z_{\lambda}^{+} \delta Z_{\lambda}^{-}}{\lambda} \tau_A, \quad (4.4)$$

assuming $\tau_{\text{nl}}^{\pm} \sim \lambda/\delta Z_{\lambda}^{\mp}$. By definition of the WT regime, $\tau_{\text{nl}}^{\pm} \gg \tau_A$, so the amplitude change in any one interaction is small, $\Delta(\delta Z_{\lambda}^{\pm}) \ll \delta Z_{\lambda}^{\pm}$, and many such interactions are needed in order to change the amplitude δZ_{λ}^{\pm} by an amount comparable to itself, i.e., to “cascade” the energy associated with scale λ to smaller scales. Suppose that interactions occur all the time and that the kicks (4.4) accumulate as a random walk. Then the cascade time is $\tau_c^{\pm} = N\tau_A$ if after N interactions the amplitude change is of order δZ_{λ}^{\pm} :

$$\Delta(\delta Z_{\lambda}^{\pm})\sqrt{N} \sim \delta Z_{\lambda}^{\pm} \Rightarrow \frac{\tau_A}{\tau_{\text{nl}}^{\pm}} \sqrt{\frac{\tau_c^{\pm}}{\tau_A}} \sim 1 \Rightarrow \tau_c^{\pm} \sim \frac{(\tau_{\text{nl}}^{\pm})^2}{\tau_A}. \quad (4.5)$$

The standard Kolmogorov constant-flux requirement gives

$$\varepsilon^{\pm} \sim \frac{(\delta Z_{\lambda}^{\pm})^2}{\tau_{\text{c}}^{\pm}} \sim \frac{(\delta Z_{\lambda}^{+})^2 (\delta Z_{\lambda}^{-})^2 \tau_A}{\lambda^2}. \quad (4.6)$$

Assuming for the moment that $\varepsilon^+ \sim \varepsilon^-$ and, therefore, $\delta Z_{\lambda}^+ \sim \delta Z_{\lambda}^-$, gets us the classic WT scaling¹⁰

$$\delta Z_{\lambda} \sim \left(\frac{\varepsilon}{\tau_A} \right)^{1/4} \lambda^{1/2} \Leftrightarrow E(k_{\perp}) \sim \left(\frac{\varepsilon}{\tau_A} \right)^{1/2} k_{\perp}^{-2}. \quad (4.7)$$

This scaling is indeed what one finds numerically (see figures 3 and 4)—it was first confirmed in early, semidirect simulations by Ng & Bhattacharjee (1997) and Bhattacharjee & Ng (2001), and then definitively by Perez & Boldyrev (2008) and Boldyrev & Perez (2009), leading the community to tick off WT as done and dusted.

As anticipated in § 4.1, with the scaling (4.7), the ratio of the time scales can only stay small above a certain finite scale:

$$\frac{\tau_A}{\tau_{\text{nl}}} \sim \frac{\tau_A \delta Z_{\lambda}}{\lambda} \sim \frac{\tau_A^{3/4} \varepsilon^{1/4}}{\lambda^{1/2}} \ll 1 \Leftrightarrow \lambda \gg \varepsilon^{1/2} \tau_A^{3/2} \sim \lambda_{\text{CB}}, \quad (4.8)$$

where λ_{CB} is transition scale anticipated in (4.3). For $\lambda \lesssim \lambda_{\text{CB}}$, turbulence becomes strong and, presumably, critically balanced. Thus, the WT cascade, by transferring energy to smaller scales, where nonlinear times are shorter, saws the seeds of its own destruction.

4.3. Imbalanced WT

What if $\varepsilon^+ \neq \varepsilon^-$, viz., say, $\varepsilon^+ \gg \varepsilon^-$? (If $\varepsilon^+ > \varepsilon^-$ but both are of the same order, arguably the results obtained for $\varepsilon^+ \sim \varepsilon^-$ should still work, at least on the “twiddle” level.) Alas, (4.6) is patently incapable of accommodating such a case, an embarrassment first noticed by Dobrowolny *et al.* (1980), who were attempting an IK-style, isotropic ($L_{\parallel} \sim \lambda$), imbalanced theory—quite wrong, as we now know (§ 2.3), but they correctly identified the issue with the imbalanced regime. They concluded that no imbalanced stationary state was possible except a pure Elsasser state. This may be true for (certain types of) decaying turbulence (see § 12.7), but is certainly not a satisfactory conclusion

¹⁰For the laterally curious, let me flag here one very simple consequence of this result that, however, does not appear to be well known: the Lagrangian trajectories in weak Alfvénic turbulence diverge diffusively, rather than superdiffusively (as they do in strong turbulence)—this is shown in (D 109).

for a forced case where ε^\pm are externally prescribed. Arguably, the inability to describe the imbalanced case casts a shadow of doubt also on the validity of the argument in § 4.2 for balanced WT, as introducing the imbalance just lifts a kind of “degeneracy” and perhaps highlights a problem with the whole story.

A way out of this difficulty, various versions of which have been explored by Galtier *et al.* (2000), Lithwick & Goldreich (2003), and Chandran (2008), is to accept (4.6) but notice that it allows the two Elsasser fields to have different scaling exponents, $\delta Z_\lambda^\pm \propto \lambda^{\gamma^\pm}$, as long as they satisfy $\gamma^+ + \gamma^- = 1$. The corresponding 2D spectra of the two fields are

$$E_{\text{2D}}^\pm(k_\perp, k_\parallel) = f^\pm(k_\parallel) k_\perp^{\mu^\pm}, \quad \mu^+ + \mu^- = -4, \quad (4.9)$$

because $\mu^\pm = -2\gamma^\pm - 1$ and, WT permitting no changes in k_\parallel , the scaling arguments of § 4.2 apply to each k_\parallel individually. One may then declare that the difference between ε^+ and ε^- is hidden in the prefactors $f^\pm(k_\parallel)$, which are non-universal, inaccessible to “twiddle” scaling arguments about local interactions in the WT inertial range, and have to be fixed from outside it. At the large-scale end, one has to decide whether the outer scales for the two Elsasser fields are the same or different (Chandran 2008) and whether it is the fluxes ε^\pm or the fields’ energies at the outer scale(s) that it makes better sense to consider prescribed. At the dissipation scale, one has the option of “pinning” the spectra to the same value (an idea due to Grappin *et al.* 1983 and revived by Lithwick & Goldreich 2003), and it must also be decided whether the two fields are required to start feeling viscosity at the same scale or one can do so before the other (see discussion in Beresnyak & Lazarian 2008, and, for strong imbalanced turbulence, in § 9.6.4). If WT breaks down before the dissipation scale is reached, some other set of *ad hoc* arrangements is required (see, e.g., Chandran 2008). Typically, the outcome is that the stronger field has a steeper spectrum than the weaker field, but their scalings are non-universal, i.e., they depend on the particular set up of the problem, at both macro- and micro-scales.

Another possibility is that (4.6) is wrong. Let me observe that the balanced ($\varepsilon^+ \sim \varepsilon^-$, $\delta Z_\lambda^+ \sim \delta Z_\lambda^-$) version of this scaling, i.e., the statement that the flux ε is proportional to the fourth power of the amplitude, is less likely to be wrong than any particular assignment of “+”s and “-”s to these amplitudes: all it says is that the flux ε is what it would have been in the case of strong interactions, $\sim \delta Z_\lambda^2/\tau_{\text{nl}}$ [cf. (2.9)], times the first power of the expansion parameter τ_A/τ_{nl} , i.e., the lowest order that ε can be in a perturbation expansion in that parameter. Thus, one may doubt the validity of (4.6) for the imbalanced regime without rejecting the numerically confirmed k_\perp^{-2} scaling of the balanced spectra. For example, in the (heuristic) scheme proposed by Schekochihin *et al.* (2012),

$$\varepsilon^\pm \sim \frac{(\delta Z_\lambda^\pm)^3 \delta Z_\lambda^\mp \tau_A}{\lambda^2}, \quad (4.10)$$

which changes nothing for balanced WT, but leads to a very different situation in the imbalanced case than (4.6), allowing perfectly good k_\perp^{-2} spectra for both fields.

I do not go through all this in detail because, the WT regime being largely irrelevant (§ 4.1), it would also, if it really were non-universal, not be very interesting. If it is universal and something like (4.10) holds, that is interesting, but I do not know how to make much progress beyond Schekochihin *et al.* (2012), whose theory does not quite match simulations (see § 4.4). I also do not know how to construct a theory of imbalanced WT that would connect smoothly to any believable theory of strong imbalanced turbulence (e.g., one presented in § 9.6). An interested reader will find some further, equally unsatisfactory, observations in appendix A.6.

4.4. 2D Condensate

It follows from the discussion in § 4.1 that the WT approximation in its standard form cannot, in fact, work for the turbulence of Alfvén waves, at least not formally, because in every three-wave interaction, one of the three waves has $k_{\parallel} = 0$, so is not a wave at all, but a zero-frequency 2D perturbation, for which the nonlinear interactions are the dominant influence. If such $k_{\parallel} = 0$ perturbations are forbidden, i.e., if displacements vanish at infinity, one must consider four-wave interactions (i.e., go to next order in τ_A/τ_{nl}), which gives rise to an apparently legitimate WT state, different from (4.7) (Sridhar & Goldreich 1994). There is no particular reason to think, however, that such a restriction on displacements is legitimate in a general physical situation (Ng & Bhattacharjee 1996) or, even if one starts with no energy at $k_{\parallel} = 0$, that such a state can be maintained, except in a box with field lines nailed down at the boundaries—failing such restrictions, a 2D “condensate” must emerge (and does, in numerical simulations: see Boldyrev & Perez 2009, Wang *et al.* 2011, Meyrand *et al.* 2015, 2016, and figure 4).

Mathematically, this becomes quite obvious if we represent the solutions to (3.1) as

$$\mathbf{Z}_{\perp}^{\pm}(t, \mathbf{r}) = \sum_{k_{\parallel}} \mathbf{Z}_{k_{\parallel}}^{\pm}(t, x, y) e^{ik_{\parallel}(z \pm v_A t)} \quad (4.11)$$

and separate the $k_{\parallel} = 0$ modes from the rest:

$$\partial_t \mathbf{Z}_0^{\pm} + \hat{\mathcal{P}} \mathbf{Z}_0^{\mp} \cdot \nabla_{\perp} \mathbf{Z}_0^{\pm} = - \sum_{k_{\parallel} \neq 0} \hat{\mathcal{P}} \mathbf{Z}_{k_{\parallel}}^{\mp} \cdot \nabla_{\perp} \mathbf{Z}_{-k_{\parallel}}^{\pm} e^{\mp i 2 k_{\parallel} v_A t}, \quad (4.12)$$

$$\partial_t \mathbf{Z}_{k_{\parallel}}^{\pm} + \hat{\mathcal{P}} \mathbf{Z}_0^{\mp} \cdot \nabla_{\perp} \mathbf{Z}_{k_{\parallel}}^{\pm} = - \sum_{p_{\parallel} \neq 0} \hat{\mathcal{P}} \mathbf{Z}_{p_{\parallel}}^{\mp} \cdot \nabla_{\perp} \mathbf{Z}_{k_{\parallel}-p_{\parallel}}^{\pm} e^{\mp i 2 p_{\parallel} v_A t}, \quad (4.13)$$

where $\hat{\mathcal{P}}$ is the projection operator that takes care of the pressure term [see (3.2)] and has been introduced for brevity; forcing and dissipation terms have been dropped. The first of these equations, (4.12), describes the condensate—two real fields $\mathbf{Z}_0^{\pm}(x, y)$ advecting each other in the 2D plane while subject to an oscillating “force” due to the mutual coupling of the Alfvén waves $\mathbf{Z}_{k_{\parallel}}^{\pm}$. These Alfvén waves, described by (4.13), are advected by the 2D field and also by each other, but the latter interaction has an oscillating factor and vanishes in the WT approximation. Even if only the Alfvén waves are forced and the condensate is not, the condensate will nevertheless be built up.

Returning to three-wave interactions then (where one of the waves is not a wave), the traditional approach has been to ignore the inapplicability of the WT approximation to the $k_{\parallel} = 0$ modes by conjecturing that the function $f^{\pm}(k_{\parallel})$ in (4.9) is flat around $k_{\parallel} = 0$ —the hypothesis of “spectral continuity”. One can then press on with putting MHD through the WT analytical grinder, find an evolution equation for the spectra and show that it has steady-state, constant-flux solutions of the form (4.9). This is what was done in the now-classic paper by Galtier *et al.* (2000) (see appendices A.2 and A.3). In balanced turbulence, obviously, $\mu^+ = \mu^- = 2$, and we are back to (4.7); in imbalanced turbulence, one needs further scheming—see references in § 4.3.

Nazarenko (2007) argues that the hypothesis of spectral continuity is certainly false if the nonlinear broadening of the waves’ frequencies, of order τ_{nl}^{-1} , is smaller than the linear frequency associated with the spacing of the k_{\parallel} “grid” ($= 2\pi/L_{\parallel}$, the inverse parallel “box” size)—i.e., if the Alfvénic perturbations at the longest finite parallel scale in the system are already in the WT limit (4.1), $v_A/L_{\parallel} \gg \tau_{nl}^{-1}$. He is right. Figure 4 is taken from a (sadly, unpublished) numerical study of weak RMHD turbulence by Yousef & Schekochihin (2009), who forced Alfvén waves at $k_{\parallel} = 2\pi/L_{\parallel}$, where L_{\parallel} was the box

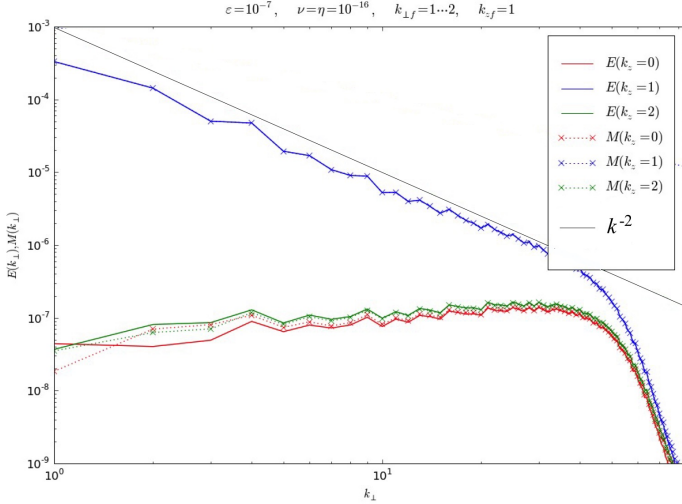


FIGURE 4. Kinetic (E , solid lines) and magnetic (M , dotted lines with crosses) energy spectra for $k_{\parallel} = 0$ (red), $k_{\parallel} = 2\pi/L_{\parallel}$ (blue) and $k_{\parallel} = 4\pi/L_{\parallel}$ (green) from an unpublished weak RMHD turbulence simulation by Yousef & Schekochihin (2009). The box size was $(L_{\perp}, L_{\parallel})$ in the perpendicular and parallel directions, respectively, and the forcing was narrow-band, at $k_{\parallel} = 2\pi/L_{\parallel}$ and $k_{\perp} = (1, 2) \times 2\pi/L_{\perp}$, deep in the WT regime ($L_{\perp} \gg \lambda_{CB}$). WT spectra for the case of broad-band forcing can be found in Perez & Boldyrev (2008) and Boldyrev & Perez (2009) and are discussed in appendix A.4.

size. It shows that, while the k_{\perp}^{-2} scaling of the $k_{\parallel} = 2\pi/L_{\parallel}$ modes is undeniable, the spectra for the unforced modes ($k_{\parallel} = 0$ and $k_{\parallel} = \text{multiples of } 2\pi/L_{\parallel}$) are dramatically shallower. Similar spectra were reported by Bigot & Galtier (2011) and by Meyrand *et al.* (2015). Qualitatively similar spectra (and a simple mechanism for how they might form) were also proposed by Schekochihin *et al.* (2012)—but their theory fails quantitatively, with the spectra that it predicts for all unforced modes at least one power of k_{\perp} steeper than the numerical ones (e.g., their $k_{\parallel} = 0$ condensate has a $\propto k_{\perp}^{-1}$ spectrum, while simulations suggest $\propto k_{\perp}^0$).

Nazarenko (2007) expects that the conventional WT theory should survive when $k_{\parallel}v_A \gg \tau_{nl}^{-1} \gg v_A/L_{\parallel}$. This is a situation that should be realisable in a system that is weakly and randomly forced in a broad band of frequencies (and, therefore, parallel wavenumbers). In appendix A.4, I discuss how, and in what sense, one might defend spectral continuity for such a system; I argue that the 2D condensate in this case is a strongly turbulent, critically balanced sub-system constantly fed by the weakly turbulent waves and developing a falsifiable set of scalings, which are, indeed, continuous with the WT scalings. While there are some indications (from the simulations by Wang *et al.* 2011; see appendix A.5) that these scalings might be right, I have not seen spectral continuity corroborated numerically in a definitive fashion, as even Perez & Boldyrev (2008) and Boldyrev & Perez (2009), who took great care to force in a broad band of k_{\parallel} to make sure the conventional WT theory did apply, saw a distinct dip in $f^{\pm}(k_{\parallel})$ at $k_{\parallel} = 0$, associated with an emergent condensate (which is magnetically dominated; see § 10.3 and appendix A.5). The same was true in the decaying simulations of Meyrand *et al.* (2015, 2016, see the upper panel of figure 3), where an initial small-amplitude (and so WT-compliant) state had the choice to evolve towards a continuous parallel spectrum, but refused to do so, again developing a $k_{\parallel} = 0$ condensate with dramatically

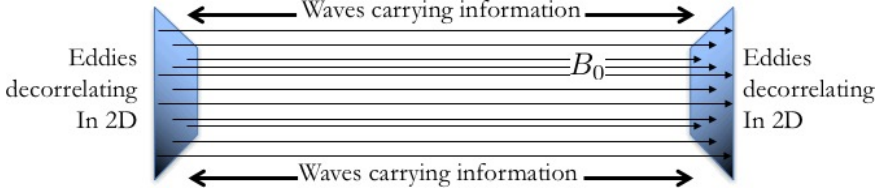


FIGURE 5. Critical balance in a (2+1)D system supporting both nonlinearity and waves (RMHD).

distinct properties, including a high degree of intermittency and a spectrum quite similar to figure 4.

Thus, the conventional WT theory is at best incomplete and at worst wrong. It is discussed further in appendix A, where I review the WT's derivation, speculate about the structure of the condensate, and discuss a number of other WT-related issues. Here, having flagged these issues, I want to halt this digression into matters that are, arguably, of little impact, and move on to the physics-rich core of the MHD-turbulence theory.

5. Critical Balance, Parallel Cascade, and Anisotropy

5.1. Critical Balance

Section 4 can be viewed as one long protracted justificatory piece in favour of critical balance: even if an ensemble of high-frequency Alfvén waves is stirred up very gently ($\tau_{\text{nl}} \gg \tau_A$), it will, at small enough scales, get itself into the strong-turbulence regime ($\tau_{\text{nl}} \sim \tau_A$). The opposite limit, a 2D regime with $\tau_{\text{nl}} \ll \tau_A$, is unsustainable for the very simple reason of causality: as information in an RMHD system propagates along \mathbf{B}_0 at speed v_A , no structure longer than $l_{\parallel} \sim v_A \tau_{\text{nl}}$ can be kept coherent and so will break up (see Boldyrev 2005, Nazarenko & Schekochihin 2011 and figure 5).

It is worth mentioning in passing that the CB turns out to be a very robust feature of the turbulence in the following interesting sense. With a certain appropriate definition of τ_{nl} (which will be explained in § 6.1), the ratio τ_A/τ_{nl} has been found (numerically) by Mallet *et al.* (2015) to have a scale-invariant distribution (figure 6), a property that they dubbed *refined critical balance (RCB)*. It gives a quantitative meaning to the somewhat vague statement $\tau_A/\tau_{\text{nl}} \sim 1$ —and becomes important in the (as it turns out, unavoidable) discussion of intermittency of MHD turbulence (§ 6.4.2).

5.2. Parallel Cascade

The most straightforward—and the least controversial—consequence of CB is the scaling of *parallel* increments. I have already derived this result in (2.10), but let me now restate it using Elsasser fields. If it is the case that the nonlinear-interaction time and, therefore, the cascade time for \mathbf{Z}_{\perp}^{\pm} are approximately the same as their propagation time $\tau_A \sim l_{\parallel}/v_A$, then the parallel increments $\delta Z_{l_{\parallel}}^{\pm}$ satisfy

$$\frac{(\delta Z_{l_{\parallel}}^{\pm})^2}{\tau_A} \sim \varepsilon^{\pm} \quad \Rightarrow \quad \delta Z_{l_{\parallel}}^{\pm} \sim \left(\frac{\varepsilon^{\pm} l_{\parallel}}{v_A} \right)^{1/2} \quad \Leftrightarrow \quad E^{\pm}(k_{\parallel}) \sim \frac{\varepsilon^{\pm}}{v_A} k_{\parallel}^{-2}. \quad (5.1)$$

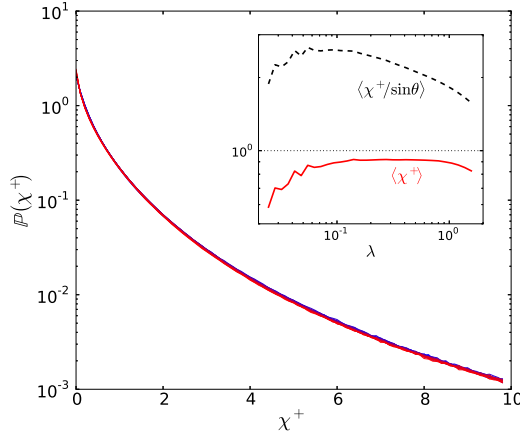


FIGURE 6. Refined critical balance: this figure, taken from [Mallet et al. \(2015\)](#), shows the probability density function (PDF) of the ratio $\chi^+ = \tau_A/\tau_{nl}^+$ with τ_{nl}^+ defined by (6.4). In fact, 17 PDFs are plotted here, taken at different scales within an approximately decade-wide inertial range (this was a 1024^3 RMHD simulation)—the corresponding lines are in colour shades from blue (smaller scales) to red (larger scales), but this is barely visible because the PDFs all collapse on top of each other. The inset shows that the self-similarity does not work if τ_{nl}^+ is defined without the alignment angle (see § 6). [Reprinted from [Mallet et al. \(2015\)](#) by permission of the Royal Astronomical Society.]

[Beresnyak \(2012a, 2015\)](#) gives two rather elegant (and related) arguments in favour of the scaling (5.1), alongside robust numerical evidence presented in the latter paper.¹¹ First, he argues that the scaling relation (5.1) can be obtained by dimensional analysis because the RMHD equations (3.1) stay invariant if v_A and $1/k_{\parallel}$ are scaled simultaneously [see (3.5)] and so these two quantities must always appear in the combination $k_{\parallel}v_A$ in scaling relations for any physical quantities—in the case of (5.1), energy, or field increment. Secondly, [Beresnyak \(2015\)](#) notes that following the structure of the fluctuating field (calculating its increments) along the field line (in the positive \mathbf{B}_0 direction) is the MHD equivalent of following its evolution forward (for \mathbf{Z}_{\perp}^-) or backward (for \mathbf{Z}_{\perp}^+) in time and it should, therefore, be possible to infer the parallel spectrum (5.1) from the Lagrangian frequency spectrum of the turbulence (as opposed to the Eulerian one, which is dominated by large-scale sweeping effects: see [Lugones et al. 2016, 2019](#)). Estimating the energy flux as the rate of change of energy in a fluid element in the Lagrangian frame (i.e., excluding sweeping by large eddies), one obtains ([Landau & Lifshitz 1987](#); [Corrsin 1963](#))

$$\varepsilon^{\pm} \sim (\delta Z_{\tau}^{\pm})^2 \tau^{-1} \Leftrightarrow E^{\pm}(\omega) \sim \varepsilon^{\pm} \omega^{-2}, \quad (5.2)$$

where δZ_{τ}^{\pm} is the Lagrangian field increment over time interval τ . Then (5.1) is recovered from (5.2) by changing variables $\omega = k_{\parallel}v_A$ and letting $E^{\pm}(\omega)d\omega = E^{\pm}(k_{\parallel})dk_{\parallel}$.

Thus, the parallel cascade and the associated scaling (5.1) appear to be a very simple

¹¹To be precise, the scaling he actually observes is closer to $k_{\parallel}^{-1.9}$, although he argues that this is a finite-resolution effect. Imperfect following of field lines might also conceivably be a factor. [Meyrand et al. \(2019\)](#), who followed field lines to a higher precision than that afforded by linear interpolation at every scale (see § 5.3), found a rather good k_{\parallel}^{-2} scaling for the magnetic-field increments, but a slightly steeper slope for velocities—although that too may be a finite-resolution issue.

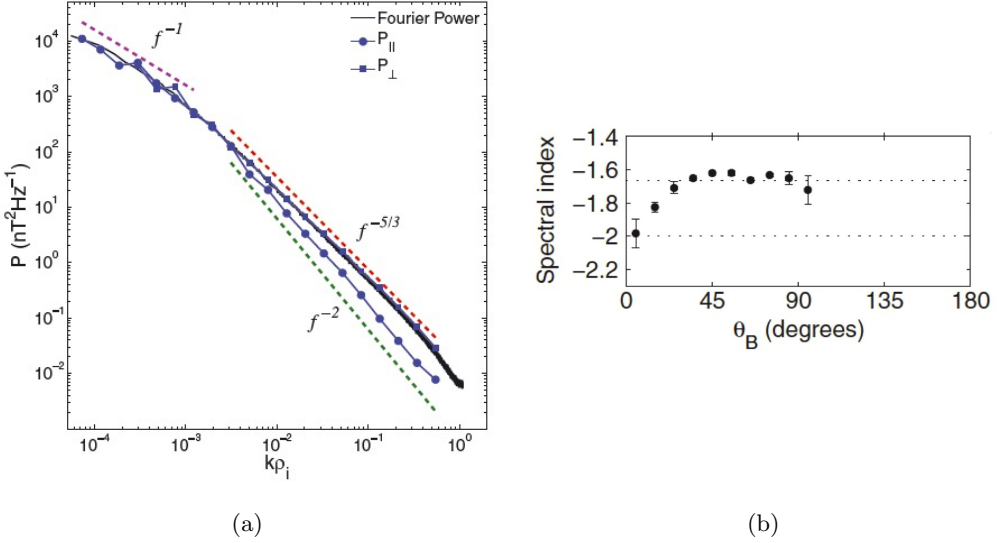


FIGURE 7. (a) Parallel (P_{\parallel}) and perpendicular (P_{\perp}) spectra (Fourier and wavelet) of the magnetic fluctuations in the solar wind, measured by the Ulysses spacecraft and computed by Wicks *et al.* (2010), with frequencies f converted to wavenumbers k using the Taylor hypothesis [reprinted from Wicks *et al.* (2010) by permission of the Royal Astronomical Society]. (b) An earlier (historic, the first ever) measurement by Horbury *et al.* (2008) of the spectral index of these spectra as a function of angle to the local mean field [reprinted with permission from Horbury *et al.* (2008), copyright (2008) by the American Physical Society].

and solid property of MHD turbulence. What happens in the perpendicular direction is a more complicated story.

5.3. Local, Scale-Dependent Anisotropy

Using instead of the parallel increments the perpendicular ones δZ_{λ}^{\pm} and substituting the nonlinear time

$$\tau_{nl}^{\pm} \sim \frac{\lambda}{\delta Z_{\lambda}^{\mp}} \quad (5.3)$$

for the cascade time, we recover (2.9):¹²

$$\begin{aligned} \frac{(\delta Z_{\lambda}^{\pm})^2}{\tau_{nl}^{\pm}} &\sim \varepsilon^{\pm} \quad \Rightarrow \quad \frac{\delta Z_{\lambda}^{+}}{\delta Z_{\lambda}^{-}} \sim \frac{\varepsilon^{+}}{\varepsilon^{-}}, \quad \delta Z_{\lambda}^{\pm} \sim (\tilde{\varepsilon}^{\pm} \lambda)^{1/3}, \quad \tilde{\varepsilon}^{\pm} \equiv \frac{(\varepsilon^{\pm})^2}{\varepsilon^{\mp}} \\ &\Rightarrow \quad E^{\pm}(k_{\perp}) \sim (\tilde{\varepsilon}^{\pm})^{2/3} k_{\perp}^{-5/3}. \end{aligned} \quad (5.4)$$

Treating δZ_{λ}^{\pm} and $\delta Z_{l_{\parallel}}^{\pm}$ as increments for the same structure, but measured across and along the field, and setting them equal to each other, we find a relationship between the parallel and perpendicular scales—the scale-dependent anisotropy (2.11):

$$l_{\parallel}^{\pm} \sim v_A (\tilde{\varepsilon}^{\mp})^{-1/3} \lambda^{2/3}. \quad (5.5)$$

The fact of scale-dependent anisotropy of MHD turbulence [if, in retrospect, not with

¹²Cf. Lithwick *et al.* (2007), the imbalanced version of the GS95 scalings (§ 9.3). This and especially whether the parallel correlations obey (5.5) is by no means uncontroversial. I am going to discuss these things in § 9, but here I keep track of ε^{\pm} purely for future convenience and invite the reader to substitute $\varepsilon^+ = \varepsilon^- = \tilde{\varepsilon}^{\pm} = \varepsilon$ whenever thinking of imbalance-related complications becomes too much to bear.

the same confidence the scaling (5.5)] was confirmed numerically by Cho & Vishniac (2000) and Maron & Goldreich (2001) and, in a rare triumph of theory correctly anticipating measurement, observed in the solar wind by Horbury *et al.* (2008), followed by many others (e.g., Podesta 2009; Wicks *et al.* 2010; Luo & Wu 2010; Chen *et al.* 2011—a complete list is impossible here as this has now become an industry, as successful ideas do; see Chen 2016 for a review). Figure 7 shows some of the first of those results. An important nuance is that, in order to see scale-dependent anisotropy, one must measure the parallel correlations along the perturbed, rather than global, mean magnetic field.¹³ The reason for this is as follows.

Both the causality argument (Boldyrev 2005; Nazarenko & Schekochihin 2011) and the Lagrangian-frequency one (Beresnyak 2015) that I invoked in §§ 5.1 and 5.2 to justify long parallel coherence lengths of the MHD fluctuations rely on the ability of Alfvénic perturbations to propagate along the magnetic field. Physically, a small such perturbation on any given scale does not know the difference between a larger perturbation on, say, a few times its scale, and the “true” mean field (whatever that is, outside the ideal world of periodic simulation boxes). Thus, it will propagate along the local field and so it is along the local field that the arguments based on this propagation will apply. What if we instead measure correlations along the global mean field or, more generally, along some coarse-grained version of the exact field? Let that coarse-grained field be the average over all perpendicular scales at and below some L_\perp (to get the global mean field, make L_\perp the outer scale). Define Elsasser-field increments between pairs of points separated by a vector \mathbf{l} ,

$$\delta \mathbf{Z}_l^\pm = \mathbf{Z}_\perp^\pm(\mathbf{r} + \mathbf{l}) - \mathbf{Z}_\perp^\pm(\mathbf{r}), \quad (5.6)$$

and consider \mathbf{l} along the exact magnetic field vs. \mathbf{l} along our coarse-grained field. The perpendicular distance by which the latter vector will veer off the field line (figure 8) will be dominated by the magnetic perturbation at the largest scale that was not included in the coarse-grained field:

$$\Delta l_\perp \sim l \frac{\delta b_{L_\perp}}{v_A}. \quad (5.7)$$

If we are trying to capture parallel correlations corresponding to perturbations with perpendicular scale $\lambda \ll L_\perp$, then, using CB, $l/v_A \sim \tau_{nl}$, and (5.3) with $\delta Z_\lambda^\pm \sim \delta b_\lambda$, we conclude that

$$\Delta l_\perp \sim \lambda \frac{\delta b_{L_\perp}}{\delta b_\lambda} \gg \lambda, \quad (5.8)$$

i.e., in such a measurement, the parallel correlations are swamped by perpendicular decorrelation, unless, in fact, $\lambda \sim L_\perp$ or larger (there is no such problem with measuring perpendicular correlations: small changes in a separation vector \mathbf{l} taken perpendicular to the global vs. exact field make no difference).

Consequently, the easiest practical way to extract correlations along the local field from either observed or numerically simulated turbulence (Chen *et al.* 2011) is to measure field increments (5.6) for many different separation vectors \mathbf{l} and to calculate for each such increment the angle between \mathbf{l} and the “local mean field” \mathbf{B}_{loc} defined as the arithmetic

¹³This detail was first understood by Cho & Vishniac (2000) and Maron & Goldreich (2001) (with Milano *et al.* 2001 coming close), but still needed restating 10 years later (Chen *et al.* 2011) and, it seems, continues (or has until recently continued) to fail to be appreciated in some particularly die-hard sanctuaries where adherents of the old religion huddle for warmth before the dying fire of the isotropic IK paradigm (I will refrain from providing citations here—and will, in § 6, offer some comfort to admirers of Robert Kraichnan, who was, in a certain sense, less wrong than it appeared in the early 2000s).

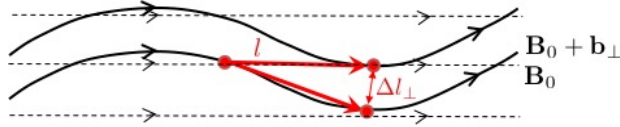


FIGURE 8. Measuring correlations along local vs. global mean field. True parallel correlations cannot be captured by a measurement along the global field \mathbf{B}_0 if the distance Δl_\perp [see (5.7)] by which the point-separation vector \mathbf{l} along \mathbf{B}_0 “slips” off the exact field line ($\mathbf{B}_0 + \mathbf{b}_\perp$) is greater than the perpendicular decorrelation length λ between “neighbouring” field lines.

mean of the magnetic field measured at the two points involved:

$$\cos \phi = \frac{\mathbf{l} \cdot \mathbf{B}_{\text{loc}}}{|\mathbf{l}| |\mathbf{B}_{\text{loc}}|}, \quad \mathbf{B}_{\text{loc}} = \mathbf{B}_0 + \frac{\mathbf{b}_\perp(\mathbf{r} + \mathbf{l}) + \mathbf{b}_\perp(\mathbf{r})}{2}. \quad (5.9)$$

This amounts to coarse-graining the field always at the right scale (just) for the correlations that are being probed. One can then measure (for example) perpendicular and parallel structure functions as conditional averages:

$$\langle (\delta Z_\lambda^\pm)^n \rangle = \langle |\delta Z_l^\pm|^n | \phi = 90^\circ \rangle, \quad (5.10)$$

$$\langle (\delta Z_{l_\parallel}^\pm)^n \rangle = \langle |\delta Z_l^\pm|^n | \phi = 0 \rangle, \quad (5.11)$$

and similarly for intermediate values of ϕ (as explained above, the difference between \mathbf{B}_0 and \mathbf{B}_{loc} matters only for small ϕ). Thus, in general, one measures

$$\langle |\delta Z_l^\pm|^n | \phi \rangle \propto l^{\zeta_n(\phi)}. \quad (5.12)$$

Alternatively, in simulations, one can simply follow field lines to get $\delta Z_{l_\parallel}^\pm$ (Cho & Vishniac 2000; Maron & Goldreich 2001) or, as was initially done in the solar wind, use local wavelet spectra (Horbury *et al.* 2008; Podesta 2009; Wicks *et al.* 2010).

It turns out (see references cited above and innumerable others) that, quite robustly, $\zeta_2(0) = 1$, consistent with (5.1), whereas $\zeta_2(90^\circ)$ is typically between $2/3$ and $1/2$, i.e., between GS95 and IK, in the solar wind, and rather closer to $1/2$ in numerical simulations—although this, as I will discuss in §§ 6.3 and 6.4, has been hotly disputed by Beresnyak (2011, 2012a, 2014b, 2019).

Thus, while little doubt remains about the reality of scale-dependent anisotropy [although not necessarily of the specific scaling (5.5)] and of the k_\parallel^{-2} spectrum (5.1), both arising from the GS95 theory, the GS95 prediction for the perpendicular spectrum (5.4) has continued to be suspect and controversial.

6. Dynamic Alignment, Perpendicular Cascade, and Intermittency

Whereas solar-wind turbulence observations were, for a period of time, viewed to be consistent with a $-5/3$ spectrum,¹⁴ leading ultimately to the GS95 revision of the IK paradigm, high-resolution numerical simulations of forced, incompressible MHD

¹⁴Matthaeus & Goldstein (1982) were possibly the first to say this. The monumental review by Bruno & Carbone (2013) contains an exhaustive historical bibliography, the shorter piece by Chen (2016) reviews the more recent state of the art: $-3/2$ is back (especially, as we are learning from the Parker Solar Probe, at lower heliocentric distances; see Chen *et al.* 2020); solar wind and simulations seem more or less in agreement (Boldyrev *et al.* 2011). Interestingly, the historical $-5/3$ period intersected by more than 10 years with the undisputed reign of the IK theory, confirming that no amount of adverse evidence can dent a dominant theoretical paradigm—or, at any rate, that it takes a long time and a hungry new generation entering the

turbulence, starting with Maron & Goldreich (2001) and Müller *et al.* (2003), have consistently shown scaling exponents closer to $-3/2$ (while strongly confirming the local anisotropy; see also Cho & Vishniac 2000; Cho *et al.* 2002b). This undermined somewhat the then still young GS95 consensus and stimulated hard questioning of the assumptions underlying its treatment of nonlinear interactions. The winning idea turned out to be that the nonlinearity in MHD turbulence might be depleted in a scale-dependent way by some form of alignment between \mathbf{Z}_\perp^+ and \mathbf{Z}_\perp^- and/or, perhaps, between the magnetic and velocity fields. Maron & Goldreich (2001) commented in passing on field alignment in their simulations, and Beresnyak & Lazarian (2006) focused on “polarisation alignment” explicitly, putting it on the table as a key effect requiring revision of GS95.¹⁵ The same possibility was mooted by Boldyrev (2005), and a year later he came up with a very beautiful (if, as we will see in § 6.3, somewhat flawed) argument based on the idea of what he referred to as “dynamic alignment” (Boldyrev 2006), which set the direction of the field for the subsequent 10 years and which I am now going to discuss.

6.1. Alignment and Anisotropy in the Perpendicular Plane

Let me, however, deviate from Boldyrev’s original case for alignment¹⁶ and follow instead Chandran *et al.* (2015) in positing that, as the two Elsasser fields advect each other, they will shear each other into an increasingly parallel configuration. As this occurs, the gradient of the advectee (say, \mathbf{Z}_\perp^-) in the direction of the advector (\mathbf{Z}_\perp^+) will get smaller than the gradient of either of them in the direction transverse to both.

In general, therefore, we must allow the possibility of a local anisotropy in the 2D plane perpendicular to the mean magnetic field (figure 9). If we do that, our “twiddle” estimate of the nonlinear term in (3.1) becomes

$$\mathbf{Z}_\perp^+ \cdot \nabla_\perp \mathbf{Z}_\perp^- \sim \frac{\delta Z_\lambda^+ \delta Z_\lambda^-}{\xi^-}, \quad (6.1)$$

where ξ^- is the scale of variation of \mathbf{Z}_\perp^- (advectee) *in the direction of* \mathbf{Z}_\perp^+ (advector), taken at scale λ , which is the scale of \mathbf{Z}_\perp^\pm ’s variation in the direction perpendicular both to \mathbf{Z}_\perp^\pm and to \mathbf{B}_0 (all interactions are still assumed local in scale). But, by elementary

field (Kuhn 1962). One wonders if, had simulations and observations showing a $-3/2$ spectrum been available at the time, IK might have survived forever.

¹⁵The first inklings of correlations naturally arising between \mathbf{u}_\perp and \mathbf{b}_\perp (the “Alfvénisation” effect) and affecting the turbulent cascade in a significant way are, in fact, traceable to Dobrowolny *et al.* (1980), Grappin *et al.* (1982, 1983), Matthaeus *et al.* (1983), and Pouquet *et al.* (1986, 1988), although there was perhaps no explicit clarity about any physical distinction between alignment as a mechanism for reduction of nonlinearity and local imbalance (see § 9.1 and appendix B)—and, of course, everybody was chained to the isotropic IK paradigm then.

¹⁶In his original case, Boldyrev (2006) follows the authors cited in footnote 15 in arguing that, in forced MHD turbulence, strong local fluctuations of cross-helicity $\mathbf{u}_\perp \cdot \mathbf{b}_\perp$ would be produced (by the external forcing, on the outer scale), this cross-helicity might then cascade to small scales less vigorously than energy (this is a conjecture), in which case \mathbf{u}_\perp and \mathbf{b}_\perp would locally align. Matthaeus *et al.* (2008) did indeed confirm numerically a fast dynamical tendency for the velocity and magnetic field to align locally, in patches, noting a formal analogy with the velocity–vorticity alignment in hydrodynamic turbulence (cf. Leovich *et al.* 1991; Leovich 2009; Bershadskii 2019). I want to alert the reader that the alignment of \mathbf{u}_\perp and \mathbf{b}_\perp , on which Matthaeus *et al.* (2008), as well as Boldyrev and his coworkers, focused their numerical investigations, is not, mathematically, the same thing as the alignment of \mathbf{Z}_\perp^+ and \mathbf{Z}_\perp^- advocated by Chandran *et al.* (2015), Mallet *et al.* (2015), and Mallet & Schekochihin (2017)—the former kind of alignment is, rather, a manifestation of emergent *local imbalance*. In practice, both types of alignment occur (Mallet *et al.* 2016). I shall discuss this topic more carefully in appendix B.

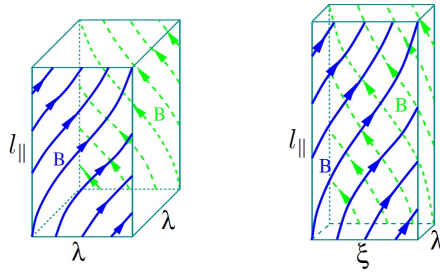


FIGURE 9. Cartoon of a GS95 eddy (left) vs. a Boldyrev (2006) aligned eddy (right). The latter has three scales: $l_\parallel \gg \xi \gg \lambda$ (along \mathbf{B}_0 , along \mathbf{b}_\perp , and transverse to both). This picture is adapted from Boldyrev (2006) [reprinted with permission from Boldyrev (2006), copyright (2006) by the American Physical Society]. In the context of my discussion, the fluctuation direction should, in fact, be thought of as along \mathbf{Z}_\perp^+ or \mathbf{Z}_\perp^- (see figure 38).

vector calculus,

$$\mathbf{Z}_\perp^+ \cdot \nabla_\perp \mathbf{Z}_\perp^- - \mathbf{Z}_\perp^- \cdot \nabla_\perp \mathbf{Z}_\perp^+ = \nabla_\perp \times (\mathbf{Z}_\perp^- \times \mathbf{Z}_\perp^+) \sim \frac{\delta Z_\lambda^+ \delta Z_\lambda^- \sin \theta_\lambda}{\lambda}, \quad (6.2)$$

where θ_λ the angle between the two Elsasser fields taken at scale λ . Under the scheme whereby the two fields shear each other into alignment in an, on average, symmetric fashion, we have $\xi^+ \sim \xi^-$ and

$$\frac{\lambda}{\xi} \sim \sin \theta_\lambda, \quad (6.3)$$

i.e., $\sin \theta_\lambda$ is the aspect ratio of the field structures in the perpendicular 2D plane.¹⁷

In view of all this, we ought to replace the estimate (5.3) of the nonlinear time with

$$\tau_{nl}^\pm \sim \frac{\xi}{\delta Z_\lambda^\mp} \sim \frac{\lambda}{\delta Z_\lambda^\mp \sin \theta_\lambda}. \quad (6.4)$$

If the last expression is correct, then the more aligned the two fields are the more the nonlinearity is reduced compared to the “naïve” GS95 estimate (5.3). The challenge is to work out the scale dependence of the reduction factor $\sin \theta_\lambda$, which is what Boldyrev (2006) did.

¹⁷Obviously, this is not a rigorous argument. It is mathematically possible for the two fields to be exactly or approximately parallel with $\mathbf{Z}_\perp^+ \cdot \nabla_\perp \mathbf{Z}_\perp^- \approx \mathbf{Z}_\perp^- \cdot \nabla_\perp \mathbf{Z}_\perp^+$ but $\lambda/\xi \sim 1$ and the latter ratio unrelated to θ_λ , a point made very forcefully by Bowen *et al.* (2021). Thus, the identification between the alignment of Elsasser fields and reduction of nonlinearity depends on a plausible dynamical scenario of how this alignment emerges—hence my insistence on the mutual shearing. If the reader is wondering whether alignment between \mathbf{u}_\perp and \mathbf{b}_\perp is a better conjecture, she will find a discussion of this in appendix B.2. In short, for balanced turbulence, assuming such an alignment amounts to the same thing, but for imbalanced one, even locally, Elsasser alignment has more to do with reducing nonlinearity.

6.2. Boldyrev's Alignment Conjecture

A version of Boldyrev's argument¹⁸ is to conjecture that the fields want to be misaligned as little as possible and that this minimal degree of misalignment is set by a kind of uncertainty principle: since the direction of the local magnetic field along which these perturbations propagate can itself only be defined within a small angle $\sim \delta b_\lambda / v_A$, the two Elsasser fields (or the velocity and the magnetic field) cannot be aligned any more precisely than this and so

$$\sin \theta_\lambda \sim \theta_\lambda \sim \frac{\delta b_\lambda}{v_A} \ll 1. \quad (6.5)$$

Alignment and imbalance (local or global), and, therefore the relative magnitudes of magnetic, velocity, and Elsasser fields, can be linked in a nontrivial way, which is still a matter of some debate, but I do not wish be distracted and so will postpone the discussion of that topic to § 9. Till then, I shall assume everywhere that

$$\varepsilon^+ \sim \varepsilon^- \Rightarrow \delta Z_\lambda^+ \sim \delta Z_\lambda^- \sim \delta u_\lambda \sim \delta b_\lambda. \quad (6.6)$$

This allows (6.5) to be combined with (6.4) and yield

$$\tau_{\text{nl}} \sim \frac{\lambda v_A}{\delta Z_\lambda^2}. \quad (6.7)$$

The constancy of flux then implies immediately¹⁹

$$\frac{\delta Z_\lambda^2}{\tau_{\text{nl}}} \sim \varepsilon \Rightarrow \delta Z_\lambda \sim (\varepsilon v_A \lambda)^{1/4} \Leftrightarrow E(k_\perp) \sim (\varepsilon v_A)^{1/2} k_\perp^{-3/2}. \quad (6.8)$$

In dimensional terms, this has brought us back to the IK spectrum (2.5), except the wavenumber is now the perpendicular wavenumber and both anisotropy and CB are retained, although the relationship between the parallel and perpendicular scales changes:

$$\tau_{\text{nl}} \sim \frac{l_\parallel}{v_A} \Rightarrow l_\parallel \sim v_A^{3/2} \varepsilon^{-1/2} \lambda^{1/2}. \quad (6.9)$$

Since CB remains in force, the parallel cascade stays the same as described in § 5.2.

For imminent use in what follows, let us compute the extent of the inertial range that this aligned cascade is supposed to span. Comparing the nonlinear cascade time (6.7) with the Ohmic diffusion time (assuming, for convenience that the magnetic diffusivity η is either the same or larger than the kinematic viscosity of our MHD fluid), we find

$$\tau_{\text{nl}} \sim \left(\frac{v_A \lambda}{\varepsilon} \right)^{1/2} \ll \tau_\eta \sim \frac{\lambda^2}{\eta} \Leftrightarrow \lambda \gg \eta^{2/3} \left(\frac{v_A}{\varepsilon} \right)^{1/3} \equiv \lambda_\eta, \quad (6.10)$$

where λ_η is the cutoff scale—the Kolmogorov scale for this turbulence. For comparison,

¹⁸His actual original argument looked somewhat more complicated than this, but in the end amounted to the same thing. In later papers (Perez *et al.* 2012, 2014b), he does appear to embrace implicitly something closer to the line of thinking that I will advocate in § 6.4.1.

¹⁹A perceptive reader might protest at this point that $\delta Z_\lambda \propto \lambda^{1/4}$ looks rather suspicious in view of the exact law (3.7), which seems to imply a $\lambda^{1/3}$ scaling. In fact, there is no contradiction: since one of the three Elsasser increments in the exact law (3.7) is the *longitudinal* one, the alignment angle successfully insinuates its way in, and (3.7) should be viewed as saying that $\delta Z_\lambda^\mp (\delta Z_\lambda^\pm)^2 \sin \theta_\lambda \sim \varepsilon^\pm \lambda$ (Boldyrev *et al.* 2009). This tells us nothing new, other than that the estimate (6.4) for the nonlinear time is reasonable.

note that the same calculation based on the GS95 scalings (5.3) and (5.4) gives

$$\tau_{\text{nl}}^{\text{GS95}} \sim \varepsilon^{-1/3} \lambda^{2/3} \ll \tau_\eta \sim \frac{\lambda^2}{\eta} \quad \Leftrightarrow \quad \lambda \gg \eta^{3/4} \varepsilon^{-1/4} \equiv \lambda_\eta^{\text{GS95}}, \quad (6.11)$$

where $\lambda_\eta^{\text{GS95}}$ is the classic Kolmogorov scale.

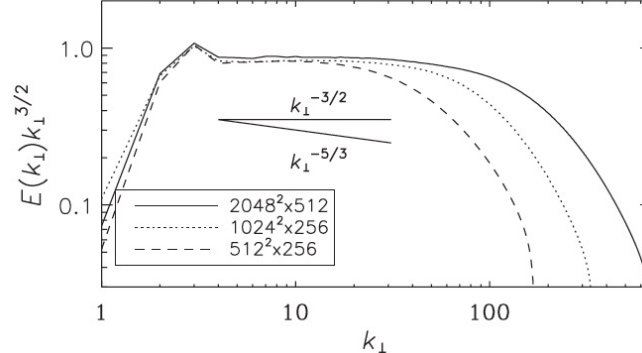
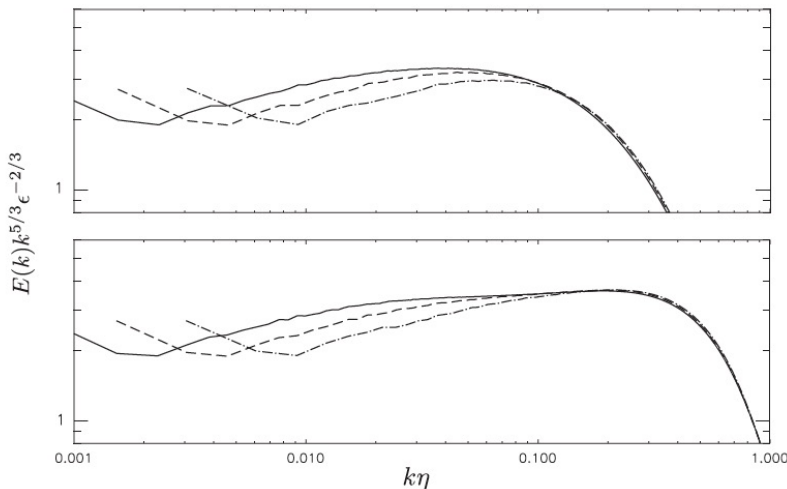
If one embraces (6.8), one could argue that Kraichnan's dimensional argument was actually right, but it should have been used with k_\perp , rather than with k , because k_\parallel is not a "nonlinear" dimension. This is the style of reasoning that Kraichnan himself might have found attractive. We are about to see, however, that the result (6.8) also runs into serious trouble and needs revision.

6.3. Plot Thickens

This is a very appealing theory, whose main conclusions were rapidly confirmed by a programme of numerical simulations undertaken by Boldyrev's group—in particular, the angle between velocity and magnetic field, measured in a certain opportune way,²⁰ was reported to scale according to $\theta_\lambda \propto \lambda^{1/4}$, as implied by (6.8) and (6.5) (Mason *et al.* 2006, 2008, 2011, 2012; Perez *et al.* 2012, 2014b). The same papers confirmed the earlier numerical claims that the spectrum of MHD turbulence indeed scaled as $k_\perp^{-3/2}$ (figure 10a). However, the legitimacy of this conclusion was contested by Beresnyak (2011, 2012a, 2014b, 2019), who had, in fact, been first to focus on the alignment effect numerically (Beresnyak & Lazarian 2006), but disputed that the numerical spectra exhibiting it were converged and argued that systematic convergence tests in fact favoured a trend towards a $k_\perp^{-5/3}$ spectrum at asymptotically small scales. His point was that convergence of spectra with increasing resolution ought to be checked from the dissipative end of the inertial interval and that rescaling the spectra in his simulations to the Kolmogorov scale (6.11) gave a better data collapse than rescaling them to Boldyrev's cutoff scale (6.10) (figure 10b; to be precise, in Beresnyak 2014b, he reports that the best numerical convergence obtained by this method is to $k_\perp^{-1.7}$). Despite the sound and fury of the ensuing debate about the quality of the two competing sets of numerics (Perez *et al.* 2014a; Beresnyak 2013, 2014a), it would not necessarily be obvious to anyone who took a look at their papers that their raw numerical results themselves were in fact all that different—certainly not as different as the interpretation of these results by their authors. Without dwelling on either, however, let me focus instead on a conceptual wrinkle in Boldyrev's original argument that Beresnyak (2011) spotted and that cannot be easily dismissed.

In the RMHD limit (whose applicability to MHD turbulence at sufficiently small scales we have no reason to doubt), $\delta b_\lambda/v_A$ is an arbitrarily small quantity, and so must then be, according to (6.5), the alignment angle $\sin \theta_\lambda$. Introducing such a large depletion of the nonlinearity into (3.1) would abolish it completely in the RMHD ordering and render

²⁰They focused on one particular measure of alignment, $\sin \theta_\lambda = \langle |\delta \mathbf{u}_\lambda \times \delta \mathbf{b}_\lambda| \rangle / \langle |\delta \mathbf{u}_\lambda| |\delta \mathbf{b}_\lambda| \rangle$, which indeed turns out to scale as $\lambda^{1/4}$ in a certain range of scales. Obviously, one can invent other proxies for the alignment angle, involving different fields ($\delta \mathbf{Z}_\lambda^\pm$) and/or different powers of the fields' increments inside the averages. This game produces many different scalings (Beresnyak & Lazarian 2006, 2009b; Mallet *et al.* 2016) (some of which can be successfully theorised about: see Chandran *et al.* 2015), and it is not *a priori* obvious which of these should be most representative of the "typical" alignment that figures in "twiddle" theories. Perhaps a better handle on the scaling of the alignment is obtained when one studies the full distribution of the "RMHD ensemble" (see § 6.4.2 and Mallet & Schekochihin 2017) and/or the 3D-anisotropic statistics (see § 6.5 and papers by Chen *et al.* 2012, Mallet *et al.* 2016 and Verdini *et al.* 2018, 2019).

(a) Perez *et al.* (2012)

(b) Beresnyak (2014b)

FIGURE 10. The best-resolved currently available spectra of RMHD turbulence. (a) From simulations by Perez *et al.* (2012) (their figure 1), with Laplacian viscosity and resolution up to $2048^2 \times 512$. (b) From simulations by Beresnyak (2014b) (his figure 1, ©AAS, reproduced with permission), with Laplacian viscosity (top panel) and with 4th-order hyperviscosity (bottom panel); the resolution for the three spectra is 1024^3 , 2048^3 and 4096^3 . His spectra are rescaled to Kolmogorov scale (6.11) (which he denotes η). He finds poorer convergence (see his figure 2) when he rescales to Boldyrev's scale (6.24). Perez *et al.* (2012) appear to get a somewhat better outcome (see their figure 8) if they plot their spectra vs. $k_\perp \lambda_\eta$ where λ_η is given by (6.24) with λ_{CB} computed in each simulation as the normalisation constant in the scaling (6.22) of $\sin \theta_\lambda$ (in their analysis, however, this is the angle between velocity and magnetic perturbations, not the Elsasser fields).

the system linear. The only way to keep the nonlinearity while assuming a small angle θ_λ is to take the angle to be small but still ordered as unity in the RMHD ordering—in other words, it cannot scale with ϵ under the RMHD rescaling symmetry (3.5). The same rescaling symmetry implies that any physical scaling that involves v_A and l_\parallel (and no other scales) must involve them in the combination l_\parallel/v_A (see § 5.2 and Beresnyak 2012a), which (6.9) manifestly does not. All this flies in the face of the fact that a substantial body of numerical evidence supporting aligned MHD turbulence was obtained by means of RMHD simulations (Mason *et al.* 2011, 2012; Perez *et al.* 2012; Beresnyak 2012a;

(Mallet *et al.* 2015, 2016)—complemented by explicit evidence that full MHD simulations produce quantitatively the same alignment—so the standard recourse to casting a cloud of suspicion on the validity of an asymptotic approximation is not available in this case.

In a further blow to the conjecture (6.5), it turns out that the alignment angle between the Elsasser fields at any given scale is *anticorrelated* with their amplitudes (Mallet *et al.* 2015), supporting the view that the dynamical alignment is indeed *dynamical*, being brought about by the mutual shearing of the Elsasser fields (Chandran *et al.* 2015), rather than by the uncertainty principle (6.5) (which would imply, presumably, a positive correlation between θ_λ and δZ_λ).

The numerical evidence in favour of alignment appears to be real and solid.²¹ While numerical simulations at currently feasible resolutions cannot definitively verify or falsify Beresnyak’s expectation that alignment is but a transient feature that disappears at asymptotically small scales, they certainly show aligned, locally 3D-anisotropic turbulence over a respectable inertial subrange at least one order of magnitude wide, and probably two. This is approaching the kind of scale separations that actually exist in Nature, e.g., in the solar wind (where the evidence for a $k_\perp^{-3/2}$ spectrum has also been firming up: see, e.g., Chen *et al.* 2020), and we cannot be casually dismissive of a physical regime, even if transient, that occupies most of the phase space that we are able to probe!

6.4. Revised Model of Aligned MHD Turbulence

6.4.1. Dimensional and RMHD-Symmetry Constraints

Let me make the restrictions implied by Beresnyak’s objection more explicit. Under the RMHD rescaling symmetry (3.5),

$$\delta Z_\lambda \rightarrow \epsilon \delta Z_\lambda, \quad \epsilon \rightarrow \frac{\epsilon^3}{a} \epsilon, \quad v_A \rightarrow v_A, \quad \lambda \rightarrow a \lambda \quad (6.12)$$

(note that ϵ is the energy flux whereas ϵ is the scaling factor). Therefore, the scaling relation (6.8) becomes $\epsilon \delta Z_\lambda \sim \epsilon^{3/4} (\epsilon v_A \lambda)^{1/4}$, which is obviously a contradiction. Indeed, trialling

$$\delta Z_\lambda \sim \epsilon^\mu v_A^\nu \lambda^\gamma \quad (6.13)$$

and mandating both the symmetry (6.12) and dimensional consistency, one finds that the GS95 solution (5.4), $\nu = 0$ and $\gamma = \mu = 1/3$, is the only possibility, which was Beresnyak’s point.

It seems obvious that the only way to rescue alignment is to allow another parameter—

²¹ Just to make it all more confusing, the real *observational* evidence for it is far from solid: in the solar wind, Podesta *et al.* (2009) and Wicks *et al.* (2013a) see scale-dependent alignment, but only for fluctuations at large scales—larger than what is normally viewed as the outer scale/the start of the inertial range (in the solar wind, this shows up as a break between f^{-1} and $f^{-5/3\dots-3/2}$ slopes in the frequency spectrum). Osman *et al.* (2011) also report alignment, on the outer scale, as far as I can tell. Chen *et al.* (2012) see alignment across the inertial range, but, to the best of their measurement, it is not scale-dependent. Verdini *et al.* (2018, 2019) managed to extract structure functions in three field-dependent directions (see § 6.5) that scale in a way that is consistent with scale-dependent alignment, but all measures of the alignment angle θ_λ that they tried had much shallower (but not flat!) scalings than $\lambda^{1/4}$. This appears to be the first time that scale-dependent alignment at small scales has (still quite timidly) shown itself in the solar wind. Most recently, Bowen *et al.* (2021) also measure scale-dependent alignment, albeit at largish scales, where fluctuations are large and it is not clear that the inertial range has properly started or that the RMHD limit applies. Theoreticians must live in hope that, as both instruments and analysis techniques become more refined, definite and universal scalings will eventually emerge from this sea of uncertainty.

and the (almost) obvious choice is L_{\parallel} , the parallel outer scale, which transforms as $L_{\parallel} \rightarrow (a/\epsilon)L_{\parallel}$. Then

$$\delta Z_{\lambda} \sim \varepsilon^{\mu} v_A^{\nu} \lambda^{\gamma} L_{\parallel}^{\delta} = \varepsilon^{(1+\delta)/3} \left(\frac{L_{\parallel}}{v_A} \right)^{\delta} \lambda^{(1-2\delta)/3}, \quad (6.14)$$

where the second expression is the result of imposing on the first the RMHD symmetry (6.12) and dimensional correctness; $\delta = 0$ returns us to GS95.²² The same argument applied to the scaling of l_{\parallel} with ε , v_A , λ and L_{\parallel} gives

$$l_{\parallel} \sim \varepsilon^{(\sigma-1)/3} v_A^{1-\sigma} L_{\parallel}^{\sigma} \lambda^{2(1-\sigma)/3}, \quad (6.15)$$

where σ is a free parameter. Note that both (6.14) and (6.15) manifestly contain the parallel scales and v_A in the solely allowed combinations l_{\parallel}/v_A and L_{\parallel}/v_A . A reassuring consistency check is to ask what perpendicular scale $\lambda = L_{\perp}$ corresponds to $l_{\parallel} = L_{\parallel}$: this turns out to be

$$L_{\perp} \sim \varepsilon^{1/2} \left(\frac{L_{\parallel}}{v_A} \right)^{3/2} \sim \lambda_{CB}, \quad (6.16)$$

the very same λ_{CB} , given by (4.3), at which weak turbulence becomes strong—thus seamlessly connecting any strong-turbulence theory expressed by (6.14) and (6.15) with the WT cascade discussed in § 4.²³ Notably, if we applied such a test to (6.9), we would find the price of consistency to be $L_{\perp} = L_{\parallel}$, which is allowed but does not have to be the case in MHD and certainly cannot be the case in RMHD.

Finally, since the parallel-cascade scaling (5.1) remains beyond reasonable doubt and, as can be readily checked, respects the rescaling symmetry (3.5) (Beresnyak 2015), combining it with (6.15) and (6.14) fixes

$$\sigma = 2\delta. \quad (6.17)$$

Alas, CB does not help with determining δ because, in aligned turbulence, the nonlinear time (6.4) contains the unknown scale ξ , or, equivalently, the alignment angle $\theta_{\lambda} \sim \lambda/\xi$. If we did know δ , CB would let us determine this angle:

$$\frac{l_{\parallel}}{v_A} \sim \tau_{nl} \sim \frac{\lambda}{\delta Z_{\lambda} \sin \theta_{\lambda}} \Rightarrow \sin \theta_{\lambda} \sim \left(\frac{\lambda}{\lambda_{CB}} \right)^{2\delta}, \quad (6.18)$$

where λ_{CB} is given by (6.16). The answer that we want to get—keeping Boldyrev’s scalings of everything with λ but not with ε or v_A —requires

$$\delta = \frac{1}{8}. \quad (6.19)$$

²²The weak-turbulence spectrum (4.7) corresponds to $\delta = -1/4$.

²³If we had included L_{\perp} with some unknown exponents into (6.14) and (6.15), we would have found that L_{\perp} had to satisfy (6.16) and so could not be treated as an independent quantity. What, might one ask, will then happen if I attempt to inject energy at some L_{\perp} that does not satisfy (6.16)? If this $L_{\perp} > \lambda_{CB}$, then the cascade set off at the outer scale will be weak and transition to the strong-turbulence regime at λ_{CB} as described in § 4; if $L_{\perp} < \lambda_{CB}$, then I am effectively forcing 2D motions, which should break up by the causality argument (§ 5.1) and it is L_{\parallel} that will be determined by (6.16). Thus, λ_{CB} can be treated without loss of generality as the perpendicular outer scale of the CB cascade.

Then, instead of (6.8), we end up with

$$\delta Z_\lambda \sim \varepsilon^{3/8} \left(\frac{L_{\parallel}}{v_A} \right)^{1/8} \lambda^{1/4}, \quad l_{\parallel} \sim \varepsilon^{-1/4} v_A^{3/4} L_{\parallel}^{1/4} \lambda^{1/2}, \quad \sin \theta_\lambda \sim \varepsilon^{-1/8} \left(\frac{v_A}{L_{\parallel}} \right)^{3/8} \lambda^{1/4}, \quad (6.20)$$

and the dissipation cutoff scale (6.10) is corrected as follows:

$$\tau_{nl} \sim \left(\frac{L_{\parallel}}{\varepsilon v_A} \right)^{1/4} \lambda^{1/2} \ll \tau_\eta \sim \frac{\lambda^2}{\eta} \quad \Leftrightarrow \quad \lambda \gg \eta^{2/3} \left(\frac{L_{\parallel}}{\varepsilon v_A} \right)^{1/6} \equiv \lambda_\eta. \quad (6.21)$$

Note that, since $\lambda_\eta \propto \eta^{2/3}$ still, this does not address Beresnyak's numerical evidence on the convergence of the spectra (§ 6.3)—I shall come back to this problem in § 7.

For future convenience, let me recast the scalings (6.20) in a somewhat simpler form:

$$\delta Z_\lambda \sim \left(\frac{\varepsilon L_{\parallel}}{v_A} \right)^{1/2} \left(\frac{\lambda}{\lambda_{CB}} \right)^{1/4}, \quad \frac{l_{\parallel}}{L_{\parallel}} \sim \left(\frac{\lambda}{\lambda_{CB}} \right)^{1/2}, \quad \sin \theta_\lambda \sim \left(\frac{\lambda}{\lambda_{CB}} \right)^{1/4}. \quad (6.22)$$

Defining the magnetic Reynolds number based on the CB scale (6.16) and the fluctuation amplitude at this scale,

$$Rm = \frac{\delta Z_{\lambda_{CB}} \lambda_{CB}}{\eta} \sim \frac{\varepsilon}{\eta} \left(\frac{L_{\parallel}}{v_A} \right)^2, \quad (6.23)$$

allows the dissipation scale (6.21) to be recast as follows:

$$\frac{\lambda_\eta}{\lambda_{CB}} \sim \left(\frac{Rm}{1 + Pm} \right)^{-2/3} = \widetilde{Re}^{-2/3}, \quad Pm = \frac{\nu}{\eta}, \quad \widetilde{Re} = \frac{\delta Z_{\lambda_{CB}} \lambda_{CB}}{\nu + \eta}. \quad (6.24)$$

I have restored the possibility that viscosity ν might be larger than the magnetic diffusivity η : if that is the case, one must replace the latter with the former in the calculation of the dissipative cutoff, whereas if $Pm \lesssim 1$, it does not matter, hence the appearance of the magnetic Prandtl number Pm in the combination $(1 + Pm)$.

Yet another way to write the first of the scaling relations (6.20) is

$$\delta Z_\lambda \sim \varepsilon^{1/3} \lambda_{CB}^{1/12} \lambda^{1/4} \quad \Leftrightarrow \quad E(k_{\perp}) \sim \varepsilon^{2/3} \lambda_{CB}^{1/6} k_{\perp}^{-3/2}. \quad (6.25)$$

This is effectively the prediction for the spectrum that Perez *et al.* (2012, 2014b) used in their numerical convergence studies. Thus, they and I are on the same page as to what the spectrum of aligned turbulence is expected to be, although the question remains why it should be that if Boldyrev's uncertainty principle (6.5) can no longer be used.

A set of RMHD-compatible scalings (6.20), or (6.25), is also effectively what was deduced by Chandran *et al.* (2015) and by Mallet & Schekochihin (2017) from a set of plausible conjectures about the dynamics and statistics of RMHD turbulence (they did not explicitly discuss the issue of the RMHD rescaling symmetry, but used normalisations that enforced it automatically). The two papers differed in their strategy for determining the exponent δ ; my exposition here will be a “heuristic” version of Mallet & Schekochihin (2017).

6.4.2. Intermittency Matters!

The premise of both Chandran *et al.* (2015) and Mallet & Schekochihin (2017) is that in order to determine the scalings of everything, including the energy spectrum, one must have a working model of intermittency, i.e., of the way in which fluctuation amplitudes and their scale lengths in all three directions— λ , ξ and l_{\parallel} —are distributed in a turbulent MHD system. It may be disturbing to the reader, or viewed by her as an

unnecessary complication, that we must involve “rare” events—as this is what the theory of intermittency is about—in the mundane business of the scaling of the energy spectra, which are usually viewed as made up from the more “typical” fluctuations. These doubts might be alleviated by the following observation. The appearance of the outer scale L_{\parallel} in (6.14) suggests that the self-similarity is broken—this is somewhat analogous to what happens in hydrodynamic turbulence, where corrections to the K41 scaling (2.2) come in as powers of λ/L (Kolmogorov 1962; Frisch 1995). We may view δ as just such a correction to the self-similar GS95 result, and alignment as the physical mechanism whereby this intermittency correction arises. The main difference with the hydrodynamic case is that δ is not all that small (MHD turbulence is “more intermittent” than the hydrodynamic one), the mechanism responsible for it has important consequences (§ 7), and so we care.

I shall forgo a detailed discussion of the intermittency model that Mallet & Schekochihin (2017) proposed; for my purposes here, a vulgarised version of their argument will suffice. They consider the turbulent field as an ensemble of structures, or fluctuations, each of which has some amplitude and three scales: parallel l_{\parallel} , perpendicular λ and fluctuation-direction ξ (they call this the “RMHD ensemble”). They make certain conjectures about the joint probability distribution of these quantities, which then allow them to fix scalings. The most crucial (and perhaps also the most arbitrary) of these conjectures is, effectively, that for all structures, $l_{\parallel} \sim \lambda^{\alpha}$ with the same exponent α , i.e., that the quantity $l_{\parallel}/\lambda^{\alpha}$ has a scale-invariant distribution (this appears to be confirmed by numerical evidence: see figure 11a). They then determine the exponent α by considering “the most intense structures”²⁴—because it is possible to work out what the probability of encountering them is as a function both of λ and of l_{\parallel} .

They then conjecture that the most intense structures in the RMHD ensemble are sheets transverse to the local perpendicular direction. Therefore, if one looks for their probability (filling fraction) in any perpendicular plane as a function of the perpendicular scale λ , one expects it to scale as

$$P \propto \lambda. \quad (6.26)$$

If, on the other hand, one is interested in their filling fraction in the plane locally tangent to a flux sheet (i.e., defined by the local mean field and the direction of the fluctuation vector), it is

$$P \propto \xi l_{\parallel}. \quad (6.27)$$

The next conjecture is the “refined critical balance” (RCB, already advertised in § 5.1), stating that not only is $\tau_{nl} \sim \tau_A$ in some vague “typical” sense, but the quantity

$$\chi = \frac{\delta Z l_{\parallel}}{\xi v_A} \sim \frac{\tau_A}{\tau_{nl}} \quad (6.28)$$

has a scale-invariant distribution in the RMHD ensemble—this was discovered by Mallet *et al.* (2015) to be satisfied with truly remarkable accuracy in numerically simulated RMHD turbulence (figure 6).²⁵ If this is true for all structures, it is true for the most intense ones—and a further assumption about those is that their amplitude δZ_{max} is not a function of scale but is simply equal to some typical outer-scale value (i.e., the most

²⁴Often an object of particular importance in intermittency theories (e.g., She & Leveque 1994; Dubrulle 1994; She & Waymire 1995; Grauer *et al.* 1994; Müller & Biskamp 2000; Boldyrev 2002; Boldyrev *et al.* 2002).

²⁵Note that it makes sense then that the alignment angle $\sin \theta_{\lambda} \sim \lambda/\xi$ should be anticorrelated, and ξ , therefore, positively correlated, with the fluctuation amplitude δZ_{λ} at any given scale λ (stronger fluctuations are more aligned—the strongest of them are the sheets being discussed here), as I mentioned in § 6.3 and as Mallet *et al.* (2015) indeed found.

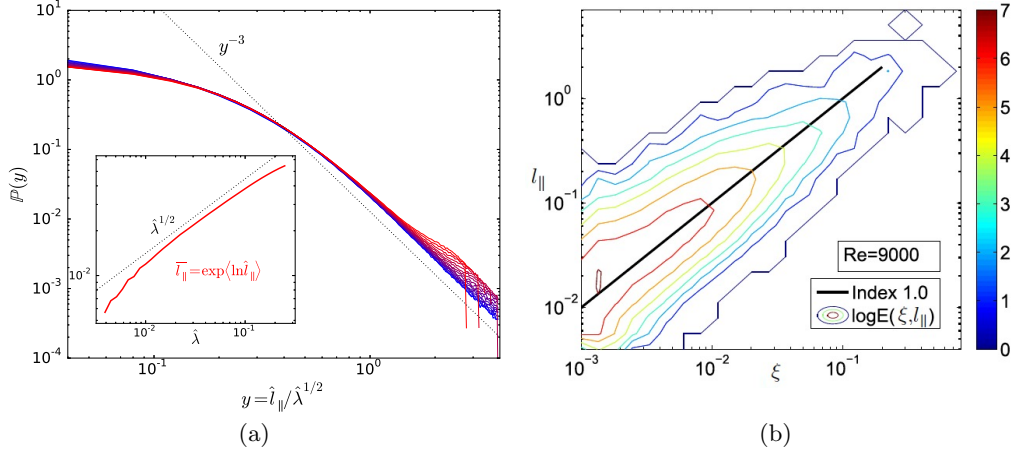


FIGURE 11. (a) Probability distribution of $l_{\parallel}/\lambda^{1/2}$ in a 1024^3 RMHD simulation (the shades of colour from blue to red correspond to PDFs at increasing scales within the inertial range). This plot is taken from Mallet & Schekochihin (2017) (where the reader will find a discussion—somewhat inconclusive—of the slope of this PDF) and illustrates how good (or otherwise) is the assumption that $l_{\parallel}/\lambda^{\alpha}$ has a scale-invariant distribution (the assumption is not as good as RCB, illustrated in figure 6 based on data from the same simulation). (b) Joint probability distribution for the length l_{\parallel} and width ξ (in my notation) of the most intense dissipative structures (adapted from Zhdankin *et al.* 2016b). This shows that $\xi \propto l_{\parallel}$, in line with (6.29). [Reprinted from Zhdankin *et al.* (2016b) with the permission of AIP Publishing.] Independent simulations by J. M. Stone (private communication, 2018) support this scaling.

intense structures are formed by the largest perturbations collapsing, or being sheared, into sheets without breaking up into smaller perturbations; see Chandran *et al.* 2015). This, together with (6.27), implies that for those structures,

$$\xi \sim l_{\parallel} \frac{\delta Z_{\max}}{v_A} \quad \Rightarrow \quad P \propto l_{\parallel}^2 \quad (6.29)$$

(Zhdankin *et al.* 2016b) confirm that $\xi \propto l_{\parallel}$ for the most intense dissipative structures: see figure 11b). Comparing (6.29) with (6.26), we conclude that $l_{\parallel} \propto \lambda^{1/2}$ for the most intense structures and, therefore, for everyone else—by the conjecture of scale invariance of $l_{\parallel}/\lambda^{\alpha}$, where we now know that $\alpha = 1/2$. Comparing this with (6.15), we see that $\alpha = 2(1 - \sigma)/3$, whence

$$\sigma = \frac{1}{4} \quad \Rightarrow \quad \delta = \frac{1}{8}, \quad (6.30)$$

the latter by virtue of (6.17). Q.e.d.: we now have the scalings (6.20).

I do not know if the reader will find this quasi-intuitive argument more (or less) convincing than the formal-looking conjectures and corollaries in Mallet & Schekochihin (2017). There is no need to repeat their algebra here, but hopefully the above sheds some (flickering) light—if not, perhaps a better argument will be invented one day, but all I can recommend for now is reading their paper. Notably, in their more formal treatment, not just the energy spectrum but the two-point structure functions of all orders are predicted—and turn out to be a decent fit to numerical data as it currently stands.²⁶The

²⁶The key tenet of their theory—a log-Poisson distribution of field increments, which follows from arguments analogous to those advanced in the hydrodynamic-turbulence theory (She & Leveque 1994; Dubrulle 1994; She & Waymire 1995)—also appears to be at least consistent with numerical evidence (Zhdankin *et al.* 2016a; Mallet & Schekochihin 2017).

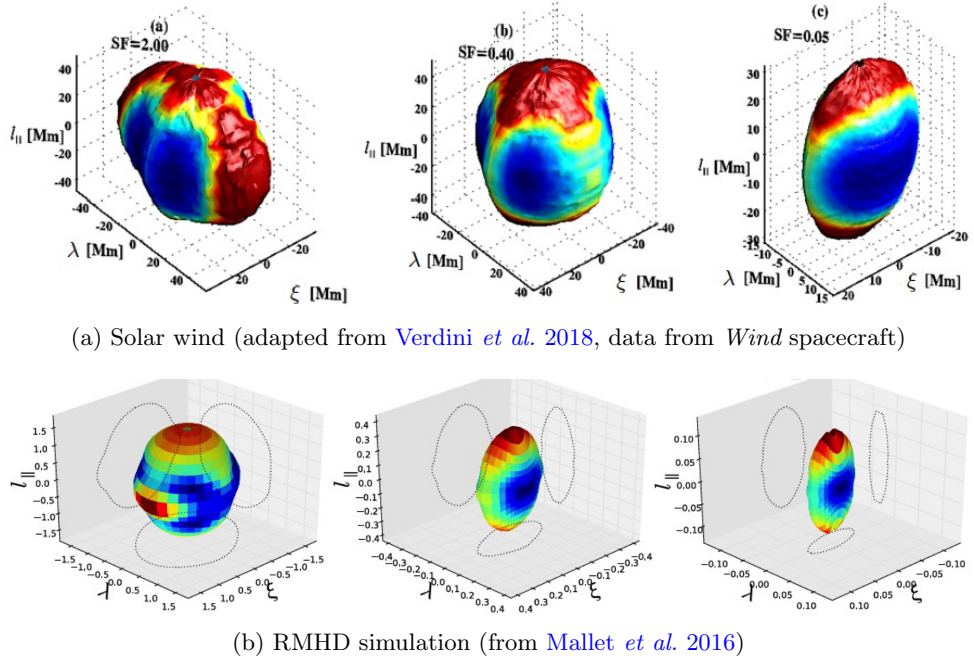


FIGURE 12. Locally 3D-anisotropic structures in the (a) solar wind [from Verdini *et al.* (2018) ©AAS, reproduced with permission] and (b) numerical simulations (here l_{\parallel} is normalised to $L_{\parallel}/2\pi$ and λ and ξ to $L_{\perp}/2\pi$, hence apparent isotropy at the outer scale). These are surfaces of constant second-order structure function of the magnetic field (a) or one of the Elsasser fields (b). The three images correspond to successively smaller fluctuations and so successively smaller scales (only the last of the three is firmly in the universal inertial range). In both cases, the emergence of statistics with $l_{\parallel} \gg \xi \gg \lambda$ is manifest. In the solar wind, the route that turbulence takes to this aligned state appears to depend quite strongly on the solar-wind expansion, which distorts magnetic-field component in the radial direction compared to the azimuthal ones (Verdini & Grappin 2015; Vech & Chen 2016). The data shown in panel (a) was carefully selected to minimise this effect; without such selection, one sees structures most strongly elongated in the ξ direction at the larger scales ($\xi > l_{\parallel} > \lambda$), although they too tend to the universal aligned regime at smaller scales (see Chen *et al.* 2012, where 3D-anisotropy plots like ones shown here first appeared).

same is true about the model proposed in the earlier paper by Chandran *et al.* (2015). Their approach is based on a much more enthusiastic engagement with dynamics: a careful analysis of how aligned and non-aligned structures might form and interact. They get $\delta \approx 0.108$, which leads to $\delta Z_{\lambda} \propto \lambda^{0.26}$ —not a great deal of difference with (6.20), considering that all of this is very far from being exact science. Their approach does have the distinction, however, of emphasising particularly strongly the dynamic nature of the dynamic alignment, which arises as Elsasser fields shear each other into sheet-like structures.

6.5. 3D Anisotropy

Before moving on, I would like to re-emphasise the 3D anisotropy of the aligned MHD turbulence—and the fact that this anisotropy is local, associated at every point with the three directions that themselves depend on the fluctuating fields: parallel to the magnetic field (l_{\parallel}), along the vector direction of the perturbed field \mathbf{Z}_{\perp}^{\mp} that advects the field \mathbf{Z}_{\perp}^{\pm} whose correlations we are measuring (ξ), and the third direction perpendicular

to the other two (λ). This local 3D anisotropy is measurable²⁷ and has indeed been observed both in the solar wind (Chen *et al.* 2012; Verdini *et al.* 2018, 2019) and in numerical simulations (Verdini & Grappin 2015; Mallet *et al.* 2016)—both are illustrated by figure 12. The main point of discrepancy between the true and virtual reality is the scale dependence of the anisotropy: confirmed solidly in simulations but only very tentatively in the solar wind (see footnote 21). However, progress never stops, and one can hope for better missions (Chen *et al.* 2020) and even more sophisticated analysis.

The scaling of the energy spectrum in the parallel direction (§ 5.2) was arguably the most robust and uncontroversial of the results reviewed thus far. We then occupied ourselves with the scalings of the Elsasser-field increments and of l_{\parallel} vs. the perpendicular scale λ , culminating in § 6.4 with a theory that one (hopefully) can believe in. The scalings with the third, fluctuation-direction coordinate ξ are very easy to obtain because the nonlinear time of the aligned cascade (6.4) has the same dependence on ξ as it did on λ in the unaligned, GS95 theory: see (5.3). Therefore,

$$\delta Z_{\xi} \sim (\varepsilon \xi)^{1/3}, \quad \xi \sim \varepsilon^{1/8} \left(\frac{L_{\parallel}}{v_A} \right)^{3/8} \lambda^{3/4} \sim \lambda_{CB}^{1/4} \lambda^{3/4}, \quad (6.31)$$

with the latter formula following from (6.3) and (6.20) or (6.22). Thus, Elsasser fields' spectra have exponents -2 in the l_{\parallel} direction, $-3/2$ in the λ direction and $-5/3$ in the ξ direction (see the $n = 2$ exponents in figure 13a). Let me note in passing that the “Kolmogorov” scaling (6.31) will play a key part in my discussion, in appendix D.7, of why the Lazarian & Vishniac (1999) notion of “stochastic reconnection” does not automatically invalidate the aligned cascade and return us to GS95, as an erudite reader might have been worried it would—the idea is that the Richardson (1926) (super)diffusion of Lagrangian trajectories in a turbulent field is always determined by the ξ -dependent scaling (6.31), regardless of the nature of the cascade in λ .

A good way of thinking physically of the inevitability of 3D anisotropy is to note that, from (6.4) and CB,

$$\xi \sim l_{\parallel} \frac{\delta Z_{\lambda}}{v_A} \sim l_{\parallel} \frac{\delta b_{\lambda}}{v_A}, \quad (6.32)$$

i.e., ξ is the typical displacement of a fluid element and also the typical perpendicular distance a field line wanders within a structure coherent on the parallel scale l_{\parallel} . Fluctuations must therefore preserve coherence in their own direction at least on the scale ξ . They are not constrained in this way in the third direction λ , and the fluctuation direction itself has an angular uncertainty of the order of the angle θ_{λ} between the two fields, so it makes sense that the aspect ratio of the structures in the perpendicular plane should satisfy (6.3).

The dependence of the anisotropy on the local direction of the fluctuating fields makes the connection between anisotropy, alignment and intermittency more obvious: when we follow perturbed field lines to extract parallel correlations or measure one Elsasser field's decorrelation along the direction of another Elsasser field, we are clearly not

²⁷A sophisticated reader interested in how this can be done, might wonder whether the prescription given in § 5.3 and based on defining the local field \mathbf{B}_{loc} at each scale according to (5.9) is still valid for aligned turbulence: indeed, would the distance (5.7) by which the point-separation vector \mathbf{l} veered off the exact field line not be $\Delta l_{\perp} \gg \lambda$ even when the coarse-graining scale is $L_{\perp} \sim \lambda$, because in (5.7), $l/v_A \sim \lambda/\delta b_{\lambda} \sin \theta_{\lambda}$? In fact, since Δl_{\perp} is clearly in the direction of \mathbf{b}_{\perp} , the fluctuation direction, all we need to do in order to preserve parallel correlations is to ensure $\Delta l_{\perp} \ll \xi$. This is indeed marginally satisfied when $L_{\perp} \sim \lambda$ because, in (5.7), $l/v_A \sim \xi/\delta b_{\lambda}$. Chen *et al.* (2012) and Verdini *et al.* (2018, 2019) observationally and Mallet *et al.* (2016) numerically used this method with apparent success.

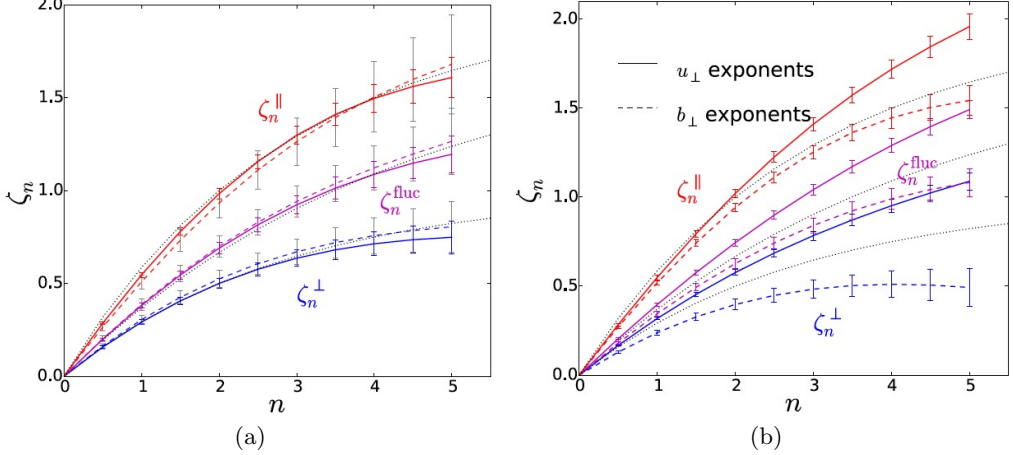


FIGURE 13. Scaling exponents of the structure functions in RMHD turbulence simulated by Mallet *et al.* (2016) (the plot is reproduced from Mallet & Schekochihin 2017). (a) Structure functions of the Elsasser-field increments (5.6): by definition, $\langle |\delta Z_l^+|^n \rangle \propto l^{\zeta_n}$ and ζ_n^{\perp} , ζ_n^{fluc} , ζ_n^{\parallel} are exponents for $l = \lambda$, ξ , l_{\parallel} , respectively (i.e., all structure functions are conditional on the point separation being in one of the three directions of local 3D anisotropy; see §§ 5.3 and 6.5). The solid lines are for a 1024^3 simulation (with hyperviscosity), the dashed ones are for a 512^3 simulation, indicating how converged, or otherwise, the exponents are, and the dotted lines, in both (a) and (b), are the theoretical model by Mallet & Schekochihin (2017). (b) Similarly defined structure functions of the velocity (solid lines) and magnetic-field (dashed lines) increments from the same 1024^3 simulation. The magnetic field is “more intermittent” than the Elsasser fields and the latter more so than velocity. An early (possibly first) numerical measurement of this kind, highlighting the differences between scalings of different fields and in different local directions, was done by Cho *et al.* (2003).

calculating second-order statistics in the strict sense—and so, in formal terms, local scale-dependent anisotropy always involves correlation functions of (all) higher orders.²⁸ Thus, it makes a certain natural sense to speak of the alignment-induced departure of MHD-turbulence spectrum from the Kolmogorovian GS95 scaling and of the 3D anisotropy of the underlying fluctuation field as an intermittency effect, as I have done here.

6.6. Higher-Order Statistics

In several places (e.g., in §§ 5.3 and 6.4.2), I have brushed against the more formal task of the intermittency theory—the calculation of the scaling exponents of higher-order structure functions or, equivalently, of the probability distributions of field increments—and recoiled every time, opting for “twiddle” algebra and statements about spectra. A fair amount of information on these matters is available from simulations and from the solar-wind measurements: what intermittency looks like in the former is illustrated by figure 13 (a survey of previous measurements of structure functions, both in simulations and in the solar wind, can be found in Chandran *et al.* 2015). Some of what is known is perhaps understood, but much remains a mystery: for example, we do not know why the higher-order scaling exponents are generally not the same for velocity, Elsasser and magnetic fields, with the latter “more intermittent” than the former, as is evident

²⁸It is easy to show that a Gaussian field cannot have scale-dependent alignment—although a solenoidal field will naturally have some modest scale-independent one (Chen *et al.* 2012; Mallet *et al.* 2016). Note also the paper by Matthaeus *et al.* (2012), where the role of higher-order statistics in locally parallel correlations is examined with great punctiliousness.

in figure 13(b) (in § 10.4, I will moot a possible connexion between intermittency and negative “residual energy”—an asymmetry between the magnetic and velocity spectra seen both in numerical simulations and in the solar wind—but I do not know how to translate this into anything resembling figure 13b).

Interesting as it is, I will now leave the problem of higher-order statistics alone. We know from the (ongoing) history of hydrodynamic-turbulence theory that once this becomes *the* unsolved problem that everyone is working on, the scope for abstract theorising expands to fill all available space (and time) while attention paid by the outside world diminishes.²⁹ This said, I hasten to dispel any possible impression that I do not consider intermittency of MHD turbulence an important problem: in fact, as I have argued above, intermittency as a physical phenomenon appears to be so inextricably hard-wired into the structure of MHD turbulence that any workable theory of the latter has to be a theory of its intermittency.

Finally, let me jump ahead of myself and mention also that we know nothing at all of the intermittency in “tearing-dominated turbulence,” which is about to be introduced (§ 7), and very little of the intermittency in the variants of MHD turbulence surveyed in §§ 9–13. In particular, the relationship between intermittency and Elsasser imbalance, local or global, appears to me to be a promising object for theoreticians’ scrutiny (see § 9.1).

7. MHD Turbulence Meets Reconnection

Finally, we wonder if it is possible that Sweet’s mechanism might modify somewhat the diffusion and dissipation of the magnetic field in hydromagnetic turbulence.

Last sentence of Parker (1957)

If we accept that MHD turbulence in the inertial range—or, at least, in some subrange of the inertial range immediately below the outer scale—has a tendency to organise itself into fettuccine-like structures whose aspect ratio in the 2D plane perpendicular to the mean magnetic field increases as their size decreases, we are opting for a state of affairs that is not sustainable asymptotically, at ever smaller scales. These structures are mini-sheets, and sheets in MHD tend to be tearing-unstable. Thus, just like WT, strong aligned turbulence too carries in it the seeds of its own destruction, making an eventual transition to some new state inevitable at sufficiently small scales.³⁰

The notion that current sheets will spontaneously form in a turbulent MHD fluid

²⁹Let me qualify this by mentioning a recent paper by Mallet *et al.* (2019) where abstract theory of intermittency is converted into insights into particle-heating physics in the solar wind (more of the Chandran *et al.* 2010 stochastic heating is found in the more intense, intermittent patches), which some might view as a more “practical” (in the astrophysical sense) preoccupation.

³⁰That this transition can and, generally speaking, will, happen *within the inertial range* is made obvious by the following rather apt observation due to Uzdensky & Boldyrev (2006). The aspect ratio of an aligned sheet-like structure at Boldyrev’s cutoff scale (6.24) is $\xi/\lambda \sim Rm^{1/6}(1 + Pm)^{-1/6}$, using (6.31) for ξ and setting $\lambda = \lambda_\eta$. The Lundquist number at this scale is $S_\xi = \delta Z_{\lambda_\eta} \xi / \eta \sim Rm^{1/3}(1 + Pm)^{2/3}$. Therefore, $\xi/\lambda \sim S_\xi^{1/2}(1 + Pm)^{-1/2}$. Apart from the Pm dependence, this is the aspect ratio of a Sweet–Parker (SP) current sheet, which is $S_\xi^{1/2}(1 + Pm)^{-1/4}$ (see appendix D.4.1). But, provided S_ξ is large enough and Pm is not too large, such a sheet will be violently (i.e., high above threshold) unstable to the plasmoid instability, which is a variety of tearing mode and has a growth rate that is much larger than the nonlinear rate at which the sheet is formed (see appendix D.4.2). Therefore, tearing should muscle its way into turbulent dynamics already at some scale that is larger than λ_η .

is not new (Matthaeus & Lamkin 1986; Politano *et al.* 1989) and the phenomenology of these structures has been studied (numerically) quite extensively, e.g., by Servidio *et al.* (2009, 2010, 2011a,b) in 2D and by Zhdankin *et al.* (2013, 2014, 2015, 2016b) in 3D (see also Wan *et al.* 2014), while solar-wind measurements (e.g., Retinò *et al.* 2007; Sundkvist *et al.* 2007; Osman *et al.* 2014; Greco *et al.* 2016) provided motivation and, perhaps, vindication. However, theoretical discussion of these results appeared to focus on the association between current sheets in MHD turbulence and its intermittent nature, identifying spontaneously forming current sheets as the archetypal intermittent events—and effectively segregating this topic from the traditional questions about the energy spectrum and the “typical” structures believed to be responsible for it, viz., Alfvénic perturbations, aligned or otherwise.

In fact, as I argued in §§ 6.4.2 and 6.5, it is impossible to separate the physics of alignment from that of intermittency. Dynamic alignment produces sheet-like, or “proto-sheet”, structures that measurably affect the energy spectrum but are also the intermittent fluctuations that can perhaps collapse into proper current sheets. The likelihood that they will do so—or, more generally, that aligned structures can survive at all—hinges on whether the nonlinear cascade time τ_{nl} at a given scale λ is longer or shorter than the typical time scale on which a tearing mode can be triggered, leading to the break up of the dynamically forming sheets into islands (Uzdensky & Loureiro 2016). Since the growth rate of the tearing mode in resistive MHD is limited by resistivity and would be zero in the limit of infinitely small η , the aligned turbulent cascade should be safe from tearing above a certain scale that must be proportional to some positive power of η . However, this need not be the same as Boldyrev’s cutoff scale (6.21) that arises from the competition between the cascade rate and vanilla Ohmic (or viscous) diffusion (τ_{nl} vs. τ_η)—so, at the very least, the cutoff scale of the aligned cascade may not be what one might have thought it was, and what happens below that scale may be more interesting than the usual dull exponential petering out of the energy spectrum in the dissipation range.

This possibility was explored by Mallet *et al.* (2017b) and Loureiro & Boldyrev (2017b) (unaware of each other’s converging preoccupations), leading to a new scaling for the aligned cascade’s cutoff and to a new model for the tail end of the MHD turbulence spectrum—mitigating some of the unsatisfactory features of the aligned-turbulence paradigm and thus providing a kind of glossy finish to the overall picture (despite their rather esoteric nature, the two papers appear to have become instant classics—so much so as to merit logarithmic corrections: Comisso *et al.* 2018). While the key idea in the two papers was the same, their takes on its consequences for the “tearing-mediated turbulence” were somewhat different—here I will follow Mallet *et al.* (2017b), but present their results in a somewhat simpler, if less general, form.³¹

Before I proceed, let me alert my erudite reader that the profound alteration of the

³¹ Namely, I will ignore the nuance that, in an intermittent ensemble, fluctuations of different strengths that are always present even at the same scale will be affected by reconnection to a different degree and so more intense structures will be disrupted at larger scales than the less intense ones. I will also not present scalings that follow from the theory of the aligned cascade by Chandran *et al.* (2015), focusing for simplicity exclusively on the model by Mallet & Schekochihin (2017) (which is the same as Boldyrev’s original theory if the latter is interpreted as explained in § 6.4). In this sense, my exposition in § 7.1 is closer in style to Loureiro & Boldyrev (2017b) than the paper by Mallet *et al.* (2017b) was. The material difference between the two arises in § 7.2 and concerns the spectrum of the tearing-mediated turbulence. This is now moot, however, as the follow-up paper by Boldyrev & Loureiro (2017) embraced the Mallet *et al.* (2017b) spectrum, if not quite the physical model that led to it (see § 7.2.1).

MHD cascade by reconnection that I will discuss here has nothing at all to do with the concept of “stochastic reconnection” in MHD turbulence associated with the work of Lazarian, Vishniac, Eyink, and their co-workers—this is explained carefully in § 8.3.3 and in appendix D.7.

7.1. Disruption by Tearing

The scale at which the aligned structures will be disrupted by tearing can be estimated very easily by comparing the nonlinear time (6.4) of the aligned cascade with the growth time of the fastest tearing mode that can be triggered in an MHD sheet of a given transverse scale λ . That this growth time is a good estimate for the time that reconnection needs to break up a sheet forming as a result of ideal-MHD dynamics is not quite as obvious as it might appear, but it is true and was carefully shown to be so by Uzdensky & Loureiro (2016). The maximum tearing growth rate is

$$\gamma \sim \frac{v_{Ay}}{\lambda} S_\lambda^{-1/2} (1 + Pm)^{-1/4}, \quad S_\lambda = \frac{v_{Ay}\lambda}{\eta}, \quad Pm = \frac{\nu}{\eta}. \quad (7.1)$$

How to derive this is reviewed in appendix D.1 [see (D 32)]. Here v_{Ay} is the Alfvén speed associated with the perturbed magnetic field that reverses at scale λ , S_λ is the corresponding Lundquist number and Pm is the magnetic Prandtl number, which only matters if the viscosity ν is larger than the magnetic diffusivity η . In application to our aligned Alfvénic structures, we should replace $v_{Ay} \sim \delta Z_\lambda$. Then, using the scalings (6.22) to work out τ_{nl} , we find that the aligned cascade is faster than tearing as long as

$$\gamma \tau_{nl} \sim \frac{S_\lambda^{-1/2} (1 + Pm)^{-1/4}}{\sin \theta_\lambda} \ll 1 \quad \Leftrightarrow \quad \lambda \gg Rm^{-4/7} (1 + Pm)^{-2/7} \lambda_{CB} \equiv \lambda_D, \quad (7.2)$$

where $Rm \sim S_{\lambda_{CB}}$, as defined in (6.23), and the scale λ_D will henceforth be referred to as the *disruption scale*. At scales $\lambda \lesssim \lambda_D$, aligned sheet-like structures can no longer retain their integrity against the onslaught of tearing.³²

7.1.1. Some Reservations and Limitations

Let me observe parenthetically that one can entertain legitimate reservations about the validity of (7.1) and other formulae based on laminar-tearing theory in a noisy, turbulent environment (see, e.g., the discussion and references in footnote 103). Here suffice it to say, that at scales where $\gamma \ll \tau_{nl}^{-1}$, the laminar formulae are, of course, unjustified, and at scales where $\gamma \gg \tau_{nl}^{-1}$, if such situations existed, they would be perfectly fine, modulo the issue of flows, which I will explain in a moment.³³ The disruption scale λ_D is where

³²This is equivalent to the idea of Pucci & Velli (2014) that one can determine the maximum allowed aspect ratio of sheets in MHD by asking when the linear-tearing time in the sheet becomes comparable to its ideal-MHD dynamical evolution time (see appendix D.5.1). Careful examination of forgotten ancient texts reveals that nothing is entirely new under the Moon and the idea that tearing might disrupt the MHD cascade in fact appeared first in an early paper by Carbone *et al.* (1990), who derived the disruption scale (7.2) (without Pm) by comparing the tearing growth rate (7.1) with the cascade rate taken from the IK theory—this gives the same scaling, $\lambda_D \propto Rm^{-4/7}$, because the IK spectrum has the same scaling as Boldyrev’s spectrum. This said, their comparison between the two rates was purely formal: as Boldyrev & Loureiro (2018) rightly observe, there is nothing in the IK theory (or in GS95) that makes tearing disruption inevitable—aligned structures are needed for that.

³³Another caveat—there is always another caveat in this business!—is that tearing mode’s growth rate can potentially be modified in at least an order-unity way by small-scale corrugations superimposed on the unstable magnetic-field profile, even when the size of these corrugations is

$\gamma \sim \tau_{\text{nl}}^{-1}$, so the laminar-tearing formulae are presumably only order-unity wrong, which I acknowledge by using “ \sim ” instead of “ $=$ ” everywhere.

Another legitimate reservation concerns application to aligned structures formed by the MHD cascade of the tearing theory derived for a magnetostatic equilibrium. Indeed, these structures are not purely magnetic sheets, but rather Elsasser ones, i.e., they have local shear flows superimposed on them. These flows are likely somewhat sub-Alfvénic (the reasons and evidence for that are explained in § 10.4), but, technically speaking, it has not been shown that they are sub-Alfvénic enough to justify application of the no-flow tearing-mode theory or even that they cannot fatally stabilise tearing (some further discussion and references on tearing with flows can be found at the end of appendix D.4.2). Since the shear rate in these flows is no larger than τ_{nl}^{-1} , I think that this difficulty is a technical one, rather than a deal breaker, i.e., that what I am doing here is again only order-unity wrong (cf. Tolman *et al.* 2018), but I cannot prove it rigorously. If this admission has not discouraged the reader, let us proceed.

The disruption scale λ_D , upon comparison with the putative resistive cutoff (6.24) of the aligned cascade turns out to supersede it provided Pm is not too large:

$$\frac{\lambda_D}{\lambda_\eta} \sim \left[\frac{Rm}{(1+Pm)^{10}} \right]^{2/21} \gg 1. \quad (7.3)$$

In view of the ridiculous exponents involved, this means that in a system with even moderately large Pm and/or not a truly huge Rm , the aligned cascade will happily make it to the dissipation cutoff (6.24) and no further chapters are necessary in this story.³⁴ However, I do want to tell the story in full and so will focus on situations in which the condition (7.3) is satisfied.

7.1.2. Debris of Disruption

I shall turn to the question of what happens at scales below λ_D in § 7.2, but to do that, it is necessary first to ask what becomes of the aligned structures that are disrupted at λ_D .

The tearing instability that disrupts them, the so-called Coppi mode, or (the fastest-growing) resistive internal kink mode (Coppi *et al.* 1976), has the wavenumber [see (D 32)]

$$k_* \sim \frac{1}{\lambda} S_\lambda^{-1/4} (1+Pm)^{1/8} \sim \frac{1}{\lambda_{CB}} Rm^{-1/4} (1+Pm)^{1/8} \left(\frac{\lambda}{\lambda_{CB}} \right)^{-21/16}, \quad (7.4)$$

where (6.22) has been used to substitute for δZ_λ inside S_λ . Therefore, at the disruption scale ($\lambda = \lambda_D$),

$$k_* \sim \frac{1}{\lambda_{CB}} Rm^{1/2} (1+Pm)^{1/2}. \quad (7.5)$$

If referred to the length of the sheet ξ_D , which depends on λ_D via (6.31), this wavenumber gives us an estimate for the number of islands in the growing perturbation:

$$N \sim k_* \xi_D \sim Rm^{1/14} (1+Pm)^{2/7}. \quad (7.6)$$

relatively small (there is a literature on this: see Militello *et al.* 2009 and references therein). In the existing solved models, however, these corrugations are required to have long-time coherence, which is unlikely in the kind of turbulent environment that we are dealing with here (the context in the literature is zonal fields generated by drift-wave turbulence in tokamaks, a different beast).

³⁴This is, in fact, not quite true: at $Pm \gg 1$, interesting things can happen between the viscous and resistive cutoffs—see § 11. In particular, if the tearing disruption fails to occur in the inertial range, it may still occur at subviscous scales (§ 11.4).

As this is always large (or at least $\gtrsim 1$), the mode fits comfortably into the sheet that it is trying to disrupt.³⁵

What happens to these islands? When the tearing mode enters the nonlinear regime, the island width is (see appendix D.2)

$$w \sim k_* \lambda_D^2, \quad (7.7)$$

which is smaller than λ_D and so, technically speaking, the aligned structures need not be destroyed by these islands. Uzdensky & Loureiro (2016) (followed by Mallet *et al.* 2017b and by Loureiro & Boldyrev 2017b) argue that, after the tearing mode goes nonlinear, the islands will grow further while the X -points between them collapse into current sheets—all of that on the same time scale (7.1) as the mode grew. It seems intuitive that, in order to break up the aligned structure (ideal-MHD sheet) that spawned them, the islands would have to get to $w \sim \lambda_D$ (Uzdensky & Loureiro 2016). If they did this in a cross-section-area-preserving way, then they would be circular at the point of disruption: from (7.7), $w k_*^{-1} \sim \lambda_D^2$. Such a set of islands (flux ropes) would be isotropic in the perpendicular plane. Another simplistic model is to imagine their width grow due to further reconnection while their length remains the same, viz., $\sim k_*^{-1}$ (simplistic because the lengthening of the inter-island current sheets is ignored). The aspect ratio of such a flux rope once it reached the width λ_D would be

$$\lambda_D k_* \sim N \frac{\lambda_D}{\xi_D} \sim N \sin \theta_{\lambda_D} \sim Rm^{-1/14} (1 + Pm)^{3/14}, \quad (7.8)$$

where N is given by (7.6). This is a degree of alignment preserved, but reduced by a (asymptotically large) factor of N . At the extreme end of the range of possibilities is the view of Boldyrev & Loureiro (2017) that, in fact, islands of size (7.7) are already sufficient to break up the aligned structure, so alignment is not abruptly reduced by tearing disruption. Both this idea and some nuances about the X -point collapse are discussed further in § 7.4.1. The key point for us here is that at the disruption scale, the aligned structures that cascade down from the inertial range are broken up by reconnection into flux ropes that are underaligned and may even be isotropic in the perpendicular plane. They are a starting point for a new kind of cascade, which I shall now proceed to consider.

7.2. Tearing-Mediated Turbulence

If you accept the argument that the disruption by tearing of an aligned structure at the scale λ_D leads to its break-up into a number of flux ropes of width $\sim \lambda_D$, then the natural conclusion is that λ_D now becomes a kind of “outer scale” for a new cascade. There need not be anything particularly different about this cascade compared to the standard aligned cascade except the alignment angle may now be reset to a greater value. As the disruption-scale structures interact with each other and break up into smaller structures, the latter should develop the same tendency to align as their inertial-range predecessors did. For a while, the structures in this new cascade are safe from tearing as their aspect ratio is not large enough, but eventually (i.e., at small enough scales),

³⁵Based on (7.4), we see that this would be the case for tearing perturbations of any inertial-range structure with $\lambda \lesssim Rm^{-4/9} (1 + Pm)^{2/9} \lambda_{CB}$. At larger scales than this, the fastest tearing mode that fits into the sheet is the FKR mode (Furth *et al.* 1963) with \sim one growing island of size $\sim \xi$ [see (D34) and the discussion at the end of appendix D.1.4]. However, both this mode and the secular Rutherford (1973) evolution that succeeds it are always slower than the Coppi mode and, therefore, than the nonlinear ideal-MHD evolution of the sheet, so there is no danger of disruption at scales greater than λ_D .

they too will become sufficiently aligned to be broken up by tearing modes. This leads to another disruption, another iteration of an aligned “mini-cascade,” and so on. Thus, if we rename our critical-balance scale $\lambda_{\text{CB}} = \lambda_0$, the disruption scale $\lambda_D = \lambda_1$, and call the subsequent disruption scales λ_n , we can think of the MHD cascade as consisting of a sequence of aligned cascades interrupted by disruption episodes. I shall calculate λ_n and the spectral exponents for this new, composite tearing-mediated cascade in § 7.2.1, the final dissipation cutoff in § 7.2.2, the cascade’s alignment properties in § 7.2.3, and its parallel scalings, again determined by CB, in § 7.2.4.

7.2.1. Mini-cascades and the Spectrum of Tearing-Mediated Turbulence

Let us calculate the disruption scales λ_n , following [Mallet et al. \(2017b\)](#). Since the “mini-cascades” that connect them are just the same as the aligned cascade whose disruption we analysed in § 7.1, we can use (7.2) to deduce a recursion relation

$$\lambda_{n+1} \sim S_{\lambda_n}^{-4/7} (1 + \text{Pm})^{-2/7} \lambda_n \quad (7.9)$$

(remembering that Rm was defined as the Lundquist number at scale $\lambda_{\text{CB}} = \lambda_0$). To work out the Lundquist number S_{λ_n} at scale λ_n , notice that, if the alignment angle θ_λ just below λ_n is increased, there must be a downward jump in the amplitude of the turbulent fluctuations at λ_n : indeed, the nonlinear time (6.4) shortens compared to what it was in the aligned cascade just above λ_n , and the cascade accelerates. I shall consider the extreme possibility that the alignment is reset to being order unity, as this will effectively bracket the range of outcomes for the scalings of this cascade. Since it still has to carry the same energy flux, we have, for amplitudes just below the disruption scale (λ_n^-),

$$\frac{(\delta Z_{\lambda_n^-})^3}{\lambda_n} \sim \varepsilon \quad \Rightarrow \quad \delta Z_{\lambda_n^-} \sim (\varepsilon \lambda_n)^{1/3}, \quad (7.10)$$

just a Kolmogorov (or GS95) scaling. Therefore, the Lundquist number of the n -th mini-cascade is

$$S_{\lambda_n} \sim \frac{\delta Z_{\lambda_n^-} \lambda_n}{\eta} \sim \frac{\varepsilon^{1/3} \lambda_n^{4/3}}{\eta} \sim \text{Rm} \left(\frac{\lambda_n}{\lambda_{\text{CB}}} \right)^{4/3}. \quad (7.11)$$

In combination with (7.9), this gives us

$$\frac{\lambda_n}{\lambda_{\text{CB}}} \sim \left[\text{Rm}^{-4/7} (1 + \text{Pm})^{-2/7} \right]^{\frac{21}{16} [1 - (\frac{5}{21})^n]} \rightarrow \text{Rm}^{-3/4} (1 + \text{Pm})^{-3/8}, \quad n \rightarrow \infty. \quad (7.12)$$

I shall return to this obviously suggestive (Kolmogorov!) scaling in § 7.2.2.

In the picture that I have just painted, the cascade in the tearing-mediated range looks like a ladder (figure 14), with amplitude dropping at each successive disruption scale as structures become unaligned (or less aligned, in which case the steps of the ladder are less tall). In between the disruption scales, there are aligned “mini-cascades” of the same kind as the original one discussed in § 6.4, with $k_\perp^{-3/2}$ spectra. This means that the overall scaling of the turbulent fluctuation amplitudes can be constrained between their scaling just below each disruption scale (λ_n^-), given by (7.10), and just above it (λ_n^+). The latter scaling, for the amplitudes of the structures just before they get disrupted can be inferred from the fact that for these structures, the tearing growth rate (7.1) must be the same as the nonlinear interaction (cascade) rate: letting $v_{Ay} \sim \delta Z_{\lambda_n^+}$ in (7.1), we get

$$\tau_{\text{nl}}^{-1} \sim \gamma \sim (\delta Z_{\lambda_n^+})^{1/2} \lambda_n^{-3/2} \eta^{1/2} (1 + \text{Pm})^{-1/4} \quad (7.13)$$

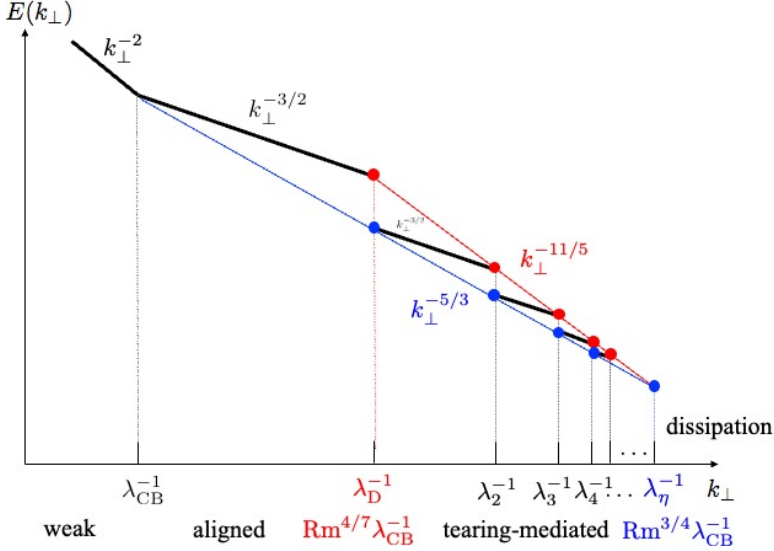


FIGURE 14. Spectrum of MHD turbulence and transition to tearing-mediated cascade [see (7.15)] (adapted from [Mallet et al. 2017b](#)). The width of the tearing-mediated range is, of course, exaggerated in this cartoon. The spectral slopes of the “mini-cascades” between λ_n^{-1} and λ_{n+1}^{-1} are all $k_\perp^{-3/2}$, but the overall envelope is $k_\perp^{-11/5}$. Note that, modulo Pm dependence, the disrupted aligned cascade and a putative unaligned GS95 $k_\perp^{-5/3}$ spectrum, starting at λ_{CB} , terminate at the same, Kolmogorov, scale (7.19).

and, therefore,

$$\begin{aligned} \frac{(\delta Z_{\lambda_n^+})^2}{\tau_{\text{nl}}} \sim \varepsilon &\Rightarrow \delta Z_{\lambda_n^+} \sim \varepsilon^{2/5} \eta^{-1/5} (1 + \text{Pm})^{1/10} \lambda_n^{3/5} \\ &\sim \left(\frac{\varepsilon L_\parallel}{v_A} \right)^{1/2} \left(\frac{\lambda_D}{\lambda_{\text{CB}}} \right)^{1/4} \left(\frac{\lambda_n}{\lambda_D} \right)^{3/5}. \end{aligned} \quad (7.14)$$

The last expression puts this result explicitly in contact with the inertial-range scaling (6.22). Thus, the tearing-mediated-range spectrum is ([Mallet et al. 2017b](#))³⁶

$$\varepsilon^{2/3} k_\perp^{-5/3} \lesssim E(k_\perp) \lesssim \varepsilon^{4/5} \eta^{-2/5} (1 + \text{Pm})^{1/5} k_\perp^{-11/5}. \quad (7.15)$$

Since the $-11/5$ upper envelope is steeper than the $-5/3$ lower one, the two converge and eventually meet at

$$\lambda_\infty \sim \eta^{3/4} \varepsilon^{-1/4} (1 + \text{Pm})^{-3/8} \sim \lambda_D^{21/16} \lambda_{\text{CB}}^{-5/16}, \quad (7.16)$$

which is, of course, the scale (7.12) in the limit $n \rightarrow \infty$. For $\text{Pm} \gg 1$, this will, in fact, be superseded by the Kolmogorov cutoff to be derived in § 7.2.2.

While in the above construction, the tearing-mediated-range spectrum is pictured as a succession of “steps” representing the “mini-cascades” that connect the successive disruption scales (figure 14), the reality will almost certainly look more like some overall power-law spectrum with a slope for which the upper $-11/5$ bound (7.15) seems to be

³⁶ [Boldyrev & Loureiro \(2017\)](#) have a somewhat differently phrased derivation of the $k_\perp^{-11/5}$ spectrum, based on assuming no increase in alignment for the debris of disruption (see § 7.4.1). The possibilities associated with fractional increase, e.g., (7.8), are bracketed by the range (7.14).

a good estimate. Indeed, the tearing disruptions will be happening within intermittently distributed aligned structures of different amplitudes and sizes, on which the disruption scales will depend (Mallet *et al.* 2017*b*). Thus, each scale λ_n will in fact be smeared over some range and, as the successive intervals $(\lambda_n, \lambda_{n+1})$ become narrower, this smear can easily exceed their width. Pending a detailed theory of intermittency in the tearing-mediated range, perhaps the best way to think of the spectrum and other scalings in this range is, therefore, in a “coarse-grained” sense, focusing on the characteristic dependence of all interesting quantities on λ_n , treated as a continuous variable.

7.2.2. Restoration of Kolmogorov Cutoff

To calculate the dissipative cutoff for the tearing-mediated cascade, one balances the larger of the viscous and resistive diffusion rates with the nonlinear cascade rate (7.13) (this is the longest of the nonlinear time scales involved): using (7.14), one gets

$$\frac{\nu + \eta}{\lambda_\eta^2} \sim \gamma \quad \Rightarrow \quad \lambda_\eta \sim \varepsilon^{-3/4} \eta^{3/4} (1 + \text{Pm})^{3/2} \sim \lambda_{\text{CB}} \text{Rm}^{-3/4} (1 + \text{Pm})^{3/2} \equiv \lambda_\eta^{\text{tearing}}. \quad (7.17)$$

For $\text{Pm} \lesssim 1$, this is the same scale as (7.16), where the $-11/5$ and $-5/3$ scalings meet; for $\text{Pm} \gg 1$, (7.17) is reached before (7.16). The condition for the range $[\lambda_D, \lambda_\eta^K]$ to be non-empty is

$$\frac{\lambda_D}{\lambda_\eta^{\text{tearing}}} \sim \left[\frac{\text{Rm}}{(1 + \text{Pm})^{10}} \right]^{5/28} \gg 1. \quad (7.18)$$

This is less stringent than (7.3), so will always be satisfied if the disruption occurs in the first place.

The good news (or, at any rate, the news) is that Kolmogorov’s scaling of the dissipative cutoff is rehabilitated for $\text{Pm} \lesssim 1$. Notably, it is not quite rehabilitated for $\text{Pm} \gg 1$, but that is likely an illusion. Indeed, while viscosity destroys velocities, aligned magnetic structures survive unscathed (cf. § 11), so tearing can keep going in the viscously dominated regime. If it breaks up the aligned structures at the scale $\lambda_\eta^{\text{tearing}}$ into flux ropes of the same width and lesser alignment, the turnover time of these structures will be shorter than the viscous-diffusion time—in just the same way as the debris of disruption had shorter turnover times than their mother sheets in § 7.2.1—and the tearing-mediated cascade can continue. A rough estimate of how small the debris have to get to be killed completely by diffusion is to set their Lundquist number (7.11) obtained on the assumption of complete lack of alignment to $S_{\lambda_n} \sim 1 + \text{Pm}$ (in other words, the cutoff occurs when either Rm or Re associated with the λ_n -scale structures is order unity). This gives

$$\lambda_\eta^K \sim \lambda_{\text{CB}} \left(\frac{\text{Rm}}{1 + \text{Pm}} \right)^{-3/4} = \lambda_{\text{CB}} \widetilde{\text{Re}}^{-3/4} \sim \frac{(\nu + \eta)^{3/4}}{\varepsilon^{1/4}}, \quad (7.19)$$

where $\widetilde{\text{Re}}$, defined in (6.24), is Rm when $\text{Pm} \lesssim 1$ and Re when $\text{Pm} \gg 1$. This is the proper, classic Kolmogorov scale.

It is interesting to recall that it is the Kolmogorov scaling at (and of) the dissipation scale that was the strongest claim made by Beresnyak (2011, 2012*a*, 2014*b*, 2019) on the basis of a convergence study of his numerical spectra (see § 6.3 and figure 10*b*). While he inferred from that an interpretation of these spectra as showing a $-5/3$ scaling in the inertial range, it is their convergence at the dissipative end of the resolved range that appeared to be the least negotiable feature of his work. He may well have been right. Indeed, his largest simulations (see figure 10) fall somewhere in between the

condition (7.18) ($\lambda_D/\lambda_\eta^K \gtrsim 3$ would require perhaps $Rm \gtrsim 10^3$ at $Pm \sim 1$) and the more stringent condition (7.3) needed to stop Boldyrev's cutoff (6.24) from taking over ($\lambda_D/\lambda_\eta \gtrsim 3$ if $Rm \gtrsim 10^5$). Thus, λ_D in Beresnyak's simulations could not have been more than a factor of order unity larger than the dissipation scale. An optimist might argue that this could have been just about enough to pick up the Kolmogorov scaling of the latter.

7.2.3. Alignment in the Tearing-Mediated Range

The structures corresponding to the lower (GS95) envelope (7.10) are unaligned, whereas the alignment corresponding to the upper envelope (7.14) is the tightest alignment sustainable in the tearing-mediated range and achieved by each aligned “mini-cascade” just before it is disrupted by tearing at the scale λ_n . This is (cf. [Boldyrev & Loureiro 2017](#))

$$\sin \theta_{\lambda_n^+} \sim \frac{\lambda_n/\delta Z_{\lambda_n^+}}{\tau_{nl}} \sim \left(\frac{\lambda_D}{\lambda_{CB}} \right)^{1/4} \left(\frac{\lambda_n}{\lambda_D} \right)^{-4/5}. \quad (7.20)$$

Equivalently, the fluctuation-direction coherence scale is

$$\xi_n \sim \frac{\lambda_n}{\sin \theta_{\lambda_n^+}} \sim \lambda_{CB} \left(\frac{\lambda_D}{\lambda_{CB}} \right)^{3/4} \left(\frac{\lambda_n}{\lambda_D} \right)^{9/5}. \quad (7.21)$$

The corresponding spectral exponent is again $-5/3$, which is automatically the case given the definitions of τ_{nl} , θ_λ and ξ [see (6.4) and § 6.5].

Thus, the smallest possible alignment angle, having reached its minimum at λ_D , gets larger through the tearing-mediated range, according to (7.20). It becomes order unity at the scale (7.16), which is the same as the Kolmogorov cutoff (7.19) for $Pm \lesssim 1$ and a bit smaller than it for $Pm \gg 1$ (but in fact there is no more alignment below the Kolmogorov cutoff).

To the (doubtful) extent that existing numerical evidence can be considered to be probing this regime, perhaps we can take heart from the numerical papers by both Beresnyak and by Boldyrev's group cited in § 6.3 all reporting that alignment fades away at the small-scale end of the inertial range—although this may also be just a banal effect of the numerical resolution cutoff.

7.2.4. Parallel Cascade in the Tearing-Mediated Range

As ever, CB should be an enduring feature of our turbulence. This means that the parallel spectrum (5.1) will not notice the disruption scale and blithely extend all the way through the tearing-mediated range. Since the unaligned (or less aligned) flux ropes produced in the wake of the disruption of aligned structures have a shorter decorrelation time than their aligned progenitors, they should break up in the parallel direction (cf. [Zhou et al. 2020](#) and § 12.6). The resulting parallel coherence scale, the same as the scale (5.5) in the GS95 theory, is the lower bound on l_{\parallel} at each λ_n . The upper bound can be inferred by equating the nonlinear time (7.13) at λ_n to the Alfvén time l_{\parallel}/v_A . The result is

$$v_A \varepsilon^{-1/3} \lambda_n^{2/3} \lesssim l_{\parallel} \lesssim v_A \varepsilon^{-1/5} \eta^{-2/5} (1 + Pm)^{1/5} \lambda_n^{6/5} \sim L_{\parallel} \left(\frac{\lambda_D}{\lambda_{CB}} \right)^{1/2} \left(\frac{\lambda_n}{\lambda_D} \right)^{6/5}. \quad (7.22)$$

Thus, the upper bound on the parallel anisotropy l_{\parallel}/λ decreases with scale in this range (turbulence becomes less anisotropic).

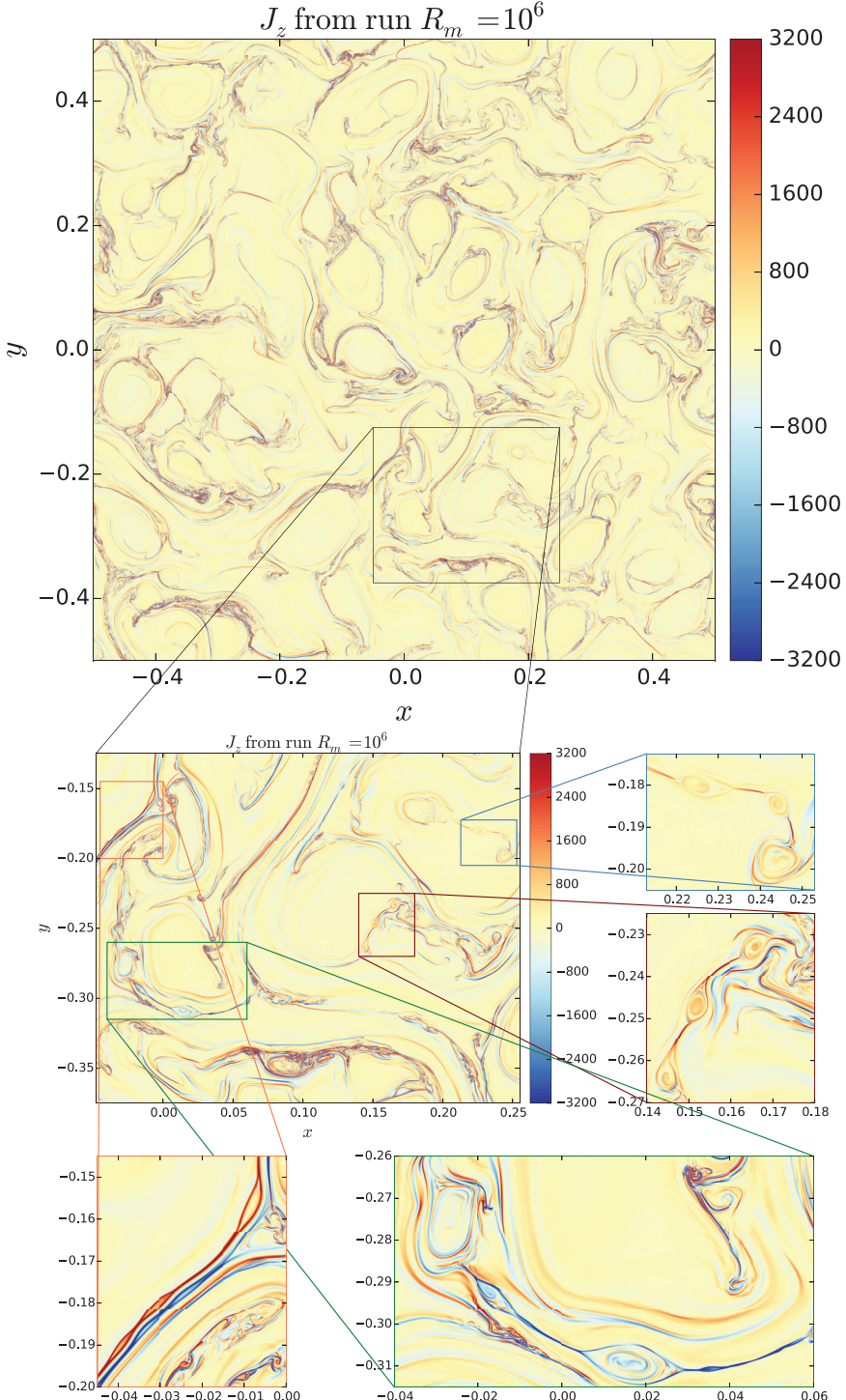


FIGURE 15. A snapshot of current density (j_z) from a 2D, $R_m = 10^6$ ($64,000^2$) MHD simulation by Dong *et al.* (2018) [reprinted with permission from Dong *et al.* (2018), copyright (2018) by the American Physical Society; I am grateful to C. Dong for letting me have the original figure file]. Zoomed areas show sheets broken up into plasmoids. The 3D versions of these visualisations reported by Dong *et al.* (2021) look generally messier, with islands less clearly delineated (they look a bit like the flux ropes in figure 50), but not, at first glance, qualitatively different in a paradigm-changing way.

7.3. Is This a Falsifiable Theory?

With considerable difficulty.

Numerically, anything like a definite confirmation of the tearing disruption (§ 7.1) and the existence of a tearing-mediated cascade (§ 7.2) requires formidably large simulations: the condition (7.3) demands $Rm \sim 10^5$ at least (estimated via the frivolous but basically sound principle that the smallest large number is 3)—and probably quite a bit larger if one is to see the scaling of the tearing-mediated-range spectrum (7.15). However, as was mooted above, an optimist might find cause for optimism in the evidence of the MHD turbulence cutoff seen in simulations appearing to obey the Kolmogorov scaling (7.19) (see discussion in § 7.2.2) or in the numerically measured alignment petering out at the small-scale end of the inertial range, as required by § 7.2.3. While the trouble to which I have gone to keep track of the Pm dependence of the tearing-mediated-range quantities did not yield anything qualitatively spectacular, there is perhaps an opportunity here for numerical tests: e.g., can one obtain Boldyrev’s scaling (6.24) of the dissipation cutoff in the limit of moderate Rm and large Pm ?—which, in view of (7.3), is unlikely to need to be very large to take over and shut down tearing.

One way to circumvent the need for getting into a hyper-asymptotic regime is to simulate directly the dynamics of structures that resemble Alfvénic sheets deep in the inertial range. Such a study by Walker *et al.* (2018), in 2D, of the decay of an Alfvénic “eddy” highly anisotropic in the perpendicular plane, has shown it breaking up promisingly into plasmoids and giving rise to a steeper spectrum than exhibited by a larger- Rm case where tearing was too slow. Dong *et al.* (2018) went further and actually demonstrated a spectral break at the disruption scale and a $k_\perp^{-11/5}$ spectrum below it, with sheets in a turbulent system very vividly breaking up into plasmoids (figure 15)—but still in 2D. So far so good, but the real prize is always for 3D. The present review has spent so long going through revisions that 3D results, of which I originally wrote in remote future tense, are in fact now on the brink of arriving, again due to Dong *et al.* (2021), who have performed the mother of all MHD simulations (with Rm comfortably over 10^5) and are claiming to see a “sub-inertial range” with a $-11/5$ spectral slope, as per (7.15); the spectral break where this scaling starts appears to be in the right place, $\lambda_D \propto Rm^{-4/7}$ as per (7.2). If I read their results correctly (based on C. Dong’s presentation at the 2021 APS DPP Meeting), hallelujah.

Observationally, our best bet for fine measurements of turbulence is the solar wind and the terrestrial magnetosphere (e.g., the magnetosheath). However, these are collisionless environments, so, before any triumphs of observational confirmation can be celebrated, all the resistive reconnection physics on which the tearing-mediated-range cascade depends needs to be amended for the cornucopia of kinetic effects that await at the small-scale end of the cascade (see § 14.1). Once the tearing disruption in MHD was proposed, such generalisations were the ripe, low-hanging fruit quite a lot of which was immediately picked (Mallet *et al.* 2017a; Loureiro & Boldyrev 2017a; Boldyrev & Loureiro 2019; see also Loureiro & Boldyrev 2018, where these ideas were ported to pair plasmas).

Pending all this validation and verification, the tearing-mediated cascade remains a beautiful fantasy—but one must be grateful that after half a century of scrutiny, MHD turbulence still has such gifts to offer.

7.4. Tearing Disruption, Plasmoid Chains, Fast Reconnection, and Reconnection-Driven Turbulence

This section deals with what many readers might feel are fairly esoteric details. They are right—and so skipping straight to § 8 will not subtract much from their experience.

In what until recently was a separate strand of research, much interest in the reconnection community has focused on stochastic plasmoid chains that arise in current sheets susceptible to the plasmoid instability (a sub-species of tearing), where a lively population of islands (plasmoids) are born, grow, travel along the sheet with Alfvénic outflows, occasionally eat each other (coalesce),³⁷ and, as shown by Uzdensky *et al.* (2010), cause reconnection in the sheet that they inhabit to be fast,³⁸ meaning independent of η as $\eta \rightarrow +0$ (a derivation of the plasmoid instability, a long list of references on stochastic plasmoid chains, and, in figure 46, an example of one, can be found in appendix D.4.2; the Uzdensky *et al.* 2010 argument is reproduced in appendix D.6). A stochastic chain can be viewed as a kind of “1D turbulence”, and has some distinctive statistical properties (see appendices D.6.1 and D.6.2). Should one imagine the disrupted aligned structures spawning multiple instances of such a turbulence, and does the simple theory presented in § 7.2 describe this situation or does it need to be revised to represent a superposition of many fast-reconnecting, plasmoid-infested sheets (as attempted in three different ways by Loureiro & Boldyrev 2017*b*, 2020 and Tenerani & Velli 2020*b*)?

7.4.1. Nature of Tearing Disruption

In considering this problem, I first want to return to the question of what the “disruption” of the aligned structures actually consists of. There are two lines of thinking on this, articulated most explicitly in the papers by Mallet *et al.* (2017*b*) and Boldyrev & Loureiro (2017), of which I have so far stuck with the former. Namely, at the end of § 7.1, I followed Uzdensky & Loureiro (2016), Mallet *et al.* (2017*b*) and Loureiro & Boldyrev (2017*b*) in invoking the collapse of the X -points separating the tearing-mode islands as a means of consummating the disruption of the aligned structure—the theory of the tearing-mediated cascade in § 7.2 was then presented as a corollary of this view.

The collapse of inter-island X -points is actually the first step in the formation of a stochastic chain. A nuance that I have previously elided is that comparing the X -point collapse rate (which is \sim the tearing growth rate γ) with the growth rate of a *secondary* tearing instability of the same X -point shows that, at asymptotically large Lundquist numbers, the latter is always greater than the former. Therefore, the collapse may itself be disrupted by tearing, producing more islands and more X -points, followed by the collapse of those, also disrupted, and so on. My take on this recursive tearing is presented in appendix D.5.2 (alongside a review of prior literature, starting with Shibata & Tanuma 2001). I argue there that the smaller-scale islands that are produced in this process are not energetically relevant and so we need not worry about including them to amend the “one-level” scenario of tearing disruption presented in § 7.1.

The recursive tearing proceeds until inter-island current sheets are short enough to be stable, at which point the true nonlinear plasmoid chain can form, involving not just multiple tearings, but also nonlinear plasmoid growth by reconnection, their coalescence, and ejection from the sheet. While the multiscale statistics of such a chain may be different from that of a tearing-mediated cascade that I described in § 7.2, I assumed there, implicitly, that the chain could not survive for a long time, if at all: indeed,

³⁷In the process of coalescence, they also give rise to transverse secondary current sheets and plasmoid chains: see Bárta *et al.* (2011).

³⁸The reconnection that is being referred to here is the true, physical reconnection of the exact magnetic-field lines, not the effective reconnection of fields coarse-grained at some inertial-range scale λ . In a turbulent environment, the latter, known as “stochastic reconnection”, is believed always to be fast (see Lazarian *et al.* 2020 and references therein), so every cascaded eddy always gets a significant amount of it. As explained in § 8.3.3 and appendix D.7, this is plausible, and does not preclude either aligned or tearing-mediated turbulence.

the characteristic time scale of the process of fully forming the sheet out of an aligned structure is the tearing time ($\sim \gamma^{-1}$), and the time to break apart that aligned structure by ideal-MHD dynamics is of the same order ($\sim \tau_{\text{nl}}$). So it seems that the “mother sheet” (collapsed aligned structure) should break apart entirely shortly after (or even before) fully forming and release its plasmoids (flux ropes) into the general turbulent wilderness, where they are free to interact with each other or with anything else that comes along, and are thus no different from turbulent fluctuations of a particular size generically splashing around in a large nonlinear system. This gives rise to the “mini-cascades” in § 7.2, with the overall $k_{\perp}^{-11/5}$ spectral envelope (7.15).

[Boldyrev & Loureiro \(2017\)](#) also derive the $k_{\perp}^{-11/5}$ spectrum by using (7.13) as the operational prescription for the cascade time ($\tau_{\text{nl}} \sim \gamma^{-1}$ at each scale in the tearing-mediated range). However, they have a different narrative about what happens dynamically: they do not believe that inter-island X -points ever collapse, but that, rather, the tearing mode upsets alignment by order unity, changing the effective nonlinear cascade rate to the tearing rate. This is based on the (correct) observation that the alignment angle at the disruption scale (7.2)

$$\sin \theta_{\lambda_D} \sim S_{\lambda_D}^{-1/2} (1 + Pm)^{-1/4} \quad (7.23)$$

is the same (at least for $Pm \lesssim 1$) as the angular distortion of the field line caused by the tearing perturbation at the onset of the nonlinear regime: indeed, using (7.7) and (7.4) at $\lambda = \lambda_D$,

$$\theta_{\text{tearing}} \sim wk_* \sim (k_* \lambda_D)^2 \sim S_{\lambda_D}^{-1/2} (1 + Pm)^{1/4}. \quad (7.24)$$

They think that this is enough to make the aligned structure “cascade”, in some unspecified manner, without much reconnection, production of flux ropes, etc. In [Loureiro & Boldyrev \(2020\)](#), they revise their view a little and allow that, since the collapse time, the tearing time and, therefore, the cascade time are comparable to each other, *some* aligned structures might, in fact, collapse into proper reconnecting sheets.³⁹

It is hard to say whether the two pictures outlined above represent a disagreement in substance or merely in the style of presentation. While in the [Mallet et al. \(2017b\)](#) interpretation, the collapse of the inter-island X -points *is* the way in which the distortion of alignment caused by tearing leads to faster nonlinear break-up of the aligned structures, [Loureiro & Boldyrev \(2020\)](#) think this is not necessary but does happen with some finite probability. This might not be sufficiently quantifiable a difference to be testable.

7.4.2. Onset of Fast Reconnection

What may be consequential physically, however, is the onset of fast reconnection in those aligned, tearing structures that do manage to collapse into proper sheets. [Loureiro & Boldyrev \(2020\)](#) conjecture that when that happens, one should start worrying about

³⁹To [Loureiro & Boldyrev \(2020\)](#), the difference between these reconnection sites and mere tearing modes is that the former dissipate a lot of energy. This matters to them because they believe that the tearing-mediated cascade can only be a constant-flux cascade if it does not involve much reconnection, as reconnection is dissipative—the spectrum would have to steepen if reconnection occurred in too many places and thus caused a finite energy drain from the cascade. Is there really a contradiction between significant reconnection and constant flux? First, it is not inevitable (although, in resistive MHD with $Pm = 1$ usually true: see, e.g., [Loureiro et al. 2012](#)) that reconnection must always involve large dissipation. Secondly, and more importantly, if collapse and reconnection of an aligned structure of scale λ do lead to significant dissipation, that dissipation does not, in fact, occur at scale λ , but at much smaller scales—the scales of the inter-island sheets and outflows. Transfer of energy to those scales could arguably be viewed as part of the turbulent cascade.

the resulting reconnecting sheets making a difference to the nature of the tearing-mediated (now reconnection-mediated) turbulence.⁴⁰ In order for such a transition to be realisable, Rm must be large enough for the characteristic time of fast reconnection to be shorter than the cascade time:

$$\tau_{\text{rec}} \sim \epsilon_{\text{rec}}^{-1} \frac{\lambda}{\delta Z_\lambda} \lesssim \tau_{\text{nl}} \sim \frac{\lambda}{\delta Z_\lambda} (\sin \theta_\lambda)^{-1} \Leftrightarrow \sin \theta_\lambda \lesssim \epsilon_{\text{rec}}, \quad (7.25)$$

where the reconnection time has been estimated as the time for all of the flux in a magnetic structure of scale λ to be reconnected, and $\epsilon_{\text{rec}} \sim 10^{-2}(1 + Pm)^{-1/2}$ is the dimensionless fast-reconnection rate in a Uzdensky *et al.* (2010) plasmoid chain (see appendix D.6), or some modified version of it appropriate for a turbulent environment. The estimate (7.25) simply says that if the alignment angle (inverse aspect ratio) of a structure manages to become smaller than the reconnection rate, such a structure might be capable of becoming a fast-reconnecting sheet.

Let us recall that the alignment angle decreases with λ according to (6.22) in an aligned MHD cascade, reaches its minimum at the disruption scale λ_D [given by (7.2)], and then increases with decreasing λ according to (7.20) in a tearing-mediated cascade. The condition (7.25) is realisable if

$$\sin \theta_{\lambda_D} \sim \left(\frac{\lambda_D}{\lambda_{\text{CB}}} \right)^{1/4} \lesssim \epsilon_{\text{rec}} \Leftrightarrow Rm \gtrsim \epsilon_{\text{rec}}^{-7}(1 + Pm)^{-1/2} \sim 10^{14}(1 + Pm)^3. \quad (7.26)$$

Obviously, this is never going to be numerically (or indeed experimentally) achievable for resistive MHD—unless ϵ_{rec} is substantially enhanced in a turbulent setting (Loureiro & Boldyrev 2020 show that this “nonlinear-reconnecting” regime might also be more easily accessible in certain kinetic settings).

In the asymptotic world where the condition (7.25) can be realised, it will be realised for $\lambda \in [\lambda_{\text{rec}}^<, \lambda_{\text{rec}}^>]$, with the two scales lying below and above λ_D : using (6.22) and (7.20) for the alignment angle in the aligned and tearing-mediated cascades, respectively, one gets

$$\lambda_{\text{rec}}^> \sim \epsilon_{\text{rec}}^4 \lambda_{\text{CB}}, \quad \lambda_{\text{rec}}^< \sim \epsilon_{\text{rec}}^{-5/4} \lambda_D^{21/16} \lambda_{\text{CB}}^{-5/16}. \quad (7.27)$$

One might argue that $\lambda_{\text{rec}}^>$ is irrelevant because at that scale ideal nonlinear interactions are faster than tearing, so the instability that assists in the formation of a plasmoid chain is too slow to get it going before the energy cascades to small scales (if this is not true, then reconnection-mediated turbulence sets in at $\lambda_{\text{rec}}^>$, an Rm -independent scale, putting a hard lower bound on the allowed alignment angles, $\sin \theta_\lambda \gtrsim \epsilon_{\text{rec}}$, and vindicating Beresnyak 2019). In contrast, the interval $[\lambda_D, \lambda_{\text{rec}}^<]$ is tearing-dominated, so plasmoid chains could be on the cards.

What might turbulence in such a situation look like? To get some idea of that, it is perhaps wise to start with numerical evidence about turbulence in individual, “stand-alone” plasmoid chains—a subject on which copious literature exists, quoted in appendix D.4.2.

⁴⁰This is because in the slow-reconnection regime (described in appendix D.4.1), the reconnection time is always longer than the tearing time. Indeed, the latter, γ^{-1} , is given by (7.1) with $v_{Ay} \sim \delta Z_\lambda$, whereas τ_{rec} is given by (7.25) but with $\epsilon_{\text{rec}}^{-1} \sim \tilde{S}_\xi^{1/2}(1 + Pm)^{1/2}$, where \tilde{S}_ξ is the Lundquist number based on the size of the structure in the fluctuation direction [see (D50)]; therefore, $\gamma \tau_{\text{rec}} \sim (\xi_\lambda / \lambda)^{1/2} \gg 1$.

7.4.3. Reconnection-Driven Turbulence

Much of that literature describes 2D simulations, but there is a handful of papers dedicated to unstable sheets in 3D. In all of these 3D numerical experiments, a large-scale reconnecting configuration—a macroscopic sheet—was set up as an initial condition and/or driven by inflows/outflows from/to the boundaries of the domain, then went violently unstable, much more so than in 2D, and ended up looking like a strip of vigorous turbulence, rather than a quasi-1D chain (see appendix D.6.3 for citations and further discussion). There does not appear to be any reason for such a configuration to stay together without external help, so it is likely that what we are witnessing in these numerical simulations is a version of a tearing-mediated cascading event prolonged by the bespoke numerical set-up and thus guaranteed to go into the fast-reconnecting regime.

If this is true, then such reconnection-driven MHD turbulence and turbulence in a homogeneous box into which energy is injected by a body force are different only inasmuch as any two different outer-scale, system-specific arrangements for stirring up turbulence are different. In the spirit of universality, it is hard to believe that small patches of a turbulent sheet would look any different in close-up than a generic box of MHD turbulence. One can imagine, however, that, due to the macroscopic “reconnection driving” of the turbulence in a sheet, the turbulent cascade starts off at the outer scale already in a highly aligned, tearing-dominated, regime (Walker *et al.* 2018 was an explicit attempt to exploit this idea). Indeed, both Bárta *et al.* (2011) and Huang & Bhattacharjee (2016) see spectra somewhat steeper than -2 , perhaps consistent with $-11/5 = -2.2$ (or with the k_{\perp}^{-2} spectrum derived in appendix D.6.2). In contrast, Beresnyak (2017) and Kowal *et al.* (2017) report small-scale statistics very similar to those found in standard MHD turbulence. Tenerani & Velli (2020b) find the same at a sufficient distance from the neutral line, whereas close to it, they see interesting anisotropic scalings dependent on the (component of) the field and the direction in which its variation is probed vis-à-vis the orientation of the sheet.

Moving from turbulence in one sheet to an ensemble of turbulent sheets, Tenerani & Velli (2020b) speculate about the spectrum of a turbulence entirely dominated by reconnecting sheets filling a scale-dependent fraction of the volume, and arrive at $k_{\perp}^{-11/5}$ by an entirely different route, perhaps a coincidence. Loureiro & Boldyrev (2020), in pursuit of the same idea, amend $k_{\perp}^{-11/5}$ to $k_{\perp}^{-12/5}$ just by assuming the volume-filling fraction $\propto \lambda$ (sheets) for energy at every scale λ in an otherwise standard tearing-mediated cascade.

This is the current state of affairs. I do not have a definitive contribution to make to the (still wide open) theory of reconnection-driven turbulence. In appendix D.6.2, I show, following Bárta *et al.* (2012) and Loureiro (2016), how to get a k_{\perp}^{-2} spectrum for a stochastic plasmoid chain envisioned by Uzdensky *et al.* (2010). I then argue tentatively, in appendix D.6.3, that if plasmoids (in 3D, flux ropes) all go unstable and thus drive small-scale turbulence, that turbulence should look like regular (possibly tearing-mediated) MHD turbulence, but with a very broad driving range featuring a k_{\perp}^{-1} spectrum, in which turbulent motions are forced with an alignment angle independent of scale and equal to the (dimensionless) fast-reconnection rate ϵ_{rec} . I have no evidence to back this up.

Finally, let me also flag here the possibility that a good example of reconnection-driven turbulence may be the inertial-range turbulence in magnetically dominated decaying MHD systems, where decay is controlled by reconnection in current sheets that separate outer-scale relaxed structures (see § 12; the discussion of spectra is in § 12.8). Another

(although more uncertain) such example may be the saturated state of the turbulent dynamo (§ 13) if the scheme mooted in § 13.4.4 turns out to have merit.

I will let the subject drop at this point, with the parting message that the last word has not been written on the intermittency effects and the role of fast plasmoid reconnection in tearing-mediated turbulence.

8. Halfway Summary

For the beginning is thought to be more than half of the whole, and many of the questions we ask are cleared up by it.

Aristotle, *Nicomachean Ethics* (translated by W. D. Ross)

8.1. Is This the End of the Road?

It never quite is (see §§ 7.4.2–7.4.3 and the second part of this review, starting from § 9), but the basic story looks roughly complete for the first time in years, at least as far as forced, balanced RMHD turbulence is concerned. The principle of critical balance gave us a sound ideology for dealing with anisotropic turbulence in a system that supports propagation of waves (§ 5) and a firm prescription for the parallel spectrum (§ 5.2). The aligned cascade (§ 6) produced a plausible prediction for the perpendicular spectrum but used to have an air of unfinished business about it, both in the sense that it gave rise to a state that appeared unsustainable at asymptotically small scales and in view of the objections, physical and numerical, raised by Beresnyak (2011, 2012a, 2014b, 2019). With the revised interpretation of alignment as an intermittency effect (§ 6.4) and with the tearing-mediated cascade (§ 7) connecting the inertial-range, aligned cascade to the Kolmogorov cutoff (7.19), these issues appear to be satisfactorily resolved. In what is also an aesthetically pleasing development, the tearing-mediated cascade has emerged as an ingenious way in which MHD turbulence contrives to thermalise its energy while shedding the excessive alignment that ideal-MHD dynamics could not help producing in the inertial range. This development joins together in a most definite way the physics of turbulence and reconnection—arguably, this was always inevitable, but it is good that we now appear to have some grip on what happens specifically.

Before I move on to the miscellany of Part II, let me make a few comments about the robustness of the general picture presented above and its connection to other schools of thought on MHD turbulence.

8.2. What Can Go Wrong?

It is only fair to spell out explicitly what is settled and what can go catastrophically wrong with this entire picture.

The principle of critical balance and, therefore, the theory of the parallel cascade (§ 5) are, in my view, quite safe. They are straightforward physically and have been quite convincingly verified both observationally and numerically (*pace* the “waves vs. structures” confusion: see § 8.3.1). The CB approach also appears to offer an attractive and credible strategy for dealing with turbulence in wave-carrying systems other than MHD, in both plasmas and hydrodynamics (e.g., Cho & Lazarian 2004; Schekochihin *et al.* 2009, 2016, 2019; Nazarenko & Schekochihin 2011; Barnes *et al.* 2011; Boldyrev *et al.* 2013; Chen & Boldyrev 2017; Passot *et al.* 2017; Loureiro & Boldyrev 2018; Avsarkisov 2020; Adkins *et al.* 2022; Skoutnev 2022), further bolstering its claim to being a universal physical principle.

In contrast, the aligned perpendicular cascade (§ 6), its tearing disruption (§ 7.1) and

replacement by a tearing-mediated cascade (§ 7.2), which have formed the bulk of my story so far, are hotly debated concepts. Arguably, it is still subject to verification (requiring currently inaccessible resolutions) that alignment is not a transient, large-scale feature, as [Beresnyak \(2019\)](#) would have it. It seems to me that we do know, however, that if we stir up unaligned turbulence, it will get aligned at smaller scales (see numerical studies cited in § 6.3), so its possible transient nature can only be due to some secondary instability of the aligned structures. The picture presented above relied on this being the tearing instability—but it is not entirely impossible that it is, in fact, an ideal MHD instability, e.g., some version of Kelvin–Helmholtz (KH) instability. The difference is that tearing required resistivity and so the disruption scale $\lambda_D \propto \eta^{4/7}$ was asymptotically separated from the outer scale λ_{CB} [see (7.2)], whereas the KH instability would kick in at some $\lambda \sim$ a finite fraction of λ_{CB} . The usual expectation is that the KH instability is quenched by the magnetic field (and indeed hence perhaps the statistical preponderance of current sheets over shear layers; see § 10.4), but this can in principle turn out not to be enough. If it does, ideal MHD will take care of limiting alignment, without alignment there will be no need for, or dynamical tendency to, the tearing-mediated remedy to it at small scales, and, presumably, we will be back to GS95, in which case I apologise to my readers for having wasted their time (this scenario is explained in another language at end of § 8.3.3 and at the beginning of appendix D.7.4).

8.3. What Is Lost in Translation?

This section is devoted to misunderstandings and arguments at cross purposes. As any vibrant, fast-evolving field, MHD turbulence is a subject talked about in many languages, and differences in vocabulary are sometimes mistaken for fundamental disagreements.

8.3.1. Waves vs. Structures

In the minds of some enthusiasts of current sheets (or, generally, of “coherent structures”) in MHD turbulence, the distinction between the sheets (“structures”) and critically balanced Alfvénic perturbations (“waves”) has become a dichotomy between two allegedly incompatible paradigms of how energy is dissipated in MHD turbulence—in strongly dissipative structures or via wave damping. This is a misunderstanding that appears to be based on the incorrect perception of CB-based theories as requiring turbulence to be an ensemble of random-phased Alfvén waves, similar to WT (§ 4). No dichotomy, and certainly no mutual exclusivity, between waves and structures, in fact, exists: while Alfvénic perturbations retain certain properties associated with the linear-wave response, their turbulence is strong (which is the whole point of the CB principle) and the tendency to form sheets dynamic (mutual shearing of Elsasser fields: see [Chandran et al. 2015; Howes 2016](#)). This nonlinear, intermittent dynamics perpendicular to \mathbf{B} produces “structures”, while the linear wave-propagation physics gives them coherence along \mathbf{B} , via CB as a causality constraint (§ 5.1).

In the recent literature, the most systematic, and sensible, discussion of the “waves vs. structures” issue can be found in [Grošelj et al. \(2019\)](#) (although their focus is on the kinetic, rather than MHD, range of scales); the transition—and key differences—between wave turbulence and CB turbulence are illustrated very vividly in [Meyrand et al. \(2016\)](#) (already referred to in § 4).

8.3.2. Cellularisation of Turbulence

The interest in dissipative structures has its origin in the long history of thinking about MHD turbulence (and generally turbulence) in a language that is, at first glance, very different from the one in which the preceding sections of this review have been written.

This line of thinking dates back to [Montgomery et al. \(1978, 1979\)](#) and [Matthaeus & Montgomery \(1980\)](#), who looked for thermal-equilibrium states in MHD turbulence, subject to conservation of various secondary invariants—e.g., in 3D, helicity and cross-helicity—and conjectured that MHD turbulence would tend to such equilibria patchwise in space. By a classic variational argument, it is possible show that nonlinear interactions would be suppressed in the regions—“cells”—of fixed helicity, which would host force-free magnetic fields ([Taylor 1974](#)). A fixed cross-helicity would push velocity and magnetic field into alignment with each other (which does indeed happen in decaying MHD turbulence: see, e.g., [Matthaeus et al. 2008](#)); if they were also equal to each other in amplitude, the result would be a pure Elsasser, non-interacting state. Global force-free or Elsasser states are usually not achievable (e.g., because the conserved net helicity and/or cross-helicity of the system are zero), so the cells would be separated by boundaries where intense nonlinear dynamics and hence dissipation would take place (e.g., current sheets). That then would be the structure of a turbulent state—relaxed cells plus nonlinear, dissipative structures on their boundaries (non-volume-filling, so intermittent).

A recent review of this philosophy, from an original source and with copious references, is [Matthaeus et al. \(2015\)](#) (a similar thinking, mostly applied to hydrodynamic turbulence, is reviewed, in a fascinatingly idiosyncratic way, by [Levich 2009](#)). While this approach is most natural in the context of decaying (freely relaxing) turbulence (and does indeed work there: see § 12; vivid illustrations of this “cellularisation” of turbulence are figures 25 and 26), similar ideas have been mooted with regard to inertial-range statistics of forced turbulence: see, e.g., the discussion in § 9.1 of Elsasser-balanced MHD turbulence proving to be a patchwork of locally imbalanced, heavily cross-helical regions (figure 17). Dynamic alignment à la Boldyrev (§ 6), its salient effect being the local reduction of nonlinearity in the MHD inertial range, was also originally argued by him ([Boldyrev 2006](#)) to have to do with conservation and cascading of cross-helicity (see footnote 16).

Thus, perhaps cellularisation and the critically-balanced, aligned dynamics that I have described above are, in fact, the same thing said in two different languages. A clear translation between the two is, however, still to be articulated, especially the kind of translation that would add something genuinely new to our understanding of the subject.

8.3.3. Stochastic Reconnection

I have touted the joining of MHD turbulence and reconnection theories as a key outcome of the developments described in §§ 6–7, but of course there exists another school of thought for which this very connection has been the defining mantra for many years, but which has been almost entirely decoupled from those developments. This school of thought, vaguely anticipated already by [Matthaeus & Lamkin \(1985, 1986\)](#) (naturally so, given reconnection’s role in the cellularisation picture discussed in § 8.3.2), was properly launched by [Lazarian & Vishniac \(1999\)](#) when they put forward the notion of “stochastic reconnection”. Appendix D.7 is my attempt to review this topic (in which task I was greatly helped by its interpretation by [Eyink et al. 2011](#)) and its connection to, and lack of contradiction with, the main narrative presented above. Here I shall try to summarise it very briefly.

The notion of turbulent viscosity has been a mainstay of the theory of hydrodynamic turbulence for nearly as long as this theory has existed (see, e.g., the textbook by [Davidson 2015](#)). The idea is simply (but not trivially) that if we “coarse-grain” the velocity field at some scale λ in the middle of the inertial range (or even at the outer scale), the effect of all the motions at scales smaller than λ can be modelled, very crudely but surprisingly adequately, by an effective viscosity $\sim \delta u_\lambda \lambda$. This is because the hydrodynamic cascade is local and (in 3D) direct, so motions at scale λ are broken

up at the rate $\delta u_\lambda/\lambda = (\delta u_\lambda \lambda)/\lambda^2$, which can be viewed as a renormalised diffusion of momentum. The rate at which momentum and energy are removed from scale λ is entirely independent of the true molecular viscosity. In a similar way, an MHD “eddy” at the outer scale or in the inertial range (but not, according to § 7, in the tearing-mediated range) will lose both its momentum and its magnetic flux on a time scale (τ_{nl} , much discussed in the above) that is entirely independent of the true viscosity and resistivity of the MHD fluid (Eyink 2015 argues this with careful attention to detail). Thus, just like there is a turbulent viscosity, there is also a turbulent resistivity, and so a turbulent reconnection with an η -independent effective rate. This has some interesting and nontrivial consequences, both physical and mathematical, for a number of problems involving reconnection (see appendix D.7, the review by Lazarian *et al.* 2020, and references in both), but it does not mean that reconnection does not need η or small scales—just that those small scales are reached at an η -independent rate.

If the turbulent resistivity were isotropic in the plane perpendicular to the mean magnetic field, no alignment effect would be possible because the aligned structures would not need tearing to break up, and we would be back to § 8.2—no alignment, no tearing-mediated cascade, no need for this review. That is, essentially, the view of Lazarian *et al.* (2020). I cannot prove that this is wrong, but I think that it is unlikely (especially given the numerical evidence announced by Dong *et al.* 2021; see § 7.3). In appendix D.7.4, I show why it is not logically inevitable, i.e., how stochastic reconnection à la Lazarian, Vishniac, and Eyink can be reconciled with an aligned cascade.

PART II

Imbalances and Loose Ends

As we know,
 There are known knowns.
 There are things we know we know.
 We also know
 There are known unknowns.
 That is to say
 We know there are some things
 We do not know.
 But there are also unknown unknowns,
 The ones we don't know
 We don't know.

D. H. Rumsfeld,⁴¹
U.S. Department of Defense News Briefing,
 12 February 2002

In the remainder of this review, I will survey some of what has been done, what remains to be done, and what, in my view, is worth doing regarding the regimes of MHD turbulence in which there is an imbalance either between the energies of the two Elsasser fields or between the kinetic and magnetic energy. Such situations are relevant—and indeed often more relevant—in many astrophysical contexts, but remain much less (or even less) well understood, than the nice, if somewhat fictional, case in which one can just assume $\delta Z_\lambda^+ \sim \delta Z_\lambda^- \sim \delta b_\lambda \sim \delta u_\lambda$. Not only the cases of Elsasser (§ 9) and Alfvénic (§ 10) imbalance can be put in this class but also the distinct regimes of MHD turbulence

⁴¹ Set to verse by Seely (2003).

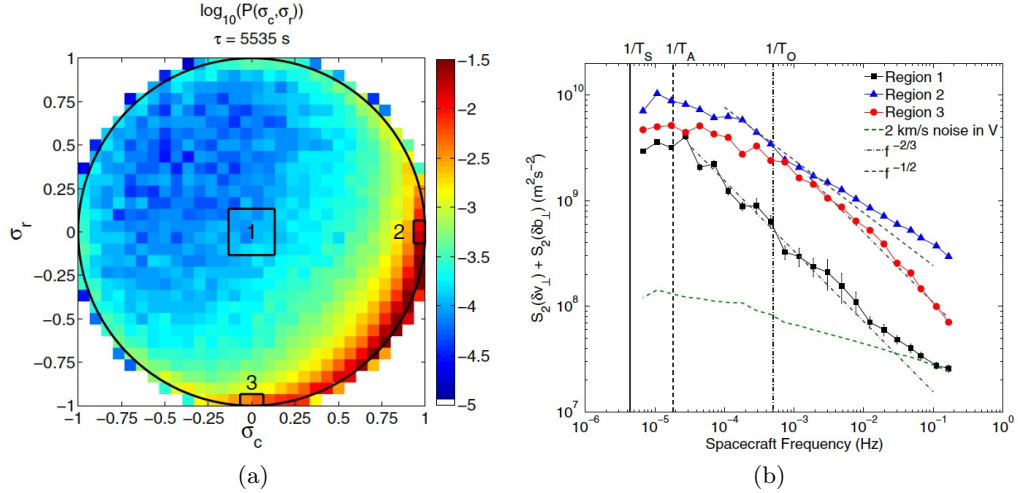


FIGURE 16. (a) Distribution of normalised cross-helicity (σ_c) and residual energy (σ_r) [defined in (B4)] in an interval of fast-solar-wind data taken by Wind spacecraft and analysed by Wicks *et al.* (2013b), from whose paper both plots in this figure are taken (©AAS, reproduced with permission). (b) Structure functions corresponding to the total energy (sum of kinetic and magnetic) conditioned on values of σ_c and σ_r and corresponding to Regions 1 (balanced), 2 (Elsasser-imbalanced), and 3 (Alfvénically imbalanced towards magnetic perturbations), indicated in panel (a). The $f^{-2/3}$ slope corresponds to a $k_\perp^{-5/3}$ spectrum, the $f^{-1/2}$ slope to a $k_\perp^{-3/2}$ one.

that arise below the viscous scale (assuming large P_m ; § 11), or when the turbulence is allowed to decay freely (§ 12), or when no mean field is imposed (the saturated MHD dynamo; § 13). For the reader’s reference, §§ 9.6, 10.4, 11, 12.6.2, and 13.3–13.4 contain some new results and arguments that have not been published elsewhere.

9. Imbalanced MHD Turbulence

9.1. Imbalance Global and Local

Since both incompressible MHD and RMHD conserve two invariants—the total energy and cross-helicity,—each of the two Elsasser fields Z_\perp^\pm has its own conserved energy [see (3.3)]. The energy fluxes ε^\pm of these fields are, therefore, independent parameters of MHD turbulence. Setting them equal to each other makes arguments simpler, but does not, in general, correspond to physical reality, for a number of reasons.

First, everyone’s favourite case of directly measurable MHD turbulence is the solar wind, where the Alfvénic perturbations propagating away from the Sun are launched from the Sun (Roberts *et al.* 1987), while the counterpropagating ones have to be supplied by some mechanism that is still under discussion and probably involves Alfvén-wave reflection as plasma density decreases outwards from the Sun (see Chandran & Perez 2019 and references therein). The counterpropagating component is usually energetically smaller, especially in the fast wind (Bruno & Carbone 2013; Chen *et al.* 2020).

Secondly—and, for a theoretical physicist interested in universality, more importantly—it is an intrinsic property of MHD turbulence to develop regions of *local* imbalance. This can be understood dynamically as a desire to evolve towards an Elsasser state, $Z_\perp^+ = 0$ or $Z_\perp^- = 0$, which is an exact solution of RMHD equations (confirmed in simulations of decaying RMHD turbulence; see § 12.7), or statistically as a tendency

for the local dissipation rates ε^\pm to fluctuate in space—a mainstay of intermittency theories since Landau’s famous objection (see Frisch 1995) to Kolmogorov (1941*b*) and the latter’s response in the form of the refined similarity hypothesis, accepting a fluctuating ε (Kolmogorov 1962) (the theories of intermittency for balanced MHD turbulence proposed by Chandran *et al.* 2015 and Mallet & Schekochihin 2017, skimmed through in § 6.4.2, were based on the same premise). In this context, a complete intermittency theory for MHD turbulence must incorporate whatever local modification (if any) of the MHD cascade is caused by $\varepsilon^+ \neq \varepsilon^-$, something that no existing theory has as yet accomplished or attempted. Another influential school of thought on the root causes of local imbalance connects it to a tendency for the cross-helicity to be less vigorously cascaded than energy, leading to local enhancements of $\mathbf{u}_\perp \cdot \mathbf{b}_\perp$ (see footnotes 15 and 16 and references therein).

That an intimate connection must exist between any verifiable theory of MHD turbulence and local imbalance is well illustrated (in figure 16) by the following piece of observational analysis, rather noteworthy, in my (not impartial) view. Wicks *et al.* (2013*b*) took a series of measurements by Wind spacecraft of magnetic and velocity perturbations in fast solar wind and sorted them according to the amount of imbalance, both Elsasser and Alfvénic (§ 10), at each scale. They then computed structure functions conditional on these imbalances. While the majority of perturbations were imbalanced one way or the other (or both), there was a sub-population with $\delta Z_\lambda^+ \sim \delta Z_\lambda^- \sim \delta b_\lambda \sim \delta u_\lambda$. Interestingly, the structure function restricted to this sub-population had what seemed to be a robust GS95 scaling (corresponding to a $k_\perp^{-5/3}$ spectrum), even though the structure functions of the imbalanced perturbations were consistent with Boldyrev’s $k_\perp^{-3/2}$ aligned-cascade scaling and indeed exhibited some alignment, unlike the GS95 population (although not necessarily an alignment with the theoretically desirable scale dependence: see footnote 21 and Wicks *et al.* 2013*a*; Podesta & Borovsky 2010 reported analogous results, conditioning on the presence of cross-helicity only). It is important to recognise that imbalance and alignment of Elsasser fields do not automatically imply each other, so balanced fluctuations are not absolutely required to be unaligned, or aligned fluctuations to be imbalanced (see appendix B.1). However, as I argued in § 6.4.2, dynamical alignment is an intermittency effect and so there may be a correlation between the emergence of imbalanced patches at ever smaller scales and Elsasser fields shearing each other into alignment (cf. Chandran *et al.* 2015).

Intuitively then, since patches of imbalance are locally ubiquitous even in globally balanced turbulence (Perez & Boldyrev 2009; see figure 17) and since the theory of balanced turbulence described in § 6.4 incorporates intermittency effects in the form of alignment, we might expect that this allows for local imbalance—and, therefore, that mildly imbalanced turbulence might look largely similar to the balanced one. Indeed, how would perturbations in the middle of inertial range “know” that the local imbalance they “see” is local rather than global? Obviously, on average, there will not be an imbalance and so the results for δZ_λ that one derives for balanced turbulence (§§ 6 and 7) are effectively averaged over the statistics of the stronger and weaker Elsasser fields—which of δZ_λ^+ and δZ_λ^- is which, depends on time and space.

If we now allow $\varepsilon^+ > \varepsilon^-$ on average, it becomes reasonable to expect $\delta Z_\lambda^+ > \delta Z_\lambda^-$ nearly everywhere or, at least, typically—unless $\varepsilon^+/\varepsilon^-$ is close enough to unity that fluctuations of local imbalance overwhelm the overall global one. In the latter case, presumably the global imbalance does not matter—at any rate, in the balanced considerations of §§ 6 and 7, we only ever required $\varepsilon^+ \sim \varepsilon^-$, rather than $\varepsilon^+ = \varepsilon^-$ exactly. What I am driving at here, perhaps with too much faffing about, is the rather obvious point that

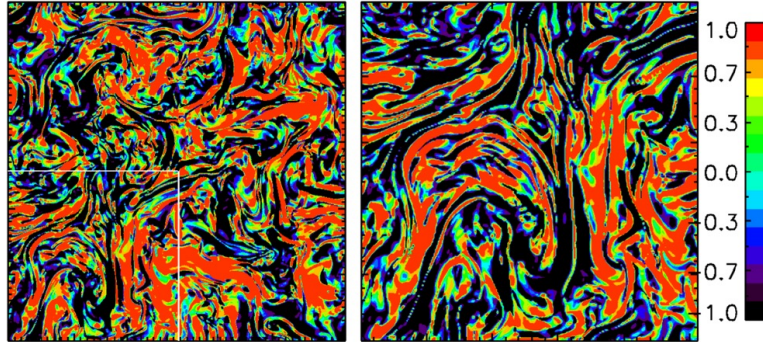


FIGURE 17. Cosine of the angle between increments $\delta\mathbf{u}_\lambda$ and $\delta\mathbf{b}_\lambda$ in the (x, y) plane, for $\lambda = L_\perp/6$ (left) and $\lambda = L_\perp/12$ (right, corresponding to the region demarcated by the white square within the left panel) in a balanced RMHD simulation by Perez & Boldyrev (2009) [reprinted with permission from Perez & Boldyrev (2009), copyright (2009) by the American Physical Society]. Since $\delta\mathbf{u}_\lambda \cdot \delta\mathbf{b}_\lambda = (|\delta\mathbf{Z}_\lambda^+|^2 - |\delta\mathbf{Z}_\lambda^-|^2)/4$, this is an illustration of patchy local imbalance, as well as of local alignment between the velocity and magnetic field.

it is only the limit of strong imbalance, $\varepsilon^+ \gg \varepsilon^-$, that can be expected to be physically distinct, in a qualitative manner, from the balanced regime.

9.2. Numerical and Observational Evidence

As usual, it is this most interesting limit that is also the hardest to resolve numerically and so we have little definitive information as to what happens in the strongly imbalanced regime. As in the case of the spectra of balanced turbulence, the debate about the numerical evidence regarding the imbalanced cascade and its correct theoretical interpretation has been dominated by the antagonistic symbiosis of Beresnyak and Boldyrev, so it is from their papers (Beresnyak & Lazarian 2008, 2009b, 2010; Beresnyak 2019; Perez & Boldyrev 2009, 2010a,b) that I derive much of the information reviewed below. Perez & Boldyrev (2010a,b) argue that large imbalances are unresolvable and refuse to simulate them. Beresnyak & Lazarian (2009b, 2010) do not necessarily disagree with this, but believe that useful things can still be learned from strongly imbalanced simulations, even if imperfectly resolved. Based (mostly) on both groups' simulations, imbalanced MHD turbulence appears to exhibit the following distinctive features (which I recount with a degree of confidence as they have been reproduced in two sets of independent, unpublished RMHD simulations by Mallet & Schekochihin 2011 and by Meyrand & Squire 2020).

(i) The stronger field has a steeper spectrum than the weaker one, with the former steeper and the latter shallower than the standard balanced-case spectra (figure 18a). However, it is fairly certain that these spectra are not converged with resolution: as resolution is increased, the tendency appears to be for the spectral slopes to get closer to each other, both when the imbalance is weak (Perez & Boldyrev 2010a) and when it is strong (Mallet & Schekochihin 2011). This led Perez & Boldyrev (2010a) to argue that numerical evidence was consistent with the two fields having the same spectral slope in the asymptotic limit of infinite Reynolds numbers. There is no agreement as to whether the two fields' spectra might be “pinned” (i.e., equal) to each other at the dissipation scale: yes, it seems, in weakly imbalanced simulations of Perez & Boldyrev (2010a), no in the strongly imbalanced ones of Beresnyak & Lazarian (2009b) and Meyrand & Squire (2020).⁴² In fact, in the latter studies, the dissipation scales of the two fields do not

⁴²Whereas the question of pinning may be subject to nontrivial discussion (Lithwick & Goldreich

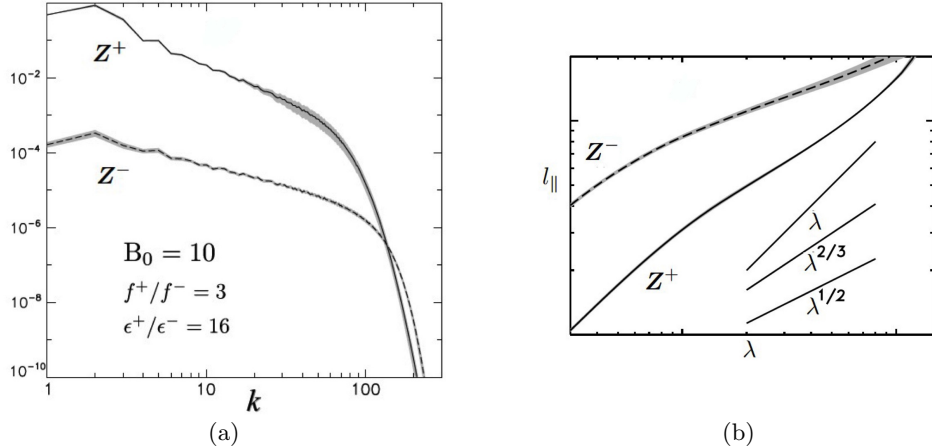


FIGURE 18. A typical MHD simulation with large imbalance: (a) spectra, (b) anisotropy, l_{\parallel}^{\pm} vs. λ . These plots are adapted from Beresnyak & Lazarian (2009b) (©AAS, reproduced with permission). Mallet & Schekochihin (2011) and Meyrand & Squire (2020) have qualitatively similar results (although the difference in slopes between the weaker and the stronger fields' spectra is much smaller in the higher-resolution simulations of Meyrand & Squire 2020—see an example of that in figure 35c, taken from Meyrand *et al.* 2021).

appear to be the same: larger for the stronger field, smaller for the weaker field (see figure 18a and figure 35c).

(ii) The ratio of stronger to weaker field's energies, a crude outer-scale quantity that Beresnyak & Lazarian (2008, 2009b, 2010) argue (reasonably, in my view) to be more likely to be numerically converged than inertial-range scalings, scales very strongly with $\varepsilon^+/\varepsilon^-$: it increases at least as fast as

$$\frac{\langle |\mathbf{Z}_\perp^+|^2 \rangle}{\langle |\mathbf{Z}_\perp^-|^2 \rangle} \sim \left(\frac{\varepsilon^+}{\varepsilon^-} \right)^2 \quad (9.1)$$

and possibly faster (which is inconsistent with the theory of Perez & Boldyrev 2009, another *casus belli* for the two groups; see § 9.4). Mallet & Schekochihin (2011, see figure 19) and Meyrand & Squire (2020) found the same scaling in their simulations for values of $\varepsilon^+/\varepsilon^-$ up to 10 (simulations with much higher imbalance are numerically suspect). In fact, early numerical evidence for (9.1) appears already in the (decaying) simulations of Verma *et al.* (1996) (see § 12.7).

(iii) According to Beresnyak & Lazarian (2008, 2009b) and Meyrand & Squire (2020), the stronger field is less anisotropic than the weaker one, in the sense that $l_{\parallel}^+ < l_{\parallel}^-$ and l_{\parallel}^+ drops faster with λ than l_{\parallel}^- (figure 18b). Beresnyak (2019) notes that this is true in

2003; Chandran 2008) in application to MHD turbulence with a viscous or resistive cutoff at small scales, it would appear that it is more straightforward in a collisionless plasma, e.g., in the solar wind. Indeed, there, the decoupling between the two Elsasser fields breaks down at the ion Larmor scale, where they are allowed to exchange energy (Schekochihin *et al.* 2009; Kunz *et al.* 2018) and, presumably, will not have very different typical amplitudes. Thus, an imbalanced turbulence theory with Larmor-scale pinning might be a desirable objective. If and when such an outcome proves impossible, this can have interesting implications for the very viability of a constant-flux cascade (and, at low beta, does, according to Meyrand *et al.* 2021: see § 14.2).

his simulations even though he forces the two fields with the same parallel scale, i.e., given an opportunity to keep $l_{\parallel}^+ = l_{\parallel}^-$, the system refuses to do so.

(iv) Mallet & Schekochihin (2011, see figure 19) found that the parallel spectrum of the weaker field (measured via its local-field-parallel structure function, as in § 5.3) was very robustly k_{\parallel}^{-2} —to be precise, the exponent varied between -1.9 and -2.1 , but in a manner that evinced no systematic dependence on $\varepsilon^+/\varepsilon^-$. For the stronger field, they found a gradual steepening of the parallel spectrum with higher imbalance.

(v) Beresnyak & Lazarian (2009b) found that the alignment angle between the Elsasser fields, defined as $\sin \theta$ in (B 1), with numerator and denominator averaged separately, decreased with scale roughly as $\lambda^{0.1}$, independently of the degree of imbalance. Mallet & Schekochihin (2011) measured the same exponent, quite robustly for a wide range of imbalances, but noticed also that the scaling exponent depended on the definition of the “alignment angle”: e.g., if root-mean-square numerator and denominator were used, the scaling was $\lambda^{0.2\dots 0.25}$, closer to the familiar theoretical result (6.20). This is not special to the imbalanced cascades—the same is true in balanced turbulence (Mallet *et al.* 2016).

(vi) The observational picture is only just emerging. A steeper scaling for the stronger field noted in item (i) appears to be consistent with the structure functions measured in the fast solar wind by, e.g., Wicks *et al.* (2011), although, besides this, they also exhibit low Alfvén ratio (see § 10), which simulations do not, and a rather-hard-to-interpret (or, possibly, to trust) scale dependence of the anisotropy. In contrast, Podesta & Borovsky (2010) report a scale-independent Elsasser ratio and $k^{-3/2}$ spectra for both fields in a number of reasonably imbalanced cases of solar-wind turbulence at 1 AU. The same result has been reported by Chen *et al.* (2020) from the very recent measurements by the Parker Solar Probe made closer to the Sun, where the imbalance gets larger ($\langle |\mathbf{Z}^+|^2 \rangle / \langle |\mathbf{Z}^-|^2 \rangle \approx 15$)—this may be damning for any theory or simulation where the two fields’ spectra scale differently, at least insomuch as these theories or simulations aspire to apply to the solar wind.

(vii) As the solar wind offers practically the only chance of observational testing of theory—a chance greatly enhanced by the launch of the Parker Solar Probe—there is a growing industry of direct numerical modelling of the generation of inward-propagating (\mathbf{Z}^-) perturbations by reflection of the outward-propagating ones (\mathbf{Z}^+), which is what is supposed to happen in the expanding solar wind. The latest and most sophisticated study of this kind is Chandran & Perez (2019) (who also provide an excellent overview of previous work). Their results appear to be quite different from the idealised periodic-box, artificially-forced studies discussed above: the stronger field’s spectrum is actually *shallower* than the weaker one’s (sometimes as shallow as k^{-1}), but both asymptote towards $k^{-3/2}$ with increasing heliocentric distance—good news for modelling, in view of what Chen *et al.* (2020) have found. Chandran & Perez (2019) acknowledge, however, that they can break these results by fiddling with how their turbulence is forced in the photosphere. Thus, the nature of large-scale energy injection appears to matter,⁴³ at least at finite resolutions, perhaps reinforcing the doubts expressed above about the convergence of even the more idealised simulations.

For a short while still, the field appears set to remain open to enterprising theoreticians.

⁴³Chandran & Perez (2019) have a theory as to why that is, which will be explained in § 9.3.

$\varepsilon^+/\varepsilon^-$	μ_\perp^+	μ_\parallel^+	μ_\perp^-	μ_\parallel^-	R_E
1	-1.6	-1.9	-1.6	-1.9	1
2	-1.6	-1.9	-1.5	-2.0	5
5	-1.8	-2.0	-1.5	-2.0	35
8	-1.8	-2.1	-1.5	-2.0	45
10	-1.9	-2.2	-1.4	-2.1	110
100	-2.3	-2.3	-1.4	-2.0	2200
1000	-2.5	-2.6	-1.3	-2.0	13000

FIGURE 19. Scalings found in (unpublished) 512^3 RMHD numerical simulations by [Mallet & Schekochihin \(2011\)](#): perpendicular (parallel) spectral indices μ_\perp (μ_\parallel) (inferred from structure functions calculated as explained in §5.3) for both fields, denoted by the \pm superscripts. In terms of the scaling exponents $\gamma_{\perp,\parallel}^\pm$ of the field increments ($\delta Z_\lambda^\pm \propto \lambda^{\gamma_\perp^\pm}$, $\delta Z_{l_\parallel}^\pm \propto l_\parallel^{\gamma_\parallel^\pm}$), these are $\mu_{\perp,\parallel}^\pm = -2\gamma_{\perp,\parallel}^\pm - 1$. The last column shows the overall Elsasser ratio $R_E = \langle |\mathbf{Z}_\perp^+|^2 \rangle / \langle |\mathbf{Z}_\perp^-|^2 \rangle$. The parallel scalings of the weaker field were converged with resolution, while the perpendicular scalings of the stronger (weaker) field at $\varepsilon^+/\varepsilon^- = 10$ became shallower (steeper) as resolution was increased from 256^3 to 512^3 to $1024^2 \times 512$; the parallel scaling of the stronger field also appeared to become shallower. Simulations with $\varepsilon^+/\varepsilon^- = 100, 1000$ should be viewed as numerically suspect.

9.3. [Lithwick et al. \(2007\)](#)

In what follows, in view of the discussion in §6.1 and in appendix B.2, I shall stick with my use of the Elsasser-field alignment angle θ in the expression (6.4) for τ_{nl}^\pm . This angle is obviously the same for both fields, so

$$\tau_{nl}^\pm \sim \frac{\lambda}{\delta Z_\lambda^\mp \sin \theta_\lambda} \quad \Rightarrow \quad \frac{\tau_{nl}^+}{\tau_{nl}^-} \sim \frac{\delta Z_\lambda^+}{\delta Z_\lambda^-} > 1, \quad (9.2)$$

i.e., the cascade of the stronger field is slower (because it is advected by the weaker field). Assuming nevertheless that both cascades are strong, we infer immediately

$$\frac{(\delta Z_\lambda^\pm)^2}{\tau_{nl}^\pm} \sim \varepsilon^\pm \quad \Rightarrow \quad \frac{\delta Z_\lambda^+}{\delta Z_\lambda^-} \sim \frac{\varepsilon^+}{\varepsilon^-}. \quad (9.3)$$

Thus, the two fields' increments have the same scaling with λ (the same k_\perp spectra) and the ratio of their energies is $\sim (\varepsilon^+/\varepsilon^-)^2$, in agreement with (9.1). This is the conclusion at which [Lithwick et al. \(2007\)](#), henceforth LGS07 arrived—they considered unaligned GS95-style turbulence ($\sin \theta \sim 1$), but that does not affect (9.3) [note that this result already appeared in (5.4)].

Things are, however, not as straightforward as they might appear. LGS07 point out that it is, in fact, counterintuitive that the weaker δZ_λ^- perturbation, which is distorted by δZ_λ^+ on a shorter time scale τ_{nl}^+ , can nevertheless coherently distort δZ_λ^+ for a longer time τ_{nl}^+ . Their solution to this is to argue that, while the weaker field is strongly distorted *in space* by the stronger one, it remains correlated *in time* for as long as the stronger field does (coherence time of the long-correlated advector inherited by the advectee). In other words, during its (long) correlation time τ_{nl}^+ , the stronger field (in its reference frame travelling at v_A) sees a weak field that has been rendered multiscale by the spatial variation of the stronger field, but remains approximately constant for a time τ_{nl}^+ and so can keep distorting the stronger field in a time-coherent way.

This argument can only work, it seems, if the long-term coherence of the weaker field

is not upset by the way in which it is forced, so one must assume that it is forced at the outer scale with the same (long!) correlation time as the cascade time of the stronger field, in the Alfvénic frame of the latter. [Chandran & Perez \(2019\)](#) dub this the “coherence assumption”. While hard to justify in general,⁴⁴ it is great for them as, in their model, the weaker field is generated by the reflection of the stronger one as the latter propagates outwards in an expanding solar wind, and so one should indeed expect the two fields to be tightly correlated at the outer scale. Their endorsement of LGS07—perhaps with an amendment that θ_λ should have some scaling with λ determined by alignment/intermittency ([§ 6.4.2](#))—is backed up by their numerical results, where both fields’ spectra approach $k_\perp^{-3/2}$ (and their alignment increases) with increasing heliocentric distance.

9.4. *Perez & Boldyrev (2009)*

[Perez & Boldyrev \(2009\)](#) disagree with the entire approach leading to ([9.3](#)): they think that the two Elsasser fields should have two different alignment angles θ_λ^\pm , both small, and posit that those ought to be the angles that they make with the velocity field.⁴⁵ Why that should be the case they do not explain, but if one takes their word for it, then (as is obvious from the geometry in figure [38](#))

$$\delta Z_\lambda^+ \sin \theta_\lambda^+ \sim \delta Z_\lambda^- \sin \theta_\lambda^- \quad \Rightarrow \quad \tau_{\text{nl}}^+ \sim \tau_{\text{nl}}^- \sim \frac{\lambda}{\delta Z_\lambda^\pm \sin \theta_\lambda^\pm} \quad \Rightarrow \quad \frac{\delta Z_\lambda^+}{\delta Z_\lambda^-} \sim \sqrt{\frac{\varepsilon^+}{\varepsilon^-}}. \quad (9.4)$$

The last result follows from the first relation in ([9.3](#)) with $\tau_{\text{nl}}^+ \sim \tau_{\text{nl}}^-$. The equality of cascade times also conveniently spares them having to deal with the issue, discussed above, of long-time correlatedness, or otherwise, of the weaker field (or with $l_\parallel^+ \neq l_\parallel^-$; see [§ 9.5](#)).

[Perez & Boldyrev \(2009, 2010a,b\)](#) are not forthcoming with any detailed tests of this scheme (viz., either of the details of alignment or of the energy-ratio scaling), while [Beresnyak & Lazarian \(2010\)](#) present numerical results that contradict very strongly the expectation of the energy ratio scaling as $\varepsilon^+/\varepsilon^-$ [as implied by ([9.4](#))] and possibly

⁴⁴It is, however, worth pointing out in this context a curious result reported by [Lugones et al. \(2019\)](#): they studied frequency-wavenumber spectra of externally forced (not reflection-driven) imbalanced MHD turbulence and spotted, in some of their runs (those, it seems to me, that were more likely to have been in a strong-turbulence regime), that, counterintuitively, the weaker field moved in the same direction as the stronger one, implying perhaps just the kind of coherence that LGS07 conjectured, without reflection driving. [Lugones et al. \(2019\)](#) interpret this result in terms of reflections off inhomogeneities of the local mean field, but perhaps that is another way of saying the same thing—that the weaker field gets locked into long-time coherence with the stronger one.

⁴⁵[Podesta & Bhattacharjee \(2010\)](#) base their theory on the same assumption (also unexplained), but have a different scheme for generalising Boldyrev’s aligned cascade to the imbalanced regime. They imagine the geometric configuration of the fields to be such that $|\delta \mathbf{u}_\lambda| = |\delta \mathbf{b}_\lambda|$ and, consequently, $\delta \mathbf{Z}_\lambda^+$ and $\delta \mathbf{Z}_\lambda^-$ are perpendicular to each other. This does not appear to be what actually happens, at least in simulations [see [§ 9.2](#), item (v)]. [Podesta & Bhattacharjee \(2010\)](#) also inherit from Boldyrev’s original construction the incompatibility of their scalings with the RMHD symmetry (see [§ 6.4.1](#)). There is an interesting angle in their paper though: they notice, in solar-wind observations, that the probabilities with which aligned or anti-aligned (in the sense of the sign of $\delta \mathbf{u}_\lambda \cdot \delta \mathbf{b}_\lambda$) perturbations occur are independent of scale throughout the inertial range; they then use the ratio of these probabilities as an extra parameter in the theory. This is a step in the direction of incorporating patchy imbalance into the game—something that seems important and inevitable.

support $(\varepsilon^+/\varepsilon^-)^2$ [i.e., (9.3)].⁴⁶ Perez & Boldyrev (2010b) reply that (9.4) should only be expected to hold for local fluctuating values of the amplitudes and of ε^\pm and not for their box averages. It is not impossible that this could make a difference for cases of weak imbalance ($\varepsilon^+/\varepsilon^- \sim 1$), with local fluctuations of energy fluxes superseding the overall imbalance, although it seems to me that if it does, we are basically dealing with balanced turbulence anyway: I do not see any fundamental physical difference between $\varepsilon^+ = \varepsilon^-$ and $\varepsilon^+ \sim \varepsilon^-$ on the level of “twiddle” arguments by which everything is done in these theories. At strong imbalance, (9.3) seems to work better (Beresnyak & Lazarian 2009b, 2010) for the overall energy ratio, but not for spectra, which do not have the same slope (figure 18a). Perez & Boldyrev (2010a,b) argue that such cases in fact cannot be properly resolved, the limiting factor being the weaker field providing too slow a nonlinearity to compete with dissipation and produce a healthy inertial range. If so, the interesting case is inaccessible and the accessible case is uninteresting, we know nothing.

9.5. Parallel Scales and Two Flavours of CB

By the CB conjecture (§ 5.1), the parallel coherence lengths of the two fields are, in the “naïve” theory leading to (9.3),

$$l_\parallel^\pm \sim v_A \tau_{nl}^\pm \quad \Rightarrow \quad \frac{l_\parallel^+}{l_\parallel^-} \sim \frac{\varepsilon^+}{\varepsilon^-} > 1, \quad (9.5)$$

whereas in the Perez & Boldyrev (2009) theory (9.4), the equality of cascade times implies $l_\parallel^+ \sim l_\parallel^-$, end of story. LGS07 argue that, in fact, also (9.5) should be replaced by

$$l_\parallel^+ \sim l_\parallel^- \sim v_A \tau_{nl}^- \quad (9.6)$$

because Z_\perp^+ perturbations separated by distance l_\parallel^- in the parallel direction are advected by completely spatially decorrelated Z_\perp^- perturbations, which would then imprint their parallel coherence length on their stronger cousins (the parallel coherence length of the short-correlated advector imprinted on the advectee).

Furthermore, if one accepts the LGS07 argument that the correlation time of the Z_\perp^- field is τ_{nl}^+ , not τ_{nl}^- (see § 9.3), then $l_\parallel^- \sim v_A \tau_{nl}^-$ must be justified not by temporal (causal) decorrelation but by the weaker field being spatially distorted beyond recognition on the scale l_\parallel^- , even if remaining temporally coherent. This is more or less what Beresnyak & Lazarian (2008) call “propagation CB” (the other CB being “causality CB”). They note that the typical uncertainty in the parallel gradient of any fluctuating field at scale λ is

$$\delta k_\parallel \sim \frac{\mathbf{b}_\perp \cdot \nabla_\perp}{v_A} \sim \frac{\delta b_\lambda}{\xi_\lambda v_A}. \quad (9.7)$$

In balanced turbulence, $\delta k_\parallel^{-1} \sim v_A \tau_{nl} \sim l_\parallel$ [cf. (6.32)], so this is just a consistency check. In imbalanced turbulence,

$$\delta b_\lambda \sim \delta Z_\lambda^+ \quad \Rightarrow \quad \delta k_\parallel^{-1} \sim \frac{\xi_\lambda v_A}{\delta Z_\lambda^+} \sim v_A \tau_{nl}^-, \quad (9.8)$$

where τ_{nl}^- , given by (9.2), is the spatial-distortion time of δZ_λ^- , not necessarily its correlation time. The parallel scale of any field will be the shorter of δk_\parallel^{-1} and whatever

⁴⁶ Podesta (2011) collated both groups’ data and concluded that the results of Perez & Boldyrev (2010b) were entirely compatible with Beresnyak & Lazarian (2010) and with (9.1).

is implied by the causality CB. In the LGS07 theory, the latter is $v_A \tau_{\text{nl}}^+$ for both fields. Since $\tau_{\text{nl}}^+ \gg \tau_{\text{nl}}^-$, we must set $l_{\parallel}^+ \sim l_{\parallel}^- \sim \delta k_{\parallel}^{-1}$, which is the same as (9.6).

Thus, we end up with both Elsasser fields having $\tau_A \sim l_{\parallel}^- / v_A$ that is smaller than their correlation time τ_{nl}^+ (even though the weaker field has a shorter spatial distortion time $\tau_{\text{nl}}^- \sim \tau_A$), but their cascades are nevertheless strong. Whatever you think of the merits of the above arguments, neither (9.5) nor (9.6) appear to be consistent with any of the cases reported by Beresnyak & Lazarian (2009b), weakly or strongly imbalanced, which all have $l_{\parallel}^+ < l_{\parallel}^-$ (see, e.g., figure 18b). No other numerical evidence on the parallel scales in imbalanced turbulence is, as far as I know, available in print.

9.6. Towards a New Theory of Imbalanced MHD Turbulence

The Beresnyak & Lazarian (2008) argument was, in fact, more complicated than presented in § 9.5, because they did not agree with LGS07 about the long correlation time of the weaker field, assumed the stronger field to be weakly, rather than strongly, turbulent, and were keen to accommodate $l_{\parallel}^+ < l_{\parallel}^-$. Their key innovation was to allow interactions to be nonlocal. I will not review their theory here, because it depends on a number of *ad hoc* choices that I do not know how to justify, and does not, as far as I can tell, lead to a fully satisfactory set of predictions, but I would like to seize on their idea of nonlocality of interactions, although in a way that is somewhat different from theirs. The resulting scheme captures most of the properties of imbalanced turbulence observed in numerical simulations (§ 9.2) and reduces to the already established theory for the balanced case when $\varepsilon^+ / \varepsilon^- \sim 1$, so perhaps it deserves at least some benefit of the doubt.

9.6.1. Two Semi-Local Cascades

Let me assume *a priori* that, as suggested by numerics (Beresnyak & Lazarian 2009b; Beresnyak 2019), $l_{\parallel}^+ \ll l_{\parallel}^-$ in the inertial range, viz.,

$$\frac{l_{\parallel\lambda}^+}{l_{\parallel\lambda}^-} \sim \left(\frac{\lambda}{L_{\perp}} \right)^{\alpha}, \quad (9.9)$$

where $\alpha > 0$ and L_{\perp} is the perpendicular outer scale (so the two Elsasser fields are assumed to have the same parallel correlation length, L_{\parallel} , at the outer scale—e.g., by being forced that way, as was done by Beresnyak 2019).

This implies that, at the same λ , the stronger field δZ_{λ}^+ oscillates much faster than the weaker field δZ_{λ}^- . I shall assume therefore that the interaction between the two fields local to the scale λ is not efficient: even though δZ_{λ}^- is buffeted quite vigorously by the stronger field δZ_{λ}^+ , most of this cancels out. Rather than attempting to pick up a contribution arising for the resulting weak interaction, let me instead posit that the dominant, strong nonlinear distortion of δZ_{λ}^- will be due to the stronger field $\delta Z_{\lambda'}^+$ at a scale $\lambda' > \lambda$ such that

$$l_{\parallel\lambda'}^+ \sim l_{\parallel\lambda}^-. \quad (9.10)$$

In other words, the interaction is nonlocal in λ but local in l_{\parallel} .⁴⁷ The constancy of the

⁴⁷Beresnyak & Lazarian (2008) proposed the same, but to describe *weak* cascading of $\delta Z_{\lambda'}^+$ by δZ_{λ}^- . Thus, their cascade of the stronger field is weak and nonlocal and that of the weaker field is strong and local. In the scheme I am proposing here, both cascades are strong and it is the weaker field's one that is nonlocal.

flux of the weaker field then requires

$$\frac{(\delta Z_\lambda^-)^2 \delta Z_{\lambda'}^+}{\xi_{\lambda'}} \sim \varepsilon^-, \quad (9.11)$$

where $\xi_{\lambda'}$ has been introduced to account for a possible depletion of the nonlinearity due to alignment:

$$\frac{\xi_{\lambda'}}{L_\perp} \sim \left(\frac{\lambda'}{L_\perp} \right)^\beta. \quad (9.12)$$

In the absence of alignment, $\beta = 1$. For aligned, balanced, locally cascading ($\lambda' \sim \lambda$) turbulence, $\beta = 3/4$ [see (6.31)]. By the usual CB argument, the parallel coherence scale of the weaker field is

$$l_{\parallel\lambda}^- \sim \frac{v_A \xi_{\lambda'}}{\delta Z_{\lambda'}^+}. \quad (9.13)$$

Note that, in the terminology of §9.5, this is both the causality CB and the propagation CB, because δk_\parallel for δZ_λ^- is determined by the propagation of the latter along the “local mean field” $\delta b_{\lambda'}$ [see (9.7)].

Now consider the cascading of the stronger field by the weaker one. Since $l_{\parallel\lambda}^+ \ll l_{\parallel\lambda}^-$, the δZ_λ^- fluctuations are, from the point of view of the δZ_λ^+ ones, slow and quasi-2D, and so the weaker field can cascade the strong one locally, in the same way as it does in any of the theories described above:

$$\frac{(\delta Z_\lambda^+)^2 \delta Z_\lambda^-}{\xi_\lambda} \sim \varepsilon^+. \quad (9.14)$$

Causality CB would imply $l_{\parallel\lambda}^+ \sim v_A \xi_\lambda / \delta Z_\lambda^-$, but that is long compared to δk_\parallel^{-1} given by (9.7), so I shall use propagation CB instead, just like LGS07 and Beresnyak & Lazarian (2008) did:

$$l_{\parallel\lambda}^+ \sim \frac{v_A \xi_\lambda}{\delta Z_\lambda^+}. \quad (9.15)$$

Reassuringly, this choice immediately clicks into consistency with the requirement of parallel locality (9.10) if $l_{\parallel\lambda}^-$ is given by (9.13).

There are two nuances here. First, in order for the δZ_λ^- field to be able to distort δZ_λ^+ according to (9.14), it needs to remain coherent for a time $\sim \xi_\lambda / \delta Z_\lambda^-$. To make it do so, let me invoke the LGS07 argument already rehearsed in §9.3: according to (9.11), δZ_λ^- stays coherent as long as $\delta Z_{\lambda'}^+$ does, which, according to (9.14) with $\lambda = \lambda'$, is $\xi_{\lambda'} / \delta Z_{\lambda'}^+$ —long enough!

Secondly, in (9.14), I used the same fluctuation-direction scale ξ_λ as in (9.11), except at λ , rather than at λ' . This may be a somewhat simplistic treatment of alignment in local vs. nonlocal interactions, but I do not know how to do better, and the scalings that I get this way will have all the right properties. A reader who finds this unconvincing may assume $\xi_\lambda \sim \lambda$ and treat what follows as a GS95-style theory that ignores alignment altogether.

To summarise, I am considering here an imbalanced turbulence that consists of two “semi-local” cascades: that of the stronger field, local in λ but not in l_\parallel , and that of the weaker one, local in l_\parallel but not in λ (figure 20).

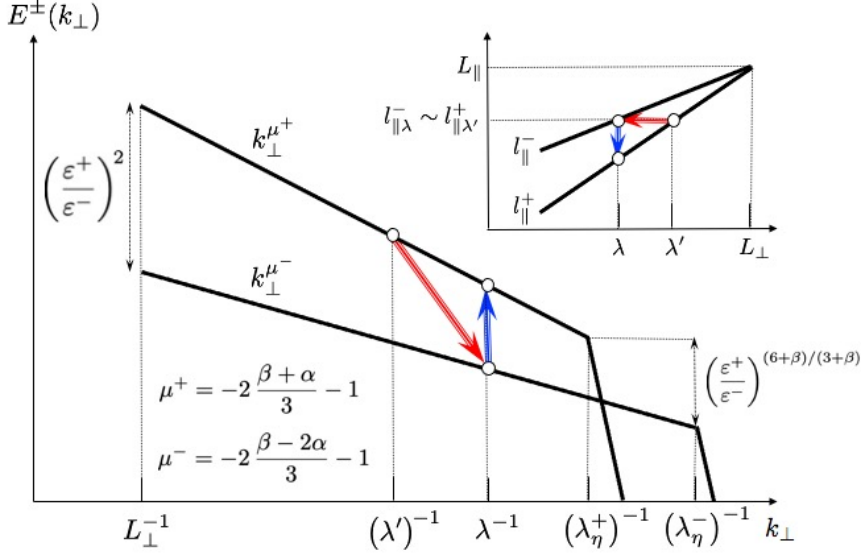


FIGURE 20. Cartoon of the spectra of imbalanced turbulence. The interactions are shown by arrows: red (advection of the weaker field by the stronger field, nonlocal in λ but local in l_{\parallel}) and blue (advection of the stronger field by the weaker field, local in λ but nonlocal in l_{\parallel}). The inset shows the parallel scales l_{\parallel}^{\pm} vs. the perpendicular scale λ .

9.6.2. Perpendicular Spectra

In view of (9.13) and (9.15), (9.11) can be rewritten as follows:

$$\frac{(\delta Z_{\lambda}^-)^2 \delta Z_{\lambda}^+}{\xi_{\lambda}} \sim \varepsilon^{-} \frac{\xi_{\lambda'} \delta Z_{\lambda}^+}{\xi_{\lambda} \delta Z_{\lambda'}^+} \sim \varepsilon^{-} \frac{l_{\parallel \lambda}^-}{l_{\parallel \lambda'}^+} \sim \varepsilon^{-} \left(\frac{\lambda}{L_{\perp}} \right)^{-\alpha}, \quad (9.16)$$

the last step being a recapitulation of the assumption (9.9). Dividing (9.14) by (9.16), one gets

$$\frac{\delta Z_{\lambda}^+}{\delta Z_{\lambda}^-} \sim \frac{\varepsilon^+}{\varepsilon^-} \left(\frac{\lambda}{L_{\perp}} \right)^{\alpha}. \quad (9.17)$$

Thus, the ratio of the energies at the outer scale ($\lambda = L_{\perp}$) is $(\varepsilon^+/\varepsilon^-)^2$, likely the correct scaling [see § 9.2, item (ii) and § 9.4], and the spectrum of the stronger field is steeper than that of the weaker field, also in agreement with numerics [§ 9.2, item (i)].

Now, by using (9.14), (9.17) and the alignment assumption (9.12), it becomes possible to determine the scalings of both fields:

$$\delta Z_{\lambda}^+ \sim \left[\frac{(\varepsilon^+)^2}{\varepsilon^-} L_{\perp} \right]^{1/3} \left(\frac{\lambda}{L_{\perp}} \right)^{(\beta+\alpha)/3}, \quad \delta Z_{\lambda}^- \sim \left[\frac{(\varepsilon^-)^2}{\varepsilon^+} L_{\perp} \right]^{1/3} \left(\frac{\lambda}{L_{\perp}} \right)^{(\beta-2\alpha)/3}. \quad (9.18)$$

Comparing the first of these with (9.11), one can also work out how nonlocal the interactions are:

$$\frac{\lambda}{\lambda'} \sim \left(\frac{\lambda}{L_{\perp}} \right)^{3\alpha/(2\beta-\alpha)}. \quad (9.19)$$

With $\alpha = 0$ and $\beta = 1$ in (9.18), we are back to GS95 (§ 5.3), whereas with $\alpha = 0$ and $\beta = 3/4$, we recover the aligned theory of § 6.4.

9.6.3. Parallel Spectra

Now, from (9.15), (9.12), (9.18), and (9.9), the parallel scales are

$$\frac{l_{\parallel\lambda}^+}{L_{\parallel}} \sim \left(\frac{\lambda}{L_{\perp}} \right)^{(2\beta-\alpha)/3}, \quad \frac{l_{\parallel\lambda}^-}{L_{\parallel}} \sim \left(\frac{\lambda}{L_{\perp}} \right)^{2(\beta-2\alpha)/3}, \quad (9.20)$$

where the parallel outer scale is [cf. (6.16)]

$$L_{\parallel} = v_A L_{\perp}^{2/3} \left[\frac{(\varepsilon^+)^2}{\varepsilon^-} \right]^{-1/3}. \quad (9.21)$$

Combining (9.20) with (9.18) gives us the parallel scalings of the field increments:

$$\delta Z_{l_{\parallel}}^+ \sim \left[\frac{(\varepsilon^+)^2 L_{\parallel}}{\varepsilon^- v_A} \right]^{1/2} \left(\frac{l_{\parallel}}{L_{\parallel}} \right)^{(\beta+\alpha)/(2\beta-\alpha)}, \quad \delta Z_{l_{\parallel}}^- \sim \left(\frac{\varepsilon^- l_{\parallel}}{v_A} \right)^{1/2}. \quad (9.22)$$

Whereas the stronger field's scaling is (for small α , slightly) steeper than $l_{\parallel}^{1/2}$, the weaker one's is exactly that, corresponding to a k_{\parallel}^{-2} spectrum, as is indeed seen in numerical simulations [§ 9.2, item (iv) and figure 19]. This makes sense because the weaker field was assumed to have a local parallel cascade with the usual CB conjecture, so the standard arguments for its parallel spectrum given in § 5.2 remain valid.

9.6.4. Pinning

It turns out that it is possible to determine α by considering what happens at the dissipation scale(s). The dissipation cutoffs λ_{η}^{\pm} for the two Elsasser fields can be worked out by balancing their fluxes with their dissipation rates:

$$\varepsilon^{\pm} \sim \frac{\nu + \eta}{(\lambda_{\eta}^{\pm})^2} \left(\delta Z_{\lambda_{\eta}^{\pm}}^{\pm} \right)^2. \quad (9.23)$$

Using (9.18) to work out the field amplitudes at λ_{η}^{\pm} , one gets

$$\frac{\lambda_{\eta}^+}{L_{\perp}} \sim \left(\frac{\varepsilon^-}{\varepsilon^+} \widetilde{\text{Re}} \right)^{-1.5/(3-\beta-\alpha)}, \quad \frac{\lambda_{\eta}^-}{L_{\perp}} \sim \widetilde{\text{Re}}^{-1.5/(3-\beta+2\alpha)}, \quad \widetilde{\text{Re}} = \frac{\delta Z_{L_{\perp}}^+ L_{\perp}}{\nu + \eta}, \quad (9.24)$$

where, as before, $\widetilde{\text{Re}}$ is the smaller of Re and Rm . There are two possibilities: either $\lambda_{\eta}^+ < \lambda_{\eta}^-$ or $\lambda_{\eta}^+ > \lambda_{\eta}^-$. The first of these is, in fact, impossible: if the weaker field is cut off at λ_{η}^- , there is nothing to cascade the stronger field at $\lambda < \lambda_{\eta}^-$ (locally in λ , as I assumed in § 9.6.1). The second possibility is $\lambda_{\eta}^+ > \lambda_{\eta}^-$. Since the weaker field is cascaded by the stronger one nonlocally, a self-consistent situation would be one in which λ_{η}^+ were the scale λ' corresponding to $\lambda = \lambda_{\eta}^-$. Using (9.19), we must therefore “pin” the dissipation scales together in the following way:

$$\frac{\lambda_{\eta}^+}{L_{\perp}} \sim \left(\frac{\lambda_{\eta}^-}{L_{\perp}} \right)^{2(\beta-2\alpha)/(2\beta-\alpha)} \Rightarrow 1 - \frac{2(\beta-2\alpha)(3-\beta-\alpha)}{(2\beta-\alpha)(3-\beta+2\alpha)} = \frac{\ln(\varepsilon^+/\varepsilon^-)}{\ln \widetilde{\text{Re}}}. \quad (9.25)$$

Assuming $\alpha \ll 1$, we get

$$\alpha \approx \frac{2(3-\beta)\beta}{3(3+\beta)} \frac{\ln(\varepsilon^+/\varepsilon^-)}{\ln \widetilde{\text{Re}}}. \quad (9.26)$$

Thus, indeed, $\alpha \rightarrow 0$ as $\widetilde{\text{Re}} \rightarrow \infty$, but very slowly, with very large $\widetilde{\text{Re}}$ needed to achieve a modicum of asymptoticity at larger imbalances. For the record, this implies, from (9.24),

$$\frac{\lambda_\eta^+}{L_\perp} \sim \widetilde{\text{Re}}^{-1.5/(3-\beta)} \left(\frac{\varepsilon^+}{\varepsilon^-} \right)^{0.5(9+\beta)/(9-\beta^2)}, \quad \frac{\lambda_\eta^-}{L_\perp} \sim \widetilde{\text{Re}}^{-1.5/(3-\beta)} \left(\frac{\varepsilon^+}{\varepsilon^-} \right)^{2\beta/(9-\beta^2)}. \quad (9.27)$$

It actually does appear to be the case that $\lambda_\eta^+ > \lambda_\eta^-$ in figure 18(a) (Beresnyak & Lazarian 2009b) and figure 35(c) (Meyrand *et al.* 2021)—perhaps the strongest evidence that we have of the nonlocality of imbalanced cascades.

While what I have proposed above is a kind of “pinning,” it is not the conventional “pinning” that means equating the amplitudes of the two fields to each other at the dissipation scale—one of the tenets of the theory of weak imbalanced turbulence (§ 4.3). Indeed, (9.23) implies that the ratio of the Elsasser amplitudes at their respective dissipation scales is

$$\frac{\delta Z_{\lambda_\eta^+}^+}{\delta Z_{\lambda_\eta^-}^-} \sim \sqrt{\frac{\varepsilon^+}{\varepsilon^-}} \frac{\lambda_\eta^+}{\lambda_\eta^-} \sim \left(\frac{\varepsilon^+}{\varepsilon^-} \right)^{(3+\beta)/2}, \quad (9.28)$$

where I have used (9.27), valid in the limit $\widetilde{\text{Re}} \rightarrow \infty$. Notably, the amplitude ratio is independent of $\widetilde{\text{Re}}$ in this limit, but is not equal to $(\varepsilon^+/\varepsilon^-)^{1/2}$, as one might have concluded from (9.23) for $\lambda_\eta^+ = \lambda_\eta^-$ (as Beresnyak & Lazarian 2008 did).

Arguably, this is a rather attractive theory: asymptotically, the spectra are parallel, interactions are local, etc., but in any finite-width inertial range, there are finite- Re logarithmic corrections to scalings, locality, etc., accounting for all of the distinctive features of imbalanced turbulence seen in non-asymptotic simulations (§ 9.2).

9.6.5. Alignment, Intermittency, Reconnection

Like in balanced turbulence, alignment is likely related to intermittency in imbalanced turbulence as well. Since, for imbalanced turbulence, we are still litigating such basic things as spectra, there is not much we know about its intermittency—and I do not propose to engage with this topic here any more than I have done already with a few throw-away comments in § 9.1. The argument in § 6.4.2 that led to $\beta = 3/4$ depended on assumptions about the most intense structures being sheets and on the “refined critical balance” (Mallet *et al.* 2015, see figure 6). It seems a worthwhile project to check whether, and in what sense, these features survive in imbalanced turbulence.

Since reconnection playing an important role at the small-scale end of the inertial range depended on alignment, the equivalent of § 7 for imbalanced turbulence must wait for a better understanding of alignment. If tearing disruption does occur at some scale in (strongly) imbalanced turbulence, the pinning scheme proposed in § 9.6.4 has to be redesigned. Incidentally, it also has to be redesigned (according to Meyrand *et al.* 2021, redesigned quite dramatically) for natural plasmas like the solar wind, where the cutoff of the RMHD inertial range is accomplished by kinetic effects rather than by Laplacian viscosity—but these matters are outside the scope of this review (see §§ 14.1 and 14.2).

10. Residual Energy in MHD Turbulence

10.1. Observational and Numerical Evidence

Going back to figure 16(a), we see that real MHD turbulence observed in the solar wind is distributed between cases with a local Elsasser imbalance (cross-helicity) and those

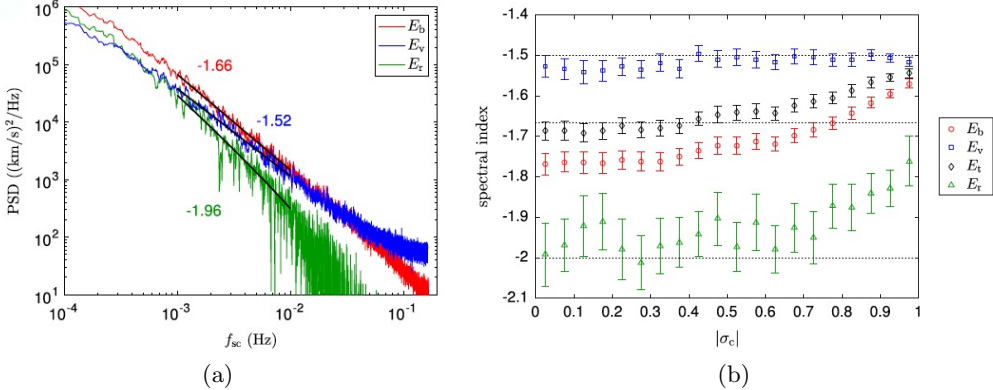


FIGURE 21. Spectra of magnetic (red), kinetic (blue), total (black) and residual (green) energies measured by [Chen et al. \(2013\)](#) (figures taken from [Chen 2016](#)): (a) typical spectra; (b) average spectral indices vs. normalised cross-helicity σ_c [defined in [\(B 4\)](#)].

with an Alfvénic one—the latter in favour of the magnetic field. Thus, the imbalanced cascades are only half of the story. According to the second relation in [\(B 6\)](#), in imbalanced turbulence ($|\sigma_c| \approx 1$), it is a geometric inevitability that $|\sigma_r| \ll 1$, as illustrated by figure 16(a) and confirmed directly in the statistical study of solar-wind data by [Bowen et al. \(2018\)](#). In contrast, when the cross-helicity is not large (i.e., when σ_c is not close to ± 1), there is flexibility for the perturbations to have finite residual energy: in the event, $\sigma_r < 0$. The definitive observational paper on this is [Chen et al. \(2013\)](#), confirming negative σ_r over a large data set obtained in the solar wind. They also report that residual energy has a spectrum consistent with k_\perp^{-2} or perhaps a little shallower, but certainly steeper than either the kinetic- or magnetic-energy spectra: the scalings of all three are reproduced in figure 21. This seems to be in agreement with earlier observational and numerical evidence ([Müller & Grappin 2005](#); [Boldyrev et al. 2011](#), figure 22).

There are two ways in which a shade of legitimate doubt extends over both numerical and observational evidence quoted above.

(i) [Beresnyak \(2014b\)](#), analysing his (largest-ever) simulations, reports that the residual energy at the small-scale end of its spectrum scales approximately as $k_\perp^{-1.7}$, same as his kinetic- and magnetic-energy spectra. His conclusion is that residual energy is merely a scale-independent finite fraction ≈ 0.15 of the total energy.

(ii) Solar wind's expansion with heliocentric distance and the resulting reflection of the outward-propagating Elsasser field leads to an increase in the negative residual energy, which has nothing to do with nonlinear interactions in the locally homogeneous turbulence (see, e.g., [Perez & Chandran 2013](#)). The steepening of the magnetic field's spectrum compared to velocity's due to this effect is captured quite clearly in, e.g., the expanding-box simulations of [Squire et al. \(2020\)](#), to whose paper I also refer the reader requiring further space-physics references on this subject. In assessing solar-wind measurements for evidence of residual energy in MHD turbulence, it may be nontrivial to separate this expansion effect from the organic local tendency of the nonlinear interactions to favour negative residual energy.

Alas, nothing is ever clear-cut in this subject, but let me press on. Obviously, it cannot be true at asymptotically small scales that, as the solar-wind data suggests, the magnetic- and kinetic-energy spectra scale as $k_\perp^{-5/3}$ and $k_\perp^{-3/2}$, respectively, while their

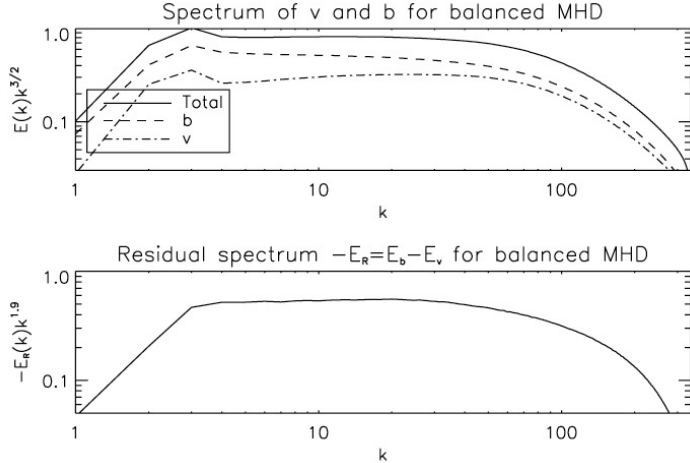


FIGURE 22. Spectra of total, magnetic, kinetic (upper panel, solid, dashed and dot-dashed lines, respectively, compensated by $k_{\perp}^{3/2}$) and residual energy (lower panel, compensated by $k_{\perp}^{1.9}$) in an RMHD simulation by Boldyrev *et al.* (2011) (©AAS, reproduced with permission). Beresnyak (2014b) does a convergence study by rescaling to the dissipative cutoff and finds instead a $k_{\perp}^{-1.7}$ scaling to be the best fit to the residual-energy spectrum (see his Figure 3), so it is possible that what is displayed here is a large-scale transient.

difference scales as k_{\perp}^{-2} —the \mathbf{b} and \mathbf{u} spectra must meet somewhere, as they indeed do in figure 21(a). The residual energy appears to peter out at the same scale (although that is also where the noise effects kick in)—but it would not be asymptotically impossible for it to retain the k_{\perp}^{-2} scaling as a subdominant correction to approximately equipartitioned \mathbf{b} and \mathbf{u} spectra (as suggested by Boldyrev *et al.* 2011)—or perhaps to parallel, finitely offset ones (à la Beresnyak 2014b). I will discuss a plausible origin for such a correction in § 10.4, but first some history.

10.2. Old Theories

The first awakening of the MHD turbulence community to the turbulence’s tendency for residual-energy generation dates back to the dawn of time (Pouquet *et al.* 1976; Grappin *et al.* 1982, 1983), when theories and simulations based on isotropic EDQNM⁴⁸ closure models of MHD turbulence predicted a negative residual energy (i.e., an excess of magnetic energy) scaling as a k^{-2} correction to the dominant $k^{-3/2}$ IK spectrum (see § 2.2). While the isotropic IK theory certainly cannot be relevant to MHD turbulence with a strong mean field (see § 2), the modern evidence (§ 10.1) looks very much like those old results, with k replaced by k_{\perp} . This led Müller & Grappin (2005) to claim a degree of vindication for the EDQNM-based theory. This vindication cannot, however, be any stronger than the vindication of IK provided by Boldyrev’s theory (§ 6.2) and its variants (§ 6.4): same scaling, different physics.

Below the turgid layers of EDQNM formalism, the basic physical idea (best summarised by Grappin *et al.* 2016) is that residual energy is generated from the total energy by nonlinear interactions that favour magnetic-field production (the “dynamo effect”)⁴⁹ and

⁴⁸Eddy-Damped Quasi-Normal Markovian. You don’t want to know.

⁴⁹That they do favour magnetic-field production and thus promote $\sigma_r < 1$ is confirmed quantitatively within the closure theory (Grappin *et al.* 1982, 1983; Gogoberidze *et al.* 2012). Physically, it is possible to argue that simple Alfvén-wave interactions will produce residual

removed by the ‘‘Alfvén effect,’’ which tends to equalise \mathbf{u}_\perp and \mathbf{b}_\perp perturbations. A balance of these two effects leads to a prediction for the residual-energy spectrum in the form

$$E_{\text{res}} \sim \frac{\tau_A}{\tau_b} E \sim \left(\frac{\tau_A}{\tau_{\text{nl}}} \right)^\alpha E, \quad (10.1)$$

where E is the total-energy spectrum, τ_b is the characteristic time scale of the generation of excess magnetic energy at a given scale, τ_A and τ_{nl} are our old friends Alfvén and nonlinear times, and the exponent α depends on one’s theory of how τ_b is related to these two basic times. For example, in the IK theory, $\tau_b \sim \tau_{\text{nl}}^2/\tau_A$ [because IK turbulence is weak; cf. (4.5) and footnote 5], so $\alpha = 2$. Using the IK scalings (2.5) and $\tau_A/\tau_{\text{nl}} \sim \delta u_\lambda/v_A$, one then gets from (10.1)

$$E_{\text{res}}(k) \sim \frac{\varepsilon}{v_A} k^{-2}. \quad (10.2)$$

I know of no unique or obvious way of adjusting this promising (but necessarily wrong because IK-based) result to fit a critically balanced cascade: indeed, the CB requires $\tau_A \sim \tau_{\text{nl}}$, implying $E_{\text{res}} \sim E$, i.e., a scale-independent ratio between the residual and total energy (this was also the conclusion of Gogoberidze *et al.* 2012, who undertook the heroic but thankless task of constructing an EDQNM theory of anisotropic, critically balanced MHD turbulence). Neither solar wind nor MHD simulations appear to agree with this (§ 10.1).

Obviously, once we enter the realm of intermittent scalings of the kind described in § 6.4.1, i.e., allow the outer scale to matter, there is a whole family of possibilities admitted by the RMHD symmetry and dimensional analysis: by exactly the same argument as the one that led to (6.14) (and noting that spectrum \sim amplitude²/ k_\perp), we must have

$$E_{\text{res}}(k_\perp) \sim \varepsilon^{2(1+\delta)/3} \left(\frac{L_\parallel}{v_A} \right)^{2\delta} k_\perp^{-(5-4\delta)/3}, \quad (10.3)$$

where δ is some new exponent. In order to determine it, one must input some physical or mathematical insight.

10.3. New Theories: Residual Energy in Weak MHD Turbulence

An interesting step in this direction was made in yet another characteristically clever contribution by Boldyrev’s group. They showed that even weak interactions of AW packets mathematically lead to growth of excess magnetic energy and thus of negative residual energy—Boldyrev *et al.* (2012) by analysing weak interaction of two model AW packets and Wang *et al.* (2011) within the framework of traditional WT theory. However, all the action in their derivation was in the $k_\parallel = 0$ modes, which hosted the excess magnetic energy generated by AW interactions—the 2D magnetic condensate whose awkward relationship with WT theory I discussed in § 4.4.

A version of the appropriate derivation is laid out in appendix A.5. Quantitatively, it cannot be right because the WT approximation does not apply to the condensate, which is strongly turbulent (see appendix A.4). Qualitatively, the outcome of the WT calculation—growth of excess magnetic energy at $k_\parallel = 0$ —can be understood as follows. Growth of positive (negative) residual energy is the same as growth of (anti)correlation between \mathbf{Z}_\perp^+ and \mathbf{Z}_\perp^- :

$$\langle \mathbf{Z}_\perp^+ \cdot \mathbf{Z}_\perp^- \rangle = \langle |\mathbf{u}_\perp|^2 \rangle - \langle |\mathbf{b}_\perp|^2 \rangle. \quad (10.4)$$

energy (Boldyrev *et al.* 2012)—see further discussion in §§ 10.3 and 10.4. I am not enthusiastic about dragging the dynamo effect into this.

These correlations are created with particular ease at $k_{\parallel} = 0$, where \mathbf{Z}_0^+ and \mathbf{Z}_0^- are forced by the interaction of the same pairs of AWs, $\mathbf{Z}_{k_{\parallel}}^+$ and $\mathbf{Z}_{k_{\parallel}}^-$ (which themselves are allowed to be uncorrelated): this is obvious from (4.12). The result is that a magnetic condensate emerges at $k_{\parallel} = 0$, giving rise to net negative residual energy—that it should be negative is not obvious, but the WT calculation says it is [see (A 38)], as, perhaps more convincingly, does a qualitative argument that I shall now explain.

10.4. New Theories: Residual Energy in Strong MHD Turbulence

In the strong-turbulence regime, no quantitative calculation exists, as usual, but a reasonably compelling physical case can be made.

Emergence of negative residual energy here must be discussed in very different terms than in § 10.3. As I repeatedly stated in § 6, my preferred picture of alignment is one in which Elsasser fields dynamically shear each other into intermittent structures where they are nearly parallel to each other (Chandran *et al.* 2015). That, of course, means that they become strongly correlated: indeed, alignment between Elsasser fields is mathematically impossible without non-zero residual energy, as is obvious from the first formula in (B 5) or from figure 38. That δb should be larger than δu in the resulting sheet-like structures is both a selection effect and the result of dynamics.

First, the structures that have $\delta u > \delta b$ —shear layers, rather than current sheets—are prone to be destroyed by the Kelvin–Helmholtz instability and to curl up into vortices, as they do in hydrodynamic turbulence, whereas in the current sheets, the instability is happily stabilised by the magnetic field (at least before it all hits the disruption scale and current sheets become unstable as well; see § 7, appendix D.4.2 and references therein).

Secondly, there is a dynamical tendency in RMHD that favours current sheets over shear layers: the nonlinearity pushes the “Elsasser vorticities” $\omega^+ = \hat{\mathbf{z}} \cdot (\nabla_{\perp} \times \mathbf{Z}_{\perp}^+)$ and $\omega^- = \hat{\mathbf{z}} \cdot (\nabla_{\perp} \times \mathbf{Z}_{\perp}^-)$ in opposite directions—this is obvious from the evolution equations (A 2) for these vorticities, where the nonlinear vortex-stretching terms have opposite signs for the two Elsasser fields. Thus, ω^+ and ω^- are “forced” equally and in opposite directions at every point in space and time. The result is a negative correlation between them, $\langle \omega^+ \omega^- \rangle < 0$, and thus a preference for current sheets over shear layers (see figure 23 and Zhdankin *et al.* 2016b).

Let us now imagine that this effect is strongest in the most intense structures, which in § 6.4.2 were all assumed to have the same, scale-independent amplitude. If they are current sheets with $\delta Z_{\max} \sim \delta b \gg \delta u$, they would, if they were alone in the world, have a spectrum of k_{\perp}^{-2} because they are just an ensemble of step functions in \mathbf{b}_{\perp} . The easiest way to see this is to notice that it is the spectrum of a single Heaviside step function. It is also the spectrum of many random steps: if the field flips direction randomly, with the number of flips between two points separated by a distance λ increasing $\propto \lambda$, then the field increment will accumulate as a random walk: $\langle \delta b_{\lambda}^2 \rangle \propto \lambda$, giving a k_{\perp}^{-2} spectrum.⁵⁰ In fact, there are many other fluctuations around, whose net spectrum is $k_{\perp}^{-3/2}$ and in which $\delta b \sim \delta u$. Overall, this shallower scaling would swamp k_{\perp}^{-2} . However, if the excess magnetic energy is dominated by the most intense sheets, one might imagine that the residual-energy spectrum would have a k_{\perp}^{-2} scaling.

⁵⁰That current sheets naturally forming in a turbulent MHD system do indeed have this spectrum was shown by Dallas & Alexakis (2013a, 2014), although they only looked at decaying, no-mean-field MHD turbulence with a certain class of initial conditions. Zhou *et al.* (2019) in their decaying 2D RMHD simulations, heavily dominated by current sheets, see the same spectrum and explain it the same way. Note that if current sheets break up into plasmoid chains, those too appear to favour a k_{\perp}^{-2} scaling (see appendix D.6.2).

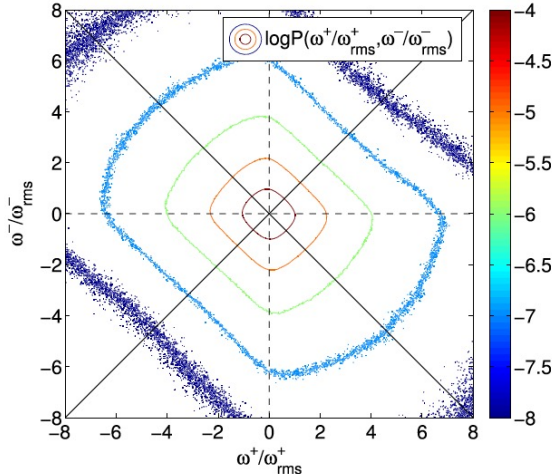


FIGURE 23. Joint probability distribution of Elsasser vorticities $\omega^\pm = \hat{z} \cdot (\nabla_\perp \times \mathbf{Z}_\perp^\pm)$ in an RMHD simulation by Zhdankin *et al.* (2016b) [reprinted from Zhdankin *et al.* (2016b) with the permission of AIP Publishing]. The contours are elongated in the SE-NW direction, indicating $\langle \omega^+ \omega^- \rangle < 0$ and thus a preponderance of current sheets over shear layers.

Encouragingly, recent analysis of solar-wind data by Bowen *et al.* (2018) directly established a positive correlation between the most intense, intermittent magnetic structures and residual energy. It is perhaps worth observing that the fact that a k_\perp^{-2} spectrum consistent with the RMHD symmetry requires $\delta = -1/4$ in (10.3) and, therefore, the presence of the outer scale L_\parallel in the expression for $E_{\text{res}}(k_\perp)$, confirms that we must again be dealing with an intermittency effect. This said, figure 13(b) appears to be at odds with the notion of a steeper magnetic spectrum, showing *smaller* scaling exponents for the magnetic field than for velocity—an effect of velocity forcing? bad statistical measurement? Sorting this out appears to be a worthwhile outstanding task.

Thus, admittedly, all this is less than a theory, but it is something.

10.5. Summary

Perhaps speaking of an “Alfvénically imbalanced regime” of MHD turbulence is misleading. Residual energy is not an RMHD invariant, so this is not something that can be viewed as a parameter in the same way as the net Elsasser imbalance can be. It is, rather, what appears to be a feature of any (approximately balanced) MHD turbulent state (but may be a large-scale transient; see § 10.1).

This feature has so far presented itself in two seemingly distinct manifestations. The first one is the tendency for sheet-like structures in the inertial range of strong MHD turbulence to be current sheets rather than shear layers and thus to have an excess of magnetic energy—it may be possible to argue that the most extreme of these structures are responsible for a subdominant k_\perp^{-2} spectrum of residual energy (§ 10.4). The second one is the emergence of a 2D magnetic condensate in weak MHD turbulence (§ 10.3).

Are these two different phenomena? Not necessarily: in the WT context, all the residual energy is generated amongst $k_\parallel \approx 0$ modes, which are, in fact, strongly turbulent (see appendices A.4 and A.5). Being strongly turbulent, this 2D condensate is strongly intermittent and appears to be dominated by sheet-like structures (Meyrand *et al.* 2015), so the physical mechanism whereby an excess of magnetic energy develops in it is likely to be the same as in strong MHD turbulence.

11. Subviscous MHD Turbulence

Let me now turn to an interesting, if somewhat boutique, regime of MHD turbulence that occurs at scales below the viscous cutoff when $Pm \gg 1$. This was first studied by Cho *et al.* (2002a, 2003) and Lazarian *et al.* (2004), and recently picked up again by Xu & Lazarian (2016, 2017), on the grounds that it is relevant to partially ionised interstellar medium, where viscosity is heavily dominated by the neutral atoms.⁵¹ This is a limit in which viscous dissipation takes over from inertia in controlling the evolution of the velocity field (one might call this “Stokes,” or “Aristotelian” dynamics; cf. Rovelli 2015), while magnetic field is still happily frozen into this viscous flow and free to have interesting MHD behaviour all the way down to the resistive scale, which, at $Pm \gg 1$, is much smaller than the viscous one. The velocity perturbations below the viscous scale will be very small compared to the magnetic ones, so this is another MHD turbulent state that features an imbalance between the two fields.

Below, I am going to present a somewhat updated qualitative theory of the subviscous cascade—with tearing disruption and the ubiquitous Kolmogorov cutoff yet again making a cameo appearance.

11.1. Viscous Cutoff

When $Pm \gg 1$, there are two possibilities for the nature of turbulence at the viscous cutoff.

The first is that Pm is large enough to break the condition (7.3), viz., $Pm \gtrsim Re^{1/9}$, so there is no tearing disruption and the (aligned) inertial-range MHD cascade encounters viscosity at the Boldyrev cutoff scale (6.24)—for $Pm \gg 1$, let me rename it λ_ν :

$$\lambda_\nu \sim \lambda_{CB} Re^{-2/3} \sim \frac{\nu^{3/4}}{\varepsilon^{1/4}} Re^{1/12} \Rightarrow \frac{\xi_\nu}{\lambda_{CB}} \sim Re^{-1/2}, \quad \frac{l_{\parallel\nu}}{L_\parallel} \sim Re^{-1/3}, \quad (11.1)$$

where λ_{CB} is given by (6.16) and Re by (6.23). The last two formulae follow via (6.31) (for the scale ξ_ν on which the perturbed fields vary along themselves) and (6.22) (for the parallel scale $l_{\parallel\nu}$).

The second (rather difficult to achieve) possibility is that $1 \ll Pm \ll Re^{1/9}$, so (7.3) does hold and we have a tearing-mediated turbulent cascade curtailed by the Kolmogorov cutoff (7.19)—for $Pm \gg 1$, it is

$$\lambda_\nu \sim \lambda_{CB} Re^{-3/4} \sim \frac{\nu^{3/4}}{\varepsilon^{1/4}}. \quad (11.2)$$

Either way, some finite fraction of ε is thermalised at λ_ν , and at $\lambda < \lambda_\nu$ velocity perturbations will have gradients that are smaller than the decorrelation rate at λ_ν . This decorrelation rate is

$$\tau_{nl}^{-1} \sim \frac{\delta u_{\lambda_\nu}}{\xi_\nu} \sim \tau_\nu^{-1} \sim \frac{\nu}{\lambda_\nu^2} \sim \left(\frac{\varepsilon}{\nu}\right)^{1/2} Re^{-1/6} \quad \text{or} \quad \left(\frac{\varepsilon}{\nu}\right)^{1/2} \quad (11.3)$$

for (11.1) and (11.2), respectively.

11.2. Magnetic Fields at Subviscous Scales

In contrast to velocities, magnetic fields are immune to viscosity and so can be pushed to scales much smaller than λ_ν . However, since velocity gradients are suppressed at

⁵¹It has also recently turned out, somewhat unexpectedly, that something very similar to this regime might be relevant in the context of collisionless gyrokinetic turbulence and ion heating in high-beta plasmas (Kawazura *et al.* 2019).

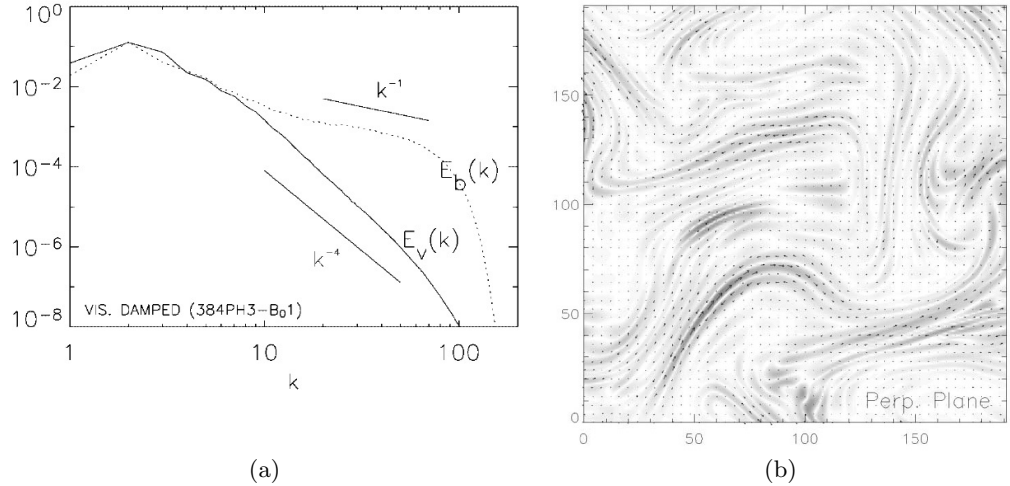


FIGURE 24. (a) Spectra of magnetic and kinetic energy for subviscous turbulence, taken from Cho *et al.* (2003). (b) Magnetic-field strength for the filtered $k > 20$ part of the field in the same simulation (from Cho *et al.* 2002a; both figures ©AAS, reproduced with permission). Stripy field structure is manifest.

these scales, these magnetic fields will be dominantly interacting with the viscous-scale velocities, in a scale-nonlocal fashion. Presumably, since the viscous-scale motions are correlated on the parallel scale $l_{\parallel\nu}$, so will be these magnetic fields, i.e., there is no parallel cascade:

$$l_{\parallel} \sim l_{\parallel\nu} = \text{const.} \quad (11.4)$$

Numerical simulations (Cho *et al.* 2002a, 2003) confirm (11.4) and show a magnetic spectrum $\propto k^{-1}$. In the mind of any minimally erudite turbulence theorist, this cannot fail to trigger a strong temptation to consider the whole situation as a variant of Batchelor (1959) advection of a passive field: assuming a cascade of magnetic energy with cascade time τ_ν at every scale, one gets (see Cho *et al.* 2002a and figure 24a):

$$\delta b_\lambda^2 \sim \varepsilon_m \tau_\nu = \text{const} \quad \Rightarrow \quad E_b(k_\perp) \sim \varepsilon_m \tau_\nu k_\perp^{-1}, \quad (11.5)$$

where ε_m is the part of the turbulent flux that is not dissipated at the viscous cutoff (possibly about half of it, since velocity and magnetic fields have the same energies at the viscous scale and are pushed into viscous dissipation and subviscous structure, respectively, at the same rate τ_ν^{-1}). The spectrum (11.5) stretches all the way to the resistive scale, where Ohmic dissipation can rival advection:

$$\tau_\nu^{-1} \sim \frac{\eta}{\lambda_\eta^2} \quad \Rightarrow \quad \lambda_\eta \sim (\tau_\nu \eta)^{1/2} \sim \lambda_\nu Pm^{-1/2}. \quad (11.6)$$

The line of reasoning leading to (11.5) should perhaps be viewed with a degree of suspicion. In a regime where magnetic fields are nonlocally advected and stretched by the viscous-scale velocity field, while the latter experiences back reaction from them while constantly being dissipated by viscosity, why can one assume that magnetic energy is an independent invariant with a constant scale-to-scale flux? While this may be a plausible proposition, I do not know how to justify it beyond reasonable doubt—but I do believe the scaling (11.5) because it is bolstered by the following alternative argument of a more dynamical nature.

The situation at subviscous scales is not entirely dissimilar to a kind of dynamo (§ 13),

or rather a 2D version of it in which the perturbed magnetic field \mathbf{b}_\perp is randomly stretched and sheared by the viscous-scale velocity and is excused from the 2D antidynamo theorem (Zeldovich 1956) by constant resupply from the inertial range. The role of \mathbf{B}_0 is just to two-dimensionalise the dynamics approximately—maintaining all fields at the single parallel correlation scale $l_{\parallel\nu}$. The stretching and shearing of \mathbf{b}_\perp leads to a folded magnetic field (figure 30) forming a stripy pattern, with multiple reversals on small scales limited from below only by λ_η (figure 24b).⁵²

Just like in the case of dynamo-generated fields (§ 13.3.1), our stripy fields are spatially correlated along themselves on scales $\sim \xi_\nu$ and so can exert coherent Lorentz forces back on the viscous-scale velocity field. These forces are tension forces consisting of two parts:

$$\mathbf{F} = \mathbf{B}_0 \cdot \nabla \mathbf{b}_\perp + \mathbf{b}_\perp \cdot \nabla \mathbf{b}_\perp. \quad (11.7)$$

Here let us think of \mathbf{b}_\perp as just the part of \mathbf{B} that contains subviscous-scale variation and absorb into \mathbf{B}_0 all inertial-range fields. The first term in (11.7) alternates sign on the scale λ_η (in the direction perpendicular to \mathbf{b}_\perp) and so its effect on the viscous-scale motions should cancel out. In contrast, the second term is quadratic in \mathbf{b}_\perp , and its size is $\sim b_\perp^2/\xi_\nu$. In order to be dynamically significant, it must be of the same order as the viscous and inertial forces, which are similar at the viscous scale:

$$\mathbf{b}_\perp \cdot \nabla \mathbf{b}_\perp \sim \nu \nabla_\perp^2 \mathbf{u}_\perp \sim \mathbf{u}_\perp \cdot \nabla \mathbf{u}_\perp \Rightarrow \frac{\delta b_\lambda^2}{\xi_\nu} \sim \frac{\delta u_{\lambda_\nu}^2}{\xi_\nu} \Rightarrow \delta b_\lambda^2 \sim \delta u_{\lambda_\nu}^2 \sim \varepsilon \tau_\nu. \quad (11.8)$$

On the face of it, this reproduces (11.5) (assuming $\varepsilon_m \sim \varepsilon$). However, we need not interpret this result as specifically vindicating a Batchelor-style cascade. Instead, we could think of the reversal scale as always being λ_η , the size of the reversing field as being $b_\perp \sim (\varepsilon \tau_\nu)^{1/2}$, and interpret δb_λ as the increment of a stripy field taken in two points separated by $\lambda_\eta \ll \lambda \ll \lambda_\nu$. The field difference between such two points will always be either $\delta b_\lambda \sim 2b_\perp$ or zero, with equal probabilities, and so $\langle \delta b_\lambda^2 \rangle \sim b_\perp^2 \sim \varepsilon \tau_\nu$ (this argument is due to Yousef *et al.* 2007, who used it to posit a k^{-1} spectrum for dynamo-generated fields at large Pm, which will be visited in § 13.4.2). In other words, cascade or no cascade, k_\perp^{-1} can be recovered as the spectrum of sharp, repeated stripes.⁵³

11.3. Velocity Field at Subviscous Scales

Numerical simulations (Cho *et al.* 2003, shown in figure 24a) reveal that the velocity field at subviscous scales is very small and has an approximately k_\perp^{-4} spectrum. This can be recovered on the basis of the picture that I proposed in § 11.2, in the following way. The balance between the viscous and magnetic forces at $k_\perp \lambda_\nu \gg 1$ gives us

$$\nu k_\perp^2 \mathbf{u}_{\perp k} \sim (\mathbf{b}_\perp \cdot \nabla \mathbf{b}_\perp)_k \Rightarrow E_u(k_\perp) \sim \frac{E_F(k_\perp)}{\nu^2 k_\perp^4} \sim \frac{\text{const}}{k_\perp^4}, \quad (11.9)$$

⁵²Subviscous-scale fields generated by randomly stirred and viscously damped flows in 2D were studied both analytically and numerically by Kinney *et al.* (2000), who found them to follow a k_\perp^{-1} spectrum (which is evident in their Fig. 11, even though they do not claim this scaling explicitly).

⁵³To pre-empt a possible confusion, let me contrast this with the k_\perp^{-2} spectrum that is usually associated with a field consisting of sharp discontinuities, e.g., the Burgers turbulence of shocks (Bec & Khanin 2007) or an ensemble of current sheets, already discussed in § 10.4. I argued there that, in a field of random step-like discontinuities, their structure function would accumulate as a random walk: $\langle \delta b_\lambda^2 \rangle \propto \lambda$. This is different from the stripy fields posited in this section, which are a repeated pattern, giving $\langle \delta b_\lambda^2 \rangle \sim \text{const}$.

where $E_u(k_\perp)$ and $E_F(k_\perp)$ are the spectra of the velocity and of the tension force, respectively. Let me explain why $E_F(k_\perp) \sim \text{const}$. If \mathbf{b}_\perp consists of stripes of field alternating direction on the scale λ_η , then $\mathbf{b}_\perp \cdot \nabla \mathbf{b}_\perp \sim |\mathbf{b}_\perp|^2 / \xi_\nu$ consists of a constant field interspersed by sharp downward spikes of width λ_η across the field and length ξ_ν along it. At $k_\perp \lambda_\eta \ll 1$ and $k_\perp \xi_\nu \gg 1$, these are effectively 1D delta functions, so $E_F(k_\perp) \sim \text{const}$, q.e.d.⁵⁴ Note that the contribution of the first term in (11.7) to E_F should scale the same as the spectrum of \mathbf{b}_\perp , viz., $\propto k_\perp^{-1}$ —or perhaps $k_\perp^{-1/2}$ from the cross-term, if it does not average to zero—this should produce steeper and, therefore, subdominant contributions to $E_u(k_\perp)$.⁵⁵

11.4. Disruption by Tearing

A reader who still remembers the developments in §7 might wonder whether these stripy fields are safe against disruption by tearing. Setting $v_{Ay} \sim \delta b_\lambda$ in (7.1), let us ask whether there is a disruption scale $\lambda_{D,\text{subvisc}}$ at which the local tearing rate would be larger than the stretching rate by the viscous-scale eddies:

$$\gamma \sim \frac{\delta b_\lambda^{1/2}}{\lambda^{3/2}} \eta^{1/2} \text{Pm}^{-1/4} \gtrsim \tau_\nu^{-1} \quad \Rightarrow \quad \lambda \lesssim \varepsilon_m^{1/6} \tau_\nu^{5/6} \eta^{1/2} \nu^{-1/6} \equiv \lambda_{D,\text{subvisc}}, \quad (11.10)$$

where (11.5) was invoked for δb_λ . Using (11.6) to estimate the putative resistive cutoff, we get

$$\frac{\lambda_{D,\text{subvisc}}}{\lambda_\eta} \sim \varepsilon_m^{1/6} \tau_\nu^{1/3} \nu^{-1/6}, \quad (11.11)$$

If we are in the parameter regime where the tearing disruption has already occurred in the inertial range ($\text{Pm} \lesssim \text{Re}^{1/9}$) and so (11.2) holds, then τ_ν is given by the second expression in (11.3), and (11.11) implies

$$\frac{\lambda_{D,\text{subvisc}}}{\lambda_\eta} \sim \left(\frac{\varepsilon_m}{\varepsilon} \right)^{1/6} \lesssim 1, \quad (11.12)$$

so no new disruption is possible in the subviscous range.⁵⁶

In contrast, if the inertial-range cascade was cut off in the aligned regime ($\text{Pm} \gtrsim \text{Re}^{1/9}$), so (11.1) and the first expression in (11.3) apply, then

$$\frac{\lambda_{D,\text{subvisc}}}{\lambda_\eta} \sim \left(\frac{\varepsilon_m}{\varepsilon} \right)^{1/6} \text{Re}^{1/18} \gg 1. \quad (11.13)$$

Modulo factors of order unity and the ludicrous smallness of the fractional power of Re

⁵⁴A version of this argument was proposed by Schekochihin *et al.* (2004b) for dynamo-generated fields. They simulated such fields (in 3D) directly and found the spectrum of tension to be flat and the velocity spectrum to satisfy (11.9) extremely well. Kinney *et al.* (2000) argued for, and saw, similar behaviour in 2D, although their E_u had a slope closer to $k_\perp^{-4.5}$. Interestingly, Cho *et al.* (2002a) also reported a steeper spectrum like this, although it was perhaps not fully numerically converged and so, in Cho *et al.* (2003), they changed their mind in favour of k_\perp^{-4} .

⁵⁵The mismatch of the spectrum obtained this way ($E_u \propto k_\perp^{-5}$) and the one observed in numerical simulations led Lazarian *et al.* (2004) to propose an ingenious scheme whereby all fields and velocities at subviscous scales had a scale-dependent volume-filling fraction, whose scaling was then determined by an additional requirement that subviscous velocities had local shears comparable to τ_ν^{-1} . Although this did give the desired k_\perp^{-4} scaling, I do not see how such an assumption can be justified.

⁵⁶If in §11.1 I had used the cutoff (7.17) instead of (7.19) to calculate τ_ν , I would have discovered now that $\lambda_{D,\text{subvisc}} \sim (\varepsilon_m / \varepsilon)^{1/6} \lambda_\nu \sim \lambda_\nu$, indicating that the tearing-mediated cascade from §7.2 in fact continued below the cutoff (7.17)—an argument that I already made in §7.2.2.

involved, this means that if the tearing disruption did not have the chance to occur in the inertial range, it will occur in the subviscous range, and that $\lambda_{D,\text{subvisc}}$ will be the field reversal scale, not λ_η . In terms of the viscous scale (11.1), which is $\lambda_\nu \sim \lambda_\eta \text{Pm}^{1/2}$,

$$\frac{\lambda_D}{\lambda_\nu} \sim \left(\frac{\varepsilon_m}{\varepsilon} \right)^{1/6} \text{Re}^{1/18} \text{Pm}^{-1/2}, \quad (11.14)$$

where I have renamed $\lambda_{D,\text{subvisc}} \rightarrow \lambda_D$, since, in this regime, this is the only disruption scale there is.

At $\lambda \lesssim \lambda_D$, a local MHD cascade is again ignited, just like it was in § 7.2. It should not seem strange that inertial motions are again possible: viscously dominated tearing of the magnetic sheets will produce λ_D -sized plasmoids whose turnover times are shorter than their viscous-dissipation times (I already argued this in a similar context in § 7.2.2). Indeed, similarly to (7.10), taking them to be unaligned and demanding that they pick up all the available energy flux ε_m , one gets their amplitude

$$\frac{\delta Z_{\lambda_D}^3}{\lambda_D} \sim \varepsilon_m \quad \Rightarrow \quad \delta Z_{\lambda_D} \sim (\varepsilon_m \lambda_D)^{1/3} \quad (11.15)$$

and the associated Reynolds number for the new cascade:

$$\text{Re}_{\lambda_D} = \frac{\delta Z_{\lambda_D} \lambda_D}{\nu} \sim \text{Re}^{5/27} \text{Pm}^{-2/3} \gg 1 \quad \text{if} \quad \text{Re} \gg \text{Pm}^{18/5}. \quad (11.16)$$

This cascade is cut off, as usual, at the scale (7.19), but with this new Re :

$$\lambda_{\nu,\text{new}} \sim \lambda_D \text{Re}_{\lambda_D}^{-3/4} \sim \frac{\nu^{3/4}}{\varepsilon_m^{1/4}}, \quad (11.17)$$

the Kolmogorov scale again, obviously.

Thus, the subviscous cascade turns out to be a complicated transitional arrangement for enabling tearing disruption and restoration of the Kolmogorov cutoff (11.17). Yet again, below this cutoff, at $\lambda < \lambda_{\nu,\text{new}}$, we are confronted with a purely magnetic, “second subviscous cascade,” but this time with the (new) viscous-scale turnover time given by the formula analogous to the second expression in (11.3), viz., $\tau_{\nu,\text{new}} \sim (\varepsilon_m/\nu)^{1/2}$. All the arguments of §§ 11.2 and 11.3 apply, but with no longer any danger of further disruption [see (11.12)].

A reader sceptical of the falsifiability of these arguments (given the proliferation of small fractional powers of Re and the piling up of twiddle algebra) might feel this is all a fiction—but it is a logical one!

12. Decaying MHD Turbulence

Decaying MHD turbulence belongs to this part of this review because it too tends to end up in “imbalanced” states dominated either by the magnetic field or by one of the Elsasser fields (and because it remains, or has done until recently, in certain important respects a “loose end”). On a very crude level, it is perhaps obvious that this should be so, because ideal MHD equations have two types of exact solutions for which nonlinear interactions vanish: Elsasser states ($\mathbf{u} = \pm \mathbf{B}$, or $\mathbf{Z}^\mp = 0$) and static force-free magnetic fields ($\mathbf{B} \times \mathbf{J} = 0$, where $\mathbf{J} = \nabla \times \mathbf{B}$). If the system finds a way towards either of these solutions, globally or locally, concentrated on scales large enough to make dissipation small, it may, subject to this small dissipation, be able to linger in those states (“may” because the stability of the force-free states, e.g., is not guaranteed: see discussion and references in Appendix A of [Hosking et al. 2020](#)). We shall see below that

both magnetically dominated scenarios and convergence to Elsasser states are possible and that recent developments point to magnetic reconnection muscling its way into this topic as well.

The usual theoretical attitude to decaying turbulence, dating back to Kolmogorov (1941b,c), is to assume that its energy would decay slowly compared to the nonlinear interactions at small scales (simply because turnover times τ_{nl} are shorter at smaller scales) and hence to expect the situation in the inertial range (below the outer scale) to be the same as in the forced case: a constant-flux energy cascade, etc. I shall discuss the numerical evidence in § 12.8, but for now let us accept this philosophy as sound. With the small scales thus taken care of, the interesting question is the large-scale behaviour: since decaying turbulence is not interfered with “externally”, it has the freedom to decide how fast various types of energy (kinetic, magnetic, Elsasser) decay and how the outer scale evolves. These are the “zeroth-order” questions that any theory of decay must be able to answer.⁵⁷

12.1. Selective Decay

How to answer these questions was, like most other things in turbulence, understood already by Kolmogorov (1941c): one assumes that energy decays on some appropriate nonlinear time scale subject to some other invariant(s) staying constant (i.e., decaying only due to dissipation, which, at $\text{Re} \rightarrow \infty$, vanishes at the outer scale); this allows one to impose enough constraints on the energy and the outer scale to determine the evolution of both. In MHD, this principle is sometimes called the “selective-decay hypothesis”, originating from the idea of Taylor (1974) relaxation—early proponents of this view of decaying MHD turbulence were Montgomery *et al.* (1978, 1979) and Matthaeus & Montgomery (1980).

In § 12.4, I will return to what the additional invariant was for Kolmogorov, and how that can be generalised to MHD, but let me start with the most straightforward (and, historically, the earliest and most successful) application of the philosophy of selective decay—MHD turbulence in 2D.

12.1.1. Decay of 2D MHD Turbulence

In 2D MHD, there are two positive-definite invariants: energy and “anastrophy” $\langle A_z^2 \rangle$, where A_z is the out-of-plane component of the vector potential, which in 2D behaves as a passive scalar:

$$\frac{\partial A_z}{\partial t} + \mathbf{u}_\perp \cdot \nabla_\perp A_z = \eta \nabla^2 A_z. \quad (12.1)$$

⁵⁷These are also questions that preoccupy a certain subcommunity of cosmologists seeking to relate extragalactic magnetic fields observed in “cosmic voids” to theories of primordial genesis of magnetic fields, of which those observed ones are conjectured to be decayed relics. How this is done is described in Hosking & Schekochihin (2022a), where the reader will also find all the relevant cosmological references. Because of this cosmological “relevance”, decaying MHD turbulence has been a popular topic amongst MHD theorists and simulators for nearly half a century. The resulting literature that I am familiar with will be reviewed in what follows. Note that another way in which, more recently, the decaying MHD turbulence and, especially, the phenomenon of inverse transfer (§ 12.5), have been tied to the problem of the origin of cosmic magnetic fields is via attempts to construct a seed field for the cosmic dynamo (§ 13) out of decaying magnetic flux tubes generated by Weibel instability in a primordial plasma (Zhou *et al.* 2020, 2022; Pucci *et al.* 2021).

Like energy, it is, of course, only truly conserved when $\eta = 0$, but at finite but small η , it is “better conserved” than energy: assuming that the latter is finite as $\eta \rightarrow +0$,

$$\frac{d\langle A_z^2 \rangle}{dt} = -2\eta\langle B^2 \rangle \rightarrow 0. \quad (12.2)$$

Thus, energy must decay subject to the constraint that

$$\langle A_z^2 \rangle \sim B^2 L^2 \sim \text{const}, \quad (12.3)$$

where L is the outer scale. Assuming (faithfully to [Kolmogorov 1941b,c](#)) that the (magnetic) energy decays at a rate independent of the dissipation coefficients and set instead by the outer-scale nonlinear time $\sim L/U$, one gets ([Hatori 1984](#))

$$\frac{dB^2}{dt} \sim -\frac{UB^2}{L} \sim -\frac{B^3}{L} \propto -B^4 \Rightarrow \langle B^2 \rangle \sim \langle U^2 \rangle \propto t^{-1}, \quad L \propto t^{1/2}, \quad (12.4)$$

where U has been linked to B by assuming ideal Alfvénic dynamics ($U \sim B$), and L to B via anastrophy conservation (12.3). The scalings (12.4) were confirmed numerically by [Biskamp & Welter \(1989\)](#) in one of the early triumphs of high-resolution MHD simulations (earlier, lower-resolution studies were by [Matthaeus & Montgomery 1980](#) and [Ting et al. 1986](#), who explored the 2D MHD decay subject to anastrophy conservation as part of the early discussions around the “selective-decay hypothesis”).

12.1.2. Decay of Helical MHD Turbulence

There is an immediate, direct generalisation of the above argument to 3D MHD *without a mean field*. Instead of anastrophy, the magnetic invariant in 3D MHD is helicity, $\langle H \rangle = \langle \mathbf{A} \cdot \mathbf{B} \rangle$, which again is “better conserved” than energy. Indeed, assuming again that the latter decays with time in a manner independent of the dissipation coefficients, implies $\eta\langle J^2 \rangle \rightarrow \text{const}$ as $\eta \rightarrow +0$, whence

$$\frac{d\langle H \rangle}{dt} = -2\eta\langle \mathbf{B} \cdot \mathbf{J} \rangle \sim O(\eta^{1/2}) \quad \text{as } \eta \rightarrow +0. \quad (12.5)$$

[Taylor \(1974\)](#) relaxation, which inspired the selective-decay approach to decaying MHD turbulence, was precisely the idea that MHD systems would decay to states of minimal energy subject to constant helicity.

If one adopts

$$\langle H \rangle \sim B^2 L \sim \text{const} \quad (12.6)$$

as the governing constraint, the selective-decay calculation exactly analogous to (12.4) is ([Hatori 1984; Son 1999](#))

$$\frac{dB^2}{dt} \sim -\frac{UB^2}{L} \sim -\frac{B^3}{L} \propto -B^5 \Rightarrow \langle B^2 \rangle \sim \langle U^2 \rangle \propto t^{-2/3}, \quad L \propto t^{2/3}, \quad (12.7)$$

again assuming ideal Alfvénic dynamics ($U \sim B$).

Here, however, what appeared a simple and compelling theory crashed against reality, or, at any rate, against what passes for reality in the world of MHD turbulence, where figments of theoretical imaginations are tested against figments of numerical computations: the scalings (12.7) badly disagreed with the latter, by [Biskamp & Müller \(1999, 2000\)](#). Instead of $U \sim B$, these authors spotted empirically in their simulations that $U \propto B^2$ and, by modifying (12.7) accordingly, concluded

$$\langle B^2 \rangle \propto t^{-1/2}, \quad \langle U^2 \rangle \propto t^{-1}, \quad L \propto t^{1/2}. \quad (12.8)$$

These scalings did indeed appear to check out numerically, both in their simulations

and in some later ones (Christensson *et al.* 2001; Banerjee & Jedamzik 2004; Frick & Stepanov 2010; Berera & Linkmann 2014; Brandenburg *et al.* 2019).⁵⁸

The status of the scalings (12.7) and (12.8) will become clear in what follows, but I want to preface what is to come by observing that the assumption $U \sim B$ underpinning (12.7) is not as intuitively obvious as it might appear to be at first glance. Formally, a system relaxing according to J. B. Taylor's principle will tend to a static state consisting of linear force-free fields. Linear force-free fields are one-scale ($\mathbf{B} \times \mathbf{J} = 0$ implies $\nabla^2 \mathbf{B} = -k^2 \mathbf{B}$, where k is a single number that depends on the initial $\langle H \rangle$ and boundary conditions), so can hardly be thought of as a proper turbulent state, but one could nevertheless imagine MHD turbulence decaying through a sequence of magnetically dominated states featuring local patches of such fields at large scales, with flows constantly re-excited by these local patches crashing into each other (and/or going unstable). It then makes sense that the kinetic energy should be smaller than the magnetic one, and perhaps one could even hope to find magnetically dominated states in which $U/B \rightarrow 0$ with $t \rightarrow \infty$, as in (12.8).

This argument is not a proof of anything, but it should be enough to motivate one to look carefully at the dynamical nature of the processes that underpin the decay—and, as I have emphasised repeatedly in this review, when one starts to look carefully into the nonlinear dynamics in MHD, especially in magnetically dominated configurations, sooner or later reconnection makes an entrance.

12.2. Reconnection Takes Over

12.2.1. Reconnection-Controlled Decay of 2D MHD Turbulence

The argument at the end of § 12.1.2 casting doubt on the assumption $U \sim B$ in fact applies equally well to the 2D case considered in § 12.1.1, with anastrophy substituted for helicity (minimum-energy states subject to constant anastrophy are also static, linear force-free states). Except in 2D, unlike in 3D, theory (12.4) was confirmed by numerics, so why worry?

It may well be that the only thing worse for theory than to disagree with numerics is to agree with them. It has taken 30 years since Biskamp & Welter (1989) for a clear realisation to emerge that the assumption of ideal dynamics ($U \sim B$) in § 12.4 was flawed. The self-similar decaying state in which 2D MHD turbulence ends up is, in fact, quite significantly dominated by magnetic fields and, if one examines it visually, consists of magnetic islands separated by current sheets (figure 25), via which they reconnect and coalesce into bigger islands—that is how L grows. While Biskamp & Welter (1989) did observe that this process was occurring in their simulations (see also Politano *et al.* 1989; Servidio *et al.* 2009, 2010, 2011a,b), it was Zhou *et al.* (2019, 2021) who drew the logical conclusion that the characteristic nonlinear time scale for the energy decay must then be the reconnection time:

$$\tau_{\text{rec}} \sim \epsilon_{\text{rec}}^{-1} \frac{L}{B}, \quad \epsilon_{\text{rec}}^{-1} = (1 + \text{Pm})^{1/2} \min\{\tilde{S}_L^{1/2}, \tilde{S}_{\text{c}}^{1/2}\}, \quad \tilde{S}_L = \frac{BL}{\eta\sqrt{1 + \text{Pm}}}, \quad (12.9)$$

where ϵ_{rec} is the dimensionless reconnection rate, \tilde{S}_L is the Lundquist number (adjusted for a visco-Alfvénic outflow when $\text{Pm} \gg 1$) and $\tilde{S}_{\text{c}} \sim 10^4$ is its critical value above which

⁵⁸Some of these authors, nevertheless, prefer the scalings (12.7). Banerjee & Jedamzik (2004) hope that (12.7) will be recovered at a greater resolution; Brandenburg & Kahniashvili (2017) deem their turbulence to evolve gradually towards, if not quite achieve, (12.7); Brandenburg *et al.* (2019) think that (12.8) is a transient regime on the way to (12.7). In a certain sense, they are right—I will explain this in §§ 12.2.2 and 12.4.3.

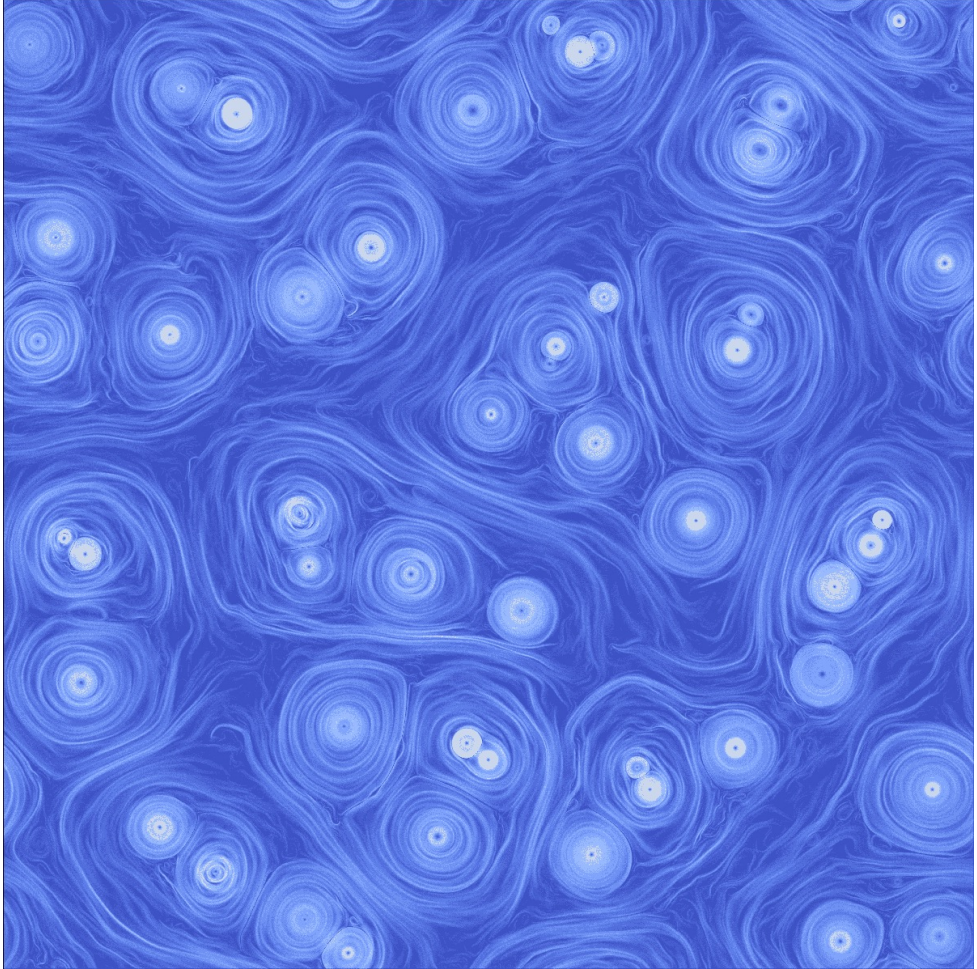


FIGURE 25. A snapshot of $|\mathbf{B}|$ from a decaying 2D MHD turbulence simulation, courtesy of D. Hosking. This run had the resolution of 4608^2 and used $n = 4$ equal hyperviscosity and hyperresistivity (the run with $\nu_4 = \eta_4 = 2 \times 10^{-11}$ from [Hosking & Schekochihin 2021](#)).

reconnection switches from the Sweet–Parker (SP) regime (appendix D.4.1) to the fast, plasmoid-dominated regime (appendix D.6).⁵⁹

This means that the first relation in (12.4) must, in fact, be rewritten as

$$\frac{dB^2}{dt} \sim -\frac{B^2}{\tau_{\text{rec}}} \sim -\epsilon_{\text{rec}} \frac{B^3}{L}. \quad (12.10)$$

Remarkably, this does not change the decay laws (12.4) because ϵ_{rec} does not change with time: in the fast-reconnection regime, because \tilde{S}_c is a numerical constant, and in the SP regime, because $\tilde{S}_L \sim \text{const}$ by anastrophy conservation (12.3) (which, for pairs of reconnecting/coalescing magnetic islands of size $\sim L$, is just the conservation of their

⁵⁹If reconnection is stochastic in the sense advocated by [Lazarian et al. \(2020\)](#) (see § 8.3.3 and appendix D.7), then, presumably, $\epsilon_{\text{rec}} \sim 1$. This does not appear to be the case in either 2D or 3D simulations of [Zhou et al. \(2019, 2020\)](#), [Bhat et al. \(2021\)](#), and [Hosking & Schekochihin \(2021\)](#), viz., they all see $\epsilon_{\text{rec}} \sim S_L^{-1/2}$, but there is no telling what might happen at higher resolutions.

flux $\sim BL$). However, by including ϵ_{rec} into the rescaling of the time histories of $\langle B^2 \rangle$ at different S_L , Zhou *et al.* (2019) did confirm that it was the reconnection time scale (12.9), with its η dependence, rather than just the Alfvén time L/B , that controlled the decay in their simulations (their S_L was small enough to stay in the SP regime). Another way to prove this is to replace the Laplacian resistivity with a hyperresistivity (dissipation operator $\eta_n \nabla^n$), which, in the “hyper-SP” regime, makes ϵ_{rec} time-dependent and thus produces different decay laws than (12.4)—these indeed turn out to be the ones seen in such a numerical experiment (Hosking & Schekochihin 2021, the 2D case is described in their Appendix A).

What about the kinetic energy? The turbulence that Zhou *et al.* (2019) studied had none at the outset (they started with just a grid of magnetic islands), so all flows that emerged with time were due to reconnection processes. These are Alfvénic outflows (ignoring the $Pm \gg 1$ case for now), so $U \sim B$, but their mean energy over the system’s volume is not same as the magnetic energy because they are localised to reconnection sites, i.e., to sheets of length L and width $\delta \sim \epsilon_{\text{rec}} L$ (Hosking & Schekochihin 2021). Therefore,

$$\langle U^2 \rangle \sim \frac{\delta}{L} \langle B^2 \rangle \sim \epsilon_{\text{rec}} \langle B^2 \rangle. \quad (12.11)$$

The turbulence is magnetically dominated because $\epsilon_{\text{rec}} \ll 1$, even though the kinetic and magnetic energies’ decay laws are still the same because $\epsilon_{\text{rec}} \sim \text{const}$.

12.2.2. Reconnection-Controlled Decay of Helical MHD Turbulence

The same arguments can be ported immediately to the 3D helical case considered in § 12.1.2. In doing so, I follow the paper by Hosking & Schekochihin (2021).

While the 3D dynamics might not be as vividly dominated by coalescence of magnetic structures as the 2D one is, let us nonetheless assume that the main dynamical process controlling the energy decay and transfer to larger scales is reconnection between blobs of helicity-conserving magnetic fields. To work out the consequences of this assumption, let us again replace (12.7) with (12.10), where ϵ_{rec} is given by (12.9). If reconnection is fast, $\epsilon_{\text{rec}} \sim \text{const}$ again, so the decay laws (12.7) survive, with the only amendment that kinetic energy, while decaying at the same rate as magnetic, is only a small fraction of it given by (12.11).

This outcome still disagrees with (12.8) and most extant numerical simulations, but it is, in fact, highly unlikely that any of these simulations are large enough to reach the fast-reconnection regime. Let us therefore work out what happens when ϵ_{rec} is set by the \tilde{S}_L -dependent SP formula in (12.9). As anastrophy is no longer conserved, $\tilde{S}_L \neq \text{const}$ and (12.10) becomes

$$\frac{dB^2}{dt} \sim -\frac{\eta^{1/2}}{(1+Pm)^{1/4}} \frac{B^{5/2}}{L^{3/2}} \propto -B^{11/2} \Rightarrow \langle B^2 \rangle \propto t^{-4/7}, \quad L \propto t^{4/7}. \quad (12.12)$$

Therefore, $\epsilon_{\text{rec}} \propto \tilde{S}_L^{-1/2} \propto (BL)^{-1/2} \propto t^{-1/7}$, whence the kinetic energy’s decay law is, by (12.11),

$$\langle U^2 \rangle \sim \epsilon_{\text{rec}} \langle B^2 \rangle \propto t^{-5/7}. \quad (12.13)$$

Note that, since the Lundquist number gets larger with time under this scheme (albeit quite slowly), this regime is transient, with reconnection eventually becoming fast and the scalings (12.7) and (12.11) with $\epsilon_{\text{rec}} \sim \text{const}$ taking over in the long run.

Even if we assume that simulations cannot run long enough (or to extend to large enough L) to reach this state, the transient scalings (12.12) and (12.13) are not particularly close to the Biskamp–Müller scalings (12.8) seen in simulations, so it would seem

that these new developments bring us no confirmatory joy. In fact, things are better than they look, for two reasons.

First, most numerical simulations use hyperresistivity, and the generalisation of the above scaling to the “hyper-SP” reconnection does push scaling exponents of the magnetic and kinetic energy away from each other and somewhat closer to $-1/2$ and -1 , respectively. At any rate, the important point is that the decay laws in hyperresistive simulations that fall short of the fast-reconnection regime depend quite sensitively on the order n of the hyperresistivity and so the entire idea of reconnection-controlled decay can be tested by varying n —[Hosking & Schekochihin \(2021\)](#) did that and found that the decay exponents measured in such simulations agreed passably with the theoretical ones obtained in the same way as above but for different n , and disagreed fairly decisively with other theoretical schemes mooted in the literature (e.g., that of [Campanelli 2004](#), discussed in § 12.2.3).

Secondly, the reconnection-controlled decay is, in fact, only justifiable if the amount of kinetic energy in the initial state is not much larger than (12.11), i.e., it is a good theory only for magnetically dominated MHD turbulence. If one starts with $\langle U^2 \rangle \sim \langle B^2 \rangle$, as [Biskamp & Müller \(1999, 2000\)](#) did (or $\langle U^2 \rangle \gg \langle B^2 \rangle$ followed by dynamo, as in [Brandenburg et al. 2019](#)), a different theory is needed to describe the initial stage of the decay (if kinetic energy still ends up decaying faster than magnetic, the system will eventually transition to the magnetically dominated regime). I shall need to introduce some further new ideas before I discuss such a theory, also proposed by [Hosking & Schekochihin \(2021\)](#), in § 12.4.3 and recover the precise scalings (12.8).

12.2.3. Lack of Rescaling Symmetry for Dissipation Coefficients

Before I do that, let me, as a historical footnote, mention the theory of helical decay by [Campanelli \(2004\)](#), which can now be falsified in what appears to be a definitive way. A reader not interested in history can skip this section, as well as § 12.3, and move directly to § 12.4, where new things happen.

The theory in question is formulated in the clever language for discussing self-similar decay pioneered by [Olesen \(1997\)](#). He observed that MHD (and, indeed, also HD) equations have the following rescaling symmetry: $\forall a$ and h ,

$$\mathbf{r} \rightarrow a\mathbf{r}, \quad t \rightarrow a^{1-h}t, \quad \mathbf{u} \rightarrow a^h\mathbf{u}, \quad \mathbf{B} \rightarrow a^h\mathbf{B}, \quad \nu \rightarrow a^{1+h}\nu, \quad \eta \rightarrow a^{1+h}\eta. \quad (12.14)$$

He then posited that decaying MHD turbulence would simply go through a sequence of these transformations, with the rescaling parameter being a power of time, $a = (t/t_0)^{1/(1-h)}$, where t_0 is some reference (not necessarily initial) time. Then

$$\langle U^2 \rangle \propto \langle B^2 \rangle \propto t^{2h/(1-h)}, \quad L \propto t^{1/(1-h)}. \quad (12.15)$$

The tricky part is, of course, to find h . Conservation of helicity, $B^2L \sim \text{const}$, would require $h = -1/2$, which gives the scalings (12.7). To get something else, [Campanelli \(2004\)](#) reasoned that if the magnetic field were approximately force-free, it would fall out of the momentum equation, and, the induction equation being linear, this force-free magnetic field could, therefore, be rescaled by an arbitrary constant: $\mathbf{B} \rightarrow a^m\mathbf{B}$, where m did not need to be the same as h . Conservation of helicity combined with the scaling of L in (12.15) then fixes m in terms of h :

$$B^2L \sim \text{const} \Rightarrow m = -\frac{1}{2} \Rightarrow \langle B^2 \rangle \propto t^{-1/(1-h)}, \quad (12.16)$$

with h still undetermined; $\langle U^2 \rangle$ still satisfies (12.15). He then argued that $h = -1$ because

the dissipation coefficients should stay constant under the rescaling (12.14). This got him the Biskamp–Müller scalings (12.8).⁶⁰

Campanelli’s argument looks neat, but, on reflection, it is counterintuitive that everything should depend on the specific form of dissipation: indeed, if one were formally to replace viscosity and resistivity with hyperviscosity and hyperresistivity, $\eta \nabla^2 \rightarrow \eta_n \nabla^n$, then keeping η_n unchanged by the scaling (12.14) would require a different value of h . Should we then expect different decay laws? This seems unlikely in the limit $\eta_n \rightarrow +0$. In any event, at finite η_n , if Campanelli is right, his theory, straightforwardly generalised, provides specific predictions for decay laws that are different for different n . So does the theory of reconnection-controlled decay, in the “hyper-SP” regime (§ 12.2.2)—and its prediction is different from Campanelli’s. Numerical simulations with hyperdissipation are consistent with the former and rule out the latter quite convincingly (Hosking & Schekochihin 2021).

The conclusion seems to be that dissipation coefficients need not be invariant under the rescaling (12.14). This means that any decay theory that involves dissipative effects—as is the case for reconnection-controlled decay when the reconnection is not fast—need not obey Olesen’s scalings (12.15) for any h (and indeed the helical decay in § 12.2.2 does not).

12.3. Decay of Non-helical MHD Turbulence: Simulations and Theories

What about 3D MHD turbulence with no mean field and zero helicity? Unlike anastrophy in 2D, $\langle H \rangle$ is not a sign-definite quantity and, in mirror-symmetric systems, $\langle H \rangle = 0$. This destroys the usefulness of the constant-helicity constraint (12.6) and re-opens the problem of the decay laws.⁶¹ Physically, one might think of the helical MHD turbulence as decaying from an initial state produced by dynamo action of a helical flow (see review by Rincon 2019); similarly, the starting point for non-helical decay might be the saturated state of a non-helical fluctuation dynamo (§ 13).

How to handle the non-helical decay has until recently remained unsettled, although quite a lot of numerical evidence about what happens in it does exist, alongside some theoretical arguments, which I will survey in a moment. I shall get to what I believe to be the right way to think about this regime in § 12.4, to which an impatient reader is welcome to turn immediately.

The conversation in the literature about non-helical decay has been heavily influenced by the fact that the 2D scalings (12.4) appear to work quite well also in 3D with zero helicity. This was reported with various degrees of certainty in a number of numerical experiments (Mac Low *et al.* 1998; Biskamp & Müller 1999, 2000; Christensson *et al.* 2001; Banerjee & Jedamzik 2004; Frick & Stepanov 2010; Berera & Linkmann 2014; Brandenburg *et al.* 2015; Brandenburg & Kahniashvili 2017; Reppin & Banerjee 2017; Bhat *et al.* 2021). The 2D analogy did not escape their authors: e.g., Brandenburg *et al.*

⁶⁰Christensson *et al.* (2005) have an argument for $L \propto t^{1/2}$ that is essentially a version of Campanelli’s. It is based on the self-similar solution (12.35) for the energy spectrum. It is hard-wired into this solution that $L \propto t^{1/(1-h)}$, but if one now assumes self-similarity all the way down to the dissipation scales, the dissipative cutoff must have the same scaling, so $\lambda_\eta \propto t^{1/(1-h)}$. In a nutshell, Christensson *et al.* (2005) then set $\lambda_\eta \sim (\eta t)^{1/2}$ by dimensional analysis and hence conclude that $h = -1$. It is, of course, far from obvious that λ_η depends only on η and t but not also on L , B and/or U (and, therefore, on the initial energy and scale of the turbulence), as the Kolmogorov scale does in a turbulence with constant energy flux.

⁶¹The constant-helicity constraint is also absent when there is an external mean field, hence in RMHD, because there is no helicity conservation in this approximation (the mean field always “sticks out” of the volume). I shall deal with this regime in § 12.6.

(2015) speculated about “near conservation” of a local version of anastrophy (*pace* the gauge-non-invariance of $\langle A^2 \rangle$). While it is true that, as observed, e.g., by Bhat *et al.* (2021), $\langle A^2 \rangle$, while not a 3D invariant, decays slower with time than energy—indeed it does, since $A \sim BL$, B decays, and L grows under any sensible decay law,—it is perhaps a stretch that this is the cause rather than a corollary of the latter.

Another scheme for rationalising $BL \sim \text{const}$ is to argue that dynamically, the decay of the magnetic energy and the increase of the scale at which it sits are driven by mergers, via reconnection, of long flux tubes, as appears to be the case in 3D RMHD (Zhou *et al.* 2020, see § 12.6)—Bhat *et al.* (2021) make a long and careful empirical case for such a scenario. In fact, in an earlier paper, Reppin & Banerjee (2017) already mention (albeit gingerly and amongst other options) the possibility that ever larger magnetic structures might be generated via mergers of reconnecting flux ropes, an idea that they attribute to Müller *et al.* (2012), who in turn credit the 2D study by Biskamp & Bremer (1994). While it is not at all obvious (and, in fact, not true: see § 12.4.2) that flux tubes in 3D MHD without a mean field should reconnect while conserving their “2D poloidal flux” ($\sim BL$), it is true that the 3D non-helical decay is controlled by reconnection, just like the 2D and the 3D helical decays turned out to be in § 12.2—the theory that I will present in § 12.4.2 will utilise this.

Campanelli (2004) also has a theory of non-helical decay. This follows from his argument, already rehearsed in § 12.2.3, that the decay exponents are fixed by the requirement that the dissipation coefficients in MHD must stay constant under Olesen’s rescaling symmetry (12.14), implying $h = -1$. In the non-helical case, he does not assume a force-free magnetic field, and so does not rescale it separately from (12.14). The result is the scalings (12.15), which, with $h = -1$, are the same as the 2D scalings (12.4). Olesen (2015) commented that under this self-similarity, $\langle A^2 \rangle = \text{const}$, so anastropy would be conserved regardless of the dimensionality of the problem (he called this “dimensional reduction”). Just as in the helical case, Campanelli’s theory is testable numerically via its generalisation to hyperviscous and hyperresistive dissipation, and fails the numerical tests in comparison with the reconnection-controlled decay described in § 12.4.2 (Hosking & Schekochihin 2021).

12.4. Selective Decay Constrained by Saffman Invariants

Let me now outline a new way (or, rather, a new version of a very old way) of thinking about the non-helical MHD decay and similar problems, proposed by David Hosking (Hosking & Schekochihin 2021).

The basic idea is that $\langle H \rangle = 0$ does not mean (except in very artificial set-ups) that no part of the turbulence has any local magnetic links or twists and thus local helicity (figure 26). While helicity has to sum up to zero over the entire system, these local helical features will still impose topological constraints on the system’s decay. The challenge is to express these constraints mathematically.

We shall draw inspiration from the long experience of thinking of such questions that exists in the context of (various flavours of) hydrodynamic turbulence.⁶² Since Kolmogorov (1941c), the decay of hydrodynamic turbulence has been treated as selective decay subject to conservation of certain invariants related to the conservation of the momentum and angular momentum of the motions—but these conserved quantities, while present locally in the turbulent “eddies”, sum up to zero over the entire system, so

⁶²A magisterial tutorial on this subject, with all the key ideas, nuances, fallacies, historical triumphs and setbacks narrated in a friendly and clear style, can be found in the books by Davidson (2013, 2015), whose own contributions form a significant part of the emerging canon.

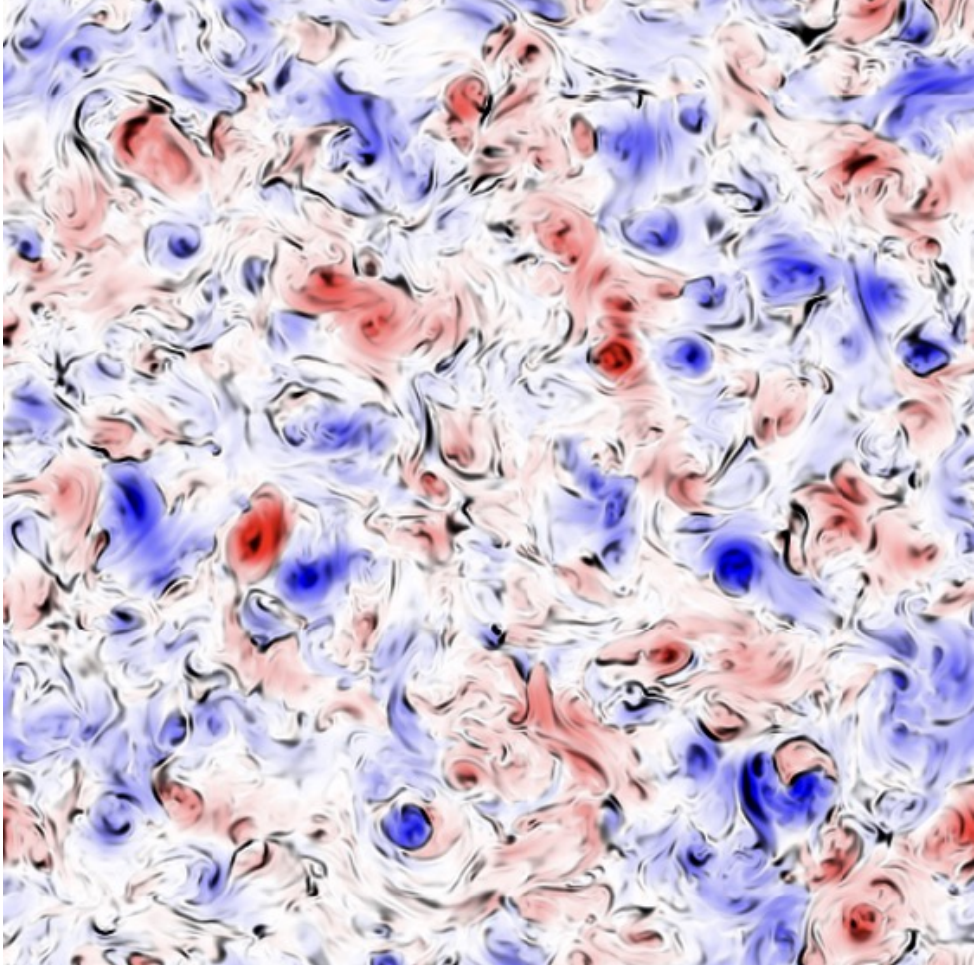


FIGURE 26. A cross-section of helicity density $H = \mathbf{A} \cdot \mathbf{B}$ (in Coulomb gauge, $\nabla \cdot \mathbf{A} = 0$) from a decaying 3D MHD turbulence simulation (512^3) with zero net helicity, taken from Hosking & Schekochihin (2022a). Red is $H > 0$, blue is $H < 0$. The superimposed grey scale shows the magnitude of the current density $J = |\nabla \times \mathbf{B}|$, so the black patches are strong currents between, and on the edges of, local blobs of non-zero helicity—presumably, these are reconnection sites where decay occurs, at constant Hosking invariant (12.25), i.e., conserving the mean square helicity fluctuations.

cannot simply be fixed in the same way as $\langle A_z^2 \rangle$ or $\langle H \rangle$ were in §§ 12.1 and 12.2. Thus, the situation is somewhat analogous to the MHD case with $\langle H \rangle = 0$.

12.4.1. Generalised Saffman Invariants

Consider a conserved quantity that has a local density ψ and that is not sign-definite. That $\langle \psi \rangle$ is conserved is expressed generically by ψ satisfying a dynamical equation of the form

$$\frac{\partial \psi}{\partial t} + \nabla \cdot \boldsymbol{\Gamma} = \text{diss. terms}, \quad (12.17)$$

where $\boldsymbol{\Gamma}$ is the flux of ψ . In the context of the upcoming derivations, ψ might be, e.g., (a component of) the fluid velocity \mathbf{u} or the helicity density $H = \mathbf{A} \cdot \mathbf{B}$. Let us now denote

$$\bar{\psi}_V = \int_V d^3\mathbf{r} \psi(\mathbf{r}), \quad (12.18)$$

where V is a finite volume, and assume that $\langle \psi \rangle \equiv \lim_{V \rightarrow \infty} \bar{\psi}_V / V = 0$. The fact that the average of ψ over the infinite space vanishes does not mean that its integral over a finite volume must do so, but, if we take $V \gg L^3$, where L is the outer scale (correlation length) of ψ , it is reasonable to assume that the integral accumulates as a random walk:⁶³

$$\bar{\psi}_V \sim \left(\frac{V}{L^3} \right)^{1/2} \delta\psi_L L^3 \Rightarrow \lim_{V \rightarrow \infty} \frac{\bar{\psi}_V^2}{V} \sim \delta\psi_L^2 L^3, \quad (12.19)$$

where $\delta\psi_L$ is the typical size of the fluctuation of ψ at its correlation scale L . This suggests that the mean square fluctuation of ψ is a finite, V -independent quantity. It can be expressed in terms of the two-point correlation function of ψ :

$$\lim_{V \rightarrow \infty} \frac{\bar{\psi}_V^2}{V} = \lim_{V \rightarrow \infty} \frac{1}{V} \iint_V d^3\mathbf{r} d^3\mathbf{r}' \psi(\mathbf{r}) \psi(\mathbf{r}') = \int d^3\mathbf{l} \langle \psi(\mathbf{r}) \psi(\mathbf{r} + \mathbf{l}) \rangle \equiv I_\psi. \quad (12.20)$$

The integral I_ψ is finite provided correlations decay faster than $1/l^3$ as $l \rightarrow \infty$. Furthermore, I_ψ is an invariant because, from (12.17),

$$\frac{\partial}{\partial t} \langle \psi(\mathbf{r}) \psi(\mathbf{r} + \mathbf{l}) \rangle + \frac{\partial}{\partial l} \cdot \langle [\boldsymbol{\Gamma}(\mathbf{r} + \mathbf{l}) - \boldsymbol{\Gamma}(\mathbf{r} - \mathbf{l})] \psi(\mathbf{r}) \rangle = \text{diss. terms} \Rightarrow \frac{dI_\psi}{dt} \rightarrow 0. \quad (12.21)$$

The last formula holds as dissipation coefficients $\rightarrow +0$ if the dissipation terms can be argued to vanish in this limit and if all correlations decay faster than $1/l^3$ (so I_ψ is finite and the surface integral left of the flux term vanishes).

In a system with $\langle \psi \rangle = 0$ and $\psi \neq 0$ pointwise, it is subject to the conservation of I_ψ that one ought to assume the selective decay of energy to be happening.

Following Davidson (2013, 2015), I shall refer to quantities such as I_ψ as (generalised) ‘‘Saffman invariants’’. The original Saffman invariant was a measure of conservation of the linear momentum of the turbulent eddies, viz., $\psi = \mathbf{u}$, and was introduced by Saffman (1967), via a line of reasoning roughly analogous to the above, to constrain the decay laws for hydrodynamic turbulence with long-range correlations. His calculation, analogous to the selective-decay ones in §12.1 (but pre-dating them considerably), is

$$I_u \sim U^2 L^3 \sim \text{const} \Rightarrow \frac{dU^2}{dt} \sim -\frac{U^3}{L} \propto -U^{11/3} \Rightarrow \langle U^2 \rangle \propto t^{-6/5}, \quad L \propto t^{2/5}. \quad (12.22)$$

Kolmogorov (1941c) used (in fact, pioneered) the same method, except he assumed that $I_u = 0$ and conjectured that the decay of turbulence would be controlled by the Loitsyansky invariant, which is just I_ψ with $\psi = \mathbf{r} \times \mathbf{u} \equiv \mathbf{L}$, expressing the conservation of the angular momentum of the eddies (see Landau & Lifshitz 1987; Davidson 2013,

⁶³Modulo some subtleties and nuances that an interested reader can read about in Davidson (2013, 2015) and Hosking & Schekochihin (2021).

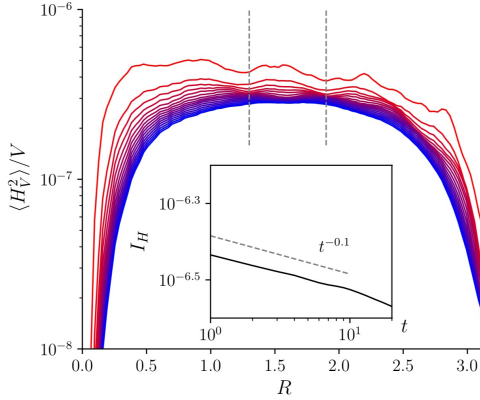


FIGURE 27. Numerical probe of the conservation of the Hosking invariant I_H , defined by (12.20) with $\psi = \mathbf{A} \cdot \mathbf{B}$. This plot, reproduced from Hosking & Schekochihin (2021), is of the mean square helicity density over a cubic volume $V = (2R)^3$, at different times in a decaying, non-helical, 3D MHD turbulence simulation started in a magnetically dominated state—red-to-blue curves correspond to earlier-to-later times. The simulation box is periodic, which is why I_H is only non-zero in a range of R intermediate between the energy-containing scale L and the box size ($2R = 2\pi$). The inset shows the near-constancy of I_H (calculated over the interval of R indicated by vertical dashed lines).

2015).⁶⁴

$$I_L = \int d^3l l^2 \langle \mathbf{u}(\mathbf{r}) \cdot \mathbf{u}(\mathbf{r} + \mathbf{l}) \rangle = \text{const} \quad \Rightarrow \quad U^2 L^5 \sim \text{const}. \quad (12.23)$$

With this constraint, one gets the famous Kolmogorov (1941c) laws of decay:

$$\frac{dU^2}{dt} \sim -\frac{U^3}{L} \propto -U^{17/5} \quad \Rightarrow \quad \langle U^2 \rangle \propto t^{-10/7}, \quad L \propto t^{2/7}. \quad (12.24)$$

12.4.2. Decay of Magnetically Dominated Non-helical MHD Turbulence

Hosking & Schekochihin (2021) introduced a new invariant, which they called the “Saffman helicity invariant” and to which I will refer as the Hosking invariant, I_H (figures 27 and 26). This invariant is I_ψ defined in (12.20) with $\psi = H = \mathbf{A} \cdot \mathbf{B}$, the helicity density (anticipating an erudite reader’s concern, yes, they did show that it was gauge-invariant).⁶⁵ They then considered the decay of non-helical MHD turbulence subject to conservation of I_H ,

$$I_H \sim (AB)^2 L^3 \sim B^4 L^5 \sim \text{const}, \quad (12.25)$$

and with the assumption that the decay occurs on the reconnection time scale (12.9).

⁶⁴Note that $\langle \mathbf{u}(\mathbf{r}) \cdot \mathbf{u}(\mathbf{r} + \mathbf{l}) \rangle$ must decay faster than $1/l^5$ as $l \rightarrow \infty$ in order for I_L to be finite, so this situation, known as Batchelor turbulence (after Batchelor & Proudman 1956), describes the decay of turbulent systems with shorter-range correlations than in Saffman turbulence. It is realised if the initial state is set up to have $I_u = 0$. Note also that the interpretation of the Loitsyansky integral in terms of the conservation of angular momentum is somewhat shaky, mathematically (see Davidson 2013, 2015).

⁶⁵It turns out that a similar idea does exist in the literature with application to pure hydrodynamical turbulence: the invariant I_ψ , with $\psi = \mathbf{u} \cdot (\nabla \times \mathbf{u})$, the kinetic helicity of the turbulent flow, was introduced by Levich & Tsinober (1983) and bears their name; it was used by Frenkel & Levich (1983) to propose an amended turbulence decay theory. I am grateful to A. Bershadskii for pointing me to these papers.

When the reconnection is fast ($\epsilon_{\text{rec}} \sim \text{const}$),

$$\frac{dB^2}{dt} \sim -\epsilon_{\text{rec}} \frac{B^3}{L} \propto -B^{19/5} \Rightarrow \langle B^2 \rangle \propto t^{-10/9}, \quad L \propto t^{4/9}, \quad \langle U^2 \rangle \sim \epsilon_{\text{rec}} \langle B^2 \rangle, \quad (12.26)$$

where the last formula is again (12.11) (in Olesen's language, § 12.2.3, this corresponds to $h = -5/4$). When the reconnection is slow, as in (12.12),

$$\frac{dB^2}{dt} \propto -\frac{B^{5/2}}{L^{3/2}} \propto -B^{37/10} \Rightarrow \langle B^2 \rangle \propto t^{-20/17}, \quad L \propto t^{8/17}, \quad \langle U^2 \rangle \propto t^{-19/17}. \quad (12.27)$$

The decay law for kinetic energy follows from (12.11) and $\epsilon_{\text{rec}} \propto \tilde{S}_L^{-1/2} \propto (BL)^{-1/2} \propto t^{1/17}$. Note that, unlike in the case of helical decay (§ 12.2.2), the reconnection rate increases (Lundquist number decreases) with time (extremely slowly), so the system never gets out of the slow-reconnection regime. In fact, even in the case of fast reconnection (12.26), the Lundquist number decreases with time, $\tilde{S}_L \propto t^{-1/9}$, so the asymptotic decay laws are ones for slow reconnection (12.27).

Whilst neither (12.26) nor (12.27) are the same as the 2D scalings (12.4) that are believed to be seen in numerical simulations (§ 12.3), they are uncannily close—and almost certainly not numerically distinguishable from either each other or (12.4). Just as in the case of helical turbulence, a way to verify them numerically is to generalise (12.27) to the hyperresistive case and test the dependence of the scaling exponents on the hyperresistivity order n —a test that the theory passes reasonably well (see Hosking & Schekochihin 2021).

As in the case of helical decay, this theory describes only magnetically dominated decay, where the kinetic energy is all due to reconnection outflows. If instead the initial state has $\langle U^2 \rangle \sim \langle B^2 \rangle$ (or $\langle U^2 \rangle \gg \langle B^2 \rangle$ followed by dynamo), working out its decay laws requires further theoretical arrangements, described in § 12.4.3.⁶⁶

12.4.3. Selective Decay Constrained by Saffman Cross-Helicity Invariant

The method of Saffman invariants (§ 12.4.1) is begging to be applied to another non-sign-definite conserved MHD quantity, the cross-helicity, whose density is $\mathbf{u} \cdot \mathbf{B} \equiv X$. In a balanced turbulence, $\langle X \rangle = 0$, arguably a natural situation in the absence of a mean field.⁶⁷ There is then the Saffman cross-helicity invariant, I_ψ of (12.20) with $\psi = X$ (which appears to have been first considered, for a different purpose, by Bershadskii 2019, who was inspired by the paper of Levich & Tsinober 1983 already mentioned in footnote 65, and its follow-ups, e.g., Levich *et al.* 1991 and Levich 2009). Unlike in the case of I_H , it is not obvious (and may not be true) that I_X is conserved better than the energy because the fields involved in it (\mathbf{u} and \mathbf{B}) are the same fields as those whose mean squares make up the energy. Let us put this issue aside for further investigation and not allow it to stop us from considering what would happen if decay of MHD turbulence were constrained by the conservation of I_X .

This is not an entirely frivolous or formalistic exercise because there is quite a lot of evidence that MHD turbulence has a tendency to break up into patches of non-zero

⁶⁶Note that, since $\langle U^2 \rangle$ in (12.27) decays a little bit slower than $\langle B^2 \rangle$, it must be the case that, if one waits long enough (longer, no doubt, than any numerical simulation has ever been able to afford to wait), the system will get out of the magnetically dominated state and into the $\langle U^2 \rangle \sim \langle B^2 \rangle$ territory. Amusingly, as we are about to see, that will push it back to a magnetically dominated state, so perhaps the system will oscillate between (12.27) and (12.29).

⁶⁷This is not to say that the case $\langle X \rangle \neq 0$ has lacked attention: there is a lively literature on it, cited in § 12.7.

cross-helicity (“imbalance”)—not only in the inertial range, as I already noted in § 9.1 (see figure 17), but also in decaying, zero-mean-field turbulence, on the outer scale (e.g., Matthaeus *et al.* 2008; Servidio *et al.* 2008). This is understandable: nonlinearity is likely to be weaker in places where the fields are closer to an Elsasser state, so decay in those places would be slower than where $Z^+ \sim Z^-$, and there would be a natural tendency for the imbalanced patches to survive Darwinianly (cf. § 12.7).

If such situations do arise, they must do so when kinetic and magnetic energies of the turbulence are (initially) not very different—precisely the case of $\langle U^2 \rangle \sim \langle B^2 \rangle$ that is not described by the theories of magnetically dominated decay outlined in §§ 12.2.2 and 12.4.2 and that I promised there to deal with later.

Let me deal with it now, following again Hosking & Schekochihin (2021). Conservation of I_X gives us a constraint,

$$I_X \sim U^2 B^2 L^3 \sim \text{const}, \quad (12.28)$$

which in this regime should replace the estimate (12.11) of $\langle U^2 \rangle$ resulting from reconnection outflows. Together with the helicity constraint (12.6), $B^2 L \sim \text{const}$, this gives $U \propto B^2$ which is precisely the relationship spotted numerically by Biskamp & Müller (1999, 2000). Since kinetic energy is now not small (at least initially), it is perhaps not as far-fetched as in the magnetically dominated regime to assume that the energy decays on the ideal time scale $\sim L/U$. Doing so and making use of our two constraints, we get

$$\frac{dB^2}{dt} \sim -\frac{UB^2}{L} \propto -B^6 \Rightarrow \langle B^2 \rangle \propto t^{-1/2}, \quad \langle U^2 \rangle \propto t^{-1}, \quad L \propto t^{1/2}. \quad (12.29)$$

These are precisely the Biskamp–Müller scalings (12.8) for helical decay. As I anticipated in § 12.2.2, since kinetic energy decays faster than magnetic, these decay laws, if correct, must be transient, eventually changing to the magnetically dominated case. This is more or less the scenario envisioned by Brandenburg *et al.* (2019) based on their simulations that started with $\langle B^2 \rangle \ll \langle U^2 \rangle$, exhibited (helical) dynamo action that brought the magnetic field to dynamical strength, and then decayed (transiently) according to (12.29).

If we instead consider the non-helical case, the helicity constraint (12.6) must be replaced by the conservation of the Hosking invariant (12.25). Combined with (12.28), this gives $U \sim B^{1/5}$, i.e., magnetic field would decay faster than velocity. But that is not a sustainable proposition: by such a decay, magnetic field would be brought down below dynamical strength, whereupon it would be re-grown by dynamo action. A natural conclusion might be that magnetic field in this regime would not be able to constrain decay and instead stay just under dynamical strength and follow the velocity field, which would decay according to a purely hydrodynamic law, probably (12.24). There might be some support for this scenario in the simulations of Bhat *et al.* (2021).

Finally, for completeness and without much supporting evidence, but just to show the joys of the new toys that are the generalised Saffman invariants for MHD, here is what happens in 2D MHD with conserved Saffman cross-helicity—again relevant, presumably, for cases in which magnetic energy does not dominate initially. In 2D,

$$I_X \sim U^2 B^2 L^2 \sim \text{const}. \quad (12.30)$$

But the anastrophy constraint (12.3) tells us that $BL \sim \text{const}$, so we must have $U \sim \text{const}$, whence

$$\frac{dB^2}{dt} \sim -\frac{UB^2}{L} \propto -B^3 \Rightarrow \langle B^2 \rangle \propto t^{-2}, \quad L \propto t, \quad \langle U^2 \rangle \sim \text{const}. \quad (12.31)$$

Thus, magnetic field will decay quite vigorously and rush to larger scales, while kinetic energy will stay constant. Just as in the case of non-helical decay in 3D, this regime

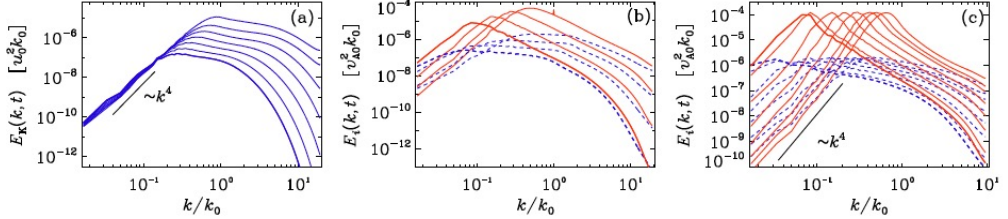


FIGURE 28. Spectra of kinetic (blue) and magnetic (red) energies in decaying turbulence: (a) pure hydrodynamic, (b) MHD with no mean field and zero helicity, (c) MHD with no mean field and finite helicity. The time evolution is from right to left (always towards larger scales). These plots are from [Brandenburg & Kahnashvili \(2017\)](#).

cannot persist because the magnetic field will soon drop below dynamical strength—but there is no dynamo in 2D ([Zeldovich 1956](#)), so it will just decay away, exponentially in the kinematic regime, leaving 2D hydrodynamic turbulence decaying by its own, slow, devices (see [Davidson 2013, 2015](#) for more). Qualitatively, this seems to be consistent with what [Kinney et al. \(2000\)](#) see in their “2D dynamo” simulations.

12.5. Permanence of Large Scales vs. Inverse Transfer

In the introduction to §12, I argued that the inertial-range spectrum of decaying turbulence is not an interesting new subject (I will return to this thought in §12.8). What is interesting though is its large-scale spectrum, at $kL \ll 1$, i.e., the presence and growth, or otherwise, of long-range correlations. Consider the 1D spectrum of a statistically isotropic field ψ and Taylor-expand it in small k :

$$E_\psi(k) = 4\pi k^2 \int \frac{d^3l}{(2\pi)^3} \langle \psi(\mathbf{r})\psi(\mathbf{r}+\mathbf{l}) \rangle e^{-ik\cdot l} = \frac{1}{2\pi^2} (I_\psi k^2 + J_\psi k^4 + \dots), \quad (12.32)$$

where I_ψ is the Saffman invariant (12.20) and $J_\psi = -(1/3) \int d^3l l^2 \langle \psi(\mathbf{r})\psi(\mathbf{r}+\mathbf{l}) \rangle$. Obviously, the Taylor expansion can only be extended to k^2 and k^4 if the coefficients I_ψ and J_ψ are finite, i.e., if correlations decay faster than $O(l^{-3})$ and $O(l^{-5})$, respectively.

If $I_\psi \neq 0$, then the large-scale spectrum is $\propto k^2$ and, moreover, the energy content at low k is frozen by the conservation of I_ψ —even though the outer scale L increases during decay, there is no energy transfer into larger scales, motions at those scales just take longer to decay. This feature is sometimes referred to as the “permanence of large scales” ([Davidson 2013, 2015](#)).

What, however, if $I_\psi = 0$, as it would normally be for $\psi = \mathbf{u}$ or $\psi = \mathbf{B}$? Then the spectrum at large scales is $\propto k^4$ and, if this is K41 turbulence decaying subject to the conservation of the Loitsyansky invariant (12.23), $I_L \propto J_u = \text{const}$, there is still permanence of large scales, although with weaker correlations. This is illustrated in figure 28(a). However, J_ψ need not be an invariant for every ψ for which I_ψ is, so, generally speaking, it will change with time. An example of that is the decay of helical MHD turbulence, the evolution of whose magnetic spectrum is shown in figure 28(c): while it still has the k^4 long-wavelength asymptotic, the prefactor J_B now is manifestly *not* conserved, but rather grows robustly with time, meaning that magnetic energy is quite vigorously transferred to larger scales—an “inverse cascade” (non necessarily local in k) associated with the conservation of magnetic helicity and its transfer to large scales, which is a well known phenomenon also in forced turbulence, often in the context of helical dynamo action ([Pouquet et al. 1976; Brandenburg 2001; Müller et al. 2012](#);

Rincon 2019).⁶⁸ A similar behaviour in non-helical decaying MHD turbulence has recently generated a flurry of excitement: an inverse magnetic-energy transfer was discovered there numerically by Zrake (2014) and Brandenburg *et al.* (2015) (accompanied by Berera & Linkmann 2014 and followed by Reppin & Banerjee 2017, Park 2017, and Bhat *et al.* 2021)—figure 28(b) is from the non-helical simulation by Brandenburg *et al.* (2015) and shows healthy magnetic-energy growth at low wavenumbers.⁶⁹

12.5.1. Scalings for Inverse Transfer of Magnetic Energy

Since we now do have a theory of the decay of MHD turbulence of any flavour, we can easily work out whether and how the large-scale spectrum grows: e.g.,

$$J_B \sim B^2 L^5 \sim \begin{cases} t^{8/3}, & (12.7), \text{ helical, ideal/fast-reconnecting, } B \gg U, \\ t^{16/7}, & (12.12), \text{ helical, SP-reconnecting, } B \gg U, \\ t^2, & (12.29), \text{ helical, ideal, } B \sim U, \\ t^{10/9}, & (12.26), \text{ non-helical, ideal/fast-reconnecting, } B \gg U, \\ t^{20/17}, & (12.27), \text{ non-helical, SP-reconnecting, } B \gg U, \\ t^{(5+2m)/(1-h)}, & \S 12.2.3, \text{ self-similar.} \end{cases} \quad (12.33)$$

Thus, in all conceivable regimes, there is some inverse transfer of energy to large scales—not altogether surprising if the underlying dynamics involves mergers (by reconnection) of structures, rather than merely slower decay of the larger ones.

Obviously, the same logic can be applied to spectra of all other fields. E.g., Hosking & Schekochihin (2021) observe (and confirm numerically) that, for reconnection-dominated decay of non-helical MHD turbulence, the spectrum of the quantity $H = \mathbf{A} \cdot \mathbf{B}$ is $\langle |H_{\mathbf{k}}|^2 \rangle \propto I_H = \text{const}$ at low k , recovering, in a certain sense, the principle of permanence of large scales (and providing another way to test the conservation of the Hosking invariant I_H).

12.5.2. Self-Similar Spectra and Inverse Energy Transfer

Let me show, for completeness, and for context, in view of the discussions that appear in the literature, how to obtain these results in the language of self-similar solutions introduced in § 12.2.3. Following Olesen (1997), let us work out what the symmetry (12.14) implies for the spectrum of any of the fields that have it. For example, for the magnetic field, the spectrum satisfies

$$E(k, t) = 4\pi k^2 \int \frac{d^3 l}{(2\pi)^3} e^{-ik \cdot l} \langle \mathbf{B}(\mathbf{r}, t) \cdot \mathbf{B}(\mathbf{r} + \mathbf{l}, t) \rangle = a^{-1-2m} E(a^{-1}k, a^{1-h}t), \quad (12.34)$$

⁶⁸In the dynamo case, forced (Brandenburg 2001) or decaying (Brandenburg *et al.* 2019), a helical velocity field generates a magnetic field from a small seed that initially has zero helicity. This field has helicity of one sign at small scales and of the opposite sign at large scales (larger than the scale of the velocity), keeping overall $H = 0$. The small-scale helicity is slowly destroyed by resistivity (which possibly makes the whole process very inefficient; see discussion in Rincon 2019), while the large-scale helicity is stuck at large scales and can, if forcing is switched off or absent from the beginning, serve as the starting point for a helical decaying regime—this scenario is nicely traced out in Brandenburg *et al.* (2019).

⁶⁹In earlier, lower-resolution non-helical simulations by Banerjee & Jedamzik (2004), no inverse transfer was detected. Reppin & Banerjee (2017) report that increasing P_m while holding Re constant also kills the effect. One can imagine that in both of these cases, reconnection might not have been able to get going properly.

where I used Campanelli's more general rescaling $\mathbf{B} \rightarrow a^m \mathbf{B}$, where $m = -1/2$ with helicity and $m = h$ without. A self-similarly evolving solution of (12.34) is

$$E(k, t) = k^{-1-2m} f(kt^{1/(1-h)}), \quad (12.35)$$

where $f(x)$ is some function that needs to be integrable in an appropriate way in order for the total energy to be finite:

$$\langle B^2 \rangle = \int_0^\infty dk E(k, t) = t^{2m/(1-h)} \int_0^\infty dx x^{-1-2m} f(x). \quad (12.36)$$

The decay laws (12.7), (12.29), and (12.26) are recovered for $(m, h) = (-1/2, -1/2)$, $(-1/2, -1)$, $(-5/4, -5/4)$, respectively [the SP-reconnecting cases (12.12) and (12.27) are non-self-similar].

If $I_{\mathbf{B}} = 0$, the magnetic-energy spectrum must be $\propto k^4$ at $kL \ll 1$. This requires $f(x) \propto x^{5+2m}$, whence

$$E(k, t) \propto t^{(5+2m)/(1-h)} k^4. \quad (12.37)$$

This is the same result as the last formula in (12.33). The solution (12.35) also implies that the peak of the spectrum, at $kL \sim 1$, is $E_{\max} \propto t^{(1+2m)/(1-h)} = \text{const}$ for the helical case (manifestly true in figure 28c) and $E_{\max} \propto t^{-1/2}$ for the non-helical one (figure 28b). Brandenburg & Kahniashvili (2017) show that rescaling their time-dependent spectra in line with (12.35), or, to be precise, with the equivalent expression $E(k, t) = L(t)^{1+2m} g(kL(t))$, where $L(t)$ is measured directly at every t , collapses them all onto a single curve, confirming self-similarity.

Let me observe, finally, that if the prefactor of the low- k asymptotic of $E(k)$ changes with time, as it does in (12.37), i.e., if $J_{\mathbf{B}}$ is not conserved, I see no reason to expect that the long-term self-similar evolution should be tied to the low- k scaling baked into the initial condition, as many authors, starting with Olesen (1997), seem to believe. The self-similar evolution need not start at $t = 0$, and it is perfectly possible that it is preceded by some initial non-self-similar rearrangement. There appears to be convincing numerical evidence that this is indeed what happens (e.g., Brandenburg & Kahniashvili 2017; Brandenburg *et al.* 2019; Hosking & Schekochihin 2021).

12.6. Decay of Magnetically Dominated RMHD Turbulence

Let me now finally return to MHD turbulence with a strong mean field (RMHD turbulence), which elsewhere in this review has been my primary preoccupation. Zhou *et al.* (2020) initialised an RMHD simulation with an array of magnetic flux tubes parallel to the mean field and found that it behaved rather similarly to the magnetically dominated 2D MHD (§ 12.2.1), with flux tubes reconnecting (coalescing) with each other in the perpendicular plane, and the system thus decaying towards a state dominated by ever-larger-scale magnetic structures. While the “perpendicular anastrophy” $\langle A_{\parallel}^2 \rangle$ is not formally conserved in RMHD, Zhou *et al.* (2020) assumed that RMHD reconnection would nevertheless proceed in a quasi-2D fashion, preserving the poloidal “2D flux”:

$$b_{\perp} L_{\perp} \sim \text{const}. \quad (12.38)$$

If one accepts this, the rest of the argument is exactly the same as in 2D MHD (§§ 12.1.1 and 12.2.1): replacing $B \rightarrow b_{\perp}$, $U \rightarrow u_{\perp}$, and $L \rightarrow L_{\perp}$, one gets

$$\langle b_{\perp}^2 \rangle \propto t^{-1}, \quad \langle u_{\perp}^2 \rangle \sim \epsilon_{\text{rec}} \langle b_{\perp}^2 \rangle, \quad L_{\perp} \propto t^{1/2}. \quad (12.39)$$

Since (12.38) implies $\tilde{S}_{L_{\perp}} \sim \text{const}$, $\epsilon_{\text{rec}} \sim \text{const}$ in both fast and SP reconnection regimes.

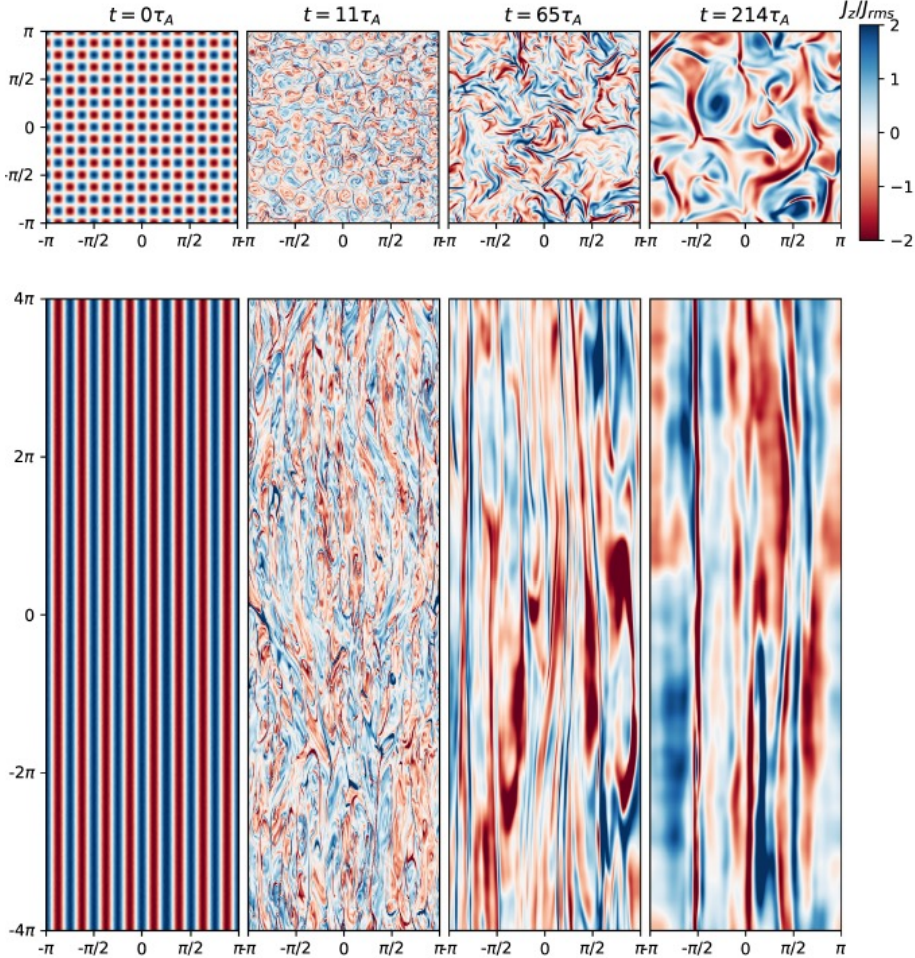


FIGURE 29. Snapshots of vertical (z) current density in the $(x, y, 0)$ (top row) and $(x, 0, z)$ (bottom row) planes, taken at a series of subsequent times in a decaying RMHD simulation by Zhou *et al.* (2020). This illustrates growth of $L_\perp \propto \sqrt{t}$ and $L_\parallel \propto t$ (the scalings confirmed quantitatively in their paper) and the presence of numerous current sheets.

A new feature is to argue that the length of the tubes along the mean field is determined by the CB condition:

$$\tau_A \sim \frac{L_\parallel}{v_A} \sim \tau_{\text{rec}} \propto \frac{L_\perp}{b_\perp} \quad \Rightarrow \quad L_\parallel \propto t. \quad (12.40)$$

Zhou *et al.* (2020) check the scalings (12.39) and (12.40) in their RMHD simulations (figure 29) and declare success. It is interesting to analyse the ingredients of this success in light of the long discussion of selective decay in MHD given in the preceding sections.

12.6.1. Saffman Cross-Helicity Invariant in RMHD

The adoption of (12.38) in 3D is, of course, a bit of a sleight of hand. This is not a flux-conservation constraint: the 3D poloidal flux through the radial cross-section of the flux tube, $\sim b_\perp L_\perp L_\parallel$, does *not* stay constant under this scheme; if it did, critical balance (12.40) would then imply $L_\perp \sim \text{const}$, which cannot be true.

There is, however, another way to justify (12.38) (Hosking & Schekochihin 2021). Since we are dealing with an RMHD system initialised with $u_\perp = 0$, the cross-helicity $\langle X \rangle = \langle \mathbf{u}_\perp \cdot \mathbf{b}_\perp \rangle$ is zero initially and will stay small as long as $u_\perp \ll b_\perp$. The logical application of the principles advocated in § 12.4 is then to posit the conservation of the Saffman cross-helicity invariant:

$$I_X \sim u_\perp^2 b_\perp^2 L_\perp^2 L_\parallel \propto b_\perp^3 L_\perp^3 \sim \text{const}, \quad \text{q.e.d.}, \quad (12.41)$$

assuming $u_\perp \propto b_\perp$ (Alfvénic flows) and $L_\parallel \propto L_\perp/b_\perp$ (CB).

It is an open question whether a decaying RMHD can stay in a balanced state, $\langle X \rangle = 0$, forever, or whether a fluctuation of $\langle X \rangle$ away from zero can eventually tip it over to another decaying regime, tending to an Elsasser state (§ 12.7).

12.6.2. Self-Similar Decay in RMHD

The reader who liked Olesen's approach (§§ 12.2.3 and 12.5.2) and remembers the RMHD symmetry (3.5) has been straining at the leash to apply the former to the latter. It is, of course, the same symmetry as (12.14) if one lets $\epsilon = a^h$, except now perpendicular and parallel gradients and, therefore, distances transform differently from each other:⁷⁰

$$\mathbf{r}_\perp \rightarrow a\mathbf{r}_\perp, \quad r_\parallel \rightarrow a^{1-h}r_\parallel. \quad (12.42)$$

This is just because v_A is now assumed to be an immutable constant, so r_\parallel transforms as time, rather than as distance (cf. Beresnyak 2015, and § 5.2). The resulting scalings,

$$\langle u_\perp^2 \rangle \propto \langle b_\perp^2 \rangle \propto t^{2h/(1-h)}, \quad L_\perp \propto t^{1/(1-h)}, \quad L_\parallel \propto t, \quad (12.43)$$

instantly reproduce (12.39) and (12.40) if $h = -1$. A useful observation perhaps is that the scaling of the parallel correlation length with time is set just by the requirement of self-similar evolution, without the need to conjecture CB explicitly, although of course the RMHD symmetry (3.5) does, in a sense, have CB hard-wired into it.

Let me make another observation that seems to be of some (possibly marginal) interest. In the same vein as (12.34), one finds, this time for the 2D spectra:

$$E_{2D}(k_\perp, k_\parallel, t) = a^{-2-h} E_{2D}(a^{-1}k_\perp, a^{-1+h}k_\parallel, a^{1-h}t). \quad (12.44)$$

The self-similar solution analogous to (12.35) is, therefore,

$$E_{2D}(k_\perp, k_\parallel, t) = k_\perp^{-2-h} F(k_\perp t^{1/(1-h)}, k_\parallel t), \quad (12.45)$$

with some unknown function $F(x, y)$. The 1D perpendicular spectrum $E(k_\perp, t)$ is found by integrating (12.45) over all k_\parallel , predictably leading to the same result as (12.35) (with $m = h$); the analog of (12.37) is

$$E(k_\perp, t) \propto t^{2(2+h)/(1-h)} k_\perp^3, \quad (12.46)$$

again manifesting inverse transfer if $h = -1$. Integrating (12.45) over k_\perp instead, one gets the 1D parallel spectrum:

$$E(k_\parallel, t) = t^{(1+h)/(1-h)} g(k_\parallel t), \quad (12.47)$$

where $g(y) = \int_0^\infty dx x^{-2-h} F(x, y)$. This result is interesting for the following reason. $E(k_\parallel, t)$ is the spectrum of a random field reflecting its dependence on a single scalar spatial coordinate, the distance along the field. The long-wavelength, $k_\parallel L_\parallel \ll 1$, asymptotic of this spectrum describes the absence of correlations at point separations $l_\parallel \gg L_\parallel$,

⁷⁰Note that this scaling of the parallel distances is correct both for distances along the global and the local mean field (cf. § 5.3), because $\mathbf{b}_\perp \cdot \nabla_\perp \rightarrow a^{h-1} \mathbf{b}_\perp \cdot \nabla_\perp$.

so it is just the spectrum of a 1D white noise (cf. appendix C.1). Therefore, $g(y) \rightarrow \text{const}$ as $y \rightarrow 0$. But (12.47) then implies that the energy content of low k_{\parallel} is frozen in time if $h = -1$. This suggests that RMHD turbulence might have a “parallel Saffman invariant” I_{\parallel} , so $E(k_{\parallel}, t) \propto I_{\parallel} k_{\parallel}^0 = \text{const}$ at $k_{\parallel} L_{\parallel} \ll 1$ (cf. § 12.5). This invariant should have the form⁷¹

$$I_{\parallel} = \int dl_{\parallel} \langle \mathbf{b}_{\perp}(r_{\parallel}) \cdot \mathbf{b}_{\perp}(r_{\parallel} + l_{\parallel}) \rangle \sim b_{\perp}^2 L_{\parallel} \quad (12.48)$$

(instead of \mathbf{b}_{\perp} , it may involve some other linear combination of the fields \mathbf{b}_{\perp} and \mathbf{u}_{\perp} , or \mathbf{Z}_{\perp}^{\pm}). If this could be shown to be the relevant conservation law for an RMHD selective decay, that would be an alternative way, to (12.41), of getting the scalings (12.39).

12.7. Decay of Imbalanced MHD Turbulence: Towards Elsasser States

Finally, let us consider RMHD (or indeed MHD) with $\langle X \rangle \neq 0$. The eventual decay of imbalanced MHD turbulence to pure Elsasser states was first mooted by Dobrowolny *et al.* (1980), in response to such states being occasionally observed in the solar wind. Since \mathbf{Z}^+ and \mathbf{Z}^- advect each other, one can easily imagine that a fluctuation of the imbalance at the outer scale in one direction, say in favour of \mathbf{Z}^+ , will lead to \mathbf{Z}^+ decaying slower and \mathbf{Z}^- faster, thus increasing the imbalance further, until \mathbf{Z}^- disappears and \mathbf{Z}^+ is left in splendid isolation. The crudest model of this is as follows (Maron & Goldreich 2001): if L is the energy-containing (outer) scale and Z^{\pm} are the two fields’ amplitudes at this scale, then

$$\frac{d(Z^{\pm})^2}{dt} \sim -\frac{Z^{\mp}(Z^{\pm})^2}{L} \Rightarrow Z^+ - Z^- \sim \text{const}, \quad \frac{d}{dt} \ln \frac{Z^+}{Z^-} \sim \frac{Z^+ - Z^-}{L}. \quad (12.49)$$

Thus, an initial imbalance in either direction will cause the (fractional) imbalance to get worse with time, until the weaker field has decayed away. In other words, cross-helicity $(Z^+)^2 - (Z^-)^2 \sim \text{const} \cdot (Z^+ + Z^-)$ decays more slowly than energy, hence the increasing imbalance. The asymptotic state is an Elsasser state with

$$Z^+(t \rightarrow \infty) \sim (Z^+ - Z^-)(t = 0). \quad (12.50)$$

Note that this simple model depends on assuming that L is the same for both fields and that any alignment effects on the strength of the nonlinear interaction can be ignored, which is far from obvious and can be hard to sustain (e.g., Hossain *et al.* 1995; Wan *et al.* 2012; Bandyopadhyay *et al.* 2019).

The above scenario did, nevertheless, appear to be confirmed (very slowly in time) in the decaying RMHD simulation by Chen *et al.* (2011), initialised by first creating a statistically steady, forced, balanced turbulence and then switching off the forcing, so the breaking of the symmetry in favour of one of the fields arose from an initial fluctuation of the imbalance. In full-MHD simulations with a strong mean field, the same result had been found in a number of earlier papers (Oughton *et al.* 1994; Maron & Goldreich 2001; Cho *et al.* 2002b), while in the absence of a mean field, it dates back to even earlier selective-decay literature (Montgomery *et al.* 1978, 1979; Matthaeus & Montgomery 1980; Ting *et al.* 1986; Stribling & Matthaeus 1991; Hossain *et al.* 1995).

Let me observe finally that, in the model (12.49), the energy fluxes

$$\varepsilon^{\pm} \sim \frac{Z^{\mp}(Z^{\pm})^2}{L} \Rightarrow \frac{\varepsilon^+}{\varepsilon^-} \sim \frac{Z^+}{Z^-} \quad (12.51)$$

⁷¹Intriguingly, (12.48) is the one-point correlator between the field and its $k_{\parallel} = 0$ part, evoking the special role of the “2D condensate” (see §§ 4.4 and 10.3).

are in the same relationship with Elsasser energies as they are reported to be in forced imbalanced turbulence: see (9.1), (9.3) and § 9.4 (there is also some direct numerical support for this relationship in decaying MHD turbulence, going back to Verma *et al.* 1996). This is perhaps another encouraging sign.

I do not have any further insights to offer about this regime, so I will stop here.

12.8. Inertial-Range Spectra of Decaying MHD Turbulence: Numerical Evidence

The philosophy articulated in the introduction to § 12 with regard to the inertial-range spectra does appear to be vindicated in the RMHD simulations of Chen *et al.* (2011), except the perpendicular spectrum was steeper than $k_{\perp}^{-3/2}$ (and closer to $k_{\perp}^{-5/3}$) and the parallel one steeper than k_{\parallel}^{-2} —this might actually be consistent with what one would expect for a system that moved gradually towards greater imbalance (see § 9.6).

The evidence from the RMHD simulations by Zhou *et al.* (2020) appears to point in the same direction: they report $k_{\perp}^{-3/2}$ spectra of both magnetic and kinetic energy, presumably of the same origin as those derived in § 6.

In the currently available decaying MHD simulations without a mean field, with or without helicity, there might not yet be sufficient resolution to tell what the asymptotic inertial-range spectra are (see, e.g., figure 28 and note particularly that there is no scale-by-scale equipartition between magnetic and kinetic energy at these resolutions)—or indeed whether they might be non-universal with respect to initial conditions (Lee *et al.* 2010), a somewhat disconcerting prospect. An oft-reported “non-universal” spectrum is k^{-2} (e.g., by Lee *et al.* 2010; Brandenburg *et al.* 2015, 2019), which might actually be another signature of reconnection (rather than of the WT regime, as some of these authors suggest): Dallas & Alexakis (2013a) and Zhou *et al.* (2019, in 2D) interpret this spectrum geometrically as describing an ensemble of current sheets, which are step-like “discontinuities” of the magnetic field (this is the same argument as I mooted for the residual energy in § 10.4; note that the spectrum of plasmoid chains would also be k^{-2} , as shown in appendix D.6.2). According to Dallas & Alexakis (2013b, 2014), however, this scaling gives way to a shallower $k^{-5/3}$ or $k^{-3/2}$ slope at sufficiently small scales in simulations with sufficiently high resolution, as current sheets curl up and/or break up (see also Mininni *et al.* 2006), so perhaps small-scale universality is safe after all and the current sheets are simply the effective energy-containing structures at which the “true” inertial range starts (cf. § 7.4.3 and appendix D.6.3).

12.9. Summary

To sum up, there appear to be at least three qualitatively different regimes, or, rather, classes of regimes,⁷² of decaying MHD turbulence:

- (i) RMHD and MHD states with some initial imbalance tend towards enduring (i.e., decaying on the viscous/resistive time scale) pure Elsasser solutions, due to relatively slower decay of the cross-helicity compared to energy (§ 12.7).
- (ii) RMHD, 2D MHD, and non-helical, zero-mean-field, 3D MHD turbulence starting in magnetically dominated and, therefore, balanced configurations, settle into a reconnection-controlled decay towards ever-larger-scale magnetic structures accompanied

⁷²It is formally possible to argue that there are many more than three regimes: Wan *et al.* (2012) take this to an amusing tongue-in-cheek extreme and count $\sim 6,500$ “conceptually distinct types of possible turbulent behaviour” for 3D MHD with no mean field and $\sim 59,000$ varieties with a mean field. No one working on decaying MHD turbulence need fear running out of options any time soon!

by flows whose kinetic energy is a time-independent fraction of the magnetic one (§§ 12.6, 12.2.1, and 12.4.2). This decay is “selective”, constrained by the conservation of certain invariants: anastrophy in 2D MHD (§ 12.1.1), the Hosking invariant (the Saffman helicity invariant) in 3D MHD (§ 12.4.2), and probably the Saffman cross-helicity invariant in RMHD (§ 12.6.1).

(iii) 3D MHD turbulence with no mean field but finite net helicity ends up in a decaying state dominated by an approximately force-free magnetic field. The decay is reconnection-controlled for magnetically dominated states (§ 12.2.2). It is constrained by the conservation of helicity (§ 12.1.2) and, if it starts in a state with comparable magnetic and kinetic energies, possibly also by the Saffman cross-helicity invariant (§ 12.4.3). In the latter case, the kinetic energy decays faster than magnetic, eventually pushing the system towards the magnetically dominated regime.

The different regimes are distinguished by different scaling laws for energies and energy-containing scales vs. time. In all cases, the energy-containing scale grows—and that is the result not just of larger structures decaying slower but also of some actual transfer of energy to larger scales, unlike in hydrodynamic turbulence (§ 12.5). In reconnection-controlled regimes, this transfer is achieved dynamically by coalescence of magnetic structures.

At sufficiently small scales, all these different types of decaying turbulence probably behave similarly to their forced counterparts, although it remains a challenging computational task to confirm this definitively (§ 12.8). Reconnection-controlled decaying MHD turbulence below the energy-containing scale is probably a case of (many instances of) reconnection-driven turbulence discussed in § 7.4.3.

13. MHD Dynamo Meets Reconnection

As the field becomes more and more tangled, there will be places where the field is sharply reversed, and magnetic reconnection may set in, removing the sharpest kinks.

[Kulsrud & Anderson \(1992\)](#)

An interesting and distinct type of MHD turbulence about which I have so far said nothing except in the context of its decay (§ 12) is the case of no mean field. Starting with a steady-state, forced hydrodynamic turbulence and a dynamically weak, randomly tangled magnetic field, one observes exponential growth of the latter, a phenomenon known as *small-scale dynamo* (or *fluctuation dynamo*)—expected already by [Batchelor \(1950\)](#) and [Biermann & Schlüter \(1951\)](#) and since confirmed numerically ([Meneguzzi et al. 1981](#)) and experimentally ([Tzeferacos et al. 2018; Bott et al. 2021b, 2022](#)). The system eventually saturates with magnetic energy comparable to kinetic, but not, it seems, necessarily equal to it scale by scale—what the final state is remains an unsolved problem, both numerically (due to lack of resolution) and theoretically (due to lack of theoreticians). Furthermore, it matters whether the turbulence possesses net helicity (injected into the flow by the forcing) and/or has a large-scale shear superimposed on it—if it does, small-scale dynamo is accompanied by a *mean-field dynamo*, leading to growth of a large-scale field (the large scale in question being generally larger than the outer scale of the turbulence). Saturated states of such dynamos are also poorly understood, for the same reasons.

Turbulent dynamos deserve a separate review—and they have recently received a

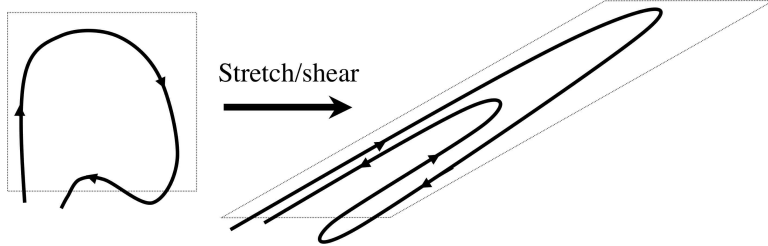


FIGURE 30. Stretching/shearing a field line produces direction reversals (cartoon from [Schekochihin & Cowley 2007](#)).

superb one, by [Rincon \(2019\)](#), to which I enthusiastically refer all interested public. This said, the ideas associated with the role of tearing in RMHD turbulence, reviewed in § 7, turn out to have some direct bearing on the “purest” (homogeneous, non-helical, unsheared) small-scale dynamo problem. This is, therefore, a natural place for some discussion of it.

13.1. Old Arguments About Saturated Dynamo at Large Pm

In regimes with $Pm > 1$,⁷³ small-scale dynamo can be understood as the process of a velocity field, restricted to scales above the viscous cutoff, randomly stretching and shearing the magnetic field, which is allowed to go to smaller scales, limited only by the Ohmic resistivity. Intuitively, it is not hard to see that embedding a tangled field line into an “eddy” will lead to the field line being stretched and folded, resulting in a configuration featuring field reversals on ever smaller scales (figure 30). A combination of numerical evidence and theoretical arguments (see [Schekochihin & Cowley 2007](#), [Rincon 2019](#), and references therein) confirms that this process does indeed lead to net amplification of

⁷³After I first worked on this problem ([Schekochihin et al. 2002, 2004a,b](#)), I grew quite sceptical about the relevance of the $Pm \gg 1$ MHD dynamo to any real-world situations: plasmas that formally have high Pm (e.g., the hot interstellar medium or the intergalactic medium in galaxy clusters) tend to be very hot and tenuous and, therefore, not very collisional, so MHD with Laplacian viscosity cannot possibly apply there (see, e.g., [Schekochihin & Cowley 2006](#), and further discussion in § 14.5). However, recent kinetic simulations of dynamo in such plasmas ([Rincon et al. 2016](#); [Kunz et al. 2016](#); [St-Onge & Kunz 2018](#); [St-Onge et al. 2020](#)) appear to be showing many familiar large- Pm features, perhaps because plasma microphysics conspire to produce an effectively collisional medium, which might not be entirely dissimilar from a large- Pm MHD fluid. Furthermore, some of the first laboratory plasma dynamos, achieved in laser-plasma experiments, have turned out to be right in the collisional, $Pm \gtrsim 1$, MHD regime ([Tzeferacos et al. 2018](#); [Bott et al. 2021b, 2022](#)). Thus, it seems that my scepticism was premature and we ought to tackle the large- Pm dynamo with renewed vigour and sense of relevance. In contrast with $Pm \gg 1$, the limit of $Pm \ll 1$ is much more straightforwardly relevant: liquid metals and plasmas in convective zones of stars are comfortably collisional MHD fluids, and there are many other examples. This case appears, however, to be quite different physically, at least in the kinematic regime, and even less well understood, although numerically we do know that there is dynamo ([Iskakov et al. 2007](#); [Schekochihin et al. 2007](#); [Brandenburg et al. 2018](#)) and that it has some kind of saturated state ([Brandenburg 2011](#); [Sahoo et al. 2011](#))—conclusions to obtain which, one still has to push at the resolution limits of currently achievable MHD simulations. A massive paper by [Sahoo et al. \(2011\)](#) contains a wealth of sophisticated statistical information but does not answer any of the more basic questions (their one distinctive physical conclusion is that the low- Pm case is less intermittent than the high- Pm one, which is plausible). I am not aware of any other systematic numerical study of how low- Pm dynamo saturates—an opportunity for a definitive contribution that some enterprising researcher with an MHD code and a large allocation of computing time should seize (there is a promise of that in [McKay et al. 2019](#)).

magnetic energy, with that energy residing preferentially in “folds”—magnetic fields that reverse direction across themselves on the resistive scale and remain approximately straight along themselves up to the scale of the velocity field. When the dynamo saturates, it does so in some poorly understood way involving these bundles of alternating fields back-reacting on the turbulent flow and arresting further amplification. Whereas in the kinematic-dynamo stage (i.e., when the field is dynamically weak), the spectrum of the magnetic energy certainly peaks at the resistive scale (Schekochihin *et al.* 2004b), what exactly happens in the saturated state is a matter of some debate. It is tempting to argue, with Biermann & Schläuter (1951) and Kraichnan (1965), that the system will sort itself out into a state where the magnetic energy is at the outer scale, while the smaller scales behave in exactly the same way as they would do in the presence of a strong mean field. Whether numerical evidence confirms this view is, at the resolutions achieved so far, in the eye of the beholder (Kida *et al.* 1991; Haugen *et al.* 2003, 2004; Cho & Ryu 2009; Beresnyak & Lazarian 2009a; Beresnyak 2012c; Teaca *et al.* 2011; Eyink *et al.* 2013; Porter *et al.* 2015; Grete *et al.* 2017, 2021; McKay *et al.* 2019; Bian & Aluie 2019; Brandenburg & Rempel 2019; Seta *et al.* 2020; see figure 33b). The alternative possibility is that the magnetic energy stays at small scales—not quite as small as in the kinematic regime, but still determined by resistivity (Schekochihin *et al.* 2002, 2004b; Maron *et al.* 2004). The claim is that the folded field structure persists in saturation, with the folds elongating to the outer scale (L) of the turbulence and direction reversals within folds occurring on the scale $\lambda_\eta \sim L \text{Rm}^{-1/2}$, where the stretching rate ($\sim \delta u_L/L$) balances the Ohmic-diffusion rate ($\sim \eta/\lambda_\eta^2$).

Despite being associated with the latter point of view, I am not going to defend it here in its original form because of certain little known but consequential numerical developments, described in § 13.2, that occurred after that debate had its heyday. Instead, drawing on the ideas of § 7, I will propose, in §§ 13.3 and 13.4, an amended view of the saturated state of turbulent dynamo, in which reconnection and MHD turbulence will again meet and collaborate.

13.2. Numerical Evidence: Reconnection Strikes Again

The existence of turbulent dynamo was definitively established by Meneguzzi *et al.* (1981) in what was then a “hero” 64^3 MHD simulation—one of those *bona fide* numerical discoveries that make computer simulations worthwhile. 20 years later, when the debate about the nature of the saturated dynamo state focused on interpreting newly accessible improved numerical evidence (Kinney *et al.* 2000; Schekochihin *et al.* 2004b; Maron *et al.* 2004; Haugen *et al.* 2003, 2004), everyone was staring at not-very-conclusive magnetic spectra with some pronounced excess of the magnetic energy over kinetic at small scales, and at visualisations of magnetic fields organised in folds (especially at large Pm). One could be a believer in universality and think of this as a non-asymptotic state that would, at infinite resolution, turn into the usual Kolmogorov-style turbulence spectrum, with magnetic energy shifting to the outer scales (Haugen *et al.* 2003, 2004; Beresnyak & Lazarian 2009a; Beresnyak 2012c)—or one could rely on a different kind of physical intuition and argue that there was no obvious physical mechanism for unwrapping fields folded at the resistive scale (that was my view).

In later, sadly unfinished, work, Iskakov & Schekochihin (2008) discovered, however, that, in simulations with moderate $\text{Pm} \geq 1$ and large Re (the former being the only affordable possibility compatible with the latter), magnetic folds in the nonlinear regime became current sheets, with very clear inflow–outflow patterns around the field reversals (figure 31). One might say that this should have been obvious from the start, although

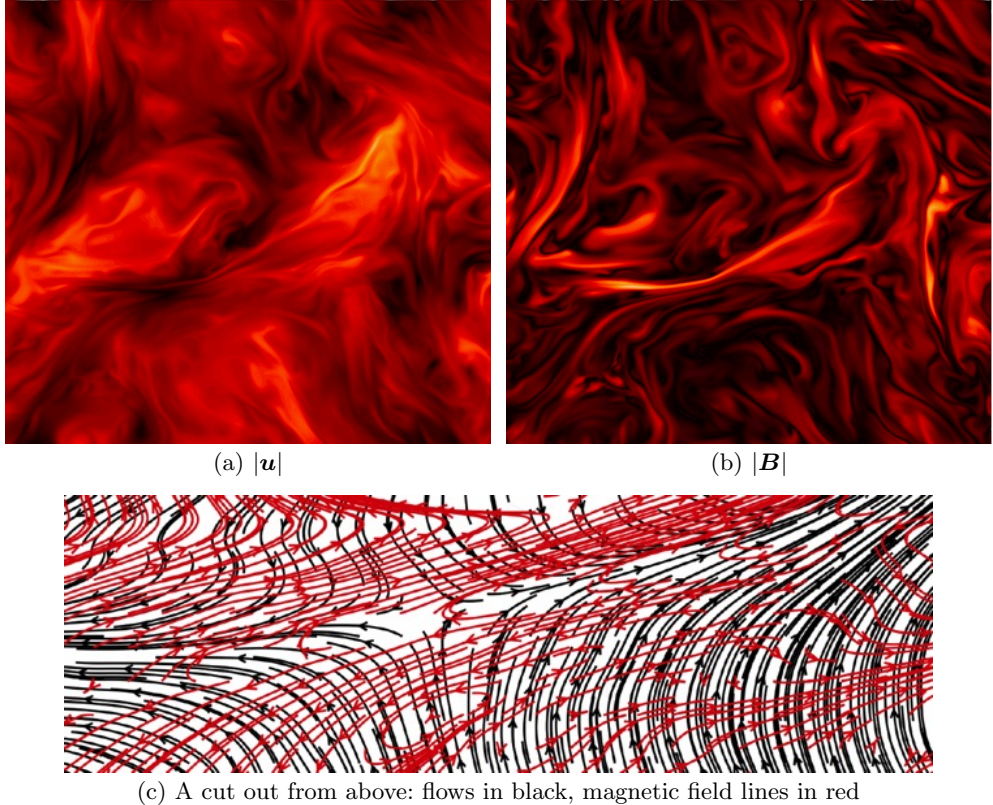


FIGURE 31. From unpublished work by [Iskakov & Schekochihin \(2008\)](#): a 512^3 incompressible-MHD simulation of saturated fluctuation dynamo, $Pm = 1$, $Re = 1360$ (defined as $u_{rms}/\nu k_0$, where $k_0 = 2\pi$ is the forcing wavenumber, corresponding to the box size; this is the same numerical set up as in [Iskakov et al. 2007](#) and [Schekochihin et al. 2007](#)). These are 2D cuts from instantaneous snapshots of absolute values of (a) velocity, (b) magnetic field. Panel (c) is a cut out from these snapshots, zooming in on the horizontal fold just down towards the left from the centre of the snapshot. Stream lines are in black and field lines are in red. A reconnecting-sheet structure, with field reversal, inflows and outflows is manifest. Very pretty 3D visualisations of this kind of reconnecting structure extracted from an MHD turbulence simulation can be found in [Lalescu et al. \(2015\)](#).

perhaps less so in the case of $Pm \gg 1$ (see § 13.3.3). We also found that the folds became corrugated, and plasmoid-like structures (probably flux ropes) formed, with (perhaps) approximately circularised cross-sections. Larger simulations by [Beresnyak \(2012b\)](#), also unpublished (except for some bits in [Beresnyak & Lazarian 2009a](#) and [Beresnyak 2012c](#)), revealed the same feature, with the numerical box now teaming with small plasmoid-like structures and rippled folds (figure 32), a result confirmed at even higher resolutions by [Galishnikova et al. \(2022\)](#). Thus, while the folds could not perhaps be literally unwrapped, they did turn out to be prone to breaking up and seeding populations of smaller structures.⁷⁴

⁷⁴Note that none of these authors saw any of this happen in the ‘‘Stokes’’ regime $Re \sim 1$, $Pm \gg 1$, which is the only numerically accessible case if one wants very large Pm , and on which much of the previous physical intuition ([Schekochihin et al. 2004b](#)) had been based: there, the saturated state just consisted of magnetic fields smoothly folded on the resistive scale. I shall argue in § 13.3.3 that this makes sense.



FIGURE 32. From unpublished work by [Beresnyak \(2012b\)](#) (reproduced with the kind permission of the author): snapshot of the absolute value of magnetic field in a $P_m = 10$ and $Re \approx 500$ simulation at 1024^3 (the same numerical set up as in [Beresnyak & Lazarian 2009a](#) and [Beresnyak 2012c](#); note that Beresnyak defines his Re in terms of the “true” integral scale of the flow calculated from its spectrum). Plasmoids/fold corrugations galore. In his other simulations within this sequence, there are even more plasmoid-like-looking features at $P_m = 1$ and $Re \approx 6000$, with some sign of them breaking up into even smaller structures (cf. § 13.3.3). In contrast, they start disappearing at $P_m = 10^2$ and $Re \approx 80$ and are gone completely in the “Stokes” regime $P_m = 10^4$ and $Re \approx 2$. Very similar results have been found by [Galishnikova et al. \(2022\)](#).

There is little definitive analysis of all this available in print. There is, however, an intriguing finding by [Brandenburg \(2014\)](#), who analysed his own simulations and those of [Sahoo et al. \(2011\)](#) and discovered that the ratio of energy dissipated resistively to that dissipated viscously decreased at larger P_m ([Beresnyak 2012b](#) also had this result,

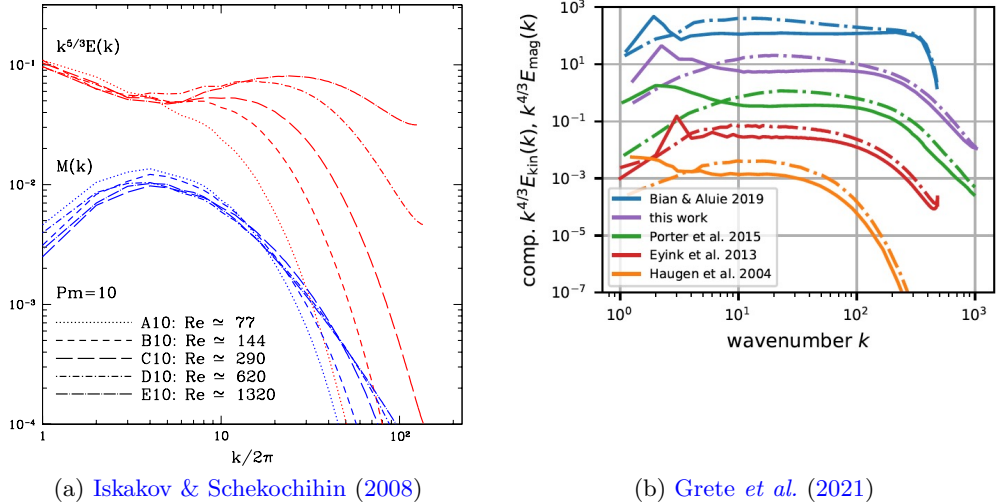


FIGURE 33. (a) Spectra of saturated MHD dynamo: kinetic-energy (red, compensated by $k^{5/3}$) and magnetic-energy (blue) spectra from a series of incompressible-MHD simulations with $Pm = 10$ and increasing Re by Iskakov & Schekochihin (2008). The numerical set up is the same as in Schekochihin *et al.* (2007); the resolution is 512^3 (so the highest- Re run may be numerically suspect). (b) A summary plot from Grete *et al.* (2021) (©AAS, reproduced with permission) of their and several other numerical studies, viz., from top to bottom, Bian & Aluie (2019); Grete *et al.* (2021); Porter *et al.* (2015); Eyink *et al.* (2013); Haugen *et al.* (2004). The kinetic-energy (solid lines) and magnetic-energy (dot-dashed lines) spectra are all compensated by $k^{4/3}$ to highlight the shallow kinetic-energy spectrum at small scales. Galishnikova *et al.* (2022) report very similar spectra and find also the magnetic spectrum steepening at even smaller scales, perhaps vindicating the prediction of § 13.3.

and Galishnikova *et al.* 2022 confirm it; McKay *et al.* 2019, however, raise a degree of doubt as to whether it will survive at larger Rm). One might plausibly argue that something like this could happen if kinetic energy, first converted into magnetic one as fields were amplified and folded by large-scale turbulent flows, were then to be recovered from magnetic energy at smaller scales as fluid motions were generated by reconnection and instabilities (presumably, tearing instabilities) in the folds. Brandenburg & Rempel (2019), while they do not engage with the notion of reconnecting folds, do confirm explicitly that, in larger- Pm simulations, there is increasing net transfer of magnetic to kinetic energy at small scales, with kinetic energy's viscous thermalisation increasingly dominating the overall dissipation rate (this was checked, and checked out, in the simulations by Galishnikova *et al.* 2022).

A signature of this behaviour is discernible if one examines the magnetic- and, especially, kinetic-energy spectra in saturated dynamo simulations at relatively high resolutions (512^3 and up), without attempting to see what one might want to see, e.g., scale-by-scale equipartition or $k^{-5/3}$. Figure 33(a), taken from the unpublished simulations by Iskakov & Schekochihin (2008), shows that the kinetic-energy spectrum steepens at large scales compared to the hydrodynamic case (the empirical slope is $k^{-7/3}$; see Schekochihin *et al.* 2004b and St-Onge *et al.* 2020), but picks up around the same wavenumber where the magnetic-energy spectrum has its peak and becomes shallower than Kolmogorov—Grete *et al.* (2021) find $k^{-4/3}$ to be a good fit, both in their simulations and, in retrospect, in many previous ones (figure 33b). By analysing energy transfers, they attribute this to significant transfer of energy from magnetic to kinetic, by means of the tension force—

this is analogous to the result of Brandenburg & Rempel (2019) and again entirely consistent with (although does not amount to a definitive confirmation of) the idea that reconnection in the folds drives small-scale motions, which come to dominate the kinetic-energy spectrum at those scales. This is perhaps reinforced by their (Grete et al. 2021) observation (in disagreement with Bian & Aluie 2019) that the energy cascade at small scales is almost entirely controlled by magnetic forces, rather than by hydrodynamic advection. The paper by Grete et al. (2021) appears to be the first one for well over a decade that, having measured different kinetic- and magnetic-energy spectra, dares to consider the possibility that this might mean something physical, rather than merely insufficient resolution for expected asymptotic recovery of $k^{-5/3}$ or $k^{-3/2}$.

Thus, reconnection appears to have caught up with dynamo, just as it did with Alfvénic turbulence in § 7, the general principle at work in both cases being that while large-scale motions push magnetic fields into small-scale, direction-reversing configurations, resistive effects invariably manage to break those up (provided $\text{Re} \gg 1$; see below).

13.3. Towards a New Theory of Reconnection-Limited Dynamo

13.3.1. Kinematic Dynamo and Onset of Tearing

Consider first a weak, tangled magnetic field being stretched by fluid motions whose scale is ℓ (why I call it ℓ rather than λ is about to become obvious). Let us imagine that these fluid motions are part of vanilla Kolmogorov turbulence, described, inevitably, by (2.2):

$$\delta u_\ell \sim (\varepsilon \ell)^{1/3}. \quad (13.1)$$

Balancing the associated stretching rate with the Ohmic-diffusion rate gives one the resistive scale:

$$\tau_{\text{nl}}^{-1} \sim \frac{\delta u_\ell}{\ell} \sim \frac{\varepsilon^{1/3}}{\ell^{2/3}} \sim \tau_\eta^{-1} \sim \frac{\eta}{\lambda_\eta^2} \quad \Rightarrow \quad \lambda_\eta(\ell) \sim (\eta \tau_{\text{nl}})^{1/2} \sim \ell \text{Rm}_\ell^{-1/2}, \quad \text{Rm}_\ell = \frac{\delta u_\ell \ell}{\eta}. \quad (13.2)$$

The scale $\lambda_\eta(\ell)$ is the reversal scale of the magnetic field generated by the dynamo of the eddies of size ℓ ; this field's typical coherence scale *along itself* will be ℓ .

Imagine now a general configuration in which magnetic field B_λ (as usual, in velocity units) reverses direction on some scale λ , not necessarily equal to λ_η . It will be subject to tearing at the rate (7.1), but with v_{Ay} replaced by B_λ :

$$\gamma \sim \frac{B_\lambda}{\lambda} S_\lambda^{-1/2} (1 + \text{Pm})^{-1/4} \sim \frac{B_\lambda^{1/2}}{\lambda^{3/2}} \eta^{1/2} (1 + \text{Pm})^{-1/4}. \quad (13.3)$$

When B_λ is infinitesimally small, as it would be in the kinematic stage of the dynamo, the tearing rate is small, $\gamma \ll \tau_\eta^{-1}$. It will become comparable to the resistive-diffusion rate at $\lambda = \lambda_\eta$ when the fields reversing at this scale grow to be at least

$$B_{\lambda_\eta} \sim \frac{\eta}{\lambda_\eta} (1 + \text{Pm})^{1/2} \sim \delta u_\ell \widetilde{\text{Re}}_\ell^{-1/2}, \quad \widetilde{\text{Re}}_\ell = \frac{\delta u_\ell \ell}{\nu + \eta} = \frac{\text{Rm}_\ell}{1 + \text{Pm}}. \quad (13.4)$$

Here $\widetilde{\text{Re}}_\ell$ is equal to the usual Reynolds number Re_ℓ when $\text{Pm} \gtrsim 1$ and to the magnetic Reynolds number Rm_ℓ when $\text{Pm} \ll 1$ [cf. (6.24)]. In the former case, since the stretching rate τ_{nl}^{-1} at the viscous scale $\ell \sim \ell_\nu = \varepsilon^{-1/4} \nu^{3/4}$ is the largest, it is the viscous-scale eddies that will play the dominant role in amplifying an infinitesimally small magnetic field, but the dynamo will go nonlinear as soon as the field's energy becomes comparable to the energy of the viscous-scale motions, $B_{\lambda_\eta} \sim \delta u_{\ell_\nu}$. Since, by definition of ℓ_ν , $\text{Re}_\ell \sim 1$, the estimate (13.4) also turns into $B_{\lambda_\eta} \sim \delta u_{\ell_\nu}$, i.e., tearing in the folds will start

outpacing Ohmic diffusion at exactly the same moment as the nonlinearity kicks in (this is perhaps obvious because tearing needs Lorentz force: see appendix D.1). Thus, a nonlinear dynamo is also a reconnecting dynamo, which I shall call “tearing-limited”.

In the limit of $\text{Pm} \ll 1$, the fastest eddies capable of field amplification are at the resistive scale, $\ell \sim \lambda_\eta$ (e.g., Boldyrev & Cattaneo 2004). Since $\text{Re}_{\lambda_\eta} \sim \text{Rm}_{\lambda_\eta} \sim 1$, the estimate (13.4) becomes $B_{\lambda_\eta} \sim \delta u_{\lambda_\eta}$, so it again tells us that the nonlinearity and tearing become important at the same time. Admittedly, there is no longer a scale separation between ℓ and λ_η in this situation, so the magnetic field is not, strictly speaking, “folded” (this is quite obvious from the snapshots of growing fields in Schekochihin *et al.* 2007), although one might still speculate that tearing is possible across generic X -point configurations. I shall keep my discussion general, but it might be easier for a doubtful reader just to think of large Pm in all cases.

13.3.2. Self-Similar Dynamo

It has been argued by Schekochihin *et al.* (2002, 2004b) and Maron *et al.* (2004) (with later variants by Beresnyak 2012c and Xu & Lazarian 2016) and numerically confirmed in a conclusive fashion by Cho *et al.* (2009) and Beresnyak (2012c) that, once the dynamo goes nonlinear, the field continues to be amplified, but by ever larger-scale motions that are, at a given time, just as energetic as the field is at that time.⁷⁵ That is, the scale $\ell(t)$ of the motions amplifying the field at time t is set by the condition

$$\delta u_{\ell(t)} \sim B_\lambda(t). \quad (13.5)$$

This leads, neatly, to a self-similar amplification regime:

$$\frac{dB_\lambda^2}{dt} \sim \frac{\delta u_\ell}{\ell} B_\lambda^2 \sim \frac{\delta u_\ell^3}{\ell} \sim \varepsilon \quad \Rightarrow \quad B_\lambda(t) \sim (\varepsilon t)^{1/2}, \quad \ell(t) \sim \varepsilon^{1/2} t^{3/2}. \quad (13.6)$$

After a few outer-scale eddy-turnover times, $t \sim L/\delta u_L$, the field’s energy becomes comparable to that of the flow, $B_\lambda \sim \delta u_L$, and the dynamo saturates. At any time during the self-similar growth, the cascade below ℓ presumably looks just like the cascade in the saturated state, whereas above ℓ , the turbulence is still hydrodynamic.

13.3.3. Tearing-Limited Dynamo: Universality Regained

Schekochihin *et al.* (2002, 2004b) calculated the field-reversal scale λ in the self-similar and saturated dynamo regimes by balancing $\delta u_\ell/\ell$ with the Ohmic-dissipation rate η/λ^2 . I now know, thanks to the argument in §13.3.1 (obvious in retrospect!), that the folds generated by this process will in fact tear faster than they diffuse. So let me therefore balance the tearing rate (13.3) with $\delta u_\ell/\ell$ and obtain a scale familiar from the “ideal-tearing” condition (D 57) (Pucci & Velli 2014; Tenerani *et al.* 2015a):

$$\lambda(\ell) \sim \ell \text{Rm}_\ell^{-1/3} (1 + \text{Pm})^{-1/6} \sim \varepsilon^{-1/9} \ell^{5/9} \eta^{1/3} (1 + \text{Pm})^{-1/6}. \quad (13.7)$$

⁷⁵There is a nice direct demonstration of that in the paper by Brandenburg & Rempel (2019), who measure the energy transfer from the velocity to the magnetic field and show that the sign of this transfer reverses at a scale that increases with time: the eddies above that scale act as a dynamo, while below that scale, the dynamo-generated fields drive some secondary flows, which then dissipate viscously. Analogous conclusions, by analogous means, were reached by Bian & Aluie (2019), St-Onge *et al.* (2020), Grete *et al.* (2021), and Galishnikova *et al.* (2022). The experimental dynamo observed in laser plasmas may be in this regime (Bott *et al.* 2021b, 2022).

In order for tearing to supersede Ohmic diffusion, we must have⁷⁶

$$\lambda(\ell) \gg \lambda_\eta(\ell) \Leftrightarrow \widetilde{\text{Re}}_\ell^{1/6} \gg 1, \quad (13.8)$$

where $\lambda_\eta(\ell)$ was taken from (13.2). Note that $\lambda \ll \ell$ always, except, for low Pm , at the start of the self-similar regime, when $\text{Rm}_\ell \sim 1$ (this seems to suggest that even a low- Pm dynamo may form reconnecting folds in the nonlinear regime).

Let us imagine for now that that the self-similar evolution (13.6) has run its course and the dynamo has saturated in a state where the only motions that are responsible for the (re)generation of the folds are on the outer scale, viz., $\ell \sim L$, while the motions below this scale no longer affect the magnetic field (I will experiment with relaxing this assumption in § 13.4.1). The reversal scale of the folds is then set by (13.7) with $\ell \sim L$. I shall call this scale

$$\lambda_R = \lambda(L) \sim L \text{Rm}_L^{-1/3} (1 + \text{Pm})^{-1/6}. \quad (13.9)$$

Consider a fold of length L and width λ_R . Its tearing will produce islands whose number can be inferred from (7.4):

$$N \sim k_* L \sim \frac{L}{\lambda_R} S_{\lambda_R}^{-1/4} (1 + \text{Pm})^{1/8} \sim \text{Rm}_L^{1/6} (1 + \text{Pm})^{1/3}. \quad (13.10)$$

Just as I did at the end of § 7.1, I can argue here that these islands will grow, perhaps circularise, and turn into plasmoids (flux ropes) of transverse size λ_R , while their mother fold is destroyed. Similarly to § 7.2, I can entertain the possibility that they are the outer-scale structures of a new turbulent cascade, seeded by the tearing of the fold at the scale λ_R . At scales below λ_R , this new cascade is of the usual RMHD kind considered in §§ 5–7—the mean field now is B_{λ_R} , assuming that fields that make up the folds are unlikely to be exactly anti-parallel and so there is some component of the folded field, generally of the same order as its reversing component, pointing in the direction perpendicular both to the latter and to the direction of reversal.⁷⁷

Let the flux rope have a circulation velocity δu_{λ_R} and a perturbed field $\delta b_{\lambda_R} \sim \delta u_{\lambda_R}$. One can estimate these quantities by the same logic as led to (7.10): if this new cascade is to carry (a finite fraction of) the same energy flux as produced the fold,⁷⁸ then

$$\frac{\delta u_{\lambda_R}^3}{\lambda_R} \sim \varepsilon \Rightarrow \delta u_{\lambda_R} \sim (\varepsilon \lambda_R)^{1/3} \sim \delta u_L \left(\frac{\lambda_R}{L} \right)^{1/3} \sim \delta u_L \text{Rm}_L^{-1/9} (1 + \text{Pm})^{-1/18} \sim \delta b_{\lambda_R}. \quad (13.11)$$

⁷⁶This condition means that the “Stokes” ($\text{Re} \lesssim 1$) simulations of [Kinney et al. \(2000\)](#) and [Schekochihin et al. \(2004b\)](#) could not have captured this effect. In the simulations of [Iskakov & Schekochihin \(2008\)](#) and [Beresnyak \(2012b\)](#), one can see very clearly that when Pm is increased, which, at fixed finite resolution, has to happen at the expense of Re , the magnetic folds become ever smoother and plasmoids/fold corrugations ever fewer, until they disappear entirely. Interestingly, at a given Re , larger values of Pm appear to promote the break up of the folds—perhaps because their aspect ratio ℓ/λ is, according to (13.7), larger when Pm is larger, and so is the number of islands (13.10) produced by the fastest-growing tearing mode.

⁷⁷There is perhaps a whiff of evidence for this in [Schekochihin et al. \(2004b\)](#), who found that $\langle |\mathbf{B} \cdot \mathbf{J}|^2 \rangle$ in the nonlinear regime of the dynamo had the same Rm scaling as $\langle |\mathbf{B} \times \mathbf{J}|^2 \rangle$, where $\mathbf{J} = \nabla \times \mathbf{B}$. Precisely anti-parallel fields would have had $\mathbf{B} \cdot \mathbf{J} = 0$.

⁷⁸I am assuming here that tearing, while destroying the folds, does not dissipate a significant amount of energy directly: the role of resistivity in the process of tearing is to break magnetic field lines, not to remove magnetic energy. This is not necessarily obvious, but is perhaps backed up by the following unsurprising estimate of the fraction of energy dissipated by resistivity in magnetic structures of width λ_R : $\varepsilon \lambda_R / \varepsilon \sim \eta B_{\lambda_R}^2 / \lambda_R^2 \varepsilon \sim (L/\lambda_R)^2 \text{Rm}_L^{-1} \sim \widetilde{\text{Re}}_L^{-1/3} \ll 1$.

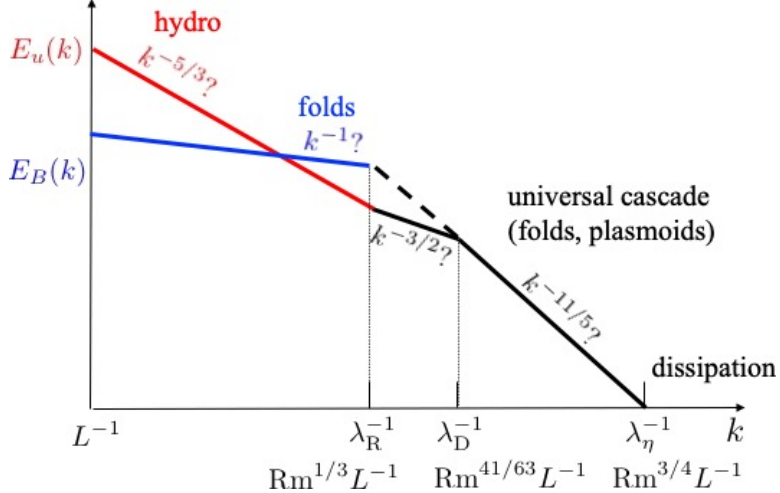


FIGURE 34. Spectrum of isotropic MHD turbulence, which is the saturated state of small-scale dynamo. The universal cascade below the fold-reversal scale λ_R [see (13.9)] is described in § 13.3.3. Various options for the spectrum at $k\lambda_R < 1$ are discussed in § 13.4; in particular, the k^{-1} magnetic spectrum is (13.18). The velocity spectrum may well be steeper than $k^{-5/3}$ at the largest scales and then shallower at smaller ones (see § 13.2), before steepening again at $k\lambda_R \gtrsim 1$. The disruption (λ_D) and dissipation (λ_η) scales are given by (13.15) and (13.16), respectively. Whether the $k^{-11/5}$ spectrum starts at λ_R (§ 13.4.1) or at λ_D (§ 13.3.3) is not obvious because how the spectra at scales below and above λ_R are connected remains an open question.

Finally, the length of the flux rope (its “parallel” scale) is set by critical balance: the scale over which coherence can be maintained by propagating information at the Alfvén speed $\sim B_{\lambda_R} \sim \delta u_L$ is

$$l_{\parallel} \sim \frac{B_{\lambda_R} \lambda_R}{\delta u_{\lambda_R}} \sim L^{1/3} \lambda_R^{2/3} \sim L \text{Rm}_L^{-2/9} (1 + \text{Pm})^{-1/9}. \quad (13.12)$$

Thus, we have got ourselves a critically balanced RMHD-type cascade, with $\delta u_L \sim B_{\lambda_R}$ being the Alfvén speed, λ_R given by (13.9) playing the role of λ_{CB} , l_{\parallel} given by (13.12) in the role of the parallel outer scale L_{\parallel} , and the outer-scale amplitude δu_{λ_R} given by (13.11). The RMHD ordering parameter for this cascade is, therefore,

$$\epsilon \sim \frac{\delta u_{\lambda_R}}{\delta u_L} \sim \frac{\lambda_R}{l_{\parallel}} \sim \text{Rm}_L^{-1/9} (1 + \text{Pm})^{-1/18} \ll 1, \quad (13.13)$$

not terribly small in any real-world situation, but perfectly legitimate in principle. The Reynolds number of this cascade will generally be large:

$$\widetilde{\text{Re}}_{\lambda_R} \sim \frac{\delta u_{\lambda_R} \lambda_R}{\nu + \eta} \sim \text{Rm}_L^{5/9} (1 + \text{Pm})^{-11/9} \gg 1 \quad \Leftrightarrow \quad \widetilde{\text{Re}}_L \gg (1 + \text{Pm})^{6/5}. \quad (13.14)$$

The latter inequality might not always be satisfied when $\text{Pm} \gg 1$, but again is a perfectly legitimate limit. When it is *not* satisfied, the motions produced by the tearing of the folds will be quickly dissipated by viscosity and thus cannot seed a proper cascade; one option then is to invoke § 13.4.1 to deal with the sub- λ_R structure.

The RMHD cascade seeded by the production of flux ropes in tearing folds, as just described, will do what an RMHD cascade does: push energy to smaller scales, become aligned and be eventually disrupted by tearing. The arguments of § 7.2 apply: a succession of mini-cascades will be seeded, etc., as per figure 14. One expects a $k^{-3/2}$ spectrum (6.25)

down to the disruption scale set by (7.2), viz.,

$$\lambda_D \sim \lambda_R Rm_{\lambda_R}^{-4/7} (1 + Pm)^{-2/7} \sim L Rm_L^{-41/63} (1 + Pm)^{-41/126}. \quad (13.15)$$

Below this scale, the mini-cascades will have a $k^{-11/5}$ spectral envelope described by (7.15) (figure 34). The final resistive cut-off is then determined by (7.19):

$$\lambda_\eta \sim \lambda_R \widetilde{Re}_{\lambda_R}^{-3/4} \sim \lambda_R Rm_L^{-5/12} (1 + Pm)^{11/12} \sim L \widetilde{Re}_L^{-3/4}, \quad (13.16)$$

the Kolmogorov scale again—reassuringly, some things in the world never change.

Thus, turbulence in the saturated state of small-scale dynamo is, at scales below λ_R , likely to be similar to the tearing-mediated turbulence of § 7.2, the only difference being that the direction of the “local mean field” will be fluctuating strongly and all the statistics will be isotropic overall (although certainly not isotropic with respect to this fluctuating local mean field, as indeed spotted by Beresnyak & Lazarian 2009a and, most recently, studied by St-Onge *et al.* 2020; in a decaying, no-mean-field set up, this was shown already by Milano *et al.* 2001). An aesthetically pleasing conclusion from all this is that universality is regained at small scales: even without the crutch of the mean field, MHD turbulence manages to turn itself into RMHD (Alfvénic) turbulence, at least in local patches where it is seeded by the tearing of the folds.

13.3.4. Outstanding Question

Just as I did in § 7.3, let me ask first whether this is a falsifiable theory. The numerical evidence that I described in § 13.2 was what encouraged me to bring reconnection into the dynamo game. However, it is clear that the state-of-the-art numerical spectra shown in figure 33 describe a still non-asymptotic situation, at best only just starting to capture reconnection in the folds. Is there hope to do better any time soon? Surprisingly, the answer is yes. Just like in the case of the tearing-mediated cascade with a mean field (§ 7.3), numerical verification that, in the earlier version of this review, I referred to as a distant hope, is becoming reality before the final version goes into print. The just-published dynamo simulations by Galishnikova *et al.* (2022), which aimed specially to assess the fold-tearing scenario proposed above and pushed the numerical resolution upwards another notch (to 2240^3), appear to offer some tentative evidence for the disruption of folds by tearing, the $\lambda_R \propto Rm^{1/3}$ scaling of the field-reversal scale,⁷⁹ and a steeper-than-Kolmogorov spectrum below that scale ($\propto k^{-2}$ or thereabouts). Thus, I present this scenario now with greater confidence than I originally thought I could. The theory appears to be on the brink of being testable by state-of-the-art numerics.

The key open question, however, both theoretically and numerically, is still what has been the central question of small-scale-dynamo theory since the founding papers of Batchelor (1950) and Biermann & Schlüter (1951) and preoccupied the authors of the long string of papers cited in § 13.1: will magnetic energy get stuck at small scales [in my current scheme, at the reversal scale λ_R given by (13.9)] or will it make its way to the outer scale L via some further step in the nonlinear evolution? The latter would be everyone’s preferred outcome: astrophysicists could then have their cosmic magnetic fields at the scales where they are observed to be,⁸⁰ while theoretical physicists could stop worrying about no-mean-field vs. strong-mean-field MHD upsetting their universalist

⁷⁹Or, as they would have it, $\lambda_R \propto Rm^{3/10} Pm^{1/5}$. Their quantitative comparisons were done for tearing of sinusoidal, rather than Harris-sheet, magnetic-field profile across the folded structure: $n = 2$ in appendix D.1.5, rather than $n = 1$ adopted in the main text of this review.

⁸⁰I am referring to extragalactic astrophysicists (the galactic ones get their large-scale field from mean-field dynamo; see Rincon 2019)—see Vacca *et al.* (2018), Vazza *et al.* (2021), and

dream by exhibiting different kinds of turbulence—the fluctuating field at L would just be the effective mean field in the inertial range, as Kraichnan (1965) prophesied.

As I already said in §§ 13.1 and 13.2, a definitive demonstration of an inverse cascade in forced, isotropic MHD turbulence has remained elusive, leaving space for disagreement over how to interpret insufficiently asymptotic simulations; the highest-resolution-to-date study by Galishnikova *et al.* (2022) does not nail the issue completely but would be much easier to interpret if a compelling argument in favour of an R_m -independent magnetic-energy-containing scale were available after all. I do not currently have such an argument—but I am able to offer, in § 13.4, a small catalogue of speculations, mine and other people’s, about some relevant physical processes—note that they are not necessarily all mutually exclusive and may coexist in a saturated dynamo state, perhaps in different spatial patches or at different times.

13.4. Saturation Scenarios

Wenn es aber Wirklichkeitssinn gibt, und niemand wird bezweifeln, daß er seine Daseinsberechtigung hat, dann muß es auch etwas geben, das man Möglichkeitssinn nennen kann. Wer ihn besitzt, sagt beispielweise nicht: Hier ist dies oder das geschehet, wird geschehen, muß geschehen; sondern er erfindet: Hier könnte, sollte oder müßte geschehen; und wenn man ihm von irgend etwas erklärt, daß es so sei, wie es sei, dann denkt er: Nun, es könnte wahrscheinlich auch anders sein. So ließe sich der Möglichkeitssinn geradezu als die Fähigkeit definieren, alles, was ebensogut sein könnte, zu denken und das, was ist, nicht wichtiger zu nehmen als das, was nicht ist. Man sieht, daß die Folgen solcher schöpferischen Anlage bemerkenswert sein können...

Robert Musil, *Der Mann ohne Eigenschaften*⁸¹

To start with, let me imagine for the time being that the state with field reversals at the scale λ_R conjectured in § 13.3.3 is the saturated state and explore what happens between λ_R and the outer scale L . I shall discuss this in §§ 13.4.1–13.4.3 before moving on to schemes for bringing magnetic energy to the outer scale in §§ 13.4.4–13.4.8. A reader wary of speculations (who has, nevertheless, inexplicably, got this far) may wish just to read §§ 13.4.2 and 13.4.4 and move on to § 14.

13.4.1. Multiscale Folds?

In § 13.3.3, I assumed that in the saturated state, the only motions capable of stretching magnetic fields into folds were the outer-scale motions and that, consequently, all folds

references therein for magnetic fields in clusters of galaxies and beyond. Interestingly, laboratory turbulent dynamo, recently achieved in a laser plasma, also appears to have its magnetic energy at the outer scale, in apparent contradiction with MHD simulations of the same experiment (Tzeferacos *et al.* 2018; Bott *et al.* 2021b).

⁸¹ “But if there is a sense of reality,—and no one will doubt that it has every right to exist,—then there must also be something that one could call a sense of possibility. A person who possesses it does not, for example, say: here this or that has happened, will happen, must happen; no, he rather starts inventing: here might, should, or could happen something or other; and if he is explained about something that it is so and so, and how it is, then he thinks: well, it could have probably also been different. Thus, one may define the sense of possibility as the ability to perceive everything that can be, and not to attach more importance to what is than to what is not. It is evident that the consequences of such creative faculty can be quite remarkable...”—Robert Musil, *The Man Without Qualities*.

had length L and reversal scale $\lambda_R = \lambda(L)$ [see (13.7) and (13.9)]. Let me now relax this assumption and inquire what would happen if motions across some scale range $\ell < L$ produced different, independent folds. As I argued in § 13.3.2, the fields produced by any given motion cannot be stronger than this motion, so let us take a bold leap and guess that, for $\lambda < \lambda_R$,

$$B_\lambda \sim \delta u_{\ell(\lambda)} \sim [\varepsilon \ell(\lambda)]^{1/3} \sim \varepsilon^{2/5} \eta^{-1/5} (1 + Pm)^{1/10} \lambda^{3/5}, \quad (13.17)$$

where $\ell(\lambda)$ is obtained by inverting the $\lambda(\ell)$ dependence (13.7). In a triumph of dimensional inevitability, this is just the same as the scaling (7.14), leading to the familiar $k^{-11/5}$ spectrum (7.15) (cf. the relationship between the ξ and λ scalings in § 7.2.3). One can now again fantasise about these folds breaking up into flux ropes as described by § 13.3.3, seeding mini-cascades similar to those produced by the successive disruptions of the RMHD cascade—those too have a $k^{-11/5}$ upper envelope, so perhaps this scaling emerges as an inevitable outcome at small scales of pretty much any scenario that involves resistivity.

Note that in the scheme leading to (13.17), interactions between velocities and magnetic fields are nonlocal in scale: velocities at scale ℓ interact with magnetic fields at scale $\lambda(\ell) \ll \ell$, and vice versa.⁸² This nonlocality is more extreme than, e.g., Beresnyak (2012c) would have it, because λ/ℓ in (13.7) scales with Rm_ℓ and Pm , which are asymptotically large numbers (although it scales with quite modest fractional powers of them). Below λ_R , however, this nonlocality should get swamped by the local RMHD cascade proposed in § 13.3.3.

13.4.2. Spectra Above the Reversal Scale

In the absence, as yet, of any mechanism for magnetic structures at scales longer than λ_R to emerge dynamically, the magnetic spectrum at scales above λ_R should reflect the volume-filling properties of folds and the distribution of their reversal scales (all of this is certain to be highly intermittent). The simplest, perhaps too simple, guess is that it will be (Yousef *et al.* 2007),

$$E_B(k) \propto k^{-1}, \quad (13.18)$$

which follows if one assumes that magnetic increments across any point separation $> \lambda_R$ will tend to have, in an averaged sense, the same value, roughly equal to the rms field

⁸²It is easy to see how a large-scale flow directly produces small-scale fields (figure 30). Since the fields' *parallel* scale is ℓ , these formally smaller-scale fields can in turn exert ℓ -scale Lorentz forces: these are quadratic in the field, $\sim \mathbf{B} \cdot \nabla \mathbf{B}$, so they do not know about direction reversals but do depend on the parallel scale (Schekochihin *et al.* 2004b)—consequently, they are able to fight back coherently against the ℓ -scale flow. This is, of course, only a heuristic argument and one could legitimately wonder if it might be simplistic and misleading. It might be, but not, it seems to me, for any of the reasons that have so far been aired in the literature. The most categorical statement of locality in MHD turbulence can be found in Aluie & Eyink (2010). Their proof depends on the assumption that both velocity and magnetic spectra have scaling exponents in the range $(-3, -1)$ —equivalently, that $\delta u_\lambda \propto \lambda^{\gamma^u}$ and $B_\lambda \propto \lambda^{\gamma^B}$ with $\gamma^u, \gamma^B \in (0, 1)$ (it is probably also true, conversely, that if interactions are local, the scaling exponents should be in this range). This makes sense because, in very simple terms, the contribution from field increments at a larger scale (Λ) to those at a smaller scale (λ) is $\delta u_{\Lambda \rightarrow \lambda} \sim \lambda \delta u_\Lambda / \Lambda \sim \delta u_\lambda (\lambda / \Lambda)^{1-\gamma} \ll \delta u_\lambda$ (provided $\gamma < 1$) and the contribution from the smaller-scale increments to the larger-scale ones is $\delta u_{\lambda \rightarrow \Lambda} \sim \delta u_\lambda \sim \delta u_\lambda (\lambda / \Lambda)^\gamma \ll \delta u_\Lambda$ (provided $\gamma > 0$). In RMHD turbulence, all this holds and interactions are indeed likely to be local (as I always assumed them to be in §§ 4–7). In the case of saturated dynamo, however, the unresolved issue is precisely whether velocity and magnetic field have scaling exponents $\in (0, 1)$ across the same range of scales—and also whether velocities at every scale are of the kind, dynamically, that can stretch magnetic fields at the same scale.

B_{λ_R} , i.e., that there is the same magnetic energy at every scale $\in [\lambda_R, L]$ (cf. § 11.2). The spectrum (13.18) has the unique property that, while its peak would sit at some $k_{\text{peak}} \sim L^{-1}$, its energy is weakly (logarithmically) dominated by its small-scale cutoff, viz., $k \sim \lambda_R^{-1}$. Remarkably, this appears to be consistent, or at least not inconsistent, with what was found by [Galishnikova et al. \(2022\)](#), who see the spectral peak at a wavenumber (approximately) independent of Rm , but a fairly flat profile of $kE_B(k)$ up to $k \sim \lambda_R^{-1}$.

There is still the question of what the velocity field does in the interval $[\lambda_R, L]$. In (13.17), I blithely assumed that it continued to obey the Kolmogorov scaling (13.1). If this were true, that would connect nicely onto the flux-rope amplitude (13.11) (and hence onward to the universal tearing-mediated cascade). Admittedly, however, the justification for a Kolmogorov scaling in that case is difficult as (13.17) implies energy exchanges with the folds at smaller scales and thus undermines the assumption of a constant flux through the scale range between L and λ_R . If the energy flux ε were depleted in favour of the folds at each scale ℓ on the same typical time scale $\ell/\delta u_\ell$ as the cascade of δu_ℓ proceeded, then the velocity field would have a steeper-than-Kolmogorov spectrum. The most elementary way to see this is to model the evolution of the spectrum E_k as (cf. [Batchelor 1953](#))

$$\frac{\partial E_k}{\partial t} = -\frac{\partial \varepsilon_k}{\partial k} - \gamma_k E_k, \quad \varepsilon_k = \frac{k E_k}{\tau_k}, \quad \tau_k^{-1} = \text{const} \times k \sqrt{k E_k}, \quad (13.19)$$

where ε_k is the energy flux through wavenumber k , τ_k is the cascade time ($\sim \tau_{\text{nl}}$), and γ_k is the rate of transfer of the kinetic energy into the folds. Letting $\gamma_k \tau_k = \sigma = \text{const}$ and seeking a steady-state solution gives

$$\frac{\partial \varepsilon_k}{\partial k} = -\sigma \frac{\varepsilon_k}{k} \Rightarrow \varepsilon_k \propto k^{-\sigma} \Rightarrow E_k \propto k^{-(5+2\sigma)/3}. \quad (13.20)$$

Note that, via a calculation analogous to (13.17), this would lead to a steeper-than- $k^{-11/5}$ spectrum of folds, meaning that folds with reversal scales smaller than λ_R would get swamped by the tearing-mediated cascade originating from the longest, λ_R -scale folds, and we would be back to the scenario described in § 13.3.3.

[Cho et al. \(2009\)](#) and [Beresnyak \(2012c\)](#) report that the fraction of the energy flux transferred into magnetic fields during the self-similar regime described in § 13.3.2 is numerically quite small—between 0.04 and 0.07. This suggests that any steepening of the velocity spectrum compared to the Kolmogorov scaling should, in theory, be very slight. The numerical evidence on velocity spectra was reviewed at the end of § 13.2 (see figure 33)—there is some steepening at low k and shallowing at higher k , as magnetic fields’ back reaction kicks in, effectively making $\gamma_k < 0$ in (13.19), but none of the extant simulations is likely to have reached asymptotically large Re or Rm .

13.4.3. Magnetoelastic Turbulence?

Let us now explore what happens in the scale interval $[\lambda_R, L]$ if we abandon (13.17) and return to the scenario in which the velocity field at the outer scale L constantly passes a certain fraction of the injected power ε to the folds with reversals at λ_R and hence into the tearing-mediated cascade, while the rest of the injected power goes into some motions on scales $[\lambda_R, L]$ that do not exchange energy with that cascade, i.e., do not stretch the field or cause it to develop sub- λ_R structure. What kind of motions can these be?

In search of the answer to this question, I wish to revisit the old idea ([Moffatt 1986](#); [Gruzinov & Diamond 1996](#); [Chandran 1997](#); [Schekochihin et al. 2002](#); [Maron et al. 2004](#)) that a tangled mess of small-scale magnetic fields provides an elastic background through which larger-scale Alfvén waves can propagate isotropically. The relevant calculation is

straightforward. Consider the equations of incompressible MHD without a mean field:

$$\partial_t u_i + u_j \partial_j u_i = -\partial_i p + \partial_j M_{ij}, \quad (13.21)$$

$$\partial_t B_i + u_n \partial_n B_i = B_n \partial_n u_i, \quad (13.22)$$

where the equation for pressure p is $\partial_i u_i = 0$ and $M_{ij} = B_i B_j$ is the Maxwell stress tensor (the magnetic field is in velocity units). We can recast the induction equation (13.22) in terms of M_{ij} and forget about B_i :

$$\partial_t M_{ij} + u_n \partial_n M_{ij} = M_{nj} \partial_n u_i + M_{in} \partial_n u_j. \quad (13.23)$$

The information about magnetic fields' reversals is now hidden away and only their ability to exert Lorentz force, quadratic in B_i , is retained. Let us expand the flows and the Maxwell stresses around a time- and space-averaged state:

$$\langle u_i \rangle = 0, \quad \langle M_{ij} \rangle = v_A^2 \delta_{ij}, \quad v_A^2 = \frac{1}{3} \langle B^2 \rangle, \quad M_{ij} = \langle M_{ij} \rangle + \delta M_{ij}. \quad (13.24)$$

Linearising (13.21) and (13.23) around this “equilibrium” filled with tangled fields, we get isotropically propagating Alfvén waves whose dispersion relation and eigenvector are⁸³

$$\omega^2 = k^2 v_A^2, \quad \delta M_{ij} = v_A^2 (\partial_i \xi_j + \partial_j \xi_i), \quad (13.25)$$

where ξ_i is the displacement ($\partial_t \xi_i = u_i$). These can be dubbed *magnetoelastic waves* to highlight the formal mathematical (Ogilvie & Proctor 2003) and obvious physical analogy between a magnetised plasma and certain types of polymeric fluids. Admittedly, this analogy between magnetic field lines and polymer strands moving with the fluid and elastically back-reacting on it becomes precarious if one looks beyond the ideal description: there is no such thing as “antiparallel” polymers strands, and so there is no reconnection. It is not obvious whether fast reconnection of field lines can foil their ability to make plasma an elastic medium: do tangled fields spring back when pushed at or just reconnect quickly to accommodate the push? Here, I shall imagine that they do spring back and explore the consequences.

One of the consequences appears to be a surprising return of the IK turbulence (§ 2.2), which I have so far thoroughly dismissed—perhaps an indication that a clever idea, however wrong, never goes to waste. The reason that the IK scheme was wrong in the presence of a strong mean magnetic field was that Alfvén waves could not be legitimately expected to run around isotropically at small scales. Well, according to (13.25), the magnetoelastic waves do run around isotropically, and so the IK theory is back in business. While Kraichnan's dimensional argument leading to (2.5) may or may not be compelling, the version of the IK theory outlined in footnote 5 is perhaps sensible. Indeed, whereas at the outer scale L , the nonlinear time $\tau_{nl} \sim L/\delta u_L$ and the Alfvén time $\tau_A \sim L/v_A$ are certainly comparable (because $\langle B^2 \rangle \sim \delta u_L^2$ for saturated dynamo), the former will shorten less quickly than the latter at smaller scales ($\tau_A \propto \ell$, while $\tau_{nl} \propto$ a fractional power of ℓ). Thus, at scales $\ell \ll L$, the magnetoelastic turbulence might be expected to be weak. The cascade time is then worked out from the random-walk

⁸³Schekochihin *et al.* (2002) argued that if the small-scale magnetic fields were organised in long-scale folds, these Alfvén waves would propagate as a kind of ripple along these folds, thus making them locally anisotropic. Mathematically, this led to the disappearance of the factor of 1/3 in v_A^2 , because the tensor of magnetic-field directions $B_i B_j / B^2$ was a long-scale object. Since, however, I now propose that the folds will break up into flux ropes, etc., it seems more logical to think of the resulting magnetic tangle as an isotropic mess, at least from the point of view of long-scale perturbations.

argument (4.5), and the spectrum follows from the constancy of flux:

$$\tau_c \sim \frac{\tau_{nl}^2}{\tau_A} \sim \frac{\ell v_A}{\delta u_\ell^2}, \quad \frac{\delta u_\ell^2}{\tau_c} \sim \varepsilon \quad \Rightarrow \quad \delta u_\ell \sim (\varepsilon v_A \ell)^{1/4} \quad \Leftrightarrow \quad E(k) \sim (\varepsilon v_A)^{1/2} k^{-3/2}. \quad (13.26)$$

Presumably, this cascade terminates when it hits $k \sim \lambda_R^{-1}$, where the scale separation between the magnetoelastic waves and the magnetic fields associated with the tearing-mediated cascade of § 13.3.3 breaks down.

There is some numerical evidence in favour of an isotropic $k^{-3/2}$ spectrum of perturbations with a sound-like isotropic dispersion relation $\omega \propto k$ —the MHD fast (magnetoacoustic) waves: see Cho & Lazarian (2002, 2003), who were inspired by the same scaling derived for weak turbulence of sound waves by Zakharov & Sagdeev (1970); a later study by Kowal & Lazarian (2010) appears to be less certain about the scaling exponent.

One might have thought that some evidence as to how much of a fiction, or otherwise, the spectrum (13.26) were in an elastic medium, could be found in simulations of polymer-laden turbulence. Surprisingly, the state of the art in this area features much smaller resolutions than in MHD. The most recent relevant numerical papers appear to be Valente *et al.* (2016) and Fathali & Khoei (2019) (see references therein for the paper trail). They report significant energy transfer in the inertial range from the motions of the solvent fluid to the elastic polymer admixture and back (quite a lot of it nonlocal in k , from large-scale flows to small-scale polymer structure, perhaps analogous to dynamo); they also see spectral exponents in the $[-5/3, -3/2]$ range, at modest resolutions. They do not appear to be aware of, or interested in, the possibility of elastic waves.⁸⁴

Since polymer-laden turbulence has the advantage of being (relatively) easy to set up and measure in the laboratory, numerical simulations are not the only evidence available—there is a lively history of real experiments, amongst which some recent ones appear to have been important breakthroughs. Thus, Varshney & Steinberg (2019) have, for the first time, it seems, managed to excite and measure elastic waves experimentally. Zhang *et al.* (2021) report detailed measurements of scalings in the inertial range that imply an energy flux, increasing with k , from the fluid motions into the elastic energy of the polymers, and kinetic-energy spectra that have a well-developed power law, $k^{-2.38}$, which is steeper than what numerics show but shallower than what theoreticians (cited in footnote 84) predict. An open field for further theorising then, with not much more known definitively than in MHD.

In MHD turbulence, even whether the magnetoelastic cascade (13.26), or indeed the magnetoelastic waves, exist at all remains an open question. Hosking *et al.* (2020) have shown numerically that magnetoelastic waves do exist in certain tangled, force-free magnetic configurations, and are well described by (13.25) (modulo some further nuance that can mean that v_A is somewhat reduced for tangled fields that are spatially intermittent). What is still unknown is whether they can propagate against the background of a

⁸⁴In contrast, Balkovsky *et al.* (2001) and Fouxon & Lebedev (2003) are fully aware of it, as well as of the MHD analogy with Alfvén waves. They have a theory of turbulence of these waves at scales where elasticity is important, below the so-called Lumley (1969) scale (this is set by the balance between the turbulent rate of strain and the polymer relaxation time, a quantity without a clear MHD analogue because magnetic field lines have no interest in curling up the way polymers do, entropically; in our problem, the corresponding scale should be the outer scale L). They think that in this scale range, the waves will be nonlocally advected by the Lumley-scale motions, resulting in spectra steeper than k^{-3} because otherwise the nonlocality assumption fails. I do not see why such an assumption should hold, either for polymer-laden turbulence or in MHD.

saturated dynamo state or are quickly damped by small-scale motions and thus rendered irrelevant.

13.4.4. Fast-Reconnection-Limited Dynamo?

The narrative arc that in § 7.4.2 led me to examine, with Loureiro & Boldyrev (2020), the possibility of a competition between tearing and fast plasmoid reconnection (reviewed in appendix D.6), naturally invites doing the same for dynamo. For magnetic folds with reversals at scale λ driven by motions at scale ℓ and energetically comparable to those motions, let us compare the fast-reconnection time given by a formula analogous to (7.25) with the characteristic time of the flow:

$$\tau_{\text{rec}} \sim \epsilon_{\text{rec}}^{-1} \frac{\lambda}{B_\lambda} \sim \epsilon_{\text{rec}}^{-1} \frac{\lambda}{\delta u_\ell} \lesssim \frac{\ell}{\delta u_\ell} \quad \Leftrightarrow \quad \lambda \lesssim \epsilon_{\text{rec}} \ell \equiv \lambda_{\text{rec}}, \quad (13.27)$$

where $\epsilon_{\text{rec}} \sim \tilde{S}_c^{-1/2}(1 + \text{Pm})^{-1/2}$ and $\tilde{S}_c \sim 10^4$ (see appendix D.4.2). In order for any possible effect of the onset of fast reconnection to matter, λ_{rec} must be larger than the reversal scale (13.7) set by tearing, which is achieved provided

$$\text{Rm}_\ell \gtrsim \epsilon_{\text{rec}}^{-3}(1 + \text{Pm})^{-1/2} \sim 10^6(1 + \text{Pm}), \quad (13.28)$$

a tough ask, but not as bad as (7.26). Note that this condition, if satisfied, amply guarantees that the fast-reconnection regime actually is reached, i.e., that the slow-reconnection rate (see appendix D.4.1) is slower than fast one, or

$$\tilde{S}_c \lesssim \tilde{S}_\ell \sim \text{Rm}_\ell(1 + \text{Pm})^{-1/2} \quad \Leftrightarrow \quad \text{Rm}_\ell \gtrsim 10^4(1 + \text{Pm})^{1/2}. \quad (13.29)$$

What would happen if (13.28) were achieved? In principle, this means that a fast-reconnecting plasmoid chain could be formed out of such a fold, seeding a reconnection-driven cascade (§ 7.4.3). In order for this to happen, the folds, rather than being destroyed by tearing and/or swept away by the flow, would have to stick around long enough for the plasmoids (flux ropes) in them to gobble up more flux and grow to bigger sizes than the reversal scale set by tearing (λ_R for $\ell = L$), eventually to λ_{rec} . If this were to be the fate of most folds, λ_{rec} would be the effective reversal scale, independent of Rm , as ideally desired.

I shall not go as far as claiming that this outcome accords with simulations—both because they do not usually have Rm anywhere close to (13.28) and because (13.27) with $\ell = L$ would imply a magnetic-energy-containing scale $\sim 10^2$ shorter than the outer scale, which is rather too short. However, if ϵ_{rec} were closer to 10^{-1} than to 10^{-2} in a turbulent environment characteristic of the saturated dynamo, both the condition (13.28) and the prediction (13.27) would start looking much more realistic (alternatively, another method of increasing the field's scale is needed; see, e.g., § 13.4.8). Thus, a promising scenario, but still very much to be confirmed—and it is far from clear that it can be confirmed at the numerical resolutions likely to be available any time soon (cf. Galishnikova *et al.* 2022).

It cannot have escaped the reader that an even more attractive possibility would be $\epsilon_{\text{rec}} \sim 1$, which would absolve us from any constraints on Rm and set $\lambda_{\text{rec}} \sim L$ in the saturated state. That possibility is effectively the one associated with the other type of fast reconnection—stochastic reconnection (appendix D.7)—and is the currently trending dynamo-evolution scenario examined in § 13.4.5.

13.4.5. Xu & Lazarian (2016)

Xu & Lazarian (2016) propose that, in a $\text{Pm} \gg 1$ system, once the magnetic energy has grown to be comparable to the energy of the viscous-scale eddies ($B_{\lambda_\eta} \sim \delta u_{\ell_\nu}$;

cf. § 13.3.1), its spectrum will embark on a rearrangement exercise in which its spectral peak moves from the resistive to the viscous scale while the overall magnetic energy stays constant (I will discuss this proposition in a moment). Once it reaches the viscous scale, a self-similar secular regime follows, of the kind described in § 13.3.2⁸⁵ except the scale of B_λ is now the same as the scale of the motions that are performing the dynamo action, $\lambda \sim \ell(t)$, whereas below that scale, a GS95-type turbulent cascade forms, with $B_{\ell(t)}$ playing the role of the mean field (this is also the view of Beresnyak 2012c). As time advances, $\ell(t) \rightarrow L$, and the dynamo saturates with scale-by-scale equipartitioned $k^{-5/3}$ magnetic and velocity spectra, just like everyone since Biermann & Schliuter (1951) has always wanted it to do.

In the narrative of Xu & Lazarian (2016), this pleasing outcome depends on the assumption, unproven, but not in principle impossible, that fast stochastic reconnection (reviewed in appendix D.7) will always provide just enough turbulent magnetic diffusivity to prevent the dynamo-generated field from organising into folds with reversals at scales much below $\ell(t)$. I cannot rule this out definitively without a clear dynamical picture of the turbulence in the presence of dynamically significant dynamo-generated fields.⁸⁶

If this assumption proves true, the Xu & Lazarian (2016) scenario for the $Pm \gg 1$ case still needs the earlier transitional stage to move the magnetic energy (i.e., the field-reversal scale) from the resistive to the viscous scale. They justify this by arguing that, since the spectrum of the magnetic field is $\propto k^{3/2}$ at $k \ll \lambda_\eta^{-1}$ (Kazantsev 1968; Kulsrud & Anderson 1992), the magnetic modes with $k \ll \lambda_\eta^{-1}$ can continue being amplified by the viscous-scale motions after those with $k \sim \lambda_\eta^{-1}$ have reached energetic equipartition with those motions—if the overall magnetic energy is assumed to stay constant, this then leads to a gradual “overturning” of the spectrum and shifts its peak towards the viscous scale.

I do not think this argument is entirely satisfactory, for two reasons. First, the $k^{3/2}$ spectrum is a Fourier-space representation of the growing, folding field—it seems dubious to me to disaggregate it into individual Fourier modes and view each of them as an independent entity that back-reacts on the velocity field or is amplified by the latter separately from all others (amplification of the field is always accompanied by a change in its scale and the $k^{3/2}$ spectrum is the resulting mean distribution of the magnetic energy amongst wavenumbers during its growth; see, e.g., lecture notes by Schekochihin 2022). Secondly, I do not see why the energy should stay constant, putting the self-similar stage on hold until magnetic fields and motions are at the same scale, rather than proceeding to grow in the way described in § 13.3.2. It seems to me that if the Xu & Lazarian (2016) scheme were correct, we should see their spectral rearrangement at constant energy already in numerical simulations with $Pm \gg 1$ and $Re \sim 1$, which is the only glimpse of truly scale-separated large-Pm dynamics that we currently have. In the event, we do see the spectrum in the nonlinear stage of such simulations become

⁸⁵Xu & Lazarian (2016) believe that they can derive very precisely the fraction of the energy flux going into magnetic fields quoted at the end of § 13.4.2 (it is = 3/38, they say) from a semi-quantitative theory that contains adjustable constants of order unity and is a variant of the dynamo-with-reconnection model by Kulsrud & Anderson (1992) (who also derived that number)—see further discussion at the end of § 13.4.6.

⁸⁶It may, however, be worth observing that, according to the numerical results reported by Busse *et al.* (2007), Lagrangian particles in MHD turbulence without a mean field tend to separate along the local field direction, rather than across it. An enthusiast of field-line folding might interpret this as an indication that stochastic reconnection might find it difficult to prevent fold creation. Eyink (2011), a strong advocate of stochastic reconnection, notes his puzzlement at this result.

shallower than $k^{3/2}$ and shift a little towards larger scales—but not all the way to the flow’s scale, with the peak still, it seems, at the resistive scale (this behaviour appears to be accounted for adequately by assuming that the magnetic folds locally anisotropise the viscous-scale flow and thus stymie its ability to amplify them: see Schekochihin *et al.* 2004a,b and St-Onge *et al.* 2020).

Thus, in my view, the Xu & Lazarian (2016) scenario, while attractive if true, remains at least as much of a speculation as anything that my exasperated reader will find elsewhere in this section.

13.4.6. Subramanian (1999)

While I am not proposing to review here the entire history of dynamo saturation schemes, it is useful to describe a model proposed a long time ago by Subramanian (1999), which, in a certain general sense, anticipated the Xu & Lazarian (2016) scenario and many other similar schemes, including § 13.4.4.

Subramanian (1999) conjectured that the effect of nonlinear back-reaction of magnetic fields on the flow would be to increase the effective magnetic diffusivity of the turbulent medium:

$$\eta_{\text{eff}} = \eta + \tau \langle B^2 \rangle, \quad (13.30)$$

where τ is some adjustable constant with dimensions of time. This would go on until the effective magnetic Reynolds number reached the critical value at which the small-scale dynamo was at its threshold—known to be $Rm_c \sim 10^{1\dots 2}$ (see, e.g., Schekochihin *et al.* 2007). He then proposed that the saturated state of the dynamo would simply be the marginal state of a kinematic dynamo with $Rm_{\text{eff}} = Rm_c$, and with magnetic energy therefore sitting at the scale

$$\lambda_B \sim L Rm_c^{-1/2}. \quad (13.31)$$

This is not far from where, quantitatively, numerical simulations have been placing the peak of the magnetic-energy spectrum in finite-resolution boxes for the last two decades (see references in §§ 13.1 and 13.2). Indeed, Subramanian’s prescription was operationalised by Schober *et al.* (2015) to produce a fully-fledged modelling tool for unfailingly successful comparisons with simulation outputs for specific values of Re and Rm, as well as of the Mach number.

The key conceptual point is that under this scheme, there is no dependence of λ_B on Rm. A slight wrinkle is that the magnetic energy in the saturated state is

$$\langle B^2 \rangle \sim \frac{\delta u_L L}{\tau Rm_c} \sim \frac{\delta u_L^2}{Rm_c} \quad (13.32)$$

if one makes the most obvious choice $\tau \sim L/\delta u_L$, i.e., $\langle B^2 \rangle$ is uncomfortably smaller than the kinetic energy (although not outrageously inconsistent with numerical evidence). Since Rm_c is, however, merely a constant, this can be fudged by judicious modelling choices or, following Subramanian (1999), by arguing that if the magnetic energy is concentrated in flux ropes of radius λ_B and length L , then $\langle B^2 \rangle \sim B^2 (\lambda_B/L)^2 \sim B^2 Rm_c^{-1}$, so the actual magnetic fields are, in fact, locally as strong as the flow.

This approach does not address any rearrangements that might be caused by the Alfvénic dynamics, nor does it produce a specific mechanism for the enhancement of magnetic diffusivity, but it does capture, conceptually, a broad general class of physically plausible models, to which both § 13.4.4 and Xu & Lazarian (2016) also belong (stochastic reconnection is, of course, turbulent magnetic diffusivity by another name). To explain the enhancement of η , Brandenburg & Subramanian (2005) introduce an effective “nonlinear drift” $\propto \mathbf{J} \times \mathbf{B}$, justified by analogy with ambipolar effects (a version of that was also

explored by [Subramanian 2003](#), where he complicated his model somewhat to produce turbulent magnetic hyperdiffusion). Interestingly, an even earlier paper by [Kulsrud & Anderson \(1992\)](#) already contained calculations of nonlinear dynamo both for a model with ambipolar damping, featuring an effective magnetic diffusivity of the form (13.30), and with magnetic reconnection (see their §4.2). In the latter case, instead of an effective magnetic diffusivity, they have a damping rate of the form $-\epsilon_{\text{rec}} \langle B^2 \rangle^{1/2} k$ modelling the removal of magnetic structure by fast reconnection with dimensionless rate ϵ_{rec} (this is just τ_{rec}^{-1} of § 13.4.4), but the outcome is similar. Their calculation of the self-similar dynamo regime with reconnection appears to be functionally equivalent to that of [Xu & Lazarian \(2016\)](#), and produces the same result.

To put all this in context, the other, competing general class of models includes schemes in which dynamically strong magnetic fields locally change the nature of the flow to stop it from amplifying them further (e.g., [Cattaneo et al. 1996](#); [Zienicke et al. 1998](#); [Kim 1999](#); [Schekochihin et al. 2004a,b](#); [Cattaneo & Tobias 2009](#); [Baggaley et al. 2010](#); [Rempel et al. 2013](#); [Seta et al. 2020](#); [St-Onge et al. 2020](#)). It is if one wants to make a theory of this type work that one is required to produce a dynamical mechanism for transferring magnetic energy from small scales to large.

13.4.7. Inverse Magnetic-Energy Transfer via Sporadic Decay?

In pursuit of such mechanisms, an interesting recent development came from simulations of *decaying* MHD turbulence without a mean field: as I already mentioned in § 12.5, [Zrake \(2014\)](#) and [Brandenburg et al. \(2015\)](#) discovered numerically that such a turbulence, even without net helicity, could support a certain amount of inverse transfer of magnetic energy from small to large scales (as expected theoretically: see § 12.5).⁸⁷ In § 12.4.2, I argued, following [Zhou et al. \(2020\)](#), [Bhat et al. \(2021\)](#), and [Hosking & Schekochihin \(2021\)](#), that the dynamical mechanism by which large-scale magnetic fields are generated in decaying, non-helical MHD turbulence starting from a magnetically dominated state is the merger of reconnecting flux ropes. Let me explore what would happen if the same mechanism were to apply locally to the magnetic structures at the reversal scale λ_R , which are flux ropes (plasmoids), released from disintegrating folds.

Imagine that, instead of being continuously forced everywhere, our saturated dynamo were to be left alone for a period of time (and/or in a region of space)—this could be due to the natural spatiotemporal intermittency of the system or to a method of forcing leading to sporadic energy-injection events with quiescent periods of decaying turbulence in between (e.g., in galaxy clusters: [Roh et al. 2019](#)). With the arrival of each quiescent period, mergers between the flux ropes should push magnetic energy to larger scales.

The salient bit of theory that is needed to assess this effect is that the magnetic-energy-containing scale will grow with time as a power law during the decay of the turbulence: thus, if the field starts at scale λ_R , its scale after a period of decay will be

$$\lambda_B \sim \lambda_R \left(\frac{t}{\tau_{\text{rec}}} \right)^\alpha, \quad \tau_{\text{rec}} \sim \epsilon_{\text{rec}}^{-1} \frac{\lambda_R}{B_{\lambda_R}}, \quad (13.33)$$

where $0 < \alpha < 1$ in all conceivable circumstances ($\alpha = 4/9$ for fast-reconnection-controlled decay; see § 12.4.2), τ_{rec} is the characteristic reconnection time (12.9) at the beginning of the decay, with the initial energy-containing scale λ_R given by (13.9) and $B_{\lambda_R} \sim \delta u_L$ (same as the outer-scale velocity field). Suppose the decay is allowed to

⁸⁷The existence of such an inverse transfer in the case of non-zero net helicity is well known and well simulated (see references in § 12.5), but is not relevant here because it is just a nonlinear counterpart of the helical mean-field dynamo, a topic reviewing which I leave to [Rincon \(2019\)](#).

proceed for about one outer-scale turnover time $L/\delta u_L$. The magnetic field's scale after that will be

$$\lambda_B \sim \epsilon_{\text{rec}}^\alpha \lambda_R^{1-\alpha} L^\alpha. \quad (13.34)$$

If reconnection is fast (appendix D.6), or stochastic (appendix D.7), λ_B will have a weaker Rm_L scaling than λ_R , but it is not a triumph of inverse transfer. Another way to reach the same tepid conclusion is by asking how long it would take to get the magnetic field to the outer scale, $\lambda_B \sim L$. The answer is

$$t \sim \tau_{\text{rec}} \left(\frac{L}{\lambda_R} \right)^{1/\alpha} \sim \frac{L}{\delta u_L} \epsilon_{\text{rec}}^{-1} \left(\frac{L}{\lambda_R} \right)^{(1-\alpha)/\alpha} \gg \frac{L}{\delta u_L}, \quad (13.35)$$

quite a long time, as expected, i.e., the forcing would have to be very sporadic to achieve this.

Obviously, all this does not amount to much more than an initial “back-of-the-envelope” assessment, and a more sophisticated treatment might still yield a more pleasing outcome.

13.4.8. Local Shear Dynamo?

Let me complete my catalogue of speculations regarding the structure of the saturated dynamo state by invoking another piece of dynamo physics that, despite being of potentially fundamental and ubiquitous nature, emerged relatively late in the game. A combination of small-scale turbulence and a large-scale shear generically leads to the emergence of large-scale magnetic field, even when the turbulence has no net helicity—an effect known as the “shear dynamo”. This was mooted theoretically in several early mean-field-dynamo schemes and then confirmed numerically by Yousef *et al.* (2008b,a) (see references therein for the precursor theories, numerics and counter-arguments). This result turned out to be due to a form of “stochastic α effect” (Heinemann *et al.* 2011; Jingade *et al.* 2018), depending, therefore, on fluctuating helicity in the flow. Interestingly, the shear dynamo turned out to work also when the small-scale turbulence was magnetic, i.e., by the combination of a large-scale shear and the saturated state of small-scale dynamo (Yousef *et al.* 2008a). Squire & Bhattacharjee (2015, 2016) made sense of that by discovering semi-analytically the “magnetic shear-current effect” and showing that small-scale magnetic fields were actively helpful in enabling the shear dynamo.

The outcome of §13.3.3 was a situation in which the outer-scale (L) field-stretching motions (plus possibly some sort of kinetic-energy cascade to smaller scales) coexisted with MHD turbulence produced by the break up of the folds, with an effective outer scale $\lambda_R \ll L$ (in §§13.4.4, 13.4.6, and §13.4.7, this scale was increased, but remained smaller than L). It seems to be an attractive speculation that the combination of this turbulence with the local shears associated with the “hydrodynamic” scales $> \lambda_R$ might act as a local shear dynamo and create “local mean fields” on scales $> \lambda_R$. It would be interesting to investigate whether such a mechanism exists and, if it does, whether it can push the magnetic-energy-containing scale closer to L .

To conclude, there are plenty of potential theories—far too many, so no convincing one theory yet. Hero numerics reaching for asymptoticity, and intelligently analysed, might help pare down this field and finally give our understanding of the saturated MHD dynamo a modicum of completeness to match what has been achieved for MHD turbulence with a mean field.

14. The Frontier: Kinetic Turbulence

We can measure the globula of matter and the distances between them, but Space plasm itself is incomputable.

Vladimir Nabokov, *Ada, or Ardor*

14.1. Sundry Microphysics at Low Collisionality

I ended the first part of this review with a proclamation in § 8.1 that the story of MHD turbulence looked reasonably complete (before spending five chapters on the loose ends!). Since the main reason for this triumphalism was that MHD cascade finally made sense at the dissipation scales—and the key role in making it make sense belonged to reconnection, a dissipative phenomenon—it is an inevitable complication that microphysics of dissipation may matter. The visco-resistive MHD description adopted here does apply to some natural plasmas, e.g., stellar convective zones or colder parts of accretion discs. These are mostly low-Pm environments. Whereas I have made an effort to keep all results general and applicable to the high-Pm limit, it is, in fact, quite hard to find naturally occurring high-Pm plasmas for which the standard visco-resistive MHD equations are a good model: this would require the particles’ collision rate to be larger than their Larmor frequency, which rarely happens at high temperatures and low densities needed to achieve high Pm (one exception, quite popular these days, is plasmas created in laser experiments: see, e.g., Bott *et al.* 2021b, 2022). In fact, most of the interesting (and observed) plasmas in this hot, rarefied category are either “dilute” (an apt term coined by Balbus 2004 to describe plasmas where turbulence is on scales larger than the mean free path, but the Larmor motion is on smaller scales that it—a good example is galaxy clusters; see, e.g., Melville *et al.* 2016 and references therein) or downright collisionless (i.e., everything happens on scales smaller than the mean free path; the most obvious example is the solar wind: see the mega-review by Bruno & Carbone 2013 or a human-sized one by Chen 2016). In either case, between the “ideal-MHD scales” and the resistive scale, there is a number of other scales at which the physics changes. These changes are of two distinct kinds.

The first is the appearance of dispersion in the wave physics: Alfvén waves become kinetic Alfvén waves (KAWs), with a different linear response and, therefore, a different variety of critically balanced cascade (Cho & Lazarian 2004; Schekochihin *et al.* 2009, 2019; Boldyrev & Perez 2012; Boldyrev *et al.* 2013; Chen & Boldyrev 2017; Passot *et al.* 2017; Milanese *et al.* 2020). The culprits here are the ion inertial scale (at which the Hall effect comes in), the ion sound scale (at which the electron-pressure-gradient force becomes important in Ohm’s law), and the ion Larmor scale (at which the finite size of ion Larmor orbits starts playing a role). Which of these matters most depends on plasma beta and on the ratio of the ion and electron temperatures, but they all are essentially ion-electron decoupling effects and lead to more or less similar kinds of turbulence, at least in what concerns the KAW cascade. Note that the subviscous regime (§ 11) is, of course, irrelevant for such plasmas—except possibly, in a somewhat exotic way, at high beta (Kawazura *et al.* 2019).

The second important modification of MHD is that reconnection in a collisionless plasma need not be done by resistivity, but can be due to other physics that breaks flux conservation, viz., electron inertia, electron finite Larmor radius (FLR) and, more generally, other kinetic features of the electron pressure tensor. Tearing modes are different in such plasmas, with a double ion-electron layer structure and a variety of

scalings in a variety of parameter regimes.⁸⁸ Since tearing is important for rounding off the MHD cascade, all these effects must be considered and appropriate modifications worked out for the theory of tearing-mediated turbulence described in § 7—some of this has been done by [Mallet et al. \(2017a\)](#) and by [Loureiro & Boldyrev \(2017a\)](#). It is going to be interesting to find out whether, where, and when any of this matters or if perhaps the aligned MHD cascade just segues directly into the KAW cascade (see, however, a discussion in a moment as to what that means). Since there are some mysteries still outstanding with regard to the scale at which the spectrum of solar-wind turbulence has a spectral break between the inertial range and the “kinetic” (KAW) range ([Chen et al. 2014a](#); [Boldyrev et al. 2015](#)), perhaps something interesting can be done here (e.g., is the break set by the onset of reconnection, rather than by the Larmor scale?—see [Vech et al. 2018](#)).

Furthermore, KAW turbulence in the kinetic range and *its* relationship with reconnection is a topic that is rapidly becoming very popular with both numerical modellers (e.g., [TenBarge & Howes 2013](#); [Bañón Navarro et al. 2016](#); [Cerri & Califano 2017](#); [Franci et al. 2017, 2018](#)) and observational space physicists (e.g., [Greco et al. 2016](#)). There is a promise of interesting physics—interesting both conceptually and because it is eminently measurable in space. In the context of the prominent role that was given in § 7 to the break up of MHD sheets in setting up the tail end of the MHD cascade, I want to highlight an intriguing suggestion (implicitly) contained in the paper by [Cerri & Califano \(2017\)](#) and further fleshed out by [Franci et al. \(2017\)](#). They look (numerically) at the formation of current sheets in kinetic turbulence and the disruption of these sheets by tearing (plasmoid) instabilities—and discover that it is precisely these processes that appear to seed the sub-Larmor-scale cascade with a steep (steeper than in the inertial range) energy spectrum usually associated with KAW turbulence. One might wonder then if such a KAW cascade is an entirely distinct phenomenon from a collisionless version of tearing-mediated turbulence. If we allow ourselves to get excited about this question, we might speculate that it rhymes nicely with the idea on which [Boldyrev & Perez \(2012\)](#) relied to advocate a steeper $(-8/3)$ slope of KAW turbulence than the $-7/3$ implied by the standard CB-based theory ([Cho & Lazarian 2004](#); [Schekochihin et al. 2009](#)). They argued that the energetically dominant perturbations at each scale were concentrated in 2D structures, thus making turbulence non-volume-filling (and perhaps monofractal; cf. [Kiyani et al. 2009](#) and [Chen et al. 2014b](#)). While [Boldyrev & Perez \(2012\)](#) did not appear to think of these 2D structures as reconnecting sheets, an interpretation of them as such does not seem *a priori* unreasonable. So perhaps this is what happens in collisionless turbulence: sheet-like structures form in the usual (MHD) way, get disrupted by collisionless tearing and/or related instabilities and seed sub-Larmor turbulence,⁸⁹ which stays mostly concentrated in those sheets or their remnants, with an effectively 2D filling fraction. Another possibility—or a version of this scheme—is to abandon the old KAW cascade altogether and declare sub-Larmor turbulence to be entirely controlled by (collisionless) tearing in a similar way to the tearing-mediated cascade of § 7.2, with

⁸⁸ Appendix B.3 of [Zocco & Schekochihin \(2011\)](#) has a review of standard results for collisionless and semicollisional tearing modes at low beta (using a convenient minimalist set of dynamical equations as a vehicle), as well as all the relevant references of which we were aware at the time. There is a huge literature on semicollisional and collisionless reconnection and, short of dedicating this review to name-checking it all (which would be a noble ambition, but a doomed one, as the literature is multiplying faster than one can keep track), I cannot give proper credit to everyone who deserves it. A useful recent treatment of electron-only tearing done with applications to space turbulence in mind is [Mallet \(2020\)](#).

⁸⁹ See [Mallet et al. \(2017a\)](#) for a discussion of what else they seed.

spectral slopes between -3 and $-8/3$, still consistent with observations and simulations (Loureiro & Boldyrev 2017a; Boldyrev & Loureiro 2019).

What I have said about kinetic physics so far might not sound like a true conceptual leap: basically, at small scales, we have different linear physics and a zoo of possibilities, depending on parameter regimes; one could work productively on porting some of the basic ideas developed in the preceding sections to these situations.⁹⁰ There are, however, ways in which kinetic physics does bring in something altogether new. Four examples of that, chosen in a very biased way, are given in what follows.

14.2. Cascade Fragility

FLR effects do not just change how linear waves propagate at sub-Larmor scales. They also change the nature of the second conserved quantity (the first being energy) possessed by the plasma: (R)MHD cross-helicity (imbalance) becomes magnetic helicity in the transition from the inertial to the sub-Larmor scale range. The trouble is that the KAW helicity is a quantity that naturally wants to cascade inversely, from small scales to large (Schekochihin *et al.* 2009; Cho 2011; Kim & Cho 2015; Cho & Kim 2016; Miloshevich *et al.* 2021). In low-beta plasmas, there is no dissipation at the ion Larmor scale (Schekochihin *et al.* 2019), so an imbalanced cascade arriving from the inertial range would get thoroughly “confused” by the sudden need to reverse the direction of the helicity cascade. The result, it turns out, is a mighty blow back from the small scales to large and a failure to achieve a constant-flux steady state (see figure 35, taken from Meyrand *et al.* 2021; some evidence of strange behaviour of energy fluxes in imbalanced solar-wind turbulence does appear to exist: see, e.g., Smith *et al.* 2009). The imbalanced cascades are fragile.

What this means for the real plasmas that these models aspire to describe (low beta, high Elsasser imbalance—typical solar-wind conditions close to the Sun, currently sampled with gusto by the Parker Solar Probe; see, e.g., Chen *et al.* 2020) is that the fluid approximation is broken—not just in the sense of requiring FLR bolt-ons, but in the sense that the system cannot accommodate a steady-state turbulent cascade while still respecting the $k_{\parallel} \ll k_{\perp}$ and low-frequency (viz., $\omega \ll$ the ion cyclotron

⁹⁰ Another class of kinetic situations for which such porting appears to be a successful strategy is relativistic plasma turbulence. As full-Vlasov kinetic simulations have gradually become more computationally affordable over the last decade, the first plasmas for which they became affordable were pair plasmas moving at relativistic speeds—computations made easier on account of the mass ratio being unity and of the frequencies associated with the turbulent motion being closer to the highest plasma-wave frequencies needing to be resolved in a Vlasov simulation anyway. A lively industry has developed and, in certain respects, kinetic, relativistic plasma turbulence is now better documented than its slower-moving, harder-to-compute counterpart. I am not aware of any qualitatively dramatic way in which the small-scale structure of the former has proven to be much different from that of the latter, or of the vanilla-MHD prototype of either—but students of this topic have not been preoccupied primarily with the structure of the turbulence, but rather followed the (observationally well-motivated) astrophysical obsession with nonthermal particle acceleration. Of this, relativistic turbulence has indeed been found guilty, provided it was stirred up with $\delta B \sim B_0$ (Zhdankin *et al.* 2017; Comisso & Sironi 2018). The most recent spate of papers on this topic, which represent the state of the art and from which the historical paper trail can be followed, are Comisso & Sironi (2021), Vega *et al.* (2022b,a), Hankla *et al.* (2022) (imbalanced turbulence), Nättilä & Beloborodov (2022) (small $\delta B/B_0$, no nonthermal acceleration), Zhdankin *et al.* (2021) (non-unity mass ratio, ion vs. electron heating), and Chernoglazov *et al.* (2021) (alignment and current sheets in fluid but relativistic MHD turbulence). It is interesting that in this context again, reconnecting structures spontaneously generated by turbulence appear to play a prominent role—this time as sites of particle acceleration.

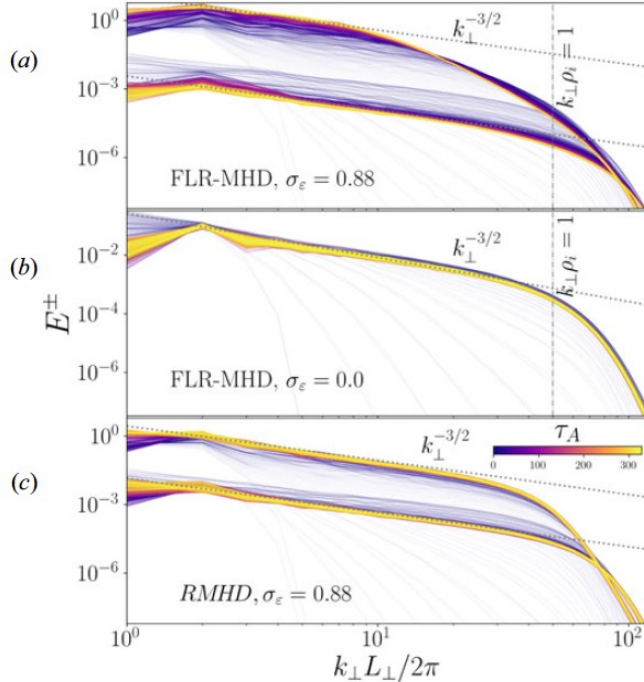


FIGURE 35. Spectra of Elsasser field for (c) heavily imbalanced RMHD turbulence ($\varepsilon^+/\varepsilon^- \approx 16$), (a) similarly imbalanced turbulence in an RMHD-like model of a low-beta collisionless plasma with FLR effects, and (b) balanced turbulence in the same model. Purple-to-yellow colour scale shows time evolution of the spectra. The spectrum of the stronger Elsasser field in (a) does not reach a steady state, with spectral break moving to larger scales. Measurement of energy fluxes in these simulations shows that (a) is not a constant-flux solution, whereas (b) is. These results are from [Meyrand et al. \(2021\)](#).

frequency) ordering associated with the gyrokinetic approximation and its various fluid-like reductions ([Howes et al. 2006](#); [Schekochihin et al. 2009, 2019](#)). A fully kinetic system deals with this problem by building up energy in the stronger Elsasser field and, therefore, shortening the nonlinear cascade times τ_{nl} , until critical balance pushes k_\parallel high enough to break the gyrokinetic approximation and open up a new dissipation channel via the ion-cyclotron resonance—a happy reconciliation, it seems, between ample observational evidence both for ion-cyclotron heating and for low-frequency cascades in the solar wind ([Squire et al. 2022](#)).

This is a relatively rare example of plasma microphysics seriously upsetting system-scale macrophysics (another possible set of such examples is flagged in § 14.5). Sadly, this renders much of § 9 almost completely irrelevant for such plasmas—unless an effective way can be found of modifying the dissipation-scale pinning scheme (§ 9.6.4) to account for the kinetic dissipation mechanism described above.

14.3. Phase-Space Turbulence

What is turbulence? Some energy is injected into some part of the phase space of a nonlinear system (in fluid systems, that simply means position or wavenumber space), which is, generally speaking, not the part of the phase space where it can be efficiently thermalised. So turbulence is a process whereby this energy finds its way from where it is injected to where it can be dissipated, and its means of doing this is nonlinear coupling,

usually from large to small scales (I am now putting to one side the upsetting example of the failure of this process discussed in § 14.2). What kind of coupling is possible and at what rate the energy can be transferred from scale to scale then determines such things as energy spectra in a stationary state with a constant flux of energy.

The same principle applies to kinetic turbulence, but now the phase space is 6D rather than 3D: the particle distribution depends on positions and velocities, and energy transfer can be from large to small scales (or vice versa) in all six coordinates. The transfer of (free) energy to small scales in velocity space, leading ultimately to activation of collisions, however small the collision rate, is known as “phase mixing”. It is not always a nonlinear phenomenon: the simplest (although not necessarily very simple) phase-mixing process is the linear Landau (1946) damping. In a magnetised plasma, this is the *parallel* (to B_0) phase mixing, whereas the *perpendicular* phase mixing is nonlinear and has to do with particles on Larmor orbits experiencing different electromagnetic fields depending on the radius of the orbit (the Larmor radius is a kinetic variable, being proportional to v_\perp). The latter phenomenon leads to an interesting phase-space “entropy cascade” (Schekochihin *et al.* 2008, 2009; Tatsuno *et al.* 2009; Plunk *et al.* 2010; Cerri *et al.* 2018; Eyink 2018; Kawazura *et al.* 2019; cf. Pezzi *et al.* 2018), which is one of the more exotic phenomena that await a curious researcher at sub-Larmor scales. Its importance in the grand scheme of things is that it channels turbulent energy into ion heat, while the KAW cascade heats electrons—the question of which dissipation channel is the more important one, and when, being both fundamental and “applied” (in the astrophysical sense of the word—e.g., to accretion flows: see Quataert & Gruzinov 1999, Event Horizon Telescope Collaboration 2019). Understanding how energy is transferred between scales in phase space requires thinking somewhat outside the standard turbulence paradigm and so perhaps counts as conceptual novelty. Not much of it has been done so far and it is worth doing more.

Returning to parallel phase mixing, this too turns out to be interesting in a nonlinear setting, even though it is a linear phenomenon itself. First theoretical (Schekochihin *et al.* 2016; Adkins & Schekochihin 2018) and numerical (Parker *et al.* 2016; Meyrand *et al.* 2019) analyses suggest that, in a turbulent system, parallel phase mixing is effectively suppressed by the stochastic plasma echo, perhaps rendering kinetic systems that are notionally subject to Landau damping effectively fluid, at least in terms of their energy-flow budgets. In the context of inertial-range MHD turbulence, this is relevant to the compressive (“slow-mode”) perturbations, which, in a collisionless plasma, are energetically decoupled from, and nonlinearly slaved to, the Alfvénic ones, while the latter are still governed by RMHD (Schekochihin *et al.* 2009; Kunz *et al.* 2015). Linearly, these compressive perturbations must be damped—but nonlinearly they are not (Meyrand *et al.* 2019), thus accounting for them exhibiting a healthy power-law spectrum and other fluid features in the solar wind (Chen 2016; Verscharen *et al.* 2017). In this vein, one might also ask whether the Landau damping of KAWs at sub-Larmor scales is always efficient or even present at all—and if it is, as TenBarge & Howes (2013), Bañón Navarro *et al.* (2016), Kobayashi *et al.* (2017), and Chen *et al.* (2019) all say, then what is different at these scales. Given that Loureiro *et al.* (2013b) see a characteristic signature of phase mixing in collisionless reconnection, reconnection might yet again turn out to be the key player, as indeed it has been conjectured to be at these scales (see § 14.1).

The broader question is whether there is generally Landau damping in turbulent systems and whether, therefore, to put it crudely, “all turbulence is fluid.” While it might be a little disappointing if it is, the way and the sense in which this seems to be achieved are surprising and pleasingly nontrivial—and possibly soon to be amenable to direct measurement if the first MMS results on velocity-space (Hermite) spectra in the

Earth's magnetosheath (Servidio *et al.* 2017) are a good indication of the possibilities that are opening up.

14.4. Statistical Thermodynamics of Collisionless Plasma

At quite uncertain times and places,
The atoms left their heavenly path,
And by fortuitous embraces,
Engendered all that being hath.
And though they seem to cling together,
And form "associations" here,
Yet, soon or late, they burst their tether,
And through the depths of space career.

J. C. Maxwell, *Molecular Evolution*

Phase-space turbulence is interesting not just in its own right, but also as a means to answering an even broader, and trickier, question, or class of questions, which concerns the equilibria underlying the fluid-like (or kinetic) dynamics of plasma turbulence. The meaning of the word “thermalised,” which I used to describe the fate of turbulent energy at the beginning of § 14.3, is really only fully clear if the underlying equilibrium is Maxwellian—i.e., if significant departures from thermal equilibrium occur, and, therefore, a kinetic description is required, only for the turbulent fluctuations. This is certainly not the case for many natural plasmas, where the overall distribution functions both of ions and of electrons, can be order-unity non-Maxwellian—the prime and most accessible example of that being the solar wind (e.g., Marsch 2006, 2018; Martinović *et al.* 2020). A number of questions then arise, all of them both unsolved and extremely fundamental on a level that should appeal to any physicist:

- (i) Do universal (i.e., not sensitive in detail to initial conditions) collisionless equilibria exist?
- (ii) If they do, is it possible to find them by constructing a statistical thermodynamics of collisionless plasma based on such staples as the maximum-entropy principle? And if so, what is the correct definition of entropy for a collisionless plasma (cf. Fowler 1968; Eyink 2018; Matthaeus *et al.* 2020; Zhdankin 2022a; Chavanis 2021; Ewart *et al.* 2022)?
- (iii) Is it then possible to have a theory of plasma relaxation to these equilibria in terms of some “collisionless collision integrals”? What is the relaxation rate (i.e., the “effective collision rate”)? It is at this step that the structure of phase-space turbulence, which was flagged as interesting in its own right in § 14.3, comes in as an essential ingredient: in the same way as the “fluid” theory of turbulent transport in, e.g., a gyrokinetic plasma, requires knowledge of the statistical properties of turbulence, which determine turbulent fluxes of conserved “fluid” quantities (e.g., Abel *et al.* 2013), the kinetic theory of collisionless relaxation requires one to know the phase-space correlation function of the perturbed distribution function, which determines the turbulent flux of phase density (Kadomtsev & Pogutse 1970; Chavanis 2021; Ewart *et al.* 2022).
- (iv) And if all, or some, of the above is accomplished, how can one then describe the passage of energy from turbulent fluctuations into the equilibrium distribution (“thermalisation”)⁹¹ in terms of some generalised free-energy cascade (one example

⁹¹Of course, collisionless equilibrium distributions do not have to be “thermal”, i.e., they can have extended tails at high energies—such tails are indeed observed by astronomers and so nonthermal particle acceleration by turbulence is an object of intense interest to astrophysicists:

of how one might approach this question can be gleaned from a comparison between Schekochihin *et al.* 2009, where a Maxwellian equilibrium is assumed, and Kunz *et al.* 2015, 2018, where the equilibrium is allowed to be pressure-anisotropic).

These questions are not new—there was some very interesting activity around them half a century ago (e.g., Fowler 1968; Kadomtsev & Pogutse 1970; Dupree 1972), which produced a flurry of follow-ups, but the subject has since gone into abeyance, due, in large part, to the impossibility at the time of numerical or observational testing of any of the theories. This is now changing: computers are big enough to handle the vastness of the 6D phase space, and the heliosphere is teeming with spacecraft full of eager and discerning instruments. This is a exciting research frontier if there has ever been one. Here is not the place to review this topic in any further detail—my own take on it, as pedagogical as I can manage, alongside a more complete set of references, can be found in Schekochihin (2022).

14.5. Macro- and Microphysical Consequences of Pressure Anisotropy

Another line of inquiry pregnant with conceptual novelty concerns the effect of self-generated pressure anisotropy on MHD dynamics. Pressure anisotropies are generated in response to any motion in a magnetised collisionless or weakly collisional plasma as long as this motion leads to a change in the strength of the magnetic field. The conservation of the magnetic moment ($\propto v_{\perp}^2/B \propto$ the angular momentum of Larmor-gyrating particles) then causes positive (if the field grows) or negative (if it decreases) pressure anisotropy to arise (see, e.g., Schekochihin *et al.* 2010). This is usually quite small, but it becomes relevant at high beta, when even small anisotropies (of order $1/\beta$) can have a dramatic effect, in two ways. Dynamically, pressure anisotropy supplies additional stress, which, when the anisotropy is negative ($p_{\perp} < p_{\parallel}$), can cancel Maxwell’s stress and thus remove magnetic tension—the simplest way to think of this is in terms of the Alfvén speed being modified so:

$$v_A \rightarrow \sqrt{v_A^2 + \frac{p_{\perp} - p_{\parallel}}{\rho}}. \quad (14.1)$$

Kinetically, pressure anisotropy is a source of free energy and will trigger fast, small-scale instabilities, most notably mirror and firehose (see Kunz *et al.* 2014 and references therein). The firehose corresponds to the Alfvén speed (14.1) turning imaginary, i.e., it is an instability caused by negative tension; the mirror is not quite as simple to explain, but is fundamentally a result of effective magnetic pressure going negative by means of some subtle resonant-particle dynamics (see Southwood & Kivelson 1993, Kunz *et al.* 2015 and references therein). These instabilities in turn can regulate the anisotropy by scattering particles or by subtler, more devious means (see Melville *et al.* 2016 and references therein).

Investigating of the dynamics of a simple finite-amplitude Alfvén wave in a collisionless, high-beta plasma, Squire *et al.* (2016, 2017b,a) showed that both of these effects did occur and altered the wave’s behaviour drastically: it first slows down to a near halt due to the removal of magnetic tension, transferring much of its kinetic energy into heat and then, having spawned a colony of particle-scattering Larmor-scale perturbations, dissipates as

see references in footnote 90. Mathematically, distribution functions with nonthermal, power-law tails can be derived as solutions of kinetic equations containing phase-space advection and diffusion with velocity-dependent coefficients (see, e.g., Wong *et al.* 2020; Vega *et al.* 2022b; Uzdensky 2022, and references therein) or as maximisers of a judiciously chosen entropy (e.g., Zhdankin 2022b; Ewart *et al.* 2022). In a complete theory, they should appear as fixed points of the “collisionless collision integrals”.

if it were propagating in a plasma with a large Braginskii (1965) parallel viscosity. Sound waves in a collisionless plasma get similarly infested by firehoses and mirrors, except the resulting effective collisionality helps them propagate in a medium that they thus render more fluid and, therefore, incapable of Landau damping (a different mechanism than discussed in § 14.3, but a similar outcome; see Kunz *et al.* 2020).

These effects occur provided the amplitude of the waves is above a certain limit that scales with plasma beta: this is because pressure anisotropy must be large enough to compete with tension in (14.1) and the amount of anisotropy that can be generated is of the order of the field-strength perturbation. For an Alfvén wave, the latter is quadratic in the wave’s amplitude:

$$\left(\frac{\delta b}{v_A}\right)^2 \sim \frac{p_\perp - p_\parallel}{p} \gtrsim \frac{v_A^2}{p/\rho} \sim \frac{1}{\beta}. \quad (14.2)$$

In formal terms, this means that in high-beta collisionless plasmas, the small-amplitude and high-beta limits do not commute. The conventional picture of Alfvénic turbulence simply obeying RMHD equations, even in a collisionless plasma (Schekochihin *et al.* 2009; Kunz *et al.* 2015), may then have to be seriously revised for such environments as galaxy clusters, for example, where $\beta \sim 10^2$ (Schekochihin & Cowley 2006) (a first step in this direction has been taken by Squire *et al.* 2019, who found that MHD turbulence with Braginskii viscosity, while looking in many respects similar to the usual Alfvénic turbulence, nevertheless manages to minimise changes in the magnetic-field strength to a much greater extent—a property they dubbed “magneto-immutability”; cf. Tenerani & Velli 2020a, who do not like the term, but explore useful dynamical scenarios for achieving just such a state).⁹²

In situations where the inequality (14.2) is not satisfied, but the pressure anisotropy is a feature of the equilibrium, it seems we can live with the current theory as long as β is not too large. This is the case for most instances of the solar wind, where negative pressure anisotropy is driven by expansion away from the Sun (so B decreases with heliocentric distance) and β ranges from $\ll 1$ closer to the Sun to $\gtrsim 1$ in our own neighbourhood. A recent investigation by Bott *et al.* (2021a) of Alfvénic turbulence in an expanding box (mimicking the solar wind) at $\beta \approx 2 - 4$ found that a kinetic version of the firehose instability, which, at these β (unlike at $\beta \gg 1$), kicks in at a (negative) value of $p_\perp - p_\parallel$ order-unity short of zeroing out the magnetic tension, generated a sea of microscale magnetic perturbations that, by scattering particles, adjusted the effective collisionality of the plasma to keep it exactly marginal to that kinetic firehose; the critically balanced, Alfvénic cascade survived unscathed, albeit with the Alfvén speed modified according to (14.1). The (potentially) more interesting things that happen at $\beta \gg 1$ are costlier to tackle numerically, but, it seems, soon will be.

Existing understanding of another basic high-beta MHD process, the small-scale dynamo, which I discussed at length in § 13, is also potentially endangered by ubiquitous pressure anisotropies—but has survived the first contact with direct numerical experimentation, which required extra-large, “hero” kinetic simulations (Rincon *et al.* 2016; Kunz *et al.* 2016; St-Onge & Kunz 2018).⁹³ So far it appears that in this problem as

⁹²Let me mention parenthetically that at the small-scale end of the turbulent cascade, electron pressure anisotropies lie in wait to mess with the way in which reconnection occurs. I will not go into this here, referring the reader to a review by Egedal *et al.* (2013). This is another microphysical effect that may need to be inserted into the sub-Larmor dynamics (see § 14.1).

⁹³“Hero” they might have been, but they were only kinetic as far as ions were concerned, whereas electrons were fluid, with the usual resistive unfreezing of flux. There is as yet no demonstration

well, changing magnetic fields render plasma more collisional in some effective sense and so large-Pm dynamo remains a relevant paradigm. The same conclusion was reached by [St-Onge et al. \(2020\)](#), who simulated dynamo action and saturation in MHD with Braginskii stress (the collisional limit of pressure-anisotropic dynamics).

This line of investigation may be particularly rich in surprises because pressure-anisotropy stress undermines much of our basic intuition for ideal-MHD dynamics, not just modifies microscale plasma physics. This said, it is not entirely inconceivable that, at the end of the day (or of the decade), in some grossly coarse-grained sense, turbulent plasmas will just turn out to supply their own effective collisionality even where Coulomb collisions are rare—and so astrophysicists, with their focus on large-scale motions, need not be too worried about the validity of fluid models beyond requiring a few easily implementable tweaks. I hope life is not quite so boring, although, as a theoretical physicist and, therefore, a believer in universality, I should perhaps expect to be pleased by such an outcome.

15. Conclusion

Let us stop here. The story of MHD turbulence is a fascinating one—both the story of what happens physically and the story of how it has been understood. It is remarkable how long it takes to figure out simple things, obvious in retrospect. It is even more remarkable (and reassuring) that we get there after all, in finite time. This story now looks reasonably complete, at least in broad-brush outline ([§ 8.1](#)) and modulo numerous caveats and many interesting loose ends ([§§ 9–13](#)). Is this an illusion? Is it all wrong again? We shall know soon enough, but in the meanwhile, the siren call of kinetic physics is too strong to resist and the unexplored terrain seems vast and fertile ([§ 14](#)). Is everything different there? Or will it all, in the end, turn out to be the same, with Nature proving itself a universalist bore and contriving to supply effective collisions where nominally there are few? Is turbulence always basically fluid or do subtle delights await us in phase space? Even if we are in danger of being disappointed by the answers to these questions, getting there is proving to be a journey of amusing twists and turns.

For a topic as broad as this, it is difficult to list all the people from whom I have learned what I know (or think I know) of this subject. The most important such influence has been Steve Cowley. The views expressed in the first part of this paper ([§§ 5–7](#)) were informed largely by my collaboration with Alfred Mallet and Ben Chandran and by conversations with Andrey Beresnyak (even if he is likely to disagree with my conclusions), Nuno Loureiro and Dmitri Uzdensky. I have learned most of what I know of reconnection from Nuno and Dmitri and of the solar wind from Chris Chen, Tim Horbury, and Rob Wicks. I owe the first epigraph of this paper to the erudition of Richard McCabe and the second (as well as the epigraph of [§ 7](#)) to that of Matt Kunz. The sections on weak turbulence ([§ 4](#), appendix [A](#) and especially appendix [A.4](#)) would have been different had Thomas Foster not convinced me to make a modicum of

of a dynamo in a plasma with kinetic electrons, and the only paper that tried to get such a dynamo, failed, because magnetic fields got Landau-damped away ([Pusztai et al. 2020](#)), but in a system with fairly low scale separations. Two other recent studies ([Pucci et al. 2021](#); [Zhou et al. 2022](#)) have got a little farther, showing that electron pressure anisotropy generated by externally driven flows in an unmagnetised plasma will lead to generation of microscale magnetic fields via Weibel instability (another pressure-anisotropy-driven instability, even smaller-scale than firehose and mirror, and, unlike them, requiring particles *not* to be magnetised); their plan is for these fields to serve as seed for a fully two-species-kinetic dynamo.

peace with the traditional theory. Ben Chandran, Nuno Loureiro, and Andrey Beresnyak have also helped me think coherently of imbalanced turbulence—without necessarily endorsing the outcome (§ 9). David Hosking demolished comprehensively my first version of § 12 (on decaying MHD turbulence) and forced a complete rewrite—in the process, he wrote what I consider to be one of the more beautiful papers that I have had the good fortune of being involved with (Hosking & Schekochihin 2021). The contents of § 13 were inspired by discussions with Andrey Beresnyak, Alisa Galishnikova, François Rincon, and Matt Kunz, re-examining my views on small-scale dynamo that had been formed in the early 2000s. The views expressed in § 14 are in large measure a result of my recent and current excursions to the kinetic frontier in the company of Toby Adkins, Lev Arzamasskiy, Michael Barnes, Archie Bott, Andrew Brown, Bill Dorland, Robbie Ewart, Yohei Kawazura, Matt Kunz, Romain Meyrand, Michael Nastac, Eliot Quataert, and Jono Squire. Besides the colleagues and friends mentioned above, conversations with Allen Boozer, Axel Brandenburg, Mike Brown, Peter Davidson, Daniele Del Sarto, Greg Eyink, Henrik Latter, Alex Lazarian, Sergey Nazarenko, Maurizio Ottaviani, Felix Parra, Marco Velli, Mahendra Verma, and Muni Zhou have helped me work out what to say, and how to say it, in various bits of this review. I would also like to thank the authors whose figures appear in the text for giving me permission to reproduce their art. I hasten to add that none of those mentioned here bear any responsibility for my many enduring confusions and biases. If, nevertheless, this paper occasionally manages to make sense to its readers, its six referees deserve some significant share of credit for that—they all provided reviews both spirited and helpful, ranging from spotting multitudinous typos to calling out preposterous stylistic bloopers to identifying important logical pitfalls, and even, in one instance, offering detailed suggestions as to the most appropriate wine selection to go with each section.

Visits to a number of pleasant places have helped bring this work to completion. I am delighted to acknowledge the hospitality of the Wolfgang Pauli Institute, Vienna, where, in meetings held annually for 12 years (2007–19), many key interactions took place and ideas were hatched. This paper started as an “opinion piece” written for the 1st JPP Frontiers of Plasma Physics Conference at the Abbazia di Spineto in 2017, when the news of tearing-mediated turbulence was very fresh. My extended stay in 2018 at the Niels Bohr International Academy, Copenhagen, where some nontrivial *i*'s were dotted and *t*'s crossed, was supported by the Simons Foundation (via Martin Pessah, to whom I am grateful for offering me NBIA's hospitality). Another place whose hospitality, in 2019, proved germane to making progress was the Kavli Institute of Theoretical Physics, Santa Barbara, during its programme on “Multiscale Phenomena in Plasma Astrophysics” led by Anatoly Spitkovsky. In the UK, my work was supported in part by grants from STFC (ST/N000919/1 and ST/W000903/1) and EPSRC (EP/M022331/1 and EP/R034737/1). The manuscript was finally finished during the first Covid-19 lockdown (in 2020) and revised during the second (2021), but I offer no thanks to the virus.

Declaration of Interests. The author reports no conflict of interest.

Appendices

Appendix A. Splendours and Miseries of WT Theory

A.1. RMHD in Scalar Form

It is convenient to rewrite the RMHD equations (3.1) in terms of two scalar fields, so-called Elsasser potentials ζ^\pm , which are the stream functions for the 2D-solenoidal

fields \mathbf{Z}_\perp^\pm (Schekochihin *et al.* 2009), viz.,

$$\mathbf{Z}_\perp^\pm = \hat{\mathbf{z}} \times \nabla_\perp \zeta^\pm, \quad (\text{A } 1)$$

where $\hat{\mathbf{z}} = \mathbf{B}_0/B_0$. Then ζ^\pm satisfy, as shown by taking the curl of (3.1) and using (A 1),

$$\frac{\partial \omega^\pm}{\partial t} \mp v_A \nabla_\parallel \omega^\pm = -\{\zeta^\mp, \omega^\pm\} + \{\partial_j \zeta^\pm, \partial_j \zeta^\mp\}, \quad (\text{A } 2)$$

where $\omega^\pm = \hat{\mathbf{z}} \cdot (\nabla_\perp \times \mathbf{Z}_\perp^\pm) = \nabla_\perp^2 \zeta^\pm$ are Elsasser vorticities, all dissipative terms have been dropped, and

$$\{\zeta^\mp, \omega^\pm\} = \frac{\partial \zeta^\mp}{\partial x} \frac{\partial \omega^\pm}{\partial y} - \frac{\partial \zeta^\mp}{\partial y} \frac{\partial \omega^\pm}{\partial x} = \mathbf{Z}_\perp^\mp \cdot \nabla_\perp \omega^\pm. \quad (\text{A } 3)$$

Note that I have written (A 2) in a slightly different (but equivalent) form than in Schekochihin *et al.* (2009). The present version emphasises that the two physical influences of the nonlinearity on the Elsasser vorticities are advection by the other Elsasser field \mathbf{Z}_\perp^\mp (the first term on the right-hand side) and ‘‘vortex stretching’’ (the second term) (cf. Zhdankin *et al.* 2016b)—this is a useful way to write these equations for, e.g., the argument in § 10.4 about the build-up of negative correlations between ω^+ and ω^- (residual energy).

In Fourier space, (A 2) has a nicely generic form

$$\partial_t \zeta_{\mathbf{k}}^\pm \mp ik_\parallel v_A \zeta_{\mathbf{k}}^\pm = \sum_{\mathbf{pq}} M_{\mathbf{k}\mathbf{pq}} \delta_{\mathbf{k},\mathbf{p}+\mathbf{q}} \zeta_{\mathbf{p}}^\mp \zeta_{\mathbf{q}}^\pm, \quad (\text{A } 4)$$

with the coupling coefficients

$$M_{\mathbf{k}\mathbf{pq}} = \hat{\mathbf{z}} \cdot (\mathbf{k}_\perp \times \mathbf{q}_\perp) \frac{\mathbf{k}_\perp \cdot \mathbf{q}_\perp}{k_\perp^2} = q_\perp^2 \sin \phi \cos \phi, \quad (\text{A } 5)$$

where ϕ is the angle between \mathbf{k}_\perp and \mathbf{q}_\perp .

A.2. Classic WT Calculation

Our objective is to derive an evolution equation for the spectra $C_{\mathbf{k}}^\pm = \langle |\zeta_{\mathbf{k}}^\pm|^2 \rangle$. Multiplying (A 4) by $\zeta_{\mathbf{k}}^{\pm*}$ and adding to the resulting equation its complex conjugate, we get

$$\partial_t C_{\mathbf{k}}^\pm = 2\text{Re} \sum_{\mathbf{pq}} M_{\mathbf{k}\mathbf{pq}} \delta_{\mathbf{k},\mathbf{p}+\mathbf{q}} \langle \zeta_{\mathbf{p}}^\mp \zeta_{\mathbf{q}}^\pm \zeta_{\mathbf{k}}^{\pm*} \rangle. \quad (\text{A } 6)$$

Similarly, the evolution equation for the triple correlator appearing in the right-hand side of (A 6) is

$$\begin{aligned} \partial_t \langle \zeta_{\mathbf{p}}^\mp \zeta_{\mathbf{q}}^\pm \zeta_{\mathbf{k}}^{\pm*} \rangle \mp i2p_\parallel v_A \langle \zeta_{\mathbf{p}}^\mp \zeta_{\mathbf{q}}^\pm \zeta_{\mathbf{k}}^{\pm*} \rangle &= \sum_{\mathbf{k}'\mathbf{k}''} [M_{\mathbf{pk}'\mathbf{k}''} \delta_{\mathbf{p},\mathbf{k}'+\mathbf{k}''} \langle \zeta_{\mathbf{k}'}^\pm \zeta_{\mathbf{k}''}^\mp \zeta_{\mathbf{q}}^\pm \zeta_{\mathbf{k}''}^{\pm*} \rangle \\ &\quad + M_{\mathbf{qk}'\mathbf{k}''} \delta_{\mathbf{q},\mathbf{k}'+\mathbf{k}''} \langle \zeta_{\mathbf{p}}^\mp \zeta_{\mathbf{k}'}^\pm \zeta_{\mathbf{k}''}^\pm \zeta_{\mathbf{k}''}^{\pm*} \rangle \\ &\quad + M_{\mathbf{kk}'\mathbf{k}''} \delta_{\mathbf{k},\mathbf{k}'+\mathbf{k}''} \langle \zeta_{\mathbf{p}}^\mp \zeta_{\mathbf{q}}^\pm \zeta_{\mathbf{k}'}^\pm \zeta_{\mathbf{k}''}^{\pm*} \rangle] \equiv A_{\mathbf{k}\mathbf{pq}}, \end{aligned} \quad (\text{A } 7)$$

where, in working out the linear term, it has been opportune to take account of $k_\parallel = p_\parallel + q_\parallel$. To lowest order in the WT expansion, with $A_{\mathbf{k}\mathbf{pq}}$ approximated as constant in time, the solution to this equation is

$$\langle \zeta_{\mathbf{p}}^\mp \zeta_{\mathbf{q}}^\pm \zeta_{\mathbf{k}}^{\pm*} \rangle = \frac{1 - e^{\mp i2p_\parallel v_A t}}{\pm i2p_\parallel v_A} A_{\mathbf{k}\mathbf{pq}} \rightarrow \frac{\pi \delta(p_\parallel)}{2v_A} A_{\mathbf{k}\mathbf{pq}} \quad \text{as } t \rightarrow \infty. \quad (\text{A } 8)$$

This is the moment when it turns out that every interaction must involve the $p_{\parallel} = 0$ mode, for which the WT approximation is, in fact, broken.

Pressing on regardless, let us adopt the random-phase approximation, as always in WT (Zakharov *et al.* 1992; Nazarenko 2011). Namely, to lowest order in the WT expansion, any wave field is only correlated with itself at the same \mathbf{k} , all odd correlators vanish [which is why I had to iterate from (A 6) to (A 7)], and all even correlators are split into products of quadratic ones, viz.,

$$\langle \zeta_{\mathbf{k}}^{\pm} \zeta_{\mathbf{k}'}^{\pm} \rangle = C_{\mathbf{k}}^{\pm} \delta_{\mathbf{k}, -\mathbf{k}'}, \quad (\text{A } 9)$$

$$\langle \zeta_{\mathbf{k}}^{+} \zeta_{\mathbf{k}'}^{-} \rangle = 0, \quad (\text{A } 10)$$

$$\langle \zeta_{\mathbf{k}''}^{\pm} \zeta_{\mathbf{k}''}^{\mp} \zeta_{\mathbf{q}}^{\pm} \zeta_{\mathbf{k}}^{\pm *} \rangle = 0, \quad (\text{A } 11)$$

$$\langle \zeta_{\mathbf{p}}^{\mp} \zeta_{\mathbf{k}'}^{\mp} \zeta_{\mathbf{k}''}^{\pm} \zeta_{\mathbf{k}}^{\pm *} \rangle = C_{\mathbf{p}}^{\mp} \delta_{\mathbf{p}, -\mathbf{k}'} C_{\mathbf{k}}^{\pm} \delta_{\mathbf{k}''}, \quad (\text{A } 12)$$

$$\langle \zeta_{\mathbf{p}}^{\mp} \zeta_{\mathbf{q}}^{\pm} \zeta_{\mathbf{k}'}^{\mp} \zeta_{\mathbf{k}''}^{\pm *} \rangle = C_{\mathbf{p}}^{\mp} \delta_{\mathbf{p}, \mathbf{k}'} C_{\mathbf{q}}^{\pm} \delta_{\mathbf{q}, \mathbf{k}''}. \quad (\text{A } 13)$$

Therefore, noticing that $M_{\mathbf{q}, -\mathbf{p}, \mathbf{k}} = -M_{\mathbf{k} \mathbf{p} \mathbf{q}} k_{\perp}^2 / q_{\perp}^2$, we get

$$A_{\mathbf{k} \mathbf{p} \mathbf{q}} = M_{\mathbf{k} \mathbf{p} \mathbf{q}} \delta_{\mathbf{k}, \mathbf{p} + \mathbf{q}} C_{\mathbf{p}}^{\mp} \left(C_{\mathbf{q}}^{\pm} - \frac{k_{\perp}^2}{q_{\perp}^2} C_{\mathbf{k}}^{\pm} \right). \quad (\text{A } 14)$$

Combining (A 14) with (A 8) and putting the latter back into (A 6), we arrive at the classic WT equation derived by Galtier *et al.* (2000):

$$\partial_t N_{\mathbf{k}}^{\pm} = \frac{\pi}{v_A} \sum_{\mathbf{pq}} \frac{k_{\perp}^2 M_{\mathbf{k} \mathbf{p} \mathbf{q}}^2}{p_{\perp}^2 q_{\perp}^2} \delta_{\mathbf{k}, \mathbf{p} + \mathbf{q}} \delta(p_{\parallel}) N_{\mathbf{p}}^{\mp} (N_{\mathbf{q}}^{\pm} - N_{\mathbf{k}}^{\pm}), \quad (\text{A } 15)$$

where $N_{\mathbf{k}}^{\pm} = k_{\perp}^2 C_{\mathbf{k}}^{\pm} = \langle |\mathbf{Z}_{\perp \mathbf{k}}^{\pm}|^2 \rangle$.

A.3. Solution of WT Equation

The wavenumber sum in (A 15) is turned into an integral in the usual fashion: taking account of the restriction $\mathbf{k} = \mathbf{p} + \mathbf{q}$ and of the fact that the integrand is even in ϕ ,

$$\sum_{\mathbf{pq}} (\dots) = 2 \frac{V}{(2\pi)^3} \int_{-\infty}^{+\infty} dq_{\parallel} \int_0^{\infty} dq_{\perp} q_{\perp} \int_0^{\pi} d\phi (\dots), \quad (\text{A } 16)$$

where $V = L_{\perp}^2 L_{\parallel}$ is the volume of the box. The angle integral can be recast as an integral with respect to p_{\perp} :

$$p_{\perp}^2 = k_{\perp}^2 + q_{\perp}^2 - 2k_{\perp} q_{\perp} \cos \phi \Rightarrow \int_0^{\pi} d\phi \sin \phi (\dots) = \int_{|k_{\perp} - q_{\perp}|}^{k_{\perp} + q_{\perp}} \frac{dp_{\perp} p_{\perp}}{k_{\perp} q_{\perp}} (\dots). \quad (\text{A } 17)$$

Finally, defining the 2D spectra $E_{2D}^{\pm}(k_{\perp}, k_{\parallel}) = k_{\perp} N_{\mathbf{k}}^{\pm} V / (2\pi)^2$, we get

$$\begin{aligned} \partial_t E_{2D}^{\pm}(k_{\perp}, k_{\parallel}) &= \frac{1}{v_A} \int_0^{\infty} dq_{\perp} \int_{|k_{\perp} - q_{\perp}|}^{k_{\perp} + q_{\perp}} dp_{\perp} \frac{k_{\perp}^2 q_{\perp}^2}{p_{\perp}} \sin \phi \cos^2 \phi \\ &\times \frac{E_{2D}^{\mp}(p_{\perp}, 0)}{p_{\perp}} \left[\frac{E_{2D}^{\pm}(q_{\perp}, k_{\parallel})}{q_{\perp}} - \frac{E_{2D}^{\pm}(k_{\perp}, k_{\parallel})}{k_{\perp}} \right], \end{aligned} \quad (\text{A } 18)$$

where $\cos \phi = (k_{\perp}^2 + q_{\perp}^2 - p_{\perp}^2) / 2k_{\perp} q_{\perp}$ and $\sin \phi = (1 - \cos^2 \phi)^{1/2}$.

Let us now, as anticipated in (4.9), assume

$$E_{2D}^{\pm}(k_{\perp}, k_{\parallel}) = f^{\pm}(k_{\parallel}) k_{\perp}^{\mu^{\pm}}, \quad E_{2D}^{\mp}(k_{\perp}, 0) = f^{\mp}(0) k_{\perp}^{\mu_0^{\mp}}, \quad (\text{A } 19)$$

substitute these into the right-hand side of (A 18) and non-dimensionalise the integral by changing the integration variables to $x = q_\perp/k_\perp$ and $y = p_\perp/k_\perp$:

$$\partial_t E^\pm(k_\perp, k_\parallel) = \frac{f^\mp(0)f^\pm(k_\parallel)}{v_A} I(\mu^\pm, \mu_0^\mp) k_\perp^{\mu^\pm + \mu_0^\mp + 3} \equiv -\frac{\partial \Pi^\pm(k_\perp, k_\parallel)}{\partial k_\perp}, \quad (\text{A 20})$$

$$I(\mu, \mu_0) = \int_0^\infty dx \int_{|1-x|}^{1+x} dy y^{-2+\mu_0} x^2 (x^{\mu-1} - 1) \sin \phi \cos^2 \phi, \quad (\text{A 21})$$

where $\cos \phi = (1 + x^2 - y^2)/2x$. The energy flux formally introduced in (A 20) is

$$\Pi^\pm(k_\perp, k_\parallel) = -\frac{f^\mp(0)f^\pm(k_\parallel)}{v_A} \frac{I(\mu^\pm, \mu_0^\mp)}{\mu^\pm + \mu_0^\mp + 4} k_\perp^{\mu^\pm + \mu_0^\mp + 4}. \quad (\text{A 22})$$

It is assumed here that the flux in (k_\perp, k_\parallel) space is in the k_\perp direction only (no parallel cascade in WT). In order for (A 22) to be independent of k_\perp , it must be the case that⁹⁴

$$\mu^\pm + \mu_0^\mp = -4, \quad (\text{A 23})$$

but then, in order for the expression in (A 22) to have a finite value, it must also be the case that $I(\mu, \mu_0) \rightarrow 0$ when $\mu + \mu_0 + 4 \rightarrow 0$. That this is indeed the case is shown by changing the integration variables to $\xi = 1/x$, $\eta = y/x$, a change that leaves the domain of integration in (A 21) the same (a *Zakharov transformation*; see [Zakharov et al. 1992](#)). In these new variables,

$$I(\mu, \mu_0) = -\int_0^\infty d\xi \int_{|1-\xi|}^{1+\xi} d\eta \eta^{-2+\mu_0} \xi^{-\mu-\mu_0-2} (\xi^{\mu-1} - 1) \sin \phi \cos^2 \phi, \quad (\text{A 24})$$

where $\cos \phi = (1 + \xi^2 - \eta^2)/2\xi$. When $\mu + \mu_0 = -4$, this is exactly the same integral as (A 21), except with a minus sign, so $I = -I = 0$, q.e.d.

The problem with this otherwise respectable-looking calculation is that $E_{2D}^\mp(p_\perp, 0)$, which plays a key role in (A 18), is the spectrum of zero-frequency, $p_\parallel = 0$ modes, for which the WT approximation cannot be used, so μ_0^\mp is certainly not determinable within WT, the random-phase approximation should not have been used for these modes (and has been explicitly shown not to hold for them by [Meyrand et al. 2015](#)), and so it is at the very least doubtful that (A 18) can be used for the determination of μ^\pm , the scaling exponents for the waves, either. For the moment, let me put aside the latter doubt and act on the assumption that if I can figure out μ_0^\mp in some way, μ^\pm will follow by (A 23).

A.4. Case of Broad-Band Forcing: Spectral Continuity

The argument that is about to be presented here is heuristic and routed in the ideas about the treatment of strong turbulence described in §§ 2.3 and 5—it turns out that, to understand weak turbulence, one must understand strong turbulence first. I will, therefore, not attempt to deal with imbalanced WT—because, even though I did, in § 9.6, attempt to construct a coherent picture of strong imbalanced turbulence, it is too tentative and too fiddly to be inserted into what follows, which will be tentative and fiddly in its own right. Thus, the “±” tags are now dropped everywhere.

In reality, the delta function $\delta(p_\parallel)$ in (A 8) has a width equal to the characteristic broadening of the frequency resonance due to nonlinear interactions, $\Delta k_\parallel \sim \tau_{nl}^{-1}/v_A$,

⁹⁴Or $\mu^\pm = 1$, in which case $I = 0$, so $\Pi^\pm = 0$. This is a (UV-divergent) thermal equilibrium spectrum, which irrelevant for a forced problem below the forcing scale, but will, in a certain sense, be resurrected in appendix C.3, at large scales.

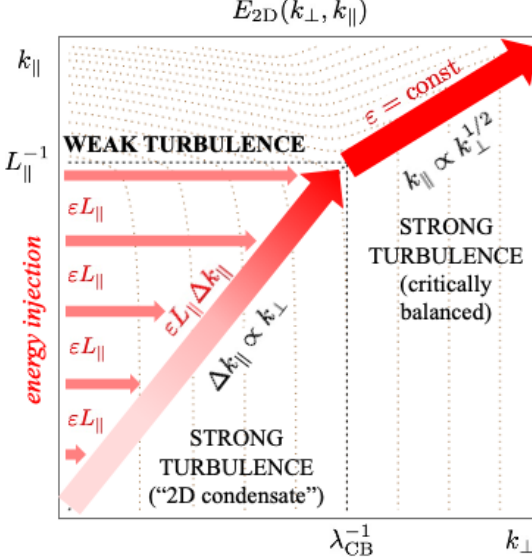


FIGURE 36. Cartoon of the 2D spectrum of broad-band-forced weak turbulence. Schematic contour lines of $E_{2D}(k_\perp, k_\parallel)$ are the brown dotted lines. Red arrows are energy fluxes: $\Pi(k_\perp, k_\parallel) \sim \varepsilon L_\parallel$ arriving from the forcing wavenumbers to the “2D condensate” at each k_\parallel , $\varepsilon L_\parallel \Delta k_\parallel$ flowing through the condensate [see (A 26)], and $\varepsilon = \text{const}$ after the transition to critically balanced cascade (cf. figure 40a).

to wit,

$$\delta(p_\parallel) = \frac{\Delta k_\parallel}{\pi} \frac{1}{p_\parallel^2 + \Delta k_\parallel^2} \quad (\text{A } 25)$$

(in the WT approximation, $\Delta k_\parallel \rightarrow 0$). At $p_\parallel \lesssim \Delta k_\parallel$, the “ $p_\parallel = 0$ ” condensate resides, whose turbulence is strong (figure 36). Let us work out the structure of this turbulence.

Let us assume that our WT is forced in a broad band of parallel wavenumbers $k_\parallel \in (0, 2\pi/L_\parallel)$ (obviously, the parallel size of “the box” must be $\gg L_\parallel$). This can happen, e.g., if the forcing is completely random with parallel coherence length L_\parallel , in which case its k_\parallel spectrum at $k_\parallel < 2\pi/L_\parallel$ is flat (a white noise). Thus, the same amount of energy is injected into each k_\parallel , this energy is cascaded weakly in k_\perp (by the still-to-be-worked-out condensate) without change in k_\parallel until it arrives at the CB scale associated with this k_\parallel , i.e., at the k_\perp for which $\Delta k_\parallel(k_\perp) \sim k_\parallel$ (equivalently, $\tau_{\text{nl}}^{-1} \sim k_\parallel v_A$), where it joins the condensate. Therefore, the flux of energy into, and via, the condensate is not scale-independent: at any given k_\perp , it is

$$\int_0^{\Delta k_\parallel(k_\perp)} dk_\parallel \Pi(k_\perp, k_\parallel) \sim \varepsilon L_\parallel \Delta k_\parallel(k_\perp), \quad \Delta k_\parallel(k_\perp) \sim \frac{\tau_{\text{nl}}^{-1}}{v_A}, \quad (\text{A } 26)$$

where I have assumed that $\Pi(k_\perp, k_\parallel) \sim \varepsilon L_\parallel$ is a constant in both of its arguments (constant in k_\perp because the WT cascade is a constant-flux one and constant in k_\parallel because the amount of energy injection is the same at every k_\parallel). Then, for the condensate at scale

$$\lambda \sim k_{\perp}^{-1},$$

$$\frac{\delta Z_{\lambda}^2}{\tau_{\text{nl}}} \sim \varepsilon L_{\parallel} \Delta k_{\parallel}(k_{\perp}) \sim \frac{\varepsilon L_{\parallel}}{\tau_{\text{nl}} v_{\text{A}}} \quad \Rightarrow \quad \delta Z_{\lambda} \sim \left(\frac{\varepsilon L_{\parallel}}{v_{\text{A}}} \right)^{1/2} \quad \Rightarrow \quad E_0(k_{\perp}) \sim \frac{\varepsilon L_{\parallel}}{v_{\text{A}}} k_{\perp}^{-1}, \quad (\text{A 27})$$

where $E_0(k_{\perp})$ is the condensate's 1D spectrum.

This 1D spectrum is the 2D spectrum $E_0(k_{\perp}, k_{\parallel})$ integrated over all parallel wavenumbers belonging to the condensate, viz.,

$$E_0(k_{\perp}) \sim \int_0^{\Delta k_{\parallel}(k_{\perp})} dk_{\parallel} E_0(k_{\perp}, k_{\parallel}) \sim E_0(k_{\perp}, k_{\parallel}) \Delta k_{\parallel}(k_{\perp}). \quad (\text{A 28})$$

The last step is valid on the assumption that $E_0(k_{\perp}, k_{\parallel})$ is, in fact, independent of k_{\parallel} , because by the usual CB assumption, there cannot be any correlations at parallel scales $k_{\parallel}^{-1} > v_{\text{A}} \tau_{\text{nl}} \sim \Delta k_{\parallel}^{-1}(k_{\perp})$ and so the corresponding k_{\parallel} spectrum is that of a white noise (cf. appendix C.1).

The cascade time for the condensate (which advects itself) is

$$\tau_{\text{nl}}^{-1} \sim \frac{\delta Z_{\lambda}}{\lambda} \sim \left(\frac{\varepsilon L_{\parallel}}{v_{\text{A}}} \right)^{1/2} \lambda^{-1} \quad \Rightarrow \quad \Delta k_{\parallel}(k_{\perp}) \sim \frac{(\varepsilon L_{\parallel})^{1/2}}{v_{\text{A}}^{3/2}} k_{\perp}. \quad (\text{A 29})$$

I am assuming that there is no dynamic alignment (§ 6) for the condensate because the condensate is effectively forced at every scale by the WT cascade—this is not a proof, but a conjecture, adopted for its simplicity and plausibility. Finally, (A 29), via (A 28) and (A 27), leads to

$$E_{0,2\text{D}}(k_{\perp}, k_{\parallel}) \sim (\varepsilon L_{\parallel} v_{\text{A}})^{1/2} k_{\perp}^{-2}, \quad k_{\parallel} \lesssim \Delta k_{\parallel}(k_{\perp}). \quad (\text{A 30})$$

Thus, $\mu_0 = -2$ for reasons that have little to do with weak interactions, and, therefore, by (A 23), $\mu = -2$ as well (in appendix C.5, the same results are rederived in a slightly different way, which may or may not shed more light).

Thus, there is, in fact, no difference between the WT spectrum at $k_{\parallel} > \Delta k_{\parallel}(k_{\perp})$ and the condensate's spectrum at $k_{\parallel} < \Delta k_{\parallel}(k_{\perp})$, even though the nature of turbulence in these two regions is quite different. The above construction can thus be viewed as a physical argument in support of spectral continuity. It does not make the derivation of the WT equation in appendix A.2 *formally* correct but it does perhaps lend it some credibility.

A.5. Residual Energy in WT

If one takes this appearance of WT credibility seriously, there is another result that can be “derived” within it. The random-phase approximation for Alfvén waves implied the absence of correlations between the counterpropagating Elsasser fields, (A 10). What if we relax this assumption—and *only* this assumption!—while still splitting fourth-order correlators into second-order ones? Namely, let us set

$$k_{\perp}^2 \langle \zeta_{\mathbf{k}}^{\pm} \zeta_{\mathbf{k}'}^{\mp} \rangle = R_{\mathbf{k}}^{\pm} \delta_{\mathbf{k}, -\mathbf{k}'}, \quad (\text{A 31})$$

where $R_{\mathbf{k}}^{-*} = R_{\mathbf{k}}^+ \equiv R_{\mathbf{k}}$, and work out the WT evolution equation for $R_{\mathbf{k}}$. This is interesting, *inter alia*, because $\text{Re}R_{\mathbf{k}}$ is the 3D residual-energy spectrum and so the derivation I am about to present (which is a version of what Wang *et al.* 2011 did) has a claim to providing theoretical backing to the presence of negative residual energy both in observed and in numerically simulated MHD turbulence (see § 10).

From the field equation (A 4), straightforwardly,

$$\partial_t R_{\mathbf{k}} - 2ik_{\parallel}v_A R_{\mathbf{k}} = k_{\perp}^2 \sum_{\mathbf{pq}} M_{\mathbf{k}\mathbf{pq}} \delta_{\mathbf{k},\mathbf{p}+\mathbf{q}} (\langle \zeta_{\mathbf{p}}^- \zeta_{\mathbf{q}}^+ \zeta_{\mathbf{k}}^{-*} \rangle + \langle \zeta_{\mathbf{p}}^{+*} \zeta_{\mathbf{q}}^{-*} \zeta_{\mathbf{k}}^+ \rangle). \quad (\text{A 32})$$

Following the same protocol as in appendix A.2, let us write the evolution equation for the third-order correlators in (A 32) in terms of fourth-order correlators and then split the latter into second-order ones, but now allowing non-zero correlations between different Elsasser fields according to (A 31):

$$\begin{aligned} \partial_t \langle \zeta_{\mathbf{p}}^{\mp} \zeta_{\mathbf{q}}^{\pm} \zeta_{\mathbf{k}}^{\mp*} \rangle \mp i2q_{\parallel}v_A \langle \zeta_{\mathbf{p}}^{\mp} \zeta_{\mathbf{q}}^{\pm} \zeta_{\mathbf{k}}^{\mp*} \rangle &= \delta_{\mathbf{k},\mathbf{p}+\mathbf{q}} \frac{\hat{\mathbf{z}} \cdot (\mathbf{k}_{\perp} \times \mathbf{q}_{\perp})}{k_{\perp}^2 p_{\perp}^2 q_{\perp}^2} [\mathbf{k}_{\perp} \cdot \mathbf{p}_{\perp} N_{\mathbf{q}}^{\pm} (N_{\mathbf{k}}^{\mp} - N_{\mathbf{p}}^{\mp}) \\ &\quad + \mathbf{k}_{\perp} \cdot \mathbf{q}_{\perp} (R_{\mathbf{p}}^{\mp} R_{\mathbf{q}}^{\pm} - R_{\mathbf{k}}^{\pm} N_{\mathbf{p}}^{\mp}) + \mathbf{p}_{\perp} \cdot \mathbf{q}_{\perp} (R_{\mathbf{k}}^{\pm} R_{\mathbf{q}}^{\pm} - R_{\mathbf{p}}^{\mp} N_{\mathbf{k}}^{\mp})]. \end{aligned} \quad (\text{A 33})$$

The presence of the first term is proof that $R_{\mathbf{k}} = 0$ is, generally speaking, not a sustainable solution. However, since growth of correlations between counterpropagating Elsasser fields contradicts the random-phase approximation and thus undermines WT, perhaps we could hope (falsely, as I will show shortly) that $R_{\mathbf{k}}$ might be small and so the terms containing $R_{\mathbf{k}}$ in (A 33) could be neglected for the time being. Then the solution of (A 33) is

$$\langle \zeta_{\mathbf{p}}^{\mp} \zeta_{\mathbf{q}}^{\pm} \zeta_{\mathbf{k}}^{\mp*} \rangle = \frac{1 - e^{\pm i2q_{\parallel}v_A t}}{\mp i2q_{\parallel}v_A} \delta_{\mathbf{k},\mathbf{p}+\mathbf{q}} \frac{\hat{\mathbf{z}} \cdot (\mathbf{k}_{\perp} \times \mathbf{q}_{\perp}) \mathbf{k}_{\perp} \cdot \mathbf{p}_{\perp}}{k_{\perp}^2 p_{\perp}^2 q_{\perp}^2} N_{\mathbf{q}}^{\pm} (N_{\mathbf{k}}^{\mp} - N_{\mathbf{p}}^{\mp}). \quad (\text{A 34})$$

Substituting this into (A 32), solving that in turn, and denoting

$$B_{\mathbf{k}\mathbf{pq}} = \frac{|\mathbf{k}_{\perp} \times \mathbf{q}_{\perp}|^2 \mathbf{k}_{\perp} \cdot \mathbf{p}_{\perp}}{k_{\perp}^2 p_{\perp}^2 q_{\perp}^2} [N_{\mathbf{q}}^+ (N_{\mathbf{k}}^- - N_{\mathbf{p}}^-) + N_{\mathbf{q}}^- (N_{\mathbf{k}}^+ - N_{\mathbf{p}}^+)], \quad (\text{A 35})$$

we find

$$\begin{aligned} \text{Re}R_{\mathbf{k}} &= \text{Re} \sum_{\mathbf{pq}} \delta_{\mathbf{k},\mathbf{p}+\mathbf{q}} \frac{1}{i2q_{\parallel}v_A} \left(\frac{1 - e^{i2k_{\parallel}v_A t}}{i2k_{\parallel}v_A} - e^{i2q_{\parallel}v_A t} \frac{1 - e^{i2p_{\parallel}v_A t}}{i2p_{\parallel}v_A} \right) B_{\mathbf{k}\mathbf{pq}}, \\ &\rightarrow \frac{\pi^2}{4v_A^2} \sum_{\mathbf{pq}} \delta_{\mathbf{k},\mathbf{p}+\mathbf{q}} \delta(p_{\parallel}) \delta(q_{\parallel}) B_{\mathbf{k}\mathbf{pq}} \quad \text{as } t \rightarrow \infty. \end{aligned} \quad (\text{A 36})$$

The 2D spectrum of residual energy is, therefore,

$$\begin{aligned} E_{\text{res},2D}(k_{\perp}, k_{\parallel}) &= \frac{V k_{\perp} \text{Re}R_{\mathbf{k}}}{(2\pi)^2} = -\frac{\pi \delta(k_{\parallel})}{4v_A^2} \int_0^{\infty} dq_{\perp} \int_{|k_{\perp}-q_{\perp}|}^{k_{\perp}+q_{\perp}} dp_{\perp} \frac{k_{\perp}^2 q_{\perp}^2}{p_{\perp}} \sin \phi \cos^2 \phi \\ &\times \left\{ \frac{E^+(q_{\perp}, 0)}{q_{\perp}} \left[\frac{E^-(k_{\perp}, 0)}{k_{\perp}} - \frac{E^-(p_{\perp}, 0)}{p_{\perp}} \right] + \frac{E^-(q_{\perp}, 0)}{q_{\perp}} \left[\frac{E^+(k_{\perp}, 0)}{k_{\perp}} - \frac{E^+(p_{\perp}, 0)}{p_{\perp}} \right] \right\}, \end{aligned} \quad (\text{A 37})$$

where the wavenumber integrals have been manipulated in exactly the same way as they were in appendix A.2, in the lead-up to (A 18). Again assuming the power-law solutions (A 19), we get

$$E_{\text{res},2D}(k_{\perp}, k_{\parallel}) = -\text{const} \frac{f^+(0)f^-(0)}{v_A^2} k_{\perp}^{\mu_0^+ + \mu_0^- + 3} \delta(k_{\parallel}). \quad (\text{A 38})$$

One establishes that the prefactor is negative (i.e., $\text{const} > 0$) by computing the wavenumber integral directly (Wang *et al.* 2011).

What does this result tell us? Primarily, it tells us that the WT calculation that has

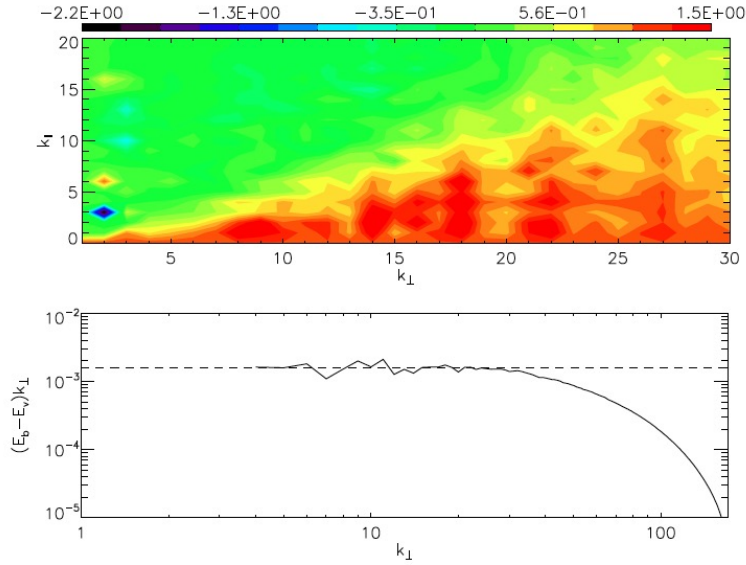


FIGURE 37. The 2D spectrum, $E_{\text{res},2\text{D}}(k_{\perp}, k_{\parallel})/E_{\text{res},2\text{D}}(k_{\perp}, 0)$ (upper panel) and the 1D, k_{\perp}^{-1} -compensated spectrum (lower panel) of residual energy from WT simulations by Wang *et al.* (2011) (512^3 , broad-band forced at $k_{\parallel} = 1, \dots, 16$ and $k_{\perp} = 1, 2$; ©AAS, reproduced with permission).

led to it is formally invalid and can, at best, be interpreted as a qualitative indication of what is going on. All the action has turned out to be concentrated in the $k_{\parallel} = 0$ condensate, while for Alfvén waves with $k_{\parallel} \neq 0$, there is no residual energy. That we were going to end up with $\delta(k_{\parallel})$ was, in fact, already obvious from the presence of the oscillatory term in (A 32). Nevertheless, without a claim to mathematical rigour, one can, as I did in appendix A.4, interpret the delta function in (A 38) as having a width $\Delta k_{\parallel} \sim \tau_{\text{nl}}^{-1}/v_A$, where $\tau_{\text{nl}} \propto k_{\perp}^{-1}$ is the cascade time for the condensate, worked out in (A 29). Taking $\mu_0^+ + \mu_0^- = -4$ and $\delta(k_{\parallel}) \sim \Delta k_{\parallel}^{-1} \propto k_{\perp}^{-1}$ in (A 38) gets us

$$E_{\text{res},2\text{D}}(k_{\perp}, k_{\parallel}) \propto -k_{\perp}^{-2}, \quad (\text{A } 39)$$

whereas the 1D spectrum can be calculated either by integrating out the delta function in (A 38) or by integrating its broadened version in (A 39) over its width $\Delta k_{\parallel} \propto k_{\perp}$:

$$E_{\text{res}}(k_{\perp}) = \int dk_{\parallel} E_{\text{res},2\text{D}}(k_{\perp}, k_{\parallel}) = -\text{const} \frac{f^+(0)f^-(0)}{v_A^2} k_{\perp}^{-1}. \quad (\text{A } 40)$$

This is the result of Wang *et al.* (2011), who, however, go to slightly greater lengths in setting up a quasi-quantitative calculation in which they introduce by hand a nonlinear relaxation rate $\tau_{\text{nl}}^{-1} \propto k_{\perp}$ into (A 32) and thus get their $\delta(k_{\parallel})$ to acquire the Lorentzian shape (A 25). They attribute this relaxation to the R_k -dependent terms in (A 33), which is qualitatively correct, but quantitatively just as invalid as is generally the application of the WT approximation (i.e., correlator splitting) to the strongly turbulent condensate.

Note that (A 40) is, in fact, the same result as (A 27)—by comparing (A 19) with (A 30), or just by dimensional analysis, it is easy to confirm that $f^{\pm}(0) \sim (\varepsilon L_{\parallel} v_A)^{1/2}$, so the dimensional prefactors match. Thus, all we have learned from the above calculation is that the condensate has residual energy and that the amount of the latter is comparable, at every scale, to the amount of energy in the condensate. One might argue that the added

value of the WT calculation was in confirming that this residual energy was negative—although the negativity of the prefactor in (A 38) is a quantitative result, not a qualitative one (one just has to calculate the appropriate integral and discover it to be negative, as Wang *et al.* 2011 did), and so, in principle, cannot be guaranteed to hold for the true, strongly turbulent condensate. I find the qualitative argument for the development of negative vorticity correlation $\langle \omega^+ \omega^- \rangle < 0$ explained in § 10.4 more compelling. The WT calculation above basically just confirms that growth of residual energy is a strong-turbulence effect.

The qualitative considerations presented above are given some credence by the numerical simulations of WT reported by Wang *et al.* (2011): their residual energy does indeed have a k_\perp^{-1} spectrum and concentrates in a wedge of wavenumber space $k_\parallel \lesssim \Delta k_\parallel \propto k_\perp$, quite convincingly (figure 37).

A.6. Imbalanced WT

As I acknowledged in § 4.3, I do not know how to construct a good theory of imbalanced WT. If imbalanced WT, like the balanced one, spawns a 2D condensate that is predominantly magnetic, that may be a helpful insight, as the presence of significant residual energy would impose geometric constraints (appendix B.1) on the “+” and “−” components of the condensate. Boldyrev & Perez (2009) do find a magnetic condensate in an imbalanced simulation, but they only have results for order-unity imbalance. They also point out that if the cross-correlations (A 31) are retained in the derivation of the WT equation (A 15) for N_k , this makes the evolution equation (A 18) for $E_{2D}^\pm(k_\perp, 0)$ acquire terms under the integral containing $E_{2D}^\pm(k_\perp, 0)E_{\text{res},2D}(p_\perp, 0) + E_{2D}^\pm(p_\perp, 0)E_{\text{res},2D}(k_\perp, 0)$. Steady-state solutions then turn out to be possible only if

$$E_{\text{res},2D}(k_\perp, 0) \propto k_\perp^{-2}, \quad E_{2D}^\pm(k_\perp, 0) \propto k_\perp^{-2}, \quad (\text{A } 41)$$

i.e., the degeneracy of the $\mu_0^+ + \mu_0^- = -4$ solution is lifted and all scalings are fixed. Perhaps this points us in the right direction, despite the fact that the WT equation for $E_{2D}^\pm(k_\perp, 0)$, whose derivation requires correlator splitting etc., is not, in fact, quantitatively valid for the condensate.

In their mildly imbalanced WT simulation, Boldyrev & Perez (2009) find that $E^+(k_\perp)$ and $E^-(k_\perp)$ have, respectively, a steeper and a shallower slope than k_\perp^{-2} , but the spectra appear to be pinned (equal) at the dissipation scale and thus get closer to each other with increased resolution. Thus, if one wants a theory that describes finite-resolution simulations, some scheme like the one I proposed in § 9.6 would need to be invented for the WT regime, generalising appendix A.4 to the imbalanced case.

Appendix B. Alignment, Imbalance, and Reduction of Nonlinearity

These topics have cropped up repeatedly (e.g., in §§ 6.1 and 9.1). This appendix is an attempt to treat them carefully.

B.1. Geometry and Types of Alignment

Let us consider the formal relationship between imbalance, residual energy, and (the two kinds of) alignment. The first salient fact is purely geometric (figure 38): the two alignment angles (defined for a particular pair of field increments)

$$\sin \theta = \frac{|\delta Z_\lambda^+ \times \delta Z_\lambda^-|}{|\delta Z_\lambda^+||\delta Z_\lambda^-|}, \quad \sin \theta^{ub} = \frac{|\delta u_\lambda \times \delta b_\lambda|}{|\delta u_\lambda||\delta b_\lambda|}, \quad (\text{B } 1)$$

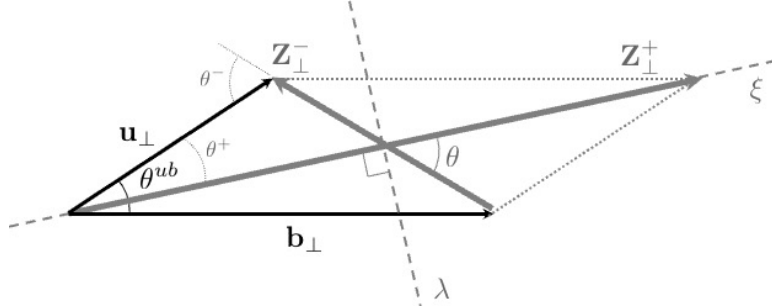


FIGURE 38. Geometry of velocity, magnetic and Elsasser fields (\mathbf{B}_0 is perpendicular to the page). All four fields are aligned: the angles θ , θ^{ub} , θ^\pm are all small (although they do not have to be). Also shown are the axes along which the λ and ξ scales in (6.4) are meant to be calculated (along and across Z_\perp^+ , respectively). The angle between these axes is $\phi = \pi/2 - \theta$ and so $\cos \phi = \sin \theta$.

and the Elsasser and Alfvén ratios

$$R_E = \frac{|\delta Z_\lambda^+|^2}{|\delta Z_\lambda^-|^2}, \quad R_A = \frac{|\delta u_\lambda|^2}{|\delta b_\lambda|^2} \quad (\text{B } 2)$$

are related by the following equations

$$\sin^2 \theta = \frac{\sin^2 \theta^{ub}}{\sin^2 \theta^{ub} + (1 - R_A)^2 / 4R_A}, \quad \sin^2 \theta^{ub} = \frac{\sin^2 \theta}{\sin^2 \theta + (1 - R_E)^2 / 4R_E}, \quad (\text{B } 3)$$

so only two of these four quantities are independent. Equivalently, in terms of the normalised local cross-helicity and residual energy, defined by

$$\sigma_c = \frac{|\delta Z_\lambda^+|^2 - |\delta Z_\lambda^-|^2}{|\delta Z_\lambda^+|^2 + |\delta Z_\lambda^-|^2} = \frac{R_E - 1}{R_E + 1} \quad \text{and} \quad \sigma_r = \frac{|\delta u_\lambda|^2 - |\delta b_\lambda|^2}{|\delta u_\lambda|^2 + |\delta b_\lambda|^2} = \frac{R_A - 1}{R_A + 1}, \quad (\text{B } 4)$$

respectively, the alignment angles are (Wicks *et al.* 2013a)⁹⁵

$$\cos \theta = \frac{\sigma_r}{\sqrt{1 - \sigma_c^2}}, \quad \cos \theta^{ub} = \frac{\sigma_c}{\sqrt{1 - \sigma_r^2}}. \quad (\text{B } 5)$$

This means that alignment between the velocity and magnetic field is not formally the same thing as alignment between the Elsasser fields, and it is a nontrivial decision which of these one believes to matter for the determination of τ_{nl}^\pm .

Before taking a side on this question in appendix B.2, let me consider a strongly imbalanced situation, where $R_E \gg 1$, i.e., the cross-helicity is large ($\sigma_c \approx 1$)—in view of the discussion in § 9.1, this is probably an asymptotic case best related to the generic situation, at least locally. In this limit, (B 3) gives us

$$\sin^2 \theta^{ub} \approx \frac{4 \sin^2 \theta}{R_E} \ll 1, \quad (1 - R_A)^2 \approx \frac{16 \cos^2 \theta}{R_E} \ll 1. \quad (\text{B } 6)$$

Mallet & Schekochihin (2011) found, unsurprisingly, that these relations were extremely well satisfied in their RMHD simulations (the first relation even in balanced ones—see figure 39). Thus, (local) imbalance implies that u_\perp and b_\perp are both closely aligned and have nearly the same amplitude (this is geometrically obvious from figure 38), but whether or not the Elsasser fields are aligned is up to the turbulence to decide. It does

⁹⁵Note the connection implied by the first of these formulae between non-zero residual energy and Elsasser alignment (cf. § 10.4).

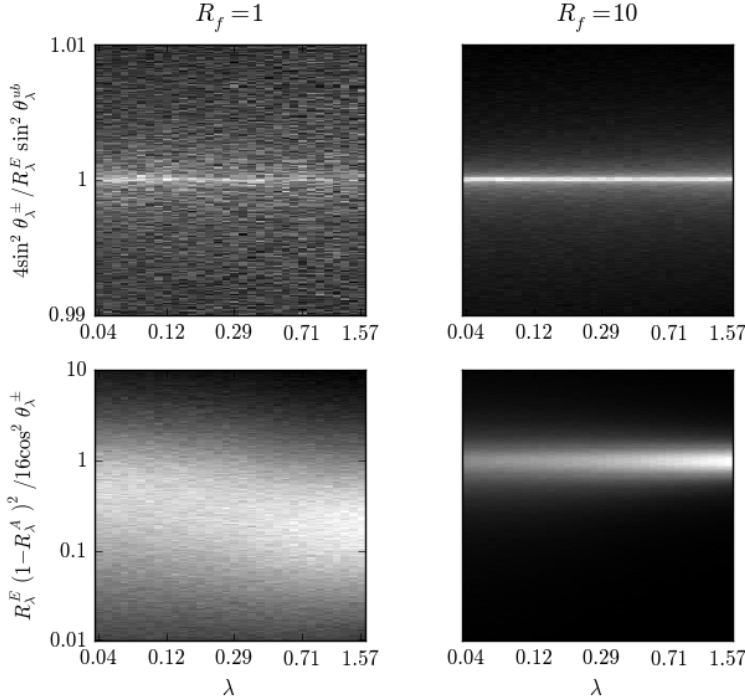


FIGURE 39. A direct test of the relations (B6) in globally balanced ($\varepsilon^+/\varepsilon^- = 1$, left column) and imbalanced ($\varepsilon^+/\varepsilon^- = 10$, right column) RMHD simulations by Mallet & Schekochihin (2011) (these are the same unpublished simulations as tabulated in figure 19). The plots show histograms of $4\sin^2 \theta / R_E \sin^2 \theta_{\lambda}^{ub}$ (upper row) and $(1 - R_A)^2 R_E / 16 \cos^2 \theta$ (lower row) vs. perpendicular point separation λ . Note that the first relation in (B6) is reasonably well satisfied even in the globally balanced simulation.

seem to decide to align them [see § 9.2, item (v)], hence the way in which I drew the field increments in figure 38.

If R_E (equivalently, σ_c) is independent of scale in the inertial range, as reported for the solar wind by Podesta & Borovsky (2010) and Chen *et al.* (2020), then the first relation in (B6) implies that θ^{ub} and θ should have the same scaling. In numerical simulations, they appear to do so, approximately, in balanced turbulence (Mallet *et al.* 2016), which, of course, is patch-wise imbalanced (§ 9.1), but not in the strongly imbalanced cases studied by Beresnyak & Lazarian (2009b) and Mallet & Schekochihin (2011) (see § 9.2). Accordingly, Mallet & Schekochihin (2011) found the dependence of θ^{ub} on λ getting shallower with increased imbalance, as R_E vs. λ got steeper (see figure 19) and θ stayed approximately the same. Alas, those simulations are in all probability not in the asymptotic regime, so a follow-up study at higher resolutions would be very welcome.

B.2. Alignment and Reduction of Nonlinearity

The nonlinear term in RMHD (3.1) can be expressed so:

$$\begin{aligned} \mathbf{Z}_\perp^+ \cdot \nabla_\perp \mathbf{Z}_\perp^- &= \mathbf{Z}_\perp^- \cdot \nabla_\perp \mathbf{Z}_\perp^+ + \nabla_\perp \times (\mathbf{Z}_\perp^- \times \mathbf{Z}_\perp^+) \\ &= \nabla_\perp \cdot (\mathbf{u}_\perp \mathbf{u}_\perp - \mathbf{b}_\perp \mathbf{b}_\perp) + \nabla_\perp \times (\mathbf{u}_\perp \times \mathbf{b}_\perp). \end{aligned} \quad (\text{B7})$$

The first of these identities already appeared as (6.2). As I already explained in § 6.1, it says, schematically,

$$\frac{1}{\xi^-} \sim \frac{1}{\xi^+} + \frac{\sin \theta}{\lambda}, \quad (\text{B } 8)$$

which makes the connection between Elsasser-field alignment ($\sin \theta \ll 1$) and reduction of nonlinearity ($\xi^\pm \gg \lambda$) a consistent choice (although not a mathematically inevitable one). This conclusion is valid regardless of the degree of imbalance.

Consider now the second identity in (B 7). Without imbalance, i.e., if $\delta Z_\lambda^+ \sim \delta Z_\lambda^- \sim \delta u_\lambda \sim \delta b_\lambda$, it implies, analogously to (B 8),

$$\frac{1}{\xi^-} \sim \frac{1}{\xi^u} + \frac{1}{\xi^b} + \frac{\sin \theta^{ub}}{\lambda}, \quad (\text{B } 9)$$

where ξ^u and ξ^b are the characteristic scales of variation of \mathbf{u}_\perp and \mathbf{b}_\perp , respectively, along themselves. Again it is a consistent choice to posit that $\xi^u \sim \xi^b \sim \xi^\pm$ and $\lambda/\xi \sim \sin \theta^{ub} \ll 1$. In contrast, if (locally or globally) $\sqrt{R_E} = \delta Z_\lambda^+ / \delta Z_\lambda^- \gg 1$, we have

$$\frac{(\delta Z_\lambda^+)^2}{\xi^- \sqrt{R_E}} \sim \frac{\delta u_\lambda^2 (1 - R_A)}{\xi^{u,b}} + \frac{\delta u_\lambda \delta b_\lambda \sin \theta^{ub}}{\lambda} \sim \left(\frac{\cos \theta}{\xi^{u,b}} + \frac{\sin \theta}{\lambda} \right) \frac{(\delta Z_\lambda^+)^2}{\sqrt{R_E}}, \quad (\text{B } 10)$$

where at the last step, I used both of the geometric relations (B 6) and $\delta u_\lambda \sim \delta b_\lambda \sim \delta Z_\lambda^+$. Again, the connection between reduced nonlinearity and alignment is consistent, but it is the alignment of Elsasser fields that matters (if $\sin \theta \sim 1$, $\xi^- \sim \lambda$, so no reduction). The alignment between \mathbf{u}_\perp and \mathbf{b}_\perp is geometrically inevitable, but does not by itself imply anything about a reduction of nonlinearity.

This is all perhaps too obvious to have needed spelling out. To summarise, in balanced turbulence (or rather in balanced regions within turbulence), which type of alignment one prefers to think about, or measure, does not appear to make a qualitative difference, whereas in the presence of imbalance, Elsasser alignment is a natural choice. Since both globally balanced and imbalanced turbulence is likely to be imbalanced locally (see § 9.1), and indeed since it is in locally imbalanced patches that most of the “action” is likely to be, I have made Elsasser alignment synonymous with “alignment” everywhere in this review.

As I stated repeatedly in the main text, the supporting physical (dynamical) argument is to think of alignment as a result of mutual shearing of Elsasser fields, following Chandran *et al.* (2015). Such a shearing will lead to simultaneous reduction of λ/ξ and $\sin \theta$. This approach is circumstantially supported by the “refined critical balance” discovered by Mallet *et al.* (2015)—the remarkable self-similarity shown by the ratio τ_A/τ_{nl}^\pm , with τ_{nl}^\pm defined by (6.4), using the angle between the Elsasser fields (see figure 6). Arguably, this says that it is this τ_{nl}^\pm that τ_A (and, therefore, t_\parallel^\pm) “knows” about, so it is this τ_{nl}^\pm that should be viewed as the decorrelation (cascade) time of the turbulent structures. The same paper spotted a pronounced anticorrelation, at a given λ , between the Elsasser alignment angle θ and the magnitudes of the Elsasser-field increments—as noted in § 6.3, this is again consistent with the shearing origin of alignment.

Another useful way to look at the relationship between alignment and nonlinearity is afforded by casting RMHD in the form (A 2), in terms of Elsasser potentials and vorticities. Alignment between \mathbf{Z}_\perp^+ and \mathbf{Z}_\perp^- is equivalent to alignment between $\nabla_\perp \zeta^+$ and $\nabla_\perp \zeta^-$, so small $\sin \theta$ will imply smallness of the second term on the right-hand side of (A 2). The first term, $\{\zeta^\mp, \omega^\pm\}$, is small if $\nabla_\perp \zeta^\mp$ and $\nabla_\perp \omega^\pm$ are approximately aligned, i.e., if contours of constant ζ^\mp and ω^\pm approximately coincide. The latter condition is indeed satisfied for perturbations that resemble tubes or sheets—and thus

for perturbations that are likely to emerge from mutual shearing of Elsasser fields (this observation is due to [Bowen et al. 2021](#)).

Finally, let me reiterate that Elsasser alignment is not formally obliged to be co-located with locally imbalanced regions, even if observations by [Wicks et al. \(2013b\)](#) discussed in § 9.1 suggest that it might be, and even though the reduction of nonlinearity in the aligned MHD cascade has originally been argued to be connected to local enhancements of cross-helicity (see footnote 16 and references therein). In numerical simulations, it remains to be checked whether such an intrinsic connection does exist.

Appendix C. 2D Spectra of RMHD Turbulence

As we trade in k_\perp (or λ) and k_\parallel (or l_\parallel) scalings, it is only natural that we might wish to have 2D spectra of RMHD turbulence, $E_{2D}(k_\perp, k_\parallel)$. It is quite easy to work them out, given the information we already have about the λ and l_\parallel scalings of the Elsasser increments.

Since, as I explained in § 5.3, the physically meaningful parallel correlations are along the local mean field, we should think of our Elsasser fields \mathbf{Z}_\perp^\pm as being mapped on a grid of values of $(\mathbf{r}_\perp, r_\parallel)$, where r_\parallel is the distance measured along the exact field line (what matters here is not that the parallel distances are slightly longer than their projection on the z axis—the difference is small in the RMHD ordering—but that we probe correlations along the exact field line rather than slipping off it; see figure 8). The Fourier transform of $\mathbf{Z}_\perp^\pm(\mathbf{r}_\perp, r_\parallel)$ is a function of k_\perp and k_\parallel , $\mathbf{Z}_\perp^\pm(\mathbf{k}_\perp, k_\parallel)$, and the 2D spectrum is defined to be

$$E_{2D}(k_\perp, k_\parallel) = 2\pi k_\perp \langle |\mathbf{Z}_\perp^\pm(\mathbf{k}_\perp, k_\parallel)|^2 \rangle. \quad (\text{C1})$$

Let us start with the premise that $E_{2D}(k_\perp, k_\parallel)$ will be a product of power laws in both of its arguments and that the scaling exponents of these power laws will be different depending on where we are in the (k_\perp, k_\parallel) space vis-à-vis the line of critical balance, which is also a power-law relation, between k_\perp and k_\parallel :

$$\tau_{nl} \sim \tau_A \Leftrightarrow k_\parallel \sim k_\perp^\sigma. \quad (\text{C2})$$

We shall treat the wavenumbers as dimensionless, $k_\parallel L_\parallel \rightarrow k_\parallel$, $k_\perp \lambda_{CB} \rightarrow k_\perp$. According to (6.22),

$$\sigma = \frac{1}{2}. \quad (\text{C3})$$

Thus, we shall look for the 2D spectrum in the form

$$E_{2D}(k_\perp, k_\parallel) \sim \begin{cases} k_\parallel^{-\alpha} k_\perp^\beta, & k_\parallel \gtrsim k_\perp^\sigma, \\ k_\parallel^\delta k_\perp^{-\gamma}, & k_\parallel \lesssim k_\perp^\sigma. \end{cases} \quad (\text{C4})$$

The four exponents α , β , γ , and δ can be determined by the following arguments, broadly analogous to those proposed by [Schekochihin et al. \(2016\)](#) for drift-kinetic turbulence except for the calculation of β (and hence of α), which will be significantly modified here in light of some new theoretical developments (appendix C.3).

C.1. Determining δ : Long Parallel Wavelengths

At long parallel wavelengths, $k_\parallel \ll k_\perp^\sigma$, the k_\parallel spectrum measures correlation between points along the field line that are separated by longer distances than an Alfvén wave can travel in one nonlinear time ($\tau_A \gg \tau_{nl}$) and, consequently, are causally disconnected

(§ 5.1). Therefore, their parallel correlation function is that of a 1D white noise and the corresponding spectrum is flat:

$$\delta = 0. \quad (\text{C } 5)$$

It may be worth belabouring this point: the flat k_{\parallel} spectrum at $k_{\parallel} \lesssim k_{\perp}^{\sigma}$ (figure 40b) is the Fourier-space signature of CB turbulence, not an indication of the presence of quasi-2D motions or of failure of local-in-scale interactions (as, e.g., Meyrand *et al.* 2016 appear to imply). This highlights the fact that the wavenumbers where energy is present are not quite the same thing as the correlation scales of the turbulent field, and so one should not expect that CB requires a spectrum peaked at $k_{\parallel} \sim k_{\perp}^{\sigma}$ (a fallacy that has made it into a number of published texts, rigorous peer review notwithstanding). The same argument applies to frequency spectra, should one want to plot them: there must be a flat spectrum at $\omega \lesssim \tau_{\text{nl}}^{-1}$ because instances separated by times longer than τ_{nl} are uncorrelated and will, therefore, have white-noise statistics.

C.2. Determining γ : Short Perpendicular Wavelengths

Let us calculate the 1D k_{\perp} spectrum: if we assume (and promise to check later) that $\alpha > 1$, then the k_{\parallel} integral over $E_{2D}(k_{\perp}, k_{\parallel})$ is dominated by the region $k_{\parallel} \lesssim k_{\perp}^{\sigma}$ and the 1D spectrum is mostly determined by the CB scales $k_{\parallel} \sim k_{\perp}^{\sigma}$ (as is indeed argued in the GS95 theory and its descendants reviewed in the main text):

$$E(k_{\perp}) \sim \int_0^{k_{\perp}^{\sigma}} dk_{\parallel} E_{2D}(k_{\perp}, k_{\parallel}) \sim k_{\perp}^{-\gamma+\sigma}. \quad (\text{C } 6)$$

Then the amplitude of an Elsasser field at scale $\lambda = k_{\perp}^{-1}$ is

$$\delta Z_{\lambda}^2 \sim \int_{k_{\perp}}^{\infty} dk'_{\perp} E(k'_{\perp}) \sim k_{\perp} E(k_{\perp}) \sim k_{\perp}^{-\gamma+\sigma+1}, \quad (\text{C } 7)$$

assuming $\gamma - \sigma > 1$. On the other hand, the usual Kolmogorov constant-flux condition coupled with the CB conjecture gives us

$$\frac{\delta Z_{\lambda}^2}{\tau_{\text{nl}}} \sim \text{const}, \quad \tau_{\text{nl}}^{-1} \sim \tau_{\text{A}}^{-1} \propto k_{\parallel} \sim k_{\perp}^{\sigma} \Rightarrow \delta Z_{\lambda}^2 \sim k_{\perp}^{-\sigma}. \quad (\text{C } 8)$$

Comparing this with (C 7), we get

$$\gamma = 2\sigma + 1 = 2. \quad (\text{C } 9)$$

The 1D spectral exponent in (C 6) is then $-\gamma + \sigma = -3/2$, as it should be [see (6.22)].

C.3. Determining β : Long Perpendicular Wavelengths

This turns out to be a somewhat subtle issue, connected to an interesting recent development in turbulence theory.

C.3.1. Kinematics

Consider first the following naïve, purely kinematic calculation. Let us write the desired spectrum (C 1) as

$$\begin{aligned} \langle |\mathbf{Z}_{\perp}^{\pm}(\mathbf{k}_{\perp}, k_{\parallel})|^2 \rangle &= \int \frac{d^2 \mathbf{r}_{\perp}}{(2\pi)^2} e^{-i\mathbf{k}_{\perp} \cdot \mathbf{r}_{\perp}} \langle \mathbf{Z}_{\perp}^{\pm}(\mathbf{r}_{\perp}, k_{\parallel}) \cdot \mathbf{Z}_{\perp}^{\pm*}(0, k_{\parallel}) \rangle \\ &= \frac{1}{2\pi} \int_0^{\infty} dr_{\perp} r_{\perp} J_0(k_{\perp} r_{\perp}) C^{\pm}(r_{\perp}, k_{\parallel}), \end{aligned} \quad (\text{C } 10)$$

where $C^\pm(r_\perp, k_\parallel)$ is the two-point correlation function of $\mathbf{Z}_\perp^\pm(\mathbf{r}_\perp, k_\parallel)$. It is only a function of the point separation r_\perp because of statistical homogeneity and isotropy in the perpendicular plane. For any given k_\parallel , it might seem reasonable, by the CB conjecture, to estimate the correlation length of the field to be $\lambda \sim k_\parallel^{-1/\sigma}$ and assume therefore that the integral in (C10) is effectively restricted by $C^\pm(r_\perp, k_\parallel)$ to $r_\perp \lesssim \lambda$. If we now let $k_\perp \lambda \ll 1$ (equivalently, $k_\perp^\sigma \ll k_\parallel$), then the Bessel function can be expanded in small argument: $J_0(k_\perp r_\perp) = 1 - k_\perp^2 r_\perp^2/4 + \dots$. The spectrum (C1) is then

$$E_{2D}(k_\perp, k_\parallel) = \frac{k_\perp}{2\pi} (C_0 + C_2 k_\perp^2 + \dots), \quad (\text{C11})$$

$$C_0 = 2\pi \int_0^\infty dr_\perp r_\perp C^\pm(r_\perp, k_\parallel), \quad C_2 = -\frac{\pi}{2} \int_0^\infty dr_\perp r_\perp^3 C^\pm(r_\perp, k_\parallel). \quad (\text{C12})$$

The first of these coefficients, $C_0 = \int d^2\mathbf{r}_\perp \langle \mathbf{Z}_\perp^\pm(\mathbf{r}_\perp, k_\parallel) \cdot \mathbf{Z}_\perp^{\pm*}(0, k_\parallel) \rangle$, vanishes if $\int d^2\mathbf{r}_\perp \mathbf{Z}_\perp^\pm(\mathbf{r}_\perp, k_\parallel) = 0$, which seems to be a reasonable assumption for a solenoidal field [see (A1)] in a box. This leaves us with the series (C11) for E_{2D} starting at the second term and so $E_{2D} \propto k_\perp^3$ to lowest order. Thus,

$$\beta = 3? \quad (\text{C13})$$

I have added a question mark to this statement because it is, in fact, not as straightforwardly obvious as the kinematic argument suggests.

C.3.2. Thermodynamics

What if one applies to the long perpendicular scales the same logic as I did to long parallel scales in appendix C.1? If the fields are decorrelated at scales longer than the CB scale, i.e., at $k_\perp \ll k_\parallel^{1/\sigma}$, assuming a 2D white-noise spectrum (at fixed k_\parallel) would imply that

$$E_{2D}(k_\perp, k_\parallel) = f(k_\parallel) k_\perp \Rightarrow \beta = 1. \quad (\text{C14})$$

This is just a thermal equilibrium spectrum, with energy equipartitioned amongst all available \mathbf{k}_\perp 's. The tendency for a thermal spectrum to emerge at large scales has indeed been recently noticed in 3D forced hydrodynamic turbulence (where the corresponding spectrum is $\propto k^2$; see [Alexakis & Brachet 2019](#) and references therein).

C.3.3. Dynamics

How then does one reconcile the thermodynamical result (C14) with the kinematic one (C13)? Let me give here the RMHD analog of the argument proposed by [Hosking & Schekochihin \(2022b\)](#) for hydrodynamic turbulence. The effect of the energy-containing scales (in our case, of the CB scales $k_\parallel \sim k_\perp^\sigma$) on the longer perpendicular scales is two-fold: modes with larger \mathbf{k}_\perp 's couple (“beat”) to feed those with smaller \mathbf{k}_\perp 's, thus creating long-scale perturbations; and those long-scale perturbations are mixed to even longer scales by the turbulent diffusion arising from the energy-containing-scale fields. It turns out that the balance between these two effects produces the thermal spectrum (C14), while pushing the kinematic asymptotic (C13) to ever smaller k_\perp 's as time goes on.

Thanks to appendix A, I already have the analytical tools to demonstrate this (semi)quantitatively. Since we are dealing with modes for which $\tau_{nl}^{-1} \ll k_\parallel v_A$, it is not unreasonable to apply the WT approximation to their description (with the usual disclaimer about its formal breakdown wherever it involves CB perturbations). Let us therefore consider (A18), but now at wavenumbers k_\perp that are much smaller than the wavenumbers at which $E_{2D}^\pm(q_\perp, k_\parallel)$ or $E_{2D}^\pm(q_\perp, 0)$ contain most of their energy. Then,

in (A 18), the integral over q_\perp can be assumed to be dominated by $q_\perp \gg k_\perp$, and the integral over $p_\perp = q_\perp + \kappa$ is, therefore,

$$\begin{aligned} \int_{|k_\perp - q_\perp|}^{k_\perp + q_\perp} dp_\perp \frac{k_\perp^2 q_\perp^2}{p_\perp^2} \sin \phi \cos^2 \phi E_{2D}^\mp(p_\perp, 0) &\approx E_{2D}^\mp(q_\perp, 0) \int_{-k_\perp}^{+k_\perp} d\kappa \kappa^2 \sqrt{1 - \frac{\kappa^2}{k_\perp^2}} \\ &= \frac{\pi}{8} k_\perp^3 E_{2D}^\mp(q_\perp, 0). \end{aligned} \quad (\text{C } 15)$$

This turns the WT equation (A 18) into

$$\frac{\partial E_{2D}^\pm}{\partial t} + D^\pm k_\perp^2 E_{2D}^\pm = k_\perp^3 F^\pm(k_\parallel). \quad (\text{C } 16)$$

The left-hand side of (C 16) features the usual turbulent diffusion with diffusivity

$$D^\pm = \frac{\pi}{8v_A} \int_0^\infty dq_\perp E_{2D}^\mp(q_\perp, 0), \quad (\text{C } 17)$$

due entirely to the $q_\parallel = 0$ modes—but these, in the context, are just the CB modes with $q_\parallel \sim q_\perp^\sigma$ (cf. appendix A.4). The right-hand side of (C 16) contains the effect of energy-containing-scale modes coupling to feed the long-scale spectrum:

$$F^\pm(k_\parallel) = \frac{\pi}{8v_A} \int_0^\infty \frac{dq_\perp}{q_\perp} E_{2D}^\mp(q_\perp, 0) E_{2D}^\pm(q_\perp, k_\parallel). \quad (\text{C } 18)$$

The fact that this enters in (C 16) with a prefactor of k_\perp^3 is a reflection of the fields being solenoidal and thus requiring the kinematic asymptotic (C 13) at $k_\perp \rightarrow 0$.

The solution of (C 16) (starting from zero initial condition) is

$$E_{2D}^\pm(k_\perp, k_\parallel) = k_\perp \left(1 - e^{-D^\pm k_\perp^2 t}\right) \frac{F^\pm(k_\parallel)}{D^\pm} \rightarrow \begin{cases} k_\perp^3 t F^\pm(k_\parallel), & k_\perp \ll (D^\pm t)^{-1/2}, \\ k_\perp F^\pm(k_\parallel)/D^\pm, & k_\perp \gg (D^\pm t)^{-1/2}, \end{cases} \quad (\text{C } 19)$$

the latter asymptotic being the steady-state solution. Thus, the kinematic asymptotic (C 13) does exist, but is constantly pushed to larger scales as time goes on. Formally this means that the correlation scale λ above which the correlation function $C^\pm(r_\perp, r_\parallel)$ in (C 10) decays sufficiently fast with r_\perp to enable the expansion (C 11), is not the CB scale $\lambda \sim k_\parallel^{-1/\sigma}$ as naïvely assumed in appendix C.3.1, but rather $\lambda \sim (D^\pm t)^{1/2}$. Since I am interested in asymptotically long times, I will adopt the thermal spectrum (C 14) in what follows.

C.4. Determining α : Short Parallel Wavelengths

Finally, α is determined simply by the requirement that the 2D spectra match along the CB line: substituting $k_\parallel \sim k_\perp^\sigma$ into (C 4) and equating powers of k_\perp , we get

$$\alpha = \frac{\beta + \gamma}{\sigma} - \delta = 6. \quad (\text{C } 20)$$

This somewhat ridiculous exponent⁹⁶ suggests that there is very little energy indeed in wave-like perturbations with $\tau_A \ll \tau_{nl}$.

⁹⁶ Amazingly, this scaling has just been confirmed by Squire *et al.* (2022, this is mentioned in passing in their §A.2), applying a new field-line-following method to the 2D spectra in the MHD inertial range of their kinetic turbulence simulation.

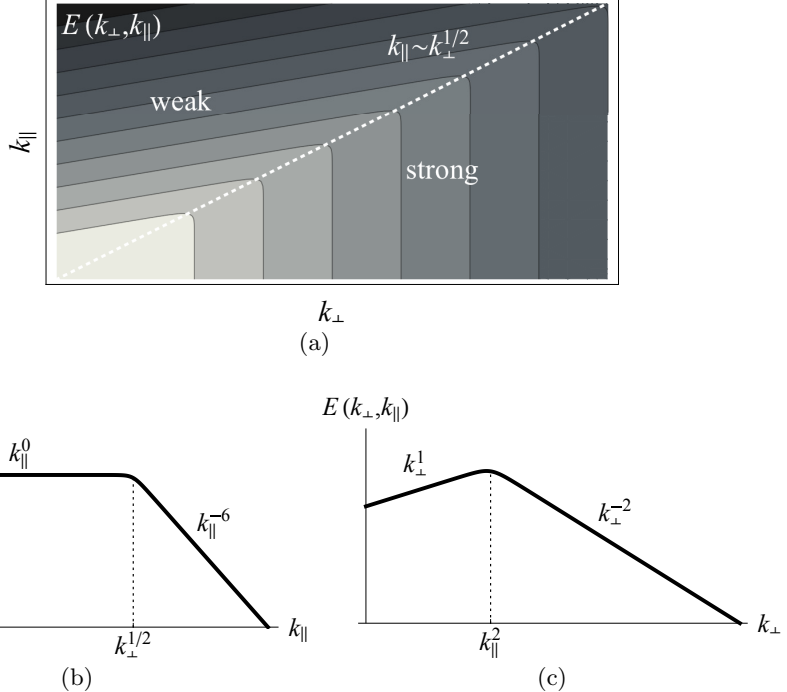


FIGURE 40. Sketch of the 2D spectra (C23) of RMHD turbulence: (a) in the 2D wave-number plane; (b) at constant k_{\perp} ; (c) at constant k_{\parallel} . Note that k_{\parallel} here is measured along the perturbed field, not the z axis (see discussion in §5.3).

Note that the consistency of what I have done above can be checked by calculating the 1D k_{\parallel} spectrum:

$$E(k_{\parallel}) = \int dk_{\perp} E_{2D}(k_{\perp}, k_{\parallel}) \sim \int_0^{k_{\parallel}^{1/\sigma}} dk_{\perp} k_{\parallel}^{-\alpha} k_{\perp}^{\beta} + \int_{k_{\parallel}^{1/\sigma}}^{\infty} dk_{\perp} k_{\parallel}^{\delta} k_{\perp}^{-\gamma} \sim k_{\parallel}^{-\zeta}, \quad (\text{C } 21)$$

where

$$\zeta = \alpha - \frac{\beta + 1}{\sigma} = \frac{\gamma - 1}{\sigma} - \delta = 2, \quad (\text{C } 22)$$

as it should be (see §5.2).

To summarise, the 2D spectrum (C4) of critically balanced Alfvénic turbulence is

$$E_{2D}(k_{\perp}, k_{\parallel}) \sim \begin{cases} k_{\parallel}^{-6} k_{\perp}^1, & k_{\parallel} \gtrsim k_{\perp}^{1/2}, \\ k_{\parallel}^0 k_{\perp}^{-2}, & k_{\parallel} \lesssim k_{\perp}^{1/2}, \end{cases} \quad (\text{C } 23)$$

leading to 1D spectra $E(k_{\perp}) \sim k_{\perp}^{-3/2}$ and $E(k_{\parallel}) \sim k_{\parallel}^{-2}$. The spectra (C23) are sketched in figure 40.

I leave it as an exercise for the reader to show that if the same scheme is applied to the tearing-mediated turbulence described in §7.2 [starting with (7.22) for σ], the exponents in (C4) are

$$\sigma = \frac{6}{5}, \quad \delta = 0, \quad \gamma = \frac{17}{5}, \quad \beta = 1, \quad \alpha = \frac{11}{3}, \quad (\text{C } 24)$$

and $\zeta = 2$, unchanged from (C 22) (as it should be, according to § 7.2.4).

C.5. 2D Spectrum of WT

The 2D spectrum of broad-band-forced WT determined in appendix A.4 can easily be obtained by arguments analogous to the above:

$$\delta = 0 \quad (\text{C } 25)$$

for the same reason as in appendix C.1,

$$\gamma = \sigma + 1 \quad (\text{C } 26)$$

similarly to appendix C.2, but now employing the non-constant-flux argument (A 27),

$$\beta = -4 + \gamma = \sigma - 3 \quad (\text{C } 27)$$

by the WT condition (A 23) with $\mu_0 = -\gamma$ and $\mu = \beta$ instead of the calculation of appendix C.3 (which would only apply above the perpendicular scale of the forcing), and, finally, matching the spectra as in appendix C.4, we get

$$\beta + \gamma = (\alpha + \delta)\sigma \Rightarrow 2(\sigma - 1) = \alpha\sigma. \quad (\text{C } 28)$$

Here we can either set $\sigma = 1$ by assuming a nonaligned cascade of the condensate, as in (A 29), and hence get $\alpha = 0$, or set $\alpha = 0$ by assuming no parallel cascade and equal forcing at all k_{\parallel} in the WT regime, in which case the matching condition (C 28) requires $\sigma = 1$ (and so I would have had to contend with discontinuous spectra if, in appendix A.4, I had allowed the condensate to have alignment). Thus,

$$\sigma = 1, \quad \delta = 0, \quad \gamma = 2, \quad \beta = -2, \quad \alpha = 0. \quad (\text{C } 29)$$

Note that the 2D spectrum in the strongly nonlinear region $k_{\parallel} \lesssim k_{\perp}^{\sigma}$ does not actually change at the transition from the WT to the CB turbulence (although the CB boundary does)—spectral continuity vindicated.

Appendix D. A Reconnection Primer

Since it is now clear that reconnection phenomena play an essential role in MHD turbulence, it is useful to provide a series of shortcuts to the key results. I will not do any precise calculations of the kind that make the theory of resistive MHD instabilities such a mathematically accomplished subject (what better example on which to teach an undergraduate class to solve ODEs with boundary layers than the many incarnations of the tearing mode!), but will instead go for “quick and dirty” ways of getting at the right scalings. Readers yearning for more exactitude will find it, e.g., in a recent treatment by Boldyrev & Loureiro (2018); those who prefer to get their instruction from the original source should start with the foundational papers by Furth *et al.* (1963) and Coppi *et al.* (1976).

When dealing with resistive MHD instabilities, it is convenient to write the RMHD equations in their original form (Strauss 1976), in terms of the stream (flux) functions for the velocity and magnetic fields:

$$\mathbf{u}_{\perp} = \hat{\mathbf{z}} \times \nabla_{\perp} \Phi, \quad \mathbf{b}_{\perp} = \hat{\mathbf{z}} \times \nabla_{\perp} \Psi. \quad (\text{D } 1)$$

Since the Elsasser potentials introduced in (A 1) are just $\zeta^{\pm} = \Phi \pm \Psi$, one can recover the equations for Φ and Ψ from (A 2), or, indeed, use (D 1) and derive them directly from

the momentum and induction equations of MHD (see Schekochihin *et al.* 2009, Oughton *et al.* 2017, and references therein):

$$\frac{\partial}{\partial t} \nabla_{\perp}^2 \Phi + \{\Phi, \nabla_{\perp}^2 \Phi\} = v_A \nabla_{\parallel} \nabla_{\perp}^2 \Psi + \{\Psi, \nabla_{\perp}^2 \Psi\} + \nu \nabla_{\perp}^4 \Phi, \quad (\text{D } 2)$$

$$\frac{\partial}{\partial t} \Psi + \{\Phi, \Psi\} = v_A \nabla_{\parallel} \Phi + \eta \nabla_{\perp}^2 \Psi, \quad (\text{D } 3)$$

where the difference between the Ohmic diffusivity η and viscosity ν has been restored.

D.1. Tearing Instability

Let us ignore the parallel derivatives in (D2–D3) and consider small perturbations of a simple static equilibrium in which the in-plane magnetic field points in the y direction and reverses direction at $x = 0$:

$$\Phi = \phi(x, y)e^{\gamma t}, \quad \Psi = \Psi_0(x) + \psi(x, y)e^{\gamma t} \Rightarrow \mathbf{b}_{\perp} = \hat{\mathbf{y}} b_0(x) + \hat{\mathbf{z}} \times \nabla_{\perp} \psi e^{\gamma t}, \quad (\text{D } 4)$$

where $b_0(x) = \Psi'_0(x)$ is an odd function describing the reversing field profile and γ is the rate at which perturbations of this profile will grow (if they are interesting). Now linearise the RMHD equations (D2–D3) and Fourier-transform them in the y direction:

$$[\gamma - \nu(\partial_x^2 - k_y^2)](\partial_x^2 - k_y^2)\phi = ik_y [b_0(x)(\partial_x^2 - k_y^2) - b_0''(x)]\psi, \quad (\text{D } 5)$$

$$[\gamma - \eta(\partial_x^2 - k_y^2)]\psi = ik_y b_0(x)\phi. \quad (\text{D } 6)$$

When η is small, this system has a boundary layer around $x = 0$, of width δ_{in} , outside which the solution is an ideal-MHD one and inside which resistivity is important and reconnection occurs.

D.1.1. Outer Solution

If we assume that the outer-region solution has scale λ and

$$\tau_{\eta}^{-1} \equiv \frac{\eta}{\lambda^2} \sim \tau_{\nu}^{-1} \equiv \frac{\nu}{\lambda^2} \ll \gamma \ll \tau_{A_y}^{-1} \equiv \frac{v_{A_y}}{\lambda}, \quad (\text{D } 7)$$

where $v_{A_y} \equiv \lambda b'_0(0)$, then the outer solution satisfies

$$\partial_x^2 \psi = \left[k_y^2 + \frac{b_0''(x)}{b_0(x)} \right] \psi, \quad \phi = -\frac{i\gamma}{k_y b_0(x)} \psi. \quad (\text{D } 8)$$

The first of these equations is the (perturbed) magnetic-force balance (inertial terms are neglected), the second describes the ideal-MHD advection of the equilibrium magnetic field by the perturbed flow.

Since ψ is even and the magnetic field $b_y = \partial_x \psi$ must reverse direction at $x = 0$, ψ has a discontinuous derivative (figure 41). This corresponds to a singular current that is developed by the ideal-MHD solution as it approaches the boundary layer—with the singularity resolved inside the layer by resistivity. The solutions outside and inside the layer are matched to each other by equating the discontinuity in the former to the total change in $\partial_x \psi$ calculated from the latter:

$$\Delta' \equiv \frac{[\partial_x \psi_{\text{out}}]_{-0}^{+0}}{\psi_{\text{out}}(0)} = \frac{2}{\delta_{\text{in}}} \int_0^{\infty} dX \frac{\partial_X^2 \psi_{\text{in}}(X)}{\psi_{\text{in}}(0)}, \quad (\text{D } 9)$$

where $\psi_{\text{out}}(x) = \psi(x)$ is the outer solution, $\psi_{\text{in}}(X) = \psi(X\delta_{\text{in}})$ is the inner one, and $X = x/\delta_{\text{in}}$ is the “inner” variable, rescaled to the current layer’s width δ_{in} .

To find Δ' from the outer solution, one must solve (D8) for some particular form

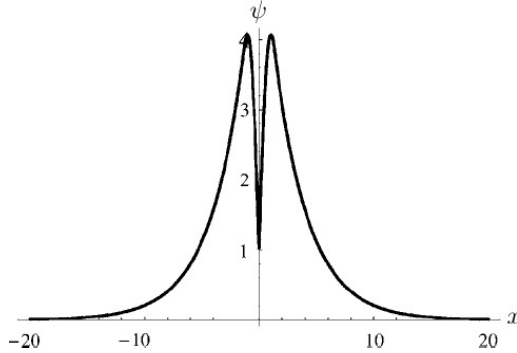


FIGURE 41. The outer solution for a tearing mode in a large-aspect-ratio sheet (adapted from Loureiro *et al.* 2007). Δ' measures the discontinuity of $\partial_x \psi$ at $x = 0$ [see (D 9)].

of $b_0(x)$. For our purposes, all that is needed is the asymptotic behaviour of Δ' in the limit of $k_y \lambda \ll 1$, where λ is the characteristic scale of $b_0(x)$. While in general this asymptotic depends on the functional form of $b_0(x)$, it is

$$\Delta' \sim \frac{1}{k_y \lambda^2} \quad (\text{D } 10)$$

if one can assume that $b_0(x)$ varies faster at $|x| \lesssim \lambda$, in the region where it reverses direction, than at $|x| \gg \lambda$, where it might be approximately flat (see appendix D.1.2). An example of such a situation is the exactly solvable and ubiquitously useful Harris (1962) sheet $b_0(x) = v_{Ay} \tanh(x/\lambda)$. This situation might be particularly relevant because in ideal MHD, field-reversing configurations of the kind that we need to support a tearing mode tend to be collapsing sheets, with λ shrinking dynamically compared to the characteristic scales in the y direction or indeed in the x direction away from the field-reversal region (see further discussion in appendix D.5).

D.1.2. Scaling of Δ'

A reader who is happy to accept (D 10) can now skip to appendix D.1.3. For those who would like to see a more detailed derivation leading to (D 10), let me put forward the following argument, which is adapted from Loureiro *et al.* (2007, 2013a).

Consider first $|x| \sim \lambda$. Since $b_0''/b_0 \sim 1/\lambda^2 \gg k_y^2$, we may neglect the k_y^2 term in (D 8) and seek a solution in the form $\psi = b_0(x)\chi(x)$. This allows us to integrate the equation directly, with the result

$$\psi = b_0(x) \left[C_1^\pm + C_2^\pm \int_{\pm x_0}^x \frac{dx'}{b_0^2(x')} \right], \quad (\text{D } 11)$$

where \pm refer to solutions at positive and negative x , respectively, $C_{1,2}^\pm$ are integration constants and $x_0 \sim \lambda$ is some integration limit, whose precise value does not matter (any difference that it makes can be absorbed into C_1^\pm). Since $b_0(x)$ is an odd function,

$$b_0(x) \approx \frac{x}{\lambda} v_{Ay} \quad \text{at} \quad |x| \ll \lambda. \quad (\text{D } 12)$$

Taking $x \rightarrow 0$ in (D 11), we can, therefore, fix the constant C_2^\pm via

$$\psi(0) = -C_2^\pm \frac{\lambda}{v_{Ay}}. \quad (\text{D } 13)$$

Now formally taking $x \rightarrow \pm\infty$ and assuming that $b_0(x) \rightarrow \pm v_{Ay,\infty} = \text{const}$ in these

limits, we find that the solution (D 11) asymptotes to

$$\psi \approx \pm C_1^\pm v_{Ay,\infty} \mp \psi(0) \frac{v_{Ay}}{v_{Ay,\infty}} \frac{x}{\lambda}. \quad (\text{D } 14)$$

Let us return to (D 8) and consider $|x| \gg \lambda$. At such distances, $b_0''/b_0 \rightarrow 0$ by assumption, so we must now solve (D 8) neglecting the b_0''/b_0 terms while retaining k_y^2 , and then match the resulting “outer-outer” solution to the large- $|x|$ asymptotic (D 14) of the “outer-inner” solution (D 11). The solution that vanishes at infinity is

$$\psi = C_3^\pm e^{\mp k_y x} \quad (\text{D } 15)$$

and its $k_y x \ll 1$ asymptotic is

$$\psi \approx C_3^\pm \mp C_3^\pm k_y x. \quad (\text{D } 16)$$

Demanding that this match (D 14), we get

$$C_3^\pm = \frac{v_{Ay}}{v_{Ay,\infty}} \frac{\psi(0)}{k_y \lambda}, \quad C_1^\pm = \pm \frac{C_3^\pm}{v_{Ay,\infty}}. \quad (\text{D } 17)$$

Finally, returning to (D 11), which, with (D 13) and (D 17), has become

$$\psi = b_0(x) \frac{v_{Ay}\psi(0)}{\lambda} \left[\pm \frac{1}{k_y v_{Ay,\infty}^2} - \int_{\pm x_0}^x \frac{dx'}{b_0^2(x')} \right], \quad (\text{D } 18)$$

and using (D 12), we obtain, for $k_y \lambda \ll 1$,

$$\Delta' = \frac{\psi'(+0) - \psi'(-0)}{\psi(0)} \approx 2 \left(\frac{v_{Ay}}{v_{Ay,\infty}} \right)^2 \frac{1}{k_y \lambda^2} \sim \frac{1}{k_y \lambda^2}, \quad \text{q.e.d.} \quad (\text{D } 19)$$

Pending detailed insight into the functional form of the aligned fluctuations in MHD turbulence, I am going to treat this scaling of Δ' with k_y and λ as generic. A more general scaling

$$\Delta' \lambda \sim \frac{1}{(k_y \lambda)^n} \quad (\text{D } 20)$$

corresponds, for $n > 1$, to $b_0(x)$ decaying to zero at large x on the same scale as it reverses direction around $x = 0$: e.g., one gets $n = 2$ for $b_0(x) = v_{Ay} \tanh(x/\lambda) / \cosh^2(x/\lambda)$ (Porcelli *et al.* 2002) or for a simple sinusoidal profile (Ottaviani & Porcelli 1993; Boldyrev & Loureiro 2018). There is some space for discussion as to whether $n = 1$ or $n = 2$ is the best model for what happens in a typical MHD-turbulent structure (cf. Walker *et al.* 2018). Generalising all the scalings derived throughout this review to arbitrary n is a tedious but straightforward exercise (Pucci *et al.* 2018; Singh *et al.* 2019; Boldyrev & Loureiro 2020), which I have opted to forgo, to avoid bulky n -dependent exponents everywhere. A meticulous reader who wishes to do this exercise will find the tearing-mode scalings for arbitrary n in appendix D.1.5 and take it from there. For the tearing-mediated RMHD cascade (§ 7), the resulting turbulence scalings were worked out by Boldyrev & Loureiro (2017, 2020); for the tearing-mediated dynamo (§ 13.3), by Galishnikova *et al.* (2022).

D.1.3. Inner Solution

In the inner region, whose width is δ_{in} , we can approximate the equilibrium magnetic field’s profile by (D 12). Since $k_y \ll \partial_x \sim \delta_{\text{in}}^{-1}$, the equations (D 5) and (D 6) for the

tearing perturbation become

$$(\gamma - \nu \partial_x^2) \partial_x^2 \phi = ik_y \frac{x}{\lambda} v_{Ay} \partial_x^2 \psi, \quad (\text{D } 21)$$

$$(\gamma - \eta \partial_x^2) \psi = ik_y \frac{x}{\lambda} v_{Ay} \phi. \quad (\text{D } 22)$$

The first of these is the balance of inertia, viscous and Lorentz forces, the second is Ohm's law in resistive MHD. Combining them, we get

$$\partial_x^2 \psi = - \left(\frac{\gamma \lambda}{k_y v_{Ay}} \right)^2 \frac{1}{x} \left(1 - \frac{\nu}{\gamma} \partial_x^2 \right) \partial_x^2 \frac{1}{x} \left(1 - \frac{\eta}{\gamma} \partial_x^2 \right) \psi. \quad (\text{D } 23)$$

This immediately tells us what the width of the boundary layer is:

$$\frac{\nu}{\gamma \delta_{in}^2} \ll 1 \Rightarrow \left(\frac{\gamma \lambda}{k_y v_{Ay}} \right)^2 \frac{\eta}{\gamma \delta_{in}^4} \sim 1 \Rightarrow \frac{\delta_{in}}{\lambda} \sim \left(\frac{\gamma \tau_{Ay}^2}{\tau_\eta} \right)^{1/4} \frac{1}{(k_y \lambda)^{1/2}}, \quad (\text{D } 24)$$

$$\frac{\nu}{\gamma \delta_{in}^2} \gg 1 \Rightarrow \left(\frac{\gamma \lambda}{k_y v_{Ay}} \right)^2 \frac{\eta \nu}{\gamma^2 \delta_{in}^6} \sim 1 \Rightarrow \frac{\delta_{in}}{\lambda} \sim \left(\frac{\tau_{Ay}^2}{\tau_\eta \tau_\nu} \right)^{1/6} \frac{1}{(k_y \lambda)^{1/3}}. \quad (\text{D } 25)$$

The latter regime, in which viscosity is large, is a slightly less popular version of the tearing mode, but it can be treated together with the classic limit (D 24) at little extra cost.

Let us now rescale $x = X \delta_{in}$ in (D 23). Then $\psi_{in}(X) \equiv \psi(X \delta_{in})$ satisfies

$$\frac{\nu}{\gamma \delta_{in}^2} \ll 1 \Rightarrow \partial_X^2 \psi_{in} = - \frac{1}{X} \partial_X^2 \frac{1}{X} (\Lambda - \partial_X^2) \psi_{in}, \quad \Lambda = \left(\frac{\gamma \lambda}{k_y v_{Ay}} \right)^2 \frac{1}{\delta_{in}^2}, \quad (\text{D } 26)$$

$$\frac{\nu}{\gamma \delta_{in}^2} \gg 1 \Rightarrow \partial_X^2 \psi_{in} = \frac{1}{X} \partial_X^4 \frac{1}{X} (\Lambda - \partial_X^2) \psi_{in}, \quad \Lambda = \left(\frac{\gamma \lambda}{k_y v_{Ay}} \right)^2 \frac{\nu}{\gamma \delta_{in}^4}. \quad (\text{D } 27)$$

In both cases, the inner solution depends on a single dimensionless parameter Λ (the eigenvalue). In view of (D 24–D 25), this parameter is, in both cases, just the ratio of the growth rate of the mode to the rate of resistive diffusion across a layer of width δ_{in} , with the appropriate scaling of δ_{in} :

$$\Lambda \sim \frac{\gamma \delta_{in}^2}{\eta} \sim \begin{cases} \frac{\gamma^{3/2} \tau_\eta^{1/2} \tau_{Ay}}{k_y \lambda} \sim \frac{(\gamma \tau_{Ay})^{3/2}}{k_y \lambda} S_\lambda^{1/2}, & \frac{\nu}{\gamma \delta_{in}^2} \sim \frac{\text{Pm}}{\Lambda} \ll 1, \\ \frac{\gamma \tau_\eta^{2/3} \tau_\nu^{-1/3} \tau_{Ay}^{2/3}}{(k_y \lambda)^{2/3}} \sim \left[\frac{(\gamma \tau_{Ay})^{3/2}}{k_y \lambda} (S_\lambda \text{Pm})^{1/2} \right]^{2/3}, & \frac{\nu}{\gamma \delta_{in}^2} \sim \frac{\text{Pm}}{\Lambda} \gg 1, \end{cases} \quad (\text{D } 28)$$

where the Lundquist number (associated with scale λ) and the magnetic Prandtl number are defined as follows:

$$S_\lambda = \frac{\tau_\eta}{\tau_{Ay}} = \frac{v_{Ay} \lambda}{\eta}, \quad \text{Pm} = \frac{\tau_\eta}{\tau_\nu} = \frac{\nu}{\eta}. \quad (\text{D } 29)$$

D.1.4. Peak Growth Rate and Wavenumber

Whatever the specific form of the solution of (D 26) (Coppi *et al.* 1976; Boldyrev & Loureiro 2018) or (D 27), Δ' calculated from it according to (D 9) (and non-dimensionalised) must be a function only of Λ :

$$\Delta' \delta_{in} = f(\Lambda). \quad (\text{D } 30)$$

Equating this to the value (D 10) calculated from the outer solution, we arrive at an equation for Λ :

$$f(\Lambda) \sim \frac{\delta_{\text{in}}}{k_y \lambda^2} \sim \begin{cases} \frac{\gamma^{1/4} \tau_{Ay}^{1/2} \tau_\eta^{-1/4}}{(k_y \lambda)^{3/2}} \sim \Lambda^{1/6} (k_y \lambda S_\lambda^{1/4})^{-4/3}, & \text{Pm} \ll \Lambda, \\ \frac{\tau_{Ay}^{1/3} (\tau_\eta \tau_\nu)^{-1/6}}{(k_y \lambda)^{4/3}} \sim (k_y \lambda S_\lambda^{1/4} \text{Pm}^{-1/8})^{-4/3}, & \text{Pm} \gg \Lambda. \end{cases} \quad (\text{D } 31)$$

Since the function $f(\Lambda)$ does not depend on any parameters apart from Λ , one might intuit that the maximum growth of the tearing mode should occur at $\Lambda \sim 1$, when $f(\Lambda) \sim 1$ (I shall confirm this momentarily). Using these estimates in (D 31) and (D 28), we find

$$k_y \lambda \sim S_\lambda^{-1/4} (1 + \text{Pm})^{1/8} \equiv k_* \lambda \Rightarrow \gamma \tau_{Ay} \sim S_\lambda^{-1/2} (1 + \text{Pm})^{-1/4}, \quad (\text{D } 32)$$

where Pm only matters if it is large. Note that if $S_\lambda \gg (1 + \text{Pm})^{1/2}$, the assumption $k_y \lambda \ll 1$ is confirmed. These are the maximum growth rate and the corresponding wavenumber of the tearing mode.⁹⁷ Note that, for this solution, since $f(\Lambda) \sim 1$, (D 31) gives us

$$\frac{\delta_{\text{in}}}{\lambda} \sim k_* \lambda. \quad (\text{D } 33)$$

If setting $\Lambda \sim 1$, $f(\Lambda) \sim 1$ did not feel inevitable to the reader, perhaps the following considerations will help. Let us consider two physically meaningful limits that do not satisfy these assumptions.

First, let us ask what happens if $\Lambda \ll 1$. This means that the mode grows slowly compared to the Ohmic diffusion rate in the current layer, $\gamma \ll \eta/\delta_{\text{in}}^2$, a situation that corresponds, in a sense that is to be quantified in a moment, to small Δ' . In this limit, $f(\Lambda) \sim \Lambda$ to lowest order in the Taylor expansion (I have not shown this rigorously, but hopefully it is plausible to the reader; for a derivation, see, e.g., [Taylor & Newton 2015](#) or [Boldyrev & Loureiro 2018](#)). Putting this into (D 31) and using (D 28) to unpack Λ , we find

$$\gamma \tau_{Ay} \sim \begin{cases} S_\lambda^{-3/5} (k_y \lambda)^{-2/5}, & k_y \lambda \ll S_\lambda^{-1/4} \text{Pm}^{-5/8}, \\ S_\lambda^{-2/3} \text{Pm}^{-1/6} (k_y \lambda)^{-2/3}, & k_y \lambda \gg S_\lambda^{-1/4} \text{Pm}^{-5/8}. \end{cases} \quad (\text{D } 34)$$

This is the famous FKR solution ([Furth *et al.* 1963](#); see also [Porcelli 1987](#) for the large-Pm case). Since, to get it, $\Lambda \ll 1$ was assumed, substituting (D 34) into (D 28) tells us that the approximation is valid at wavenumbers exceeding the wavenumber (D 32) of peak growth, $k_y \gg k_*$. Note that this imposes an upper bound on Δ' :

$$\Delta' \lambda \sim \frac{1}{k_y \lambda} \ll \frac{1}{k_* \lambda}. \quad (\text{D } 35)$$

This is sometimes (perhaps misleadingly) called the “small- Δ' ” (or weakly driven) limit.

Let us now consider the limit opposite to (D 35), i.e., when Δ' is very large and $k_y \ll k_*$. In (D 31), this corresponds to $f(\Lambda) \rightarrow \infty$ and we argue that this limit must be reached for some value $\Lambda \sim 1$ (it is not physically reasonable to expect that $\Lambda \gg 1$, i.e., that the growth rate of the mode can be much larger than the Ohmic diffusion rate in the

⁹⁷I picked up the general idea of this argument from J. B. Taylor (2010, private communication); it is a slight generalisation of his treatment of the tearing mode in [Taylor & Newton \(2015\)](#).

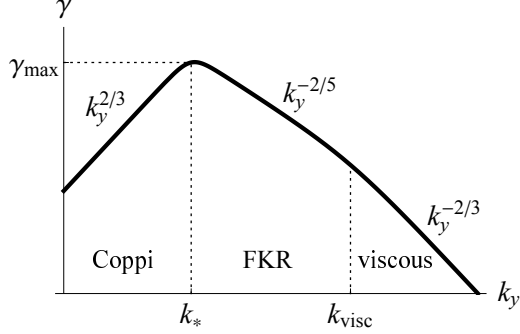


FIGURE 42. Tearing growth rate γ vs. k_y : the [Coppi et al. \(1976\)](#) solution (D 36) for $k_y \ll k_*$, where k_* is given in (D 32), and the FKR solution (D 34) at $k_y \gg k_*$. The viscous version of the latter takes over at $k_y \gg k_{\text{visc}}$, where $k_{\text{visc}}\lambda \sim S_\lambda^{-1/4}\text{Pm}^{-5/8}$. This cartoon is for $\text{Pm} \ll 1$; if $\text{Pm} \gg 1$, the viscous-FKR scaling starts at k_* .

current layer; this reasoning is confirmed by the exact solution—see [Coppi et al. 1976](#)). This implies, with the aid of (D 28),

$$\gamma\tau_{Ay} \sim S_\lambda^{-1/3}(1 + \text{Pm})^{-1/3}(k_y\lambda)^{2/3}. \quad (\text{D } 36)$$

This long-wavelength (“infinite- Δ' ,” or strongly driven) limit of the tearing mode was first derived by [Coppi et al. \(1976\)](#) (and by [Porcelli 1987](#) for the large-Pm case).

We see that the small- k_y asymptotic (D 36) is an ascending and the large- k_y one (D 34) a descending function of k_y (figure 42). The wavenumber k_* of peak growth lies in between, where these two asymptotics meet, which is quite obviously the solution (D 32).

The applicability of this solution is subject to an important caveat. The Harris-like equilibrium that was used to obtain it is a 1D configuration, implicitly assumed to extend as far in the y direction as the mode requires to develop. In reality, any sheet-like configuration forming as a result of (ideal) MHD dynamics will have a length, as well as width: $\xi \gg \lambda$, but still finite. The finiteness of ξ will limit the wavenumbers of the tearing perturbations that can be accommodated. The fastest-growing mode (D 32) will only fit into the sheet if

$$k_*\xi \gtrsim 1 \Leftrightarrow \frac{\xi}{\lambda} \gtrsim S_\lambda^{1/4}(1 + \text{Pm})^{-1/8}. \quad (\text{D } 37)$$

If this condition fails to be satisfied, i.e., if the aspect ratio of the sheet is too small, the fastest-growing mode will be the FKR mode (D 34) with the smallest possible allowed wavenumber $k_y\xi \sim 1$. Thus, low-aspect-ratio sheets will develop tearing perturbations comprising just one or two islands, whereas the high-aspect-ratio ones will spawn whole chains of them, consisting of $N \sim k_*\xi$ islands.

D.1.5. Case of Arbitrary Scaling of Δ'

As promised at the end of appendix D.1.2, here is the generalisation of the main tearing-mode scalings to the case of Δ' scaling according to (D 20). For $\Lambda \sim 1$, (D 28), which is independent of n , implies

$$\gamma\tau_{Ay} \sim (k_*\lambda)^{2/3}S_\lambda^{-1/3}(1 + \text{Pm})^{-1/3}, \quad \frac{\delta_{\text{in}}}{\lambda} \sim (k_*\lambda)^{-1/3}S_\lambda^{-1/3}(1 + \text{Pm})^{1/6}. \quad (\text{D } 38)$$

Using (D 20) in (D 30) and setting $f(\Lambda) \sim 1$ gets us, instead of (D 33),

$$\frac{\delta_{\text{in}}}{\lambda} \sim (k_*\lambda)^n. \quad (\text{D } 39)$$

Combining this with (D 38) leads to the generalised version of (D 32):

$$k_* \lambda \sim S_\lambda^{-1/(3n+1)} (1 + Pm)^{1/2(3n+1)}, \quad \gamma \tau_{Ay} \sim S_\lambda^{-(n+1)/(3n+1)} (1 + Pm)^{-n/(3n+1)}. \quad (\text{D } 40)$$

Using these scalings instead of (D 32) in (7.4) and (7.1) introduces n dependence everywhere in §§ 7, 11.4, and 13.3, but does not appear to change anything qualitatively (Boldyrev & Loureiro 2017, 2020; Galishnikova *et al.* 2022).

D.2. Onset of Nonlinearity

The tearing mode normally enters a nonlinear regime when the width w of its islands becomes comparable to δ_{in} . The islands then grow secularly (Rutherford 1973) until $w\Delta' \sim 1$. As we saw in appendix D.1.4, for the fastest-growing Coppi mode, $\Delta' \sim \delta_{\text{in}}^{-1}$, so the secular-growth stage is skipped. The width of the islands at the onset of the nonlinear regime is, therefore,

$$\frac{w}{\lambda} \sim \frac{\delta_{\text{in}}}{\lambda} \sim \frac{1}{\Delta' \lambda} \sim (k_* \lambda)^n. \quad (\text{D } 41)$$

There is little overhead here for keeping n general, as in (D 39), so I will.

The amplitudes δb_x and δb_y of the tearing perturbation at the onset of nonlinearity can be worked out by observing that the typical angular distortion of a field line due to the perturbation is

$$wk_* \sim \frac{\delta b_x}{b_0(x)|_{x \sim w}} \quad (\text{D } 42)$$

and that, by solenoidality,

$$k_* \delta b_y \sim \frac{\delta b_x}{w}. \quad (\text{D } 43)$$

Since, from (D 12), $b_0(x)|_{x \sim w} \sim (w/\lambda)v_{Ay}$, we have

$$\frac{\delta b_x}{v_{Ay}} \sim \frac{w^2 k_*}{\lambda} \sim (k_* \lambda)^{2n+1}, \quad \frac{\delta b_y}{v_{Ay}} \sim \frac{w}{\lambda} \sim (k_* \lambda)^n. \quad (\text{D } 44)$$

Note that (D 42) and (D 43) together imply that $\delta b_y \sim b_0(x)|_{x \sim w}$, i.e., the perturbed field is as large as the equilibrium field is locally at $x \sim w$ (but not as the upstream field v_{Ay} at $x \sim \lambda$).

Let us confirm that (D 41) was a good estimate for the onset of nonlinearity, i.e., that, once it is achieved, the characteristic rate of the nonlinear evolution of the tearing perturbation becomes comparable to its linear growth rate (D 40). The nonlinear evolution rate can be estimated as $k_* \delta u_y$, where δu_y is the outflow velocity from the tearing region. When $Pm \lesssim 1$, this is obviously Alfvénic, $\delta u_y \sim \delta b_y$. When $Pm \gg 1$, the situation is more subtle as the viscous relaxation of the flows is in fact faster than their Alfvénic evolution (as we are about to see). Then the outflow velocity must be determined from the force balance between viscous and magnetic stresses: using (D 44),

$$\frac{\nu}{w^2} \delta u_y \sim k_* \delta b_y^2 \quad \Rightarrow \quad \frac{\delta u_y}{\delta b_y} \sim \frac{k_* w^2 \delta b_y}{\nu} \sim \frac{k_* w^3 v_{Ay}}{\lambda \nu} \sim (k_* \lambda)^{3n+1} \frac{S_\lambda}{Pm} \sim \frac{1}{\sqrt{Pm}}. \quad (\text{D } 45)$$

Combining the small- and large-Pm cases, we get

$$\delta u_y \sim \frac{\delta b_y}{\sqrt{1 + Pm}} \quad \Rightarrow \quad k_* \delta u_y \sim \frac{(k_* \lambda)^{n+1} v_{Ay}/\lambda}{\sqrt{1 + Pm}} \sim \gamma. \quad (\text{D } 46)$$

In the last expression, (D 44) was used to estimate δb_y and then (D 40) to ascertain that the nonlinear and linear rates are indeed the same.

D.3. What Happens Next?

Once nonlinear effects come in, the tearing perturbation becomes subject to ideal-MHD evolution (for $P_m \gg 1$, also to viscous forces). This leads to collapse of the X -points separating the islands of the tearing perturbation into current sheets (Waelbroeck 1993; Jemella *et al.* 2003, 2004). The time scale for this process is the same as that for the Coppi mode's growth (Loureiro *et al.* 2005) (which, as we have just seen, is the same as the ideal-MHD time scale for a perturbation that is gone nonlinear).

In order to explain what happens as a result of this, I must cover some essential material regarding current sheets and reconnection in them, but let me preview the main ingredients of the overall story first.

- (i) The standard, resistively limited, reconnecting current sheet towards which the X -point collapse leads is described in appendix D.4.1.
- (ii) At asymptotically large Lundquist numbers, such a sheet is, in fact, violently unstable (appendix D.4.2).
- (iii) Therefore, it cannot, in fact, exist and will be disrupted in mid-formation, spawning a population of multiscale islands, or plasmoids (appendix D.5).
- (iv) If it does not fall apart as a result—e.g., if it is held together by some dynamics external to it—it turns into a stochastic plasmoid chain, which is a site of fast MHD reconnection (appendix D.6).

All of these things will be described, somewhat painstakingly, in what follows—they are the background to the blithe assumptions made at the end of § 7.1 about the nature of the debris left in the wake of the tearing disruption of the aligned turbulent structures—assumptions that I needed to construct the model of the tearing-mediated turbulence presented in § 7.2.

D.4. Sweet–Parker Sheet

Let me flesh out what was meant by the X -point collapse in appendix D.3. The idea is that, once the nonlinearity takes hold and Alfvénic (or visco-Alfvénic) outflows from the reconnection region develop, the reconnecting site will suck plasma in, carrying the magnetic field with it, thus leading to formation of an extended sheet, which is a singularity from the ideal-MHD viewpoint, resolved, of course, by resistivity and acting as a funnel both for magnetic flux and plasma (figure 43).⁹⁸ After the collapse has occurred and a sheet has been formed, the magnetic field just outside the resistive layer (the “upstream field”) is now the full equilibrium field, brought in by the incoming flow u_x of plasma (in terms of the discussion in appendix D.2, this means that now $\delta b_y \sim v_{Ay}$).

D.4.1. Sweet–Parker Reconnection

The flux brought in by the inflow u_x must be destroyed by resistivity (reconnected and turned into b_x). This translates into what formally is just a statement of balance between the advective and resistive terms in the induction equation:

$$u_x v_{Ay} \sim \eta j_z \sim \eta \frac{v_{Ay}}{\delta} \quad \Rightarrow \quad \delta \sim \frac{\eta}{u_x} \sim \frac{\ell}{S_\ell} \frac{v_{Ay}}{u_x}, \quad S_\ell = \frac{v_{Ay} \ell}{\eta}, \quad (\text{D } 47)$$

⁹⁸To avoid a misunderstanding, let me anticipate here the discussion in appendix D.5 and say that the X -point collapse at the end of the evolution of a tearing mode is not the unique scenario that can lead to the formation of a sheet, which is in fact a fairly generic dynamical feature of the evolution of X -points in *ideal* MHD. The developments in this sub-section are not in any way restricted to sheets formed from tearing modes.

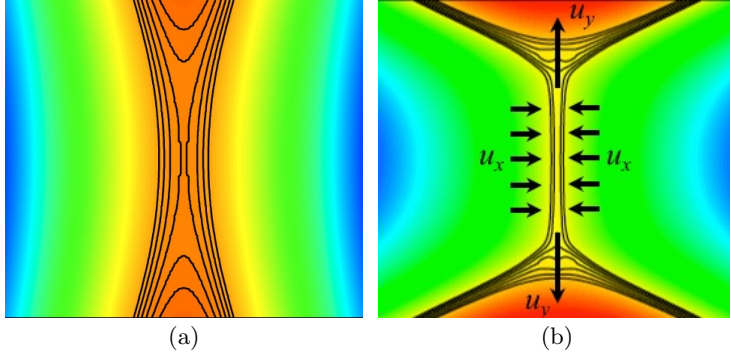


FIGURE 43. (a) An X -point, shown during the nonlinear stage of tearing mode, (b) SP current sheet, formed later on, upon collapse of that X -point (adapted from a 2D RMHD numerical simulation by Loureiro *et al.* 2005). The black lines are magnetic-field lines (constant-flux contours). The in-plane field reverses direction along the middle of the domain that is shown. In the notation of appendix D.4.1, the length of the sheet is ℓ and its width is δ .

where δ is the resistive layer's width and u_x the inflow velocity. I have, in line with the prevailing convention (and physics) of the reconnection theory, introduced a Lundquist number based on the sheet length ℓ (in the context of a sheet formed between two islands of a tearing perturbation, this length is $\ell \sim k_*^{-1}$).

Since the sheet has to process matter as well as flux and since matter must be conserved, we may balance its inflow (u_x) and outflow (u_y):

$$u_x \ell \sim u_y \delta \quad \Rightarrow \quad u_x \sim \frac{\delta}{\ell} u_y \quad \Rightarrow \quad \delta \sim \frac{\ell}{\sqrt{S_\ell}} \left(\frac{v_{Ay}}{u_y} \right)^{1/2}, \quad (\text{D } 48)$$

where the third equation is the result of combining the second with (D 47).

Finally, the outflow velocity is inevitably Alfvénic in the absence of viscosity: this follows by balancing Reynolds and Maxwell stresses (inertia and tension) in the momentum equation (in either y or x direction; note that $b_x \sim v_{Ay} \delta / \ell$). Physically, this is just saying that the tension in the “parabolic”-shaped freshly reconnected magnetic field line (manifest in figure 43a) will accelerate plasma and propel it out of the sheet. In the presence of viscosity, i.e., when $Pm \gg 1$, we must instead balance the magnetic stress with the viscous one, exactly like I did in (D 45), but with a narrower channel and a greater upstream field:

$$\frac{\nu}{\delta^2} u_y \sim \frac{v_{Ay}^2}{\ell} \quad \Rightarrow \quad \frac{u_y}{v_{Ay}} \sim \frac{v_{Ay} \delta^2}{\ell \nu} \sim \frac{1}{\sqrt{Pm}}. \quad (\text{D } 49)$$

To get the last expression, δ had to be substituted from (D 48). Just as I have done everywhere else, I will combine the low- and high- Pm cases:⁹⁹

$$u_y \sim \frac{v_{Ay}}{\sqrt{1 + Pm}} \quad \Rightarrow \quad \frac{\delta}{\ell} \sim \frac{(1 + Pm)^{1/4}}{\sqrt{S_\ell}} \equiv \frac{1}{\sqrt{\tilde{S}_\ell}}, \quad \tilde{S}_\ell = \frac{u_y \ell}{\eta}, \quad (\text{D } 50)$$

where \tilde{S}_ℓ , the Lundquist number based on the outflow velocity, is an obviously useful shorthand. Other relevant quantities can now be calculated, e.g., the rate at which flux

⁹⁹Note that replacing in this argument $\ell \rightarrow k_*^{-1}$, $u_y \rightarrow \delta u_y$, $v_{Ay} \rightarrow \delta b_y \sim v_{Ay} w / \lambda \sim v_{Ay} k_* \lambda$ gives us back the scalings associated with the tearing mode at the onset of nonlinearity (appendix D.2), with $\delta \sim \delta_{in}$. This is, of course, inevitable as both theories are based on the same balances in the reconnection region, except the tearing before X -point collapse had a smaller upstream field δb_y .

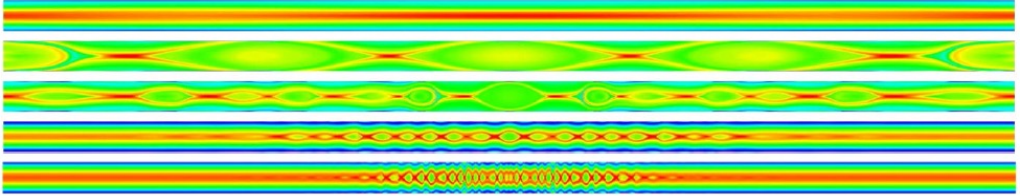


FIGURE 44. Plasmoid instability in current sheets with, from top to bottom, $S_\xi = 10^4, 10^5, 10^6, 10^7, 10^8$. The domain shown is 0.12 of the full length of the sheet. This plot is adapted from Samtaney *et al.* (2009), who confirmed the scalings (D52) numerically. [Reprinted with permission from Samtaney *et al.* (2009), copyright (2009) by the American Physical Society.]

is reconnected:

$$\frac{\partial \Psi}{\partial t} \sim u_x v_{Ay} \sim \frac{u_y v_{Ay}}{\sqrt{\tilde{S}_\ell}} \sim \frac{v_{Ay}^2}{(1 + Pm)^{1/4} \sqrt{S_\ell}}. \quad (\text{D } 51)$$

The argument that I have just presented is one of the enduring classics of the genre and is due to Sweet (1958) and Parker (1957) (hereafter SP; the large-Pm extension was done by Park *et al.* 1984). While the argument is qualitative, it does work, in the sense both that one can construct unique solutions of the SP kind, in a manner pleasing to rigorous theoreticians (Uzdensky *et al.* 1996; Uzdensky & Kulsrud 2000), and that SP reconnection has been measured and confirmed experimentally (Ji *et al.* 1998, 1999) (figure 45 shows an SP sheet measured in their MRX experiment at Princeton).

D.4.2. Plasmoid Instability

However, like for any sheet, one can work out a tearing instability for an SP sheet (this is not the same tearing instability as might have given rise to the sheet as suggested at the beginning of appendix D.4—the SP sheet is now the underlying equilibrium). The results of appendix D.1.4 can be ported directly to this situation (with some caveats that I will discuss in the next paragraph), by identifying $\delta = \lambda$ and $\ell = \xi$. This gives instantly

$$\gamma \sim \frac{u_y}{\xi} \tilde{S}_\xi^{1/4}, \quad k_* \xi \sim \tilde{S}_\xi^{3/8}, \quad \frac{\delta_{in}}{\delta} \sim \tilde{S}_\xi^{-1/8}. \quad (\text{D } 52)$$

This is the so-called *plasmoid instability* (Tajima & Shibata 1997; Loureiro *et al.* 2007, 2013a; Bhattacharjee *et al.* 2009; Comisso & Grasso 2016; see figure 44). The realisation that SP sheets must be unstable can be traced back to Bulanov *et al.* (1978, 1979), with the first numerical demonstration achieved by Biskamp (1986) (see also Biskamp 1982, Steinolfson & van Hoven 1984, Matthaeus & Lamkin 1985, Dahlburg *et al.* 1986, Lee & Fu 1986, and Malara *et al.* 1992). However, this knowledge did not seem to have impacted the field as much as it should have done¹⁰⁰ until the appearance of the analytical paper by Loureiro *et al.* (2007) and the rise of the plasmoid-chain simulation industry in 2D (Lapenta 2008; Daughton *et al.* 2009b,a; Cassak *et al.* 2009; Samtaney *et al.* 2009; Huang & Bhattacharjee 2010, 2012, 2013; Huang *et al.* 2017; Bártá *et al.* 2011; Loureiro *et al.* 2012; Shen *et al.* 2013; Tenerani *et al.* 2015b; Tenerani & Velli 2020b), followed, more recently, by its more turbulent counterpart in 3D (Oishi *et al.* 2015; Huang & Bhattacharjee 2016; Beresnyak 2017; Kowal *et al.* 2017; Stanier *et al.* 2019; Yang *et al.*

¹⁰⁰A reader interested in history will find a useful review of secondary-tearing literature in Appendix B of Del Sarto & Ottaviani (2017).

2020; Daldorff *et al.* 2022)¹⁰¹ and even some experimental undertakings (Jara-Almonte *et al.* 2016; Hare *et al.* 2017*b,a*, 2018; Peterson *et al.* 2019). Perhaps this was because plasmoids had to wait for their moment in the sun until they could be properly resolved numerically—and that required fairly large simulations. Indeed, for an SP sheet to start spawning plasmoids, a sizeable Lundquist number is needed: asking for $\delta_{\text{in}}/\delta$ to be a reasonably small number, say, at least 1/3, (D 52) gives us

$$\tilde{S}_\xi \gtrsim \tilde{S}_{\xi,c}^{(\text{plasmoid})} \sim 10^4, \quad (\text{D } 53)$$

the critical Lundquist number for the plasmoid instability (Biskamp 1986; Loureiro *et al.* 2005, 2007; Samtaney *et al.* 2009; Ni *et al.* 2010; Shi *et al.* 2018).

Let me pause briefly to discuss how (in)valid the direct application of appendix D.1 to an SP sheet in fact was. The good news is that, for such an equilibrium configuration, it is certainly true that $n = 1$ in (D 20), because the scale of the equilibrium field's reversal within the sheet is much smaller than that of its variation outside it, and so the derivation in appendix D.1.2 applies—indeed it was originally invented by Loureiro *et al.* (2007, 2013*a*) for this exact problem. The bad news is that an SP sheet is, in fact, not a static equilibrium considered in appendix D.1, but a dynamic one, featuring an Alfvénic (or, at $P_m \gg 1$, sub-Alfvénic) outflow u_y [see (D 50)], which is strongly sheared transversely to the sheet and has a positive outward gradient along it. Thus, technically, one must re-derive the tearing mode for this new equilibrium before jumping to conclusions. Doing so leads to scalings different from (D 34) in the FKR regime, but does not affect the fastest-growing mode (D 32) (a nice semi-qualitative derivation of this result is offered by Boldyrev & Loureiro 2018; the previous, quite sophisticated, if not in all cases penetrable, paper trail on tearing with flows is Bulanov *et al.* 1978, 1979, Paris & Sy 1983, Hofman 1975, Dobrowolny *et al.* 1983, Einaudi & Rubini 1986, 1989, Chen & Morrison 1990, Loureiro *et al.* 2013*a*, Shi *et al.* 2018, Tolman *et al.* 2018). This gives me licence not to worry about this complication here.

Admittedly, in an extended SP sheet, the presence of flows can also lead to a very fast Kelvin–Helmholtz instability that appears at the periphery of the sheet and is actually even faster than the plasmoid instability (Loureiro *et al.* 2013*a*). This, however, does not change the most important conclusion from (D 52), and arguably the only relevant one, which is that the instability of an SP sheet is massively supercritical: at large enough \tilde{S}_ξ , it is nowhere near marginal stability. The question therefore really is whether we should expect SP sheets ever to be formed in natural circumstances. This brings us to our next topic.

D.5. Formation and Disruption of Sheets

Let us put SP sheets aside and talk more generally about MHD sheets of the kind envisioned in appendix D.1 as the background equilibrium for tearing. The naturally occurring tearing-unstable ideal-MHD solutions are, of course, not static equilibria: they arise, basically, because of the dynamical tendency in MHD for X -points to collapse into sheets (which I invoked in appendices D.3), illustrated in figure 45. An elementary

¹⁰¹In 3D, plasmoids become flux ropes, which are prone to going kink-unstable and breaking up. Their coherence length along the mean field should then be set by a CB-style argument—a balance between the Alfvénic propagation time along the field and some typical perpendicular circulation time [see, e.g., (D 93)]. This has not, to my knowledge, been carefully checked (except, in a different set up, by Zhou *et al.* 2020). Note that most of the 3D simulations cited here were outside the RMHD regime of strong guide field—see footnote 105.

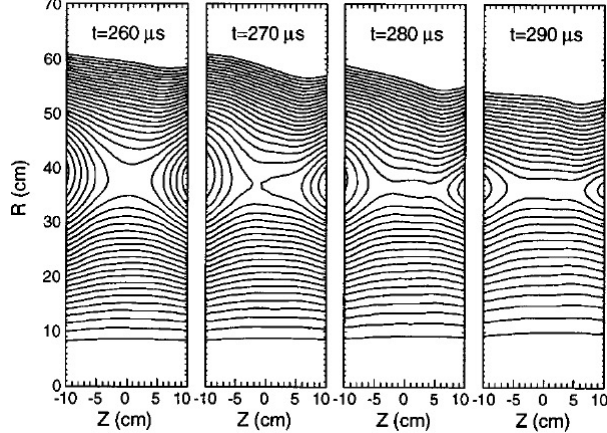


FIGURE 45. Formation of a sheet from an X -point in the MRX experiment at Princeton [reprinted from [Yamada et al. \(1997\)](#) with the permission of AIP Publishing].

example is the classic [Chapman & Kendall \(1963\)](#) collapsing solution of MHD equations:

$$\Phi_0 = \Gamma(t)xy, \quad \Psi_0 = \frac{v_{Ay}}{2} \left[\frac{x^2}{\lambda(t)} - \frac{y^2}{\xi(t)} \right]. \quad (\text{D } 54)$$

Here $\Gamma(t)$ can be specified arbitrarily and then $\lambda(t)$ and $\xi(t)$ follow upon direct substitution of (D 54) into the RMHD equations (D 2–D 3) (with $\eta = 0$). The original [Chapman & Kendall \(1963\)](#) version of this was the exponential collapse:

$$\Gamma(t) = \Gamma_0 = \text{const}, \quad \lambda(t) = \lambda_0 e^{-2\Gamma_0 t}, \quad \xi(t) = \xi_0 e^{2\Gamma_0 t}. \quad (\text{D } 55)$$

A later, perhaps more physically relevant example, due to [Uzdensky & Loureiro \(2016\)](#), is obtained by fixing the outflow velocity at the end of the sheet to be a constant parameter: if $u_y = \partial\Phi_0/\partial x = u_0 y/\xi$, then

$$\Gamma(t) = \frac{u_0}{\xi(t)}, \quad \lambda(t) = \frac{\lambda_0 \xi_0}{\xi_0 + 2u_0 t}, \quad \xi(t) = \xi_0 + 2u_0 t. \quad (\text{D } 56)$$

In this, or any other conceivable model of sheet formation, the aspect ratio increases with time as the sheet's width λ decreases and its length ξ increases.

The traditional thinking about sheets in MHD held that an ideal collapsing solution such as (D 54) (or an explosively collapsing one obtained by [Syrovatskii 1971](#) for compressible MHD) would culminate in a steady-state current sheet, which, from the ideal-MHD point of view, would be a singularity, resolved in resistive MHD by Ohmic diffusion, leading to an SP sheet. One could then discuss magnetic reconnection in such a sheet (appendix D.4.1). However, as we saw in appendix D.4.2, this object is massively unstable to tearing perturbations and will break up into a multitude of islands (“plasmoids”). [Uzdensky & Loureiro \(2016\)](#) and [Pucci & Velli \(2014\)](#) argued that, in fact, it would never form, because tearing perturbations growing against the background of a collapsing ideal-MHD solution will disrupt it before it reaches its steady-state, resistive SP limit.

The detailed demonstration of this result involves realising that not only does the instantaneous aspect ratio of a forming sheet decide what types of tearing perturbations are allowed (single-island FKR modes or multi-island fastest-growing, “Coppi” modes; see appendix D.1.4), but that, in principle, this can change as the sheet evolves, that many different modes can coexist and that these perturbations will grow on different

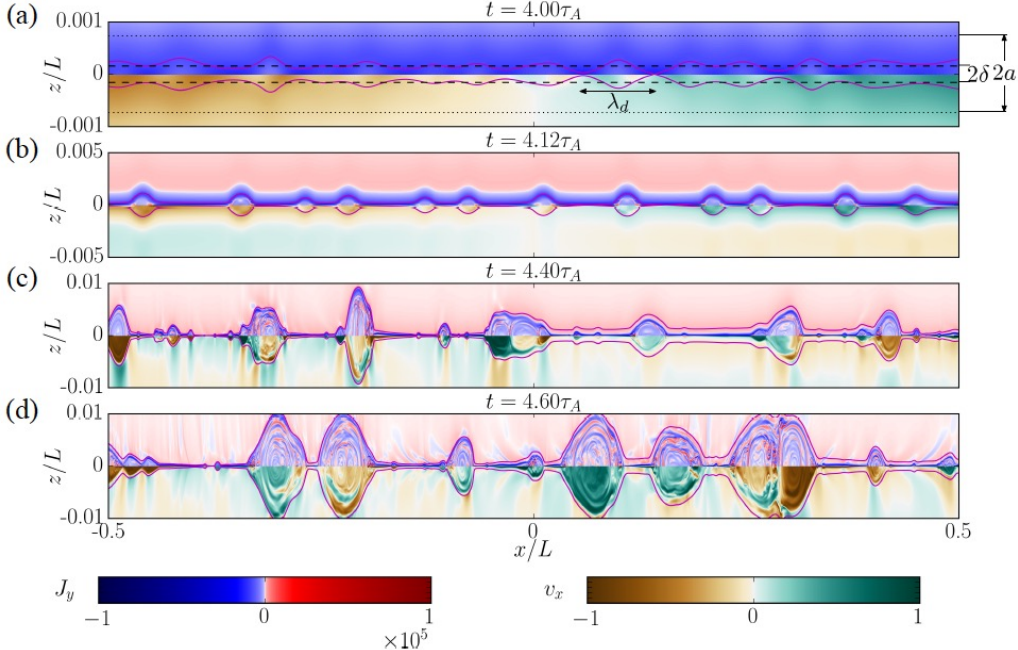


FIGURE 46. This is a plot from [Huang *et al.* \(2017\)](#) (©AAS, reproduced with permission) illustrating the evolution of tearing perturbations of an evolving sheet in a 2D MHD simulation with $S_\xi \sim 10^6$ and $\text{Pm} \ll 1$. Their (x, y, z) are my (y, z, x) , their L is my ξ (sheet length), their a is my λ (sheet width), their τ_A is my $\Gamma^{-1} \sim \xi/v_A$ (characteristic time of the sheet evolution), their δ is my δ_{in} (width of the tearing inner layer). The colour in the upper halves of their panels shows out-of-page current (colour bar “ J_y ”) and in the lower halves the outflow velocity along the sheet (colour bar “ v_x ”). The solid magenta lines are separatrices demarcating two “global” coalescing islands that they set up to form the sheet. The four snapshots are (a) at the moment when the tearing mode goes nonlinear ($w \sim \delta_{\text{in}}$; see appendix D.2), (b) a little later, showing formation of secondary sheets (and so collapse of inter-island X -points), (c) later on, with a secondary instability of these sheets manifesting itself as more plasmoids appear (cf. appendix D.5.2), and (d) in saturation, which for them is the period of stochastic but statistically steady and fast (with a rate independent of S_ξ) reconnection and which obviously also corresponds to islands reaching the width of the sheet and starting to form a stochastic chain, moving and coalescing (see appendix D.6). Note that all of this evolution happens within one Alfvén time, although the initial-growth stage does need a few Alfvén times to get going.

time scales not only linearly but also nonlinearly (the FKR modes having to go through the secular [Rutherford 1973](#) regime, the Coppi ones not). A careful analysis of all this can be found in the paper by [Uzdensky & Loureiro \(2016\)](#) (the follow-up by [Tolman *et al.* 2018](#) deals with the effect of the sheet-forming flows on the tearing mode). The summary that will suffice for my purposes here is that if the fastest-growing linear mode (D 32) fits into the sheet, it will also be the one that first reaches the nonlinear regime and disrupts the formation of the sheet. Note that at the onset of the nonlinear regime of the tearing mode, the width of the islands is given by (D 41). Since $w \ll \lambda$, islands of this size are, in fact, short of what is needed to disrupt the sheet. [Uzdensky & Loureiro \(2016\)](#) argue that the collapse of the inter-island X -points, already mooted in appendix D.3, will eventually—on the same, or faster, time scale as that of the growth of the mode—produce islands of size $w \sim \lambda$, which is what they have to get to in order to be properly disruptive. This is a key ingredient for the picture of “tearing-mediated turbulence” advocated in § 7.2 (but see caveats in § 7.4.1).

D.5.1. “Ideal Tearing”

So what kind of sheets can form before disruption occurs? Namely, what aspect ratio can a sheet reach before the growth rate of the tearing mode triggered in the sheet becomes larger than the rate at which the sheet is collapsing via its ideal-MHD evolution? The former rate is given by (D 32) and the latter is $\Gamma \sim v_{Ay}/\xi$, as is illustrated by the Uzdensky–Loureiro solution (D 56).¹⁰² Then

$$\gamma \gtrsim \Gamma \Leftrightarrow \frac{\xi}{\lambda} \gtrsim S_\lambda^{1/2}(1 + Pm)^{1/4} \Leftrightarrow \frac{\xi}{\lambda} \gtrsim S_\xi^{1/3}(1 + Pm)^{1/6}. \quad (\text{D } 57)$$

The last expression contains the Lundquist number referred to the length ξ rather than to the width λ of the sheet, as customary in magnetic-reconnection theory (cf. appendix D.4). Note that the assumption that it is the fastest-growing Coppi mode (D 32) that should be used in this estimate is confirmed *a posteriori* by checking that the mode does fit into the sheet [cf. (D 37)]: for ξ satisfying the equality in (D 57),

$$k_*\xi \sim S_\lambda^{1/4}(1 + Pm)^{3/8} \sim S_\xi^{1/6}(1 + Pm)^{1/3} \gg 1. \quad (\text{D } 58)$$

The scaling (D 57) of the aspect ratio of the sheet with S_ξ was proposed by Pucci & Velli (2014) to be the maximum possible attainable one before the sheet is destroyed by what they termed “ideal tearing,” i.e., by tearing modes that grow on the same time scale as the ideal-MHD sheet evolves (this result was checked numerically by Landi *et al.* 2015 and Del Zanna *et al.* 2016, extended to $Pm \gg 1$ by Tenerani *et al.* 2015a, and generalised by Pucci *et al.* 2018 to the case of arbitrary scaling of Δ' with k_y that I explained in appendix D.1.5). The conclusion that the sheet is indeed destroyed depends on the X -point-collapse argument described above, because the tearing modes by themselves do not produce islands as wide as the sheet (see appendix D.2).

The argument in § 7.1 about the disruption of MHD turbulence by tearing is essentially the application of the criterion (D 57) to the aligned structures of which Boldyrev’s MHD turbulent cascade consists.

Since the aspect ratio of the sheet described by (D 57) is smaller than that of the SP sheet (D 50) ($S_\xi^{1/3}$, rather than $S_\xi^{1/2}$), Pucci & Velli (2014) argued that global SP sheets could never form. An extensive numerical study by Huang *et al.* (2017) of the instability of forming current sheets has indeed confirmed explicitly that the plasmoid-instability scalings (D 52) derived for an SP sheet only survive up to a certain critical value

$$S_{\xi,c}^{(\text{ideal})} \sim 10^5 - 10^6 \quad (\text{D } 59)$$

[which obviously had to be bigger than the critical Lundquist number (D 53) for the plasmoid instability itself], with the “ideal-tearing” scalings (D 57) and (D 58) taking over at $S_\xi \gtrsim S_{\xi,c}^{(\text{ideal})}$.¹⁰³ Figure 46, taken from their paper, is an excellent illustration of the evolution of tearing perturbations and plasmoid chains.

¹⁰²Assuming an Alfvénic outflow. This is fine even when $Pm \gg 1$ as long as the sheet is macroscopic, i.e., viscosity is unimportant at the scale λ . If instead one is considering a microscopic “equilibrium,” like the secondary X -points between the islands of a tearing perturbation (appendix D.2), one should use $\Gamma \sim u_y/\xi$, where u_y is the visco-Alfvénic outflow: see (D 50). The condition (D 57) then becomes $\xi/\lambda \gtrsim \tilde{S}_\lambda^{1/2} = S_\lambda^{1/2}(1 + Pm)^{-1/4}$.

¹⁰³They also find that $S_{\xi,c}^{(\text{ideal})}$ gets smaller when larger initial background noise is present in the system and that the onset of the tearing instability (and, therefore, of fast reconnection) is generally facilitated by such noise (the same is true for the plasmoid instability of SP sheets: see Loureiro *et al.* 2009 and Sun *et al.* 2022; note also an earlier paper on the same subject by Fan *et al.* 2004). Their paper is written in a way that might give one the impression that they disagree profoundly with both Uzdensky & Loureiro (2016) and Pucci & Velli (2014): the

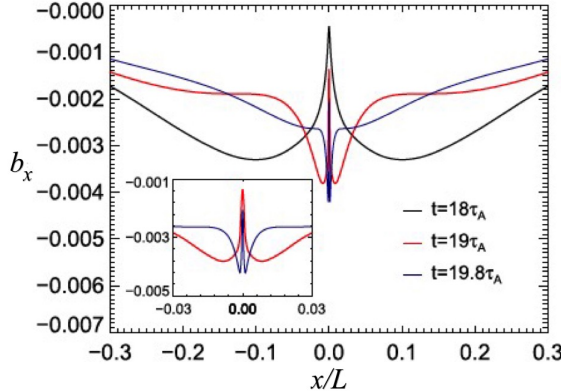


FIGURE 47. A plot, adapted from Tenerani *et al.* (2015b) (©AAS, reproduced with permission), of the $b_x = -ik_y\psi(x)$ profiles (cf. figure 41) for nested tearing modes: primary (black), secondary (red) and tertiary (blue). They extracted these from a direct numerical simulation of a recursively tearing sheet. This is a remarkably clean example of the similarity of tearing at ever smaller scales.

D.5.2. Recursive Tearing

It is not a difficult leap to realise that if a collapsing “global” MHD sheet-like configuration (which, the way it was introduced at the beginning of appendix D.5, was manifestly an X -point configuration) is unstable to tearing, the secondary X -points generated by this tearing can also be unstable to (secondary) tearing and thus might not “complete” the collapse into “proper” SP sheets that was posited for them above. This can happen if the secondary tearing has a shorter growth time than the primary one, which, as we are about to see, is always the case. This conjures up an image of recursive tearings piling up on top of each other *ad infinitum* or, rather, until the inter-island X -points have small enough Lundquist numbers to be stable. At that point, they can all collapse properly into mini-SP-sheets and we are left with a multiscale population of fully nonlinear islands, which can now break up the “mother sheet” and/or start interacting with each other and form a stochastic chain described in appendix D.6. For the purposes of the discussion in the main text (§ 7.2), the issue is whether we should be concerned that the outcome is not just a number of flux ropes of one size $\sim \lambda$, but a whole multiscale distribution of them.

The first model of recursive tearing was proposed in the seminal paper by Shibata & Tanuma (2001), and was more recently numerically tested and amended by Tenerani *et al.* (2015b, 2016) (both models are usefully reviewed by Singh *et al.* 2019). I shall

main point of disagreement is their observation that the disruption of the sheet happens when γ is equal a few times Γ , rather than $\gamma/\Gamma \approx 1$ [see (D 57)], and that exactly how many times Γ it must be depends on the initial noise level. In the context of the turbulence-disruption arguments advanced in § 7, this may be a useful practical caveat pointing to the value of λ_D [see (7.2)] possibly being an overestimate by a factor of order unity. However, all theory in this review is order-unity-inaccurate “twiddle” theory, so I am not as bothered by this complication as someone attempting a quantitative numerical study might be. In any event, the fact that the disruption of the sheet is helped by more noise is surely a good thing for the validity of $\gamma/\Gamma \sim 1$ as the disruption criterion in a turbulent environment, where there is noise aplenty. Another (related) complication that matters quantitatively but probably not qualitatively is the possible presence of logarithmic corrections and other subtleties in the tearing-instability scalings for time-dependent sheets (Comisso *et al.* 2016, 2017, 2018; Tolman *et al.* 2018; Huang *et al.* 2019).

explain their argument first, and then propose a certain modification of it that, in my view, makes it more plausible (and does lead to one important consequence).

Let us work on the assumption that the secondary tearing of an inter-island X -point works in the same way as the primary tearing described in appendix D.1.4 (see figure 47). Therefore, we can assign our old equilibrium parameters to the i -th level of tearing:

$$v_i \equiv v_{Ay}, \quad \lambda_i \equiv \lambda, \quad \xi_i \equiv \xi. \quad (\text{D } 60)$$

The same quantities at the $(i+1)$ -st level are then determined by the resulting perturbation in a way that depends on a number of assumptions.

First, as announced above, let us assume that the “equilibrium” (D 60) will produce a tearing perturbation with growth rate and wavenumber given by (D 32):

$$\gamma_i \sim \frac{u_i}{\lambda_i} \tilde{S}_i^{-1/2}, \quad k_{*,i}^{-1} \sim \lambda_i \tilde{S}_i^{1/4}, \quad (\text{D } 61)$$

where [cf. (D 46)]

$$u_i = \frac{v_i}{\sqrt{1 + \text{Pm}}}, \quad \tilde{S}_i = \frac{S_i}{\sqrt{1 + \text{Pm}}}, \quad S_i = \frac{v_i \lambda_i}{\eta}. \quad (\text{D } 62)$$

This is an assumption, not a certainty, because the local “equilibrium” set up by the i -th tearing perturbation, which features flows as well as fields, is not *a priori* obliged to be tearing unstable in exactly the same way as a very simple static equilibrium used in appendix D.1. Flows are expected to have a seriously stabilising effect if

$$\frac{u_i}{\xi_i} \sim \gamma_i \quad \Leftrightarrow \quad \frac{\xi_i}{\lambda_i} \sim \tilde{S}_i^{1/2} \quad (\text{D } 63)$$

(Bulanov *et al.* 1978, 1979; Biskamp 1986; Shi *et al.* 2018; Tolman *et al.* 2018). This is also the “ideal-tearing” threshold (D 57), at which the tearing only just outperforms the X -point collapse (except, for $\text{Pm} \gg 1$, the Alfvénic outflow here is tempered by viscosity, because secondary-sheet dynamics, as well as tearing, happen at scales where viscosity matters). Our second assumption, therefore, following both Shibata & Tanuma (2001) and Tenerani *et al.* (2015b, 2016), will be that (D 63) holds at every level, i.e., tearing at every level is ideal and marginal. It makes sense that it should not be much faster than that, otherwise the i -th-level “equilibrium” would have gone unstable earlier in its evolution.

The next steps are less obvious. We need to determine three quantities at the $(i+1)$ -st level of tearing: v_{i+1} , λ_{i+1} and ξ_{i+1} . Imposing (D 63) at every level reduces this to two, so we need two further assumptions. Shibata & Tanuma (2001) propose, first, that the length of the $(i+1)$ -st sheet is the wavelength of the i -th tearing mode (D 61), viz.,

$$\xi_{i+1} \sim k_{*,i}^{-1} \sim \lambda_i \tilde{S}_i^{1/4}, \quad (\text{D } 64)$$

and, secondly, that the X -point collapse proceeds far enough for the reconnecting field to be the same at all levels of tearing:

$$v_i \sim v_0. \quad (\text{D } 65)$$

Both of these assumptions can be doubted and revised, but, before doing this, let us see what they imply.

Using (D 65), (D 63), and (D 64), in that order, we get

$$\frac{\tilde{S}_{i+1}}{\tilde{S}_i} = \frac{v_{i+1} \lambda_{i+1}}{v_i \lambda_i} \sim \frac{\lambda_{i+1}}{\lambda_i} \sim \frac{\xi_{i+1} \tilde{S}_{i+1}^{-1/2}}{\lambda_i} \sim \tilde{S}_i^{1/4} \tilde{S}_{i+1}^{-1/2} \Rightarrow \tilde{S}_{i+1} \sim \tilde{S}_i^{5/6}. \quad (\text{D } 66)$$

This implies, *inter alia*, that the $(i+1)$ -st tearing starts only when islands grow a bit larger than the width $w \sim \delta_{\text{in}}$ that they achieved when the i -th tearing went nonlinear: using (D 41) with $n = 1$, we can estimate

$$\frac{\lambda_{i+1}}{\delta_{\text{in},i}} \sim \frac{\lambda_{i+1}}{\lambda_i \tilde{S}_i^{-1/4}} \sim \tilde{S}_i^{1/12}. \quad (\text{D } 67)$$

It is not obvious that it should be so, but it is reassuring that the secondary instability happens *after* the onset of the nonlinear stage, and not before (the conviction that, in fact, the secondary tearing must start right at the onset of nonlinearity led [Tenerani et al. 2015b, 2016](#) to their version of recursive tearing, which I will discuss at the end of this section).

The assumption (D 65) is perhaps questionable. I do not see why the local X -point “equilibria” produced in the nonlinear stage of the primary tearing should stay stable until X -point collapse makes $v_i \sim v_0$ (of course, knowing definitely whether they do so requires a careful quantitative theory of the secondary tearing, currently unavailable). It seems more natural to assume that the effective “equilibrium” upstream field for the secondary tearing (v_{i+1}) is reduced from that for the primary one (v_i) by the fact that the islands generated by the latter are not as wide (λ_{i+1}) as the primary sheet (λ_i). Then

$$v_{i+1} \sim v_i \frac{\lambda_{i+1}}{\lambda_i}. \quad (\text{D } 68)$$

This is derived in the same way as $\delta b_y/v_{Ay} \sim w/\lambda$ was from (D 42) and (D 43), but now $\delta b_y \rightarrow v_{i+1}$, $v_{Ay} \rightarrow v_i$, $w \rightarrow \lambda_{i+1}$ and $\lambda \rightarrow \lambda_i$. This idea, sometimes called the “embedding effect”, goes back to [Cassak & Drake \(2009\)](#), whose simulations appeared to support the notion that secondary tearing would get going in these circumstances (a more recent paper by [Del Sarto & Ottaviani 2017](#) took the same view).

Adopting (D 68) instead of (D 65) in the [Shibata & Tanuma \(2001\)](#) scheme for recursive tearing amounts to replacing (D 66) with

$$\frac{\tilde{S}_{i+1}}{\tilde{S}_i} \sim \frac{v_{i+1}\lambda_{i+1}}{v_i\lambda_i} \sim \left(\frac{\lambda_{i+1}}{\lambda_i} \right)^2 \sim \tilde{S}_i^{1/2} \tilde{S}_{i+1}^{-1} \Rightarrow \tilde{S}_{i+1} \sim \tilde{S}_i^{3/4}. \quad (\text{D } 69)$$

This new scheme does not lose any of the properties of the old one that made the latter plausible:

(i) since (D 67) becomes

$$\frac{\lambda_{i+1}}{\delta_{\text{in},i}} \sim \frac{\lambda_{i+1}}{\lambda_i \tilde{S}_i^{-1/4}} \sim \tilde{S}_i^{1/8}, \quad (\text{D } 70)$$

the $(i+1)$ -st tearing still sets on during the nonlinear stage of the i -th one;

(ii) the Lundquist number gets smaller at every level:

$$\tilde{S}_i \sim \tilde{S}_0^{(3/4)^i} \rightarrow 1 \quad \text{as} \quad i \rightarrow \infty; \quad (\text{D } 71)$$

(iii) the tearing growth rate nevertheless increases:

$$\gamma_i \sim \frac{u_0}{\lambda_0} \tilde{S}_0^{-(3/4)^i/2} \rightarrow \frac{u_0}{\lambda_0} \quad \text{as} \quad i \rightarrow \infty, \quad (\text{D } 72)$$

so the perturbations always grow faster than the underlying “equilibria” evolve ($\gamma_{i+1} \gg \gamma_i$). Thus, the entire hierarchy of islands is created very quickly, on the time scale of (a few times) $\gamma_0^{-1} \sim \xi_0/u_0$. If there is some critical Lundquist number \tilde{S}_c required for these

tearing modes to be unstable, (D 71) allows us to work out the maximum number of times that the recursive tearing will be iterated before X -points can collapse unimpeded into proper, stable, reconnecting current sheets:

$$i_{\max} \sim \ln \frac{\tilde{S}_0}{\ln \tilde{S}_c}. \quad (\text{D } 73)$$

It is obvious that in practice this will not be a large number at all.

The embedding assumption (D 68) enables me to argue that, while islands at all scales below λ_0 are produced, they do not contain much energy. Indeed, the effective energy density in the i -th-level islands is

$$v_{i,\text{eff}}^2 \sim v_i^2 \frac{\lambda_i}{\lambda_0} \sim v_0^2 \left(\frac{\lambda_i}{\lambda_0} \right)^3, \quad (\text{D } 74)$$

where the extra factor of λ/λ_0 represents the fraction of the volume that these islands fill, assuming that they are arranged neatly in a row. When translated into a spectral slope, this gives k_\perp^{-4} , which is easily dominated by the $k_\perp^{-11/5}$ spectrum of the tearing-mediated turbulence derived in § 7.2.1. If this is true, we should be allowed to dismiss recursive tearing as a side show in the context of the tearing-mediated cascade.

Let me conclude this section with some further nuances and caveats. After the entire tearing hierarchy has formed, the X -points fully collapse and the sheet is perhaps broken up by its spawn of islands, of which only the largest ones are energetically of any consequence [see (D 74)]. Were it instead to persist for some time (which is not impossible: see §§ 7.4.1 and 7.4.2), everything would change in the course of the subsequent dynamics of its plasmoid (island) population: plasmoid shapes, their number (they travel along the sheet, coalesce, and eventually get ejected from the sheet), field amplitudes in them (reconnection continues via elementary inter-plasmoid current sheets that are short enough to be stable). Such stochastic plasmoid chains have been studied numerically by many people (see references in appendix D.4.2). Their statistical steady state is, I believe, correctly described by the theoretical model of Uzdensky *et al.* (2010), reviewed in appendix D.6. In this context, an important caveat to the theory of recursive tearing discussed above is that imagining that all those nonlinear processes happen *after* recursive tearing has run its course was surely a gross idealisation. Namely, I assumed implicitly that secondary tearing would be the first instability to kick in once the primary tearing mode became nonlinear—and thus ignored, e.g., the possibility, raised some time ago by Malara *et al.* (1992), that the islands produced by tearing might start coalescing before secondary tearing destabilised the inter-island X -points. Tenerani *et al.* (2015b, 2016) claim to see this in their simulations.

The alternative version of recursive tearing proposed by Tenerani *et al.* (2015b, 2016) was, it seems, inspired by the notion that the nonlinear rearrangements of the island population that occurred in a plasmoid chain gave one licence to discard the Shibata & Tanuma (2001) assumption (D 64) that the number of islands at each level was decided by the wavenumber of the fastest-growing tearing mode at that level. Instead they propose (and claim confirmed in their simulations) that the width of the $(i+1)$ -st sheet is, in fact, the island width $w \sim \delta_{\text{in}}$ of the i -th tearing mode right at the onset of nonlinearity, viz., using (D 41) with $n = 1$,

$$\lambda_{i+1} \sim \delta_{\text{in},i} \sim \lambda_i \tilde{S}_i^{-1/4}. \quad (\text{D } 75)$$

Then, instead of (D 66),

$$\frac{\tilde{S}_{i+1}}{\tilde{S}_i} \sim \frac{\lambda_{i+1}}{\lambda_i} \sim \tilde{S}_i^{-1/4} \Rightarrow \tilde{S}_{i+1} \sim \tilde{S}_i^{3/4}, \quad (\text{D 76})$$

where the assumption (D 65) that the upstream field is the equilibrium field has been retained. The scaling of the Lundquist number is the same as (D 71), but for a different reason. If (D 65) were to be replaced by the embedding assumption (D 68), one gets instead

$$\frac{\tilde{S}_{i+1}}{\tilde{S}_i} \sim \frac{v_{i+1}\lambda_{i+1}}{v_i\lambda_i} \sim \left(\frac{\lambda_{i+1}}{\lambda_i} \right)^2 \sim \tilde{S}_i^{-1/2} \Rightarrow \tilde{S}_{i+1} \sim \tilde{S}_i^{1/2}. \quad (\text{D 77})$$

Under this scheme, one does not need to know ξ_i , but if one wants to know it, it is determined from the ideal-tearing condition (D 63) rather than from the wavelength of the tearing mode (D 64) (otherwise one gets a tearing growth rate γ_i that far exceeds the marginal level $\sim u_i/\xi_i$). One somewhat awkward implication is that the i -th tearing is expected to find some way of producing more numerous, smaller islands than allowed by the wavenumber k_* of its fastest-growing mode: from (D 63), (D 61), and (D 76),

$$\xi_{i+1}k_{*,i} \sim \tilde{S}_{i+1}^{1/2}\tilde{S}_i^{-1/4} \frac{\lambda_{i+1}}{\lambda_i} \sim \tilde{S}_i^{-1/8} \ll 1, \quad (\text{D 78})$$

or $\xi_{i+1}k_{*,i} \sim \tilde{S}_i^{-1/4}$ if (D 77) is used instead of (D 76).

Thus, four recursive-tearing scenarios are available: (D 66), (D 69), (D 76), and (D 77). Which of these you believe depends on which of the plausible assumptions discussed above you find most plausible—or best verified numerically (a hard task). Do the differences between them really matter? Certainly not for the qualitative picture of recursive tearing quickly leading to the formation of a fully nonlinear plasmoid chain. Once this has happened, i.e., once all X -points have fully collapsed, (D 65) will certainly be true at all levels (Uzdensky *et al.* 2010; Loureiro *et al.* 2012). However, if it were also true and, consequently, (D 68) untrue, during the initial recursive tearing, as Shibata & Tanuma (2001) and Tenerani *et al.* (2015b, 2016) would have it, then I would not be able to wave away the role of the secondary islands in the disruption process, as I did in § 7.4.1. Indeed, modifying (D 74) to have $v_i \sim v_0$, one gets

$$v_{i,\text{eff}}^2 \sim v_0^2 \frac{\lambda_i}{\lambda_0}, \quad (\text{D 79})$$

which corresponds to a spectrum of k_\perp^{-2} (cf. appendix D.6.2). This could swamp the $k_\perp^{-11/5}$ spectrum of the tearing-mediated turbulence (§ 7.2.1) unless mitigated by some volume-filling effects (as, e.g., in Tenerani & Velli 2020b). In any case, there would then be a legitimate question of how all these islands might modify, or even completely determine, the tearing-mediated-range statistics. These issues are discussed in § 7.4.3 and appendix D.6.3.

D.6. Fast MHD Reconnection

I have referred several times already to a fully nonlinear plasmoid chain being a possible end result of recursive tearing (appendix D.5.2) and making reconnection fast (§ 7.4). Let me reproduce here, in broad brush, the theory of this regime by Uzdensky *et al.* (2010).

Once all the X -points at all levels of recursive tearing have collapsed, the current sheet becomes a chain of plasmoids of different sizes connected by the longest SP sheets that

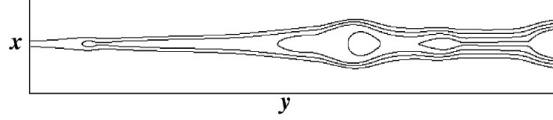


FIGURE 48. Contour plot of the magnetic flux function illustrating the open flux. This is taken from a section of a 2D MHD simulation of a plasmoid chain; the centre of the sheet is somewhere far away on the left. [Reprinted with permission from [Uzdensky et al. \(2010\)](#), copyright (2010) by the American Physical Society.]

can remain stable, i.e., ones whose “critical” length and width are

$$\ell_c \sim \frac{\tilde{S}_c \eta}{u_y}, \quad \delta_c \sim \ell_c \tilde{S}_c^{-1/2}, \quad (\text{D } 80)$$

where $u_y \sim v_{Ay}/\sqrt{1 + Pm}$ is the outflow velocity [see (D 50)] and \tilde{S}_c is the critical Lundquist number (D 53) for the plasmoid instability. The inter-plasmoid sheets cannot be any longer than ℓ_c because the moment they get stretched longer they go unstable and break up into more plasmoids. Thus, the number of plasmoids typically found in a sheet of length ℓ , in steady state, is just $N \sim \ell/\ell_c \sim \tilde{S}_\ell/\tilde{S}_c$. These plasmoids are all of different sizes, having been generated at various levels of recursive tearing or as a result of coalescence of earlier-generation plasmoids. One can think of them as belonging to many hierarchical levels, with plasmoids of the n -th level living in “local” sheets bounded by pairs of $(n - 1)$ -st-level plasmoids. At every level, they are all moving along their local sheet with a mean (visco-)Alfvénic outflow u_y , the same at every level, eventually getting ejected into (coalesced with) the previous-level plasmoids.

It is surprisingly easy to argue that reconnection in such a system (illustrated by the lowest panel of figure 46) is fast. First notice that the plasmoids travelling along the sheet and eventually ejected from it would carry no reconnected flux (no δb_x) if they only contained closed field lines. However, since the upstream (reconnecting) field v_{Ay} decreases gently from the centre of the sheet ($y = 0$) outwards along y , the reconnection on the smaller- $|y|$ side of each plasmoid is slightly faster than on the larger- $|y|$ side of it. Therefore, each plasmoid carries some open flux (figure 48) and it is the ejection of this open flux that contributes to the overall reconnection rate. At every level n in the plasmoid hierarchy, reconnection in a sheet containing n -th-and-higher-level plasmoids and bounded by two $(n - 1)$ -st-level ones adds to the open flux enveloping the $(n - 1)$ -st-level plasmoid on the larger- $|y|$ side and subtracts from the one on the smaller- $|y|$ side. The overall reconnected flux is the sum over these contributions, all of which cancel each other except for the one from the centre of the sheet. Thus, the overall reconnection rate is just the reconnection rate in the central elementary sheet, given by (D 51) with the critical Lundquist number \tilde{S}_c :

$$\frac{\partial \Psi}{\partial t} \sim \tilde{S}_c^{-1/2} u_y v_{Ay} \sim 10^{-2} (1 + Pm)^{-1/2} v_{Ay}^2, \quad (\text{D } 81)$$

independent of the actual Lundquist number \tilde{S}_ℓ and the same at every level in the hierarchy.

This result can be rederived (or re-interpreted) as a modification of the SP reconnection, proposed by [Shibata & Tanuma \(2001\)](#), in which the effective width $\delta_{\text{eff}}^{(n-1)}$ of the sheet (whose length is $\ell^{(n-1)}$) connecting the $(n - 1)$ -st-level plasmoids, for the purposes of mass (and with it, flux) ejection, is the width of the largest plasmoids in that sheet, which are the n -th-level plasmoids. Then the reconnection rate in such a sheet, i.e., the

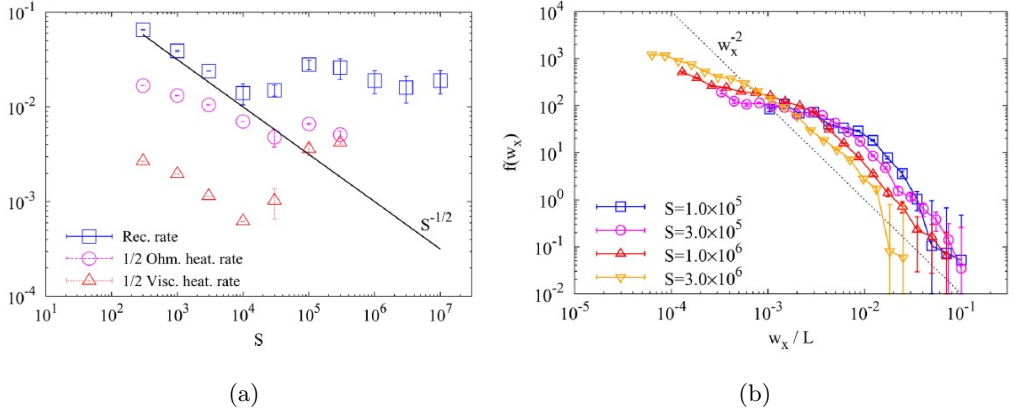


FIGURE 49. (a) Reconnection rate (blue squares), normalised, in my notation, to $u_y v_{Ay}$, in 2D MHD $\text{Pm} = 1$ simulations by Loureiro *et al.* (2012). Transition at $S_\ell \sim 10^4$ from the SP scaling to the fast-reconnection regime (D 81) is manifest. (b) Plasmoid-width distribution function in the same simulations, from the same paper, confirming the scaling predicted by Uzdensky *et al.* (2010) (see appendix D.6.1). [Reprinted from Loureiro *et al.* (2012) with the permission of AIP Publishing.]

rate of growth of the flux $\Psi^{(n-1)}$ in the $(n-1)$ -st-level plasmoids, is

$$\frac{\partial \Psi^{(n-1)}}{\partial t} \sim u_x^{(n-1)} v_{Ay} \sim \frac{\delta_{\text{eff}}^{(n-1)}}{\ell^{(n-1)}} u_y v_{Ay}, \quad \delta_{\text{eff}}^{(n-1)} \sim w^{(n)}, \quad (\text{D } 82)$$

where the inflow velocity $u_x^{(n-1)}$ has been calculated from mass conservation, as in (D 48), and the (visco-)Alfvénic outflow u_y is the same at every level of the hierarchy, because the inter-plasmoid X -points are all fully collapsed, so the upstream field is v_{Ay} at every level. The n -th-level plasmoids' width is then found by letting the perturbed field inside them be comparable to that upstream field:

$$\delta b_y^{(n)} \sim \frac{\Psi^{(n)}}{w^{(n)}} \sim v_{Ay} \quad \Rightarrow \quad w^{(n)} \sim \frac{\Psi^{(n)}}{v_{Ay}}. \quad (\text{D } 83)$$

Finally, the flux typically contained inside the n -th-level plasmoid can be estimated as the reconnection rate at that level times the time that an n -th-level plasmoid will take to travel out of the $(n-1)$ -st-level sheet:

$$\Psi^{(n)} \sim \frac{\ell^{(n-1)}}{u_y} \frac{\partial \Psi^{(n)}}{\partial t}. \quad (\text{D } 84)$$

Combining (D 82–D 84), we get

$$\frac{\partial \Psi^{(n-1)}}{\partial t} \sim \frac{\partial \Psi^{(n)}}{\partial t}, \quad (\text{D } 85)$$

so the reconnection rate is the same at every level and thus equal to the reconnection rate (D 81) at $n \rightarrow \infty$, i.e., in the most elementary sheet, q.e.d.

Thus, the basic reason for reconnection becoming fast in this way is that plasmoids make the SP sheet effectively fatter, relieving the severe constraint that pumping mass and flux through a narrow funnel would otherwise impose. The only remaining constraint is the need to get the SP sheet to be at least as long as ℓ_c in order for it to be able to break up into plasmoids.

The fact that SP reconnection transitions to a fast, plasmoid-dominated regime at

$S_\ell \gtrsim S_c \sim 10^4$, with the reconnection rate set by S_c , was confirmed numerically by Bhattacharjee *et al.* (2009), Loureiro *et al.* (2012, see figure 49a) and in numerous subsequent simulations of bespoke reconnecting configurations (many of them cited in appendix D.4.2). Whether this kind of fast reconnection and statistically steady plasmoid chains occur as local features of MHD turbulence is a tricky question: see §§ 7.4.1 and 7.4.2. Note that, in appendix D.7, I will discuss another, quite different, sense in which reconnection is sometimes described as fast when it occurs in a turbulent environment.

D.6.1. Plasmoid Flux and Width Distribution

The relation (D84), combined with the constant reconnection rate (D81), allows one to determine the distribution function of the plasmoid fluxes—not necessary for the above argument, but a nice, testable result, which will prove useful in what follows. The number of plasmoids with $\Psi > \Psi^{(n)}$, or, equivalently, $w > w^{(n)}$, in the sheet of overall length ℓ is

$$N^{(n)} \sim \frac{\ell}{\ell^{(n-1)}} \sim \frac{\tilde{S}_c^{-1/2} v_{Ay} \ell}{\Psi^{(n)}} \sim \frac{\tilde{S}_c^{-1/2} \ell}{w^{(n)}}, \quad (\text{D } 86)$$

the last expression following from (D83). Therefore, the plasmoid-flux distribution function is $f(\Psi) \propto \Psi^{-2}$ and the plasmoid-width distribution function is $f(w) \propto w^{-2}$. These scalings are indeed corroborated numerically (Loureiro *et al.* 2012, see figure 49b).

D.6.2. Spectrum of Plasmoid Chain

It is instructive to work out the spectrum of the plasmoid chain imagined by Uzdensky *et al.* (2010). This chain is a multi-scale structure, but not one that is naturally described as a local constant-flux cascade: rather, energy is brought into it by the incoming (reconnecting) field v_{Ay} and deposited by the reconnection processes (which include coalescence) into plasmoids at all levels. The field inside these plasmoids is always v_{Ay} , independently of their size [see (D83)]. However, the plasmoids are arranged in a row along the chain, rather than randomly in space, so the smaller ones fill less space than the larger ones and thus the effective energy density associated with them is smaller, viz., for n -th-level plasmoids,

$$[\delta b_{\text{eff}}^{(n)}]^2 \sim v_{Ay}^2 \frac{w^{(n)}}{w^{(1)}}, \quad (\text{D } 87)$$

where $w^{(1)}$ is the width of the largest plasmoids and, therefore, of the chain.¹⁰⁴ Note that the size of the plasmoids in the y direction (along the chain) does not matter here because the smaller plasmoids are more numerous than the larger ones by the exact same factor by which they are shorter in length ($\sim \ell/\ell^{(n)}$). Now let $\delta b_{\text{eff}}^{(n)} = \delta b_{\text{eff},\lambda}$, $\lambda = w^{(n)}$. By (D83), (D84), (D85) and (D81),

$$w^{(n)} \sim \tilde{S}_c^{-1/2} \ell^{(n-1)}, \quad (\text{D } 88)$$

so we have $w^{(1)} \sim \tilde{S}_c^{-1/2} \ell$. From (D87), therefore,

$$\delta b_{\text{eff},\lambda} \sim v_{Ay} \tilde{S}_c^{1/4} \left(\frac{\lambda}{\ell} \right)^{1/2} \Rightarrow E(k_x) \sim v_{Ay}^2 \tilde{S}_c^{1/2} \ell^{-1} k_x^{-2}. \quad (\text{D } 89)$$

I have used k_x , rather than k_\perp , because the direction of maximum variation here is very obviously x , transverse to the sheet; it is, of course, true that $k_\perp \sim k_x$.

¹⁰⁴This is exactly the same argument as I used in obtaining (D74) and (D79).

The total energy flux into the chain, per unit volume, is

$$\varepsilon \sim \frac{v_{Ay}^2 u_x \ell}{\ell w^{(1)}} \sim \frac{v_{Ay}^2 u_y}{\ell}. \quad (\text{D } 90)$$

It is, therefore, possible to recover (D 89) formally from a constant-flux argument in which the nonlinear time is the life time (ejection time) of an n -th-level plasmoid (Loureiro 2016):

$$\frac{[\delta b_{\text{eff}}^{(n)}]^2}{\tau_{\text{nl}}^{(n)}} \sim \varepsilon, \quad \tau_{\text{nl}}^{(n)} \sim \frac{\ell^{(n-1)}}{u_y} \sim \frac{\tilde{S}_c^{1/2} w^{(n)}}{u_y} \Rightarrow \delta b_{\text{eff},\lambda} \sim \left(\frac{\varepsilon}{u_y}\right)^{1/2} \tilde{S}_c^{1/4} \lambda^{1/2}, \quad (\text{D } 91)$$

which is the same as (D 89), by way of (D 90). Yet another way to derive the same result is via the plasmoid-width distribution function (D 86) (Bárta *et al.* 2012): the energy in the plasmoids of width $\lambda \sim k_x^{-1}$ is, per unit volume,

$$E(k_x) dk_x \sim \frac{v_{Ay}^2 \tilde{S}_c^{1/2} \lambda^2 dN(\lambda)}{\tilde{S}_c^{-1/2} \ell^2} \sim v_{Ay}^2 \tilde{S}_c^{1/2} \ell^{-1} d\lambda \sim v_{Ay}^2 \tilde{S}_c^{1/2} \ell^{-1} k_x^{-2} dk_x, \quad (\text{D } 92)$$

whence follows the spectrum (D 89).

All of this works on the assumption that parallel (to the mean field) dynamics do not upset things (plasmoid-width distribution etc.) in a major way. By the usual CB argument, plasmoids, which are flux ropes in 3D, cannot extend much farther along the mean field than an Alfvén wave can travel in some characteristic nonlinear time associated with the plasmoid. The most obvious estimate of this time is one in (D 91), whence (Loureiro 2016)

$$\frac{l_{\parallel}^{(n)}}{v_A} \sim \tau_{\text{nl}}^{(n)} \sim \frac{\tilde{S}_c^{1/2} w^{(n)}}{u_y} \Rightarrow l_{\parallel} \sim \frac{v_A}{u_y} \tilde{S}_c^{1/2} \lambda \Rightarrow E(k_{\parallel}) \sim \frac{v_{Ay}^2 u_y}{v_A \ell} k_{\parallel}^{-2}. \quad (\text{D } 93)$$

Thus, the chain's parallel spectrum is the same as the perpendicular one—this appears to be what Huang & Bhattacharjee (2016) report for their 3D turbulent plasmoid chain. The “fluctuation-direction” spectrum (cf. § 6.5) is the same again, because, clearly,

$$\xi \sim \tilde{S}_c^{1/2} \lambda \Rightarrow E(k_y) \sim v_{Ay}^2 \ell^{-1} k_y^{-2}. \quad (\text{D } 94)$$

The “turbulence” of plasmoids in a plasmoid chain has a fixed, scale-independent alignment angle equal to the reconnection rate, $\sim \tilde{S}_c^{-1/2}$.

A sceptical reader might observe that a k_x^{-2} spectrum for a plasmoid chain is in fact no big revelation because plasmoids are connected by elementary sheets (D 80), which, being step-like “discontinuities” of width δ_c in x , already on their own should give rise to a k_x^{-2} spectrum for all $k_x \lesssim \delta_c^{-1}$ (the same argument already appeared in §§ 10.4 and 12.8). This is true, and so the point of the above calculation is that plasmoids' energy distribution does not swamp the k_x^{-2} scaling of the spectrum; also, the same scaling in k_y and k_{\parallel} is a property of the plasmoids, not of the inter-plasmoid sheets.

D.6.3. Reconnection-Driven Turbulence

In fact, the reconnecting sheets seen in 3D simulations do not resemble all too closely the relatively orderly procession of multi-scale plasmoids envisioned by Uzdensky *et al.* (2010) and seen quite clearly in 2D simulations (see figure 46 and papers cited in appendix D.4.2). In 3D, the chain looks like a strip of vigorous turbulence (figure 50), even if flux ropes (3D plasmoids) may be identifiable there, at least when a mean field is

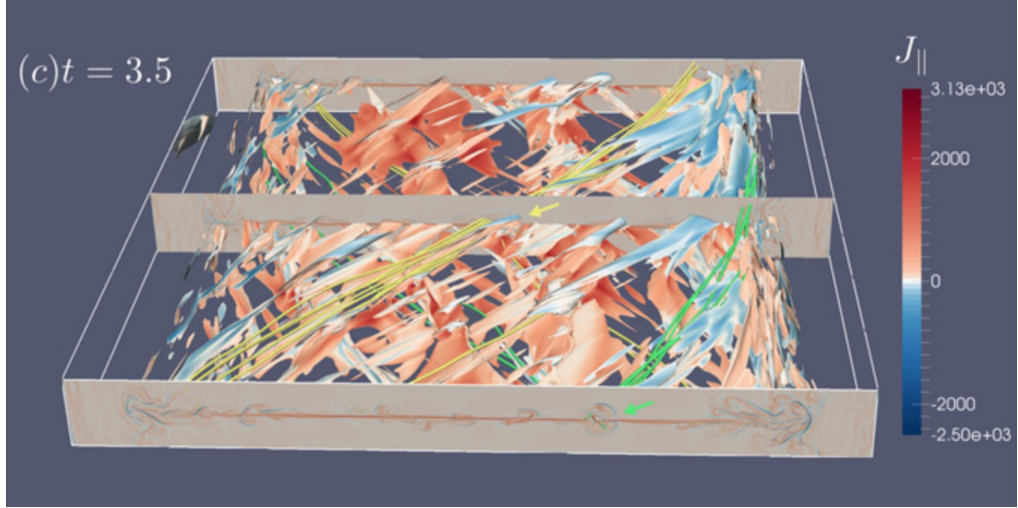


FIGURE 50. A 3D, turbulent plasmoid (flux-rope) chain obtained in the simulations of Huang & Bhattacharjee (2016) (©AAS, reproduced with permission).

imposed.¹⁰⁵ One can think of this situation as a result of the flux ropes constantly going unstable and thus seeding turbulent cascades on multiple scales. A naïve but perhaps instructive model of such “reconnection driving” of turbulence (promised in § 7.4.3) can be constructed by assuming that the energy density (D 87) in the plasmoids at each level n describes the “outer scale” of a mini-cascade, which then proceeds in some regular MHD manner. For this argument, it does not matter what exactly this cascade is like, just that it has some power-law scaling below its mother plasmoid’s scale $w^{(n)}$:

$$\delta Z_{\lambda}^{(n)} \sim \delta b_{\text{eff}}^{(n)} \left(\frac{\lambda}{w^{(n)}} \right)^{\gamma} \sim v_{Ay} \tilde{S}_c^{1/4} \frac{[w^{(n)}]^{(1-2\gamma)/2} \lambda^{\gamma}}{\ell^{1/2}}, \quad \lambda < w^{(n)}, \quad (\text{D } 95)$$

where, e.g., $\gamma = 1/4$ for an aligned MHD cascade (§ 6.4) and $\gamma = 3/5$ for a tearing-mediated one (§ 7.2.1). The cumulative energy density at scale λ from all the mini-

¹⁰⁵ According to Kowal *et al.* (2020), this turbulence is driven primarily by Kelvin–Helmholtz instability, not tearing—at least at large scales, long times, and in the outflow regions (for a theory of KH instability in reconnecting sheets, see Loureiro *et al.* 2013a). However, the simulations by Kowal *et al.* (2017) from which that conclusion was drawn had an anti-parallel, reconnecting field 10 times larger than the guide field. This is the opposite of the RMHD regime that one expects to find locally in the kind of MHD turbulence that I have discussed so far, where the in-plane field is always small, $b_{\perp} \ll B_0$. Of the rest of the 3D papers cited in appendix D.4.2, Oishi *et al.* (2015) and Yang *et al.* (2020) had $B_0 = 0$, and the others $b_{\perp} \sim B_0$, with the exception of Daldorff *et al.* (2022), who probed down to $b_{\perp} \sim 0.2B_0$ and compared 3D and 2D runs. Their conclusion is that 3D is generally messier due to flux ropes getting interlinked with each other. This somewhat impedes their ability to flow out along the sheet and be ejected from it in the way plasmoids do in 2D simulations and in the fast-reconnection model of Uzdensky *et al.* (2010)—leading, as a result, to somewhat slower reconnection. Daldorff *et al.* (2022) observe, however, that, unsurprisingly, cases with lower b_{\perp}/B_0 look more like the 2D case. There still does not appear to exist a systematic 3D study of a reconnecting sheet in RMHD—besides settling the question of convergence of reconnection rates between the 3D and 2D cases, it would be more directly relevant to aligned structures that arise in the inertial range of MHD turbulence.

cascades is then

$$\delta Z_\lambda^2 \sim \sum_{w^{(n)} > \lambda} [\delta Z_\lambda^{(n)}]^2 \sim \frac{v_{Ay}^2 \lambda^{2\gamma}}{\ell \tilde{S}_c^{-1/2}} \int_{\max\{\lambda, \delta_c\}}^{w^{(1)}} dN(w) w^{1-2\gamma} \sim v_{Ay}^2 \min \left\{ 1, \left(\frac{\lambda}{\delta_c} \right)^{2\gamma} \right\}, \quad (\text{D } 96)$$

where $N(w)$ is the plasmoid-width distribution (D 86). The upper bound of the integral is the width $w^{(1)} \sim \ell \tilde{S}_c^{-1/2}$ of the largest plasmoids, and the lower bound is the larger of the scale λ and the width $\delta_c \sim \ell_c \tilde{S}_c^{-1/2}$ of the smallest plasmoids, i.e., ones associated with the critical SP sheet (D 80). This result means that there is a k_\perp^{-1} spectrum in the reconnection-driving range $k_\perp \delta_c \lesssim 1$ followed by an MHD turbulence spectrum $\propto k_\perp^{-2\gamma-1}$ at $k_\perp \delta_c \gtrsim 1$.

What this spectrum is depends on whether the cascade is ideal/aligned or tearing-dominated. In order to work that out with confidence, one has to know rather more than we (or, at least, I) currently do about the turbulent dynamics of flux ropes. Recall however, that the structures in the driving range are already aligned with angle $\sim \tilde{S}_c^{-1/2}$. It is, therefore, possible, and indeed plausible, that the MHD cascade seeded by unstable flux ropes might be tearing-mediated, as mooted in § 7.4.3.

To conclude, under the simplistic scheme explored above, reconnection-driven turbulence at small enough scales appears to be some form of regular MHD turbulence, but with a broad scale range into which energy is injected directly by reconnection processes—broad asymptotically but certainly not captured in full asymptotic glory by any realisable numerical experiment. This might explain a degree of discord in the scalings reported in the papers cited in § 7.4.3.

D.7. Stochastic Reconnection and MHD Turbulence

As promised in § 8.3.3, here is a (biased) review of “stochastic reconnection”, the notion primarily associated today with Lazarian & Vishniac (1999, henceforth LV99)—a widely cited paper, which, however, has acquired the reputation of being rather hard to understand. Eyink *et al.* (2011) seem to me to have succeeded in explaining it with a degree of clarity by adopting somewhat different terms, based on a sizeable body of precursor work by Eyink (2009, 2011). There are many self-reviews of this school of thought, of which the most recent and comprehensive one is Lazarian *et al.* (2020), but my attempt below may be the first by an external observer. Their main idea is roughly as follows.

First, let us note that, instead of (D 47), we may follow Kulsrud (2005) and start our consideration of an SP sheet by stating that the width of the sheet must be equal to the typical distance that the field lines would diffuse resistively in the direction (x) transverse to the upstream field (which points in y) over the time that it takes the plasma to transit through the sheet and be ejected out of it, viz.,

$$\delta \sim (\eta t_{\text{out}})^{1/2}, \quad t_{\text{out}} \sim \frac{\ell}{u_y} \quad \Rightarrow \quad \delta \sim \left(\frac{\eta \ell}{u_y} \right)^{1/2} \sim \frac{\ell}{\sqrt{S_\ell}} \left(\frac{v_{Ay}}{u_y} \right)^{1/2}, \quad (\text{D } 97)$$

which is the same expression as (D 48).

LV99, as interpreted by Eyink *et al.* (2011),¹⁰⁶ argue that if the sheet is embedded in

¹⁰⁶For the connoisseurs, there is, in fact, not complete equivalence between the argument of LV99 and its interpretation by Eyink *et al.* (2011). The former paper, together with many of its successors and citers, believe that their stochastic-reconnection mechanism can only work in 3D, because magnetic-field lines are too topologically constrained in 2D. For Eyink *et al.* (2011), there is no problem in 2D as Lagrangian trajectories in 2D MHD turbulence still separate quickly.

a turbulent environment, δ should instead be calculated as the distance by which two magnetic field lines initially starting arbitrarily close-by, separate after time t_{out} , and that this distance is the same as the distance by which two Lagrangian fluid particles separate. It is this identification between stochastic particle trajectories and field lines that requires all the work contained in [Eyink \(2009, 2011\)](#). In formal terms, he is able to prove that, in the presence of resistivity, the magnetic field at any point in space and time is an average over those realisations of a certain random field that end up at that point after evolving as “virtual” magnetic fields “frozen” into a stochastic flow that is the superposition of the Lagrangian turbulent velocity field and a white noise with the diffusion constant η . However small is η , such fields diverge in the same way as Lagrangian trajectories do. [Eyink et al. \(2013\)](#) successfully tested this proposition in a large numerical simulation of MHD turbulence.¹⁰⁷

In fluid dynamics, the stochastic separation of Lagrangian trajectories is known as Richardson diffusion: one argues, with [Richardson \(1926\)](#), that the rate of change of the typical square distance Δr^2 between them is the turbulent diffusivity associated with velocities at the scale Δr :

$$\frac{d\Delta r^2}{dt} \sim D(\Delta r) \sim \delta u_{\Delta r}^2 \tau_c \sim \frac{\delta u_{\Delta r}^4}{\varepsilon} \sim \varepsilon^{1/3} \Delta r^{4/3}. \quad (\text{D } 98)$$

The last two steps follow from $\delta u_{\Delta r}^2 / \tau_c \sim \varepsilon$ and $\delta u_{\Delta r} \sim (\varepsilon \Delta r)^{1/3}$. The latter relation might appear to be valid only for standard K41 or GS95 turbulence (2.9). In fact, it is also valid for the aligned turbulence because the velocities in (D 98) must be in the direction of the particle separation Δr , so we must use the scaling of δu with ξ , not with λ —and that is always the Kolmogorov scaling, including for the aligned cascade [see (6.31)] and even for the tearing-mediated one (see § 7.2.3). Integrating (D 98) gets us “superdiffusion”:

$$\Delta r(t) \sim \varepsilon^{1/2} t^{3/2}, \quad (\text{D } 99)$$

as long as $\Delta r(t) < \lambda_{\text{CB}}$ (the outer scale of the strong turbulence), or, equivalently, as long as t is shorter than the nonlinear time τ_{nl} at scale λ_{CB} . A salient feature here is that $\Delta r(t)$ is independent of the initial separation, which can be arbitrarily small. Therefore, the width of the reconnecting sheet and the inflow speed are

$$\delta \sim \Delta r(t_{\text{out}}) \sim \varepsilon^{1/2} \left(\frac{\ell}{u_y} \right)^{3/2} \Rightarrow u_x \sim \frac{\delta}{\ell} u_y \sim \left(\frac{\varepsilon \ell}{u_y} \right)^{1/2}. \quad (\text{D } 100)$$

This result is all I need to work out what LV99 means for the theories of turbulent cascade presented in the main text. I will do this in appendices D.7.3 and D.7.4, to which a reader only interested in the effect of reconnection on turbulence can safely

[Loureiro et al. \(2009\)](#) did report fast reconnection in an SP sheet buffeted by 2D turbulence; [Kulpa-Dybel et al. \(2010\)](#) disagreed. A recent study by [Sun et al. \(2022\)](#) sides with [Loureiro et al. \(2009\)](#) but reports a scaling of the reconnection rate with the injected turbulent power that is less strong than the $\varepsilon^{1/2}$ originating from (D 100) and explained in detail in what follows. Note that a key (if possibly not sole) role in the acceleration of reconnection by turbulence in both [Loureiro et al. \(2009\)](#) and [Sun et al. \(2022\)](#) appeared to be played by the formation of plasmoids, encouraged by turbulence and thus setting in at a lower critical Lundquist number than in a laminar SP sheet [see (D 53)]. Thus, it is possible that what they see is, in fact, the kind of fast reconnection described in appendix D.6.

¹⁰⁷ [Eyink \(2015\)](#) takes another look at this topic, this time explaining in some mathematical detail how inertial-range motions and fields can be “coarse-grained” and shown to be subject to a kind of renormalised rate of reconnection controlled only by ideal MHD dynamics. The main idea is, I believe, as I summarised it in § 8.3.3—admittedly, in a simplistic, “coarse-grained” way.

skip. Appendices D.7.1 and D.7.2 are for those who are also interested in the effect of turbulence on reconnection,¹⁰⁸ and in the status of the numerical evidence on the subject.

D.7.1. Stochastic Reconnection Mediated by Strong Turbulence

LV99 formulated their prediction for the reconnection rate not in terms of its scaling with ε , as in (D 100), but with the Alfvénic Mach number, which, for the purposes of this exposition, I will define as

$$M_A \equiv \frac{\delta u_{L\perp}}{v_{Ay}}, \quad (\text{D } 101)$$

where v_{Ay} is the in-plane Alfvén speed associated with the upstream (reconnecting) magnetic field and $\delta u_{L\perp}$ is the turbulent velocity field at the outer scale L_\perp . How to express the prediction (D 100) in terms of M_A depends on how the turbulence is driven.

In LV99, it is driven weakly, so, using the standard WT scaling (4.7), they have

$$\delta u_{L\perp} \sim \left(\frac{\varepsilon v_A}{L_\parallel} \right)^{1/4} L_\perp^{1/2} \quad \Rightarrow \quad \varepsilon \sim \frac{\delta u_{L\perp}^4 L_\parallel}{v_A L_\perp^2} = M_A^4 \frac{v_A^4 L_\parallel}{v_A L_\perp^2}. \quad (\text{D } 102)$$

In their model, in fact, the driving is isotropic and the mean field is of the same order as the in-plane field: $L_\parallel \sim L_\perp \equiv L$ and $v_{Ay} \sim v_A$ (but $M_A \ll 1$, so the turbulence is indeed weak). This is outside the RMHD limit, but it is probably fine to extrapolate “twiddle” scalings to this regime: $\varepsilon \sim M_A^4 v_A^3 / L$. In what follows, I shall keep the anisotropic scaling (D 102) but show how the main results simplify in the isotropic case and reduce to LV99.

There are, obviously, two distinct possibilities: when L_\perp is much larger and much smaller than the sheet width δ . I shall deal with the latter in appendix D.7.2. In the former regime, the formula (D 100) applies if δ is small enough that turbulence is already

¹⁰⁸Let me mention very briefly another case for fast reconnection, made very vigorously in a number of recent papers by Boozer (2021, see references therein to precursor papers). The main idea is similar to LV99 and Eyink (2011): fast separation of trajectories and, therefore, of field lines, leads to accelerated reconnection. The difference is that Boozer is thinking of large-scale, system-specific motions and argues that those *laminar* flows, which nevertheless will generically have chaotic Lagrangian trajectories, are already very efficient mixers of any frozen-in, advected fields—temperature, generic passive scalar, magnetic field—and thus will do the job. The separation between trajectories is exponential in this case, at the rate $\gamma \sim u/\ell$, viz., $\Delta r(t) \sim \Delta r_0 e^{\gamma t}$. Since it depends on the initial separation, which has to be chosen to be the resistive scale, say, $\Delta r_0 \sim (\eta/\gamma)^{1/2}$, such a scheme would not help reconnection in a sheet: choosing $t_{\text{out}} \sim 1/\gamma$, we would just recover (D 97). However, Boozer wants us to abandon our fixation on reconnection in sheets, which he argues are a red herring, and instead think of generic 3D field configurations. He then estimates the reconnection timescale as the time when $\Delta r(\tau_{\text{rec}}) \sim \ell$, viz., $\tau_{\text{rec}} \sim \gamma^{-1} \ln(\ell/\Delta r_0) \sim (\ell/u) \ln Rm$. This is all fairly plausible—if he is actually wrong, that would be for some very subtle reason, e.g., if the things that a dynamically strong magnetic field had to do to a laminar chaotic flow to stop being amplified by it (see papers cited at the end of § 13.4.6) turned out also to impede the exponential separation of field lines. To be fair, Boozer & Elder (2021) did produce a specific example of a laminar flow that does what Boozer wants it to do, so his scheme appears to be realisable. However, in turbulent systems of the type that interests me here, I am not considering mean-flow effects on large scales, while on small scales, presumed aligned structures in RMHD limit are likely to have a tendency to collapse (or try to collapse) into sheets. Thus, the turbulent separation of trajectories, and field lines, according to (D 99) is a more relevant situation for me (and the validity of which Boozer does not reject).

in the strong regime at that scale, viz., if

$$L_{\perp} \gg \lambda_{CB} = \varepsilon^{1/2} \left(\frac{L_{\parallel}}{v_A} \right)^{3/2} \gtrsim \delta, \quad (\text{D } 103)$$

where the CB scale λ_{CB} is given by (4.3). Using (D 100), we find that the second inequality in (D 103) is equivalent to

$$\frac{\delta}{\lambda_{CB}} \sim \left(\frac{\ell v_A}{L_{\parallel} u_y} \right)^{3/2} \lesssim 1. \quad (\text{D } 104)$$

If this is true, then, even though turbulence is driven weakly at scale L_{\perp} , stochastic reconnection is mediated by strong turbulence at scale δ . Assuming (D 104) to be true and using (D 100) again, one gets the reconnection rate

$$\frac{u_x}{v_{Ay}} \sim M_A^2 \frac{v_{Ay} L_{\parallel}}{v_A L_{\perp}} \left(\frac{\ell v_A}{L_{\parallel} u_y} \right)^{1/2} \sim M_A^2 \left(\frac{\ell}{L} \right)^{1/2}, \quad (\text{D } 105)$$

the last expression having been obtained for the case of isotropic driving and taking also the outflow to be Alfvénic, $u_y \sim v_{Ay}$.

This is the well-known LV99 prediction $u_x \propto M_A^2$, which, to numericists, has all the attraction of a testable result. In a recent study by Yang *et al.* (2020), they tried to test it and found instead $u_x \propto M_A$, causing some concern about the validity of LV99. In fact, while their result disagrees with (D 105), it seems to me to be perfectly consistent with (D 100) if one can assume that motions comparable in size to the box-wide rms velocity exist on the scale of the sheet width—either because the sheet generates its own turbulence (as it does in such simulations when they are not externally driven: see § 7.4.3 and references therein), or because it is able locally to chop down the driven energy-containing motions to its own scale (Yang *et al.* 2020 did force their turbulence externally). Namely, let us assume that, effectively, for the sheet,

$$L_{\perp} \sim \lambda_{CB} \sim \delta \Rightarrow \frac{\ell}{u_y} \sim \frac{L_{\parallel}}{v_A}. \quad (\text{D } 106)$$

The latter relationship is a kind of CB: the time scale for the incoming matter and flux to be taken out of the sheet is the same as for an Alfvén wave to travel the correlation length along the guide field. Using $L_{\perp} \sim \lambda_{CB}$ in the strong-turbulence scaling (6.22), we get

$$\delta u_{L_{\perp}} \sim \left(\frac{\varepsilon L_{\parallel}}{v_A} \right)^{1/2} \Rightarrow \varepsilon \sim \frac{\delta u_{L_{\perp}}^2 v_A}{L_{\parallel}} \sim M_A^2 \frac{v_A v_{Ay}^2}{L_{\parallel}}. \quad (\text{D } 107)$$

The formula (D 100) now gives

$$\frac{u_x}{v_{Ay}} \sim M_A \left(\frac{\ell v_A}{L_{\parallel} u_y} \right)^{1/2} \sim M_A, \quad (\text{D } 108)$$

the last expression following from (D 106). This result is almost trivial: $u_x \sim \delta u_{L_{\perp}}$, so the sheet sucks in flux at the typical velocity of turbulent motions inside it.

D.7.2. Stochastic Reconnection Mediated by Weak Turbulence

Historically the first suite of confirmatory numerics for the LV99 theory was reported by Kowal *et al.* (2009, 2012) (usefully summarised by Lazarian *et al.* 2015), who, in their simulations of a macroscopic magnetic field reconnecting in the presence of externally injected turbulence, did indeed see the scaling $u_x \propto \varepsilon^{1/2}$, independent of η (figure 51).

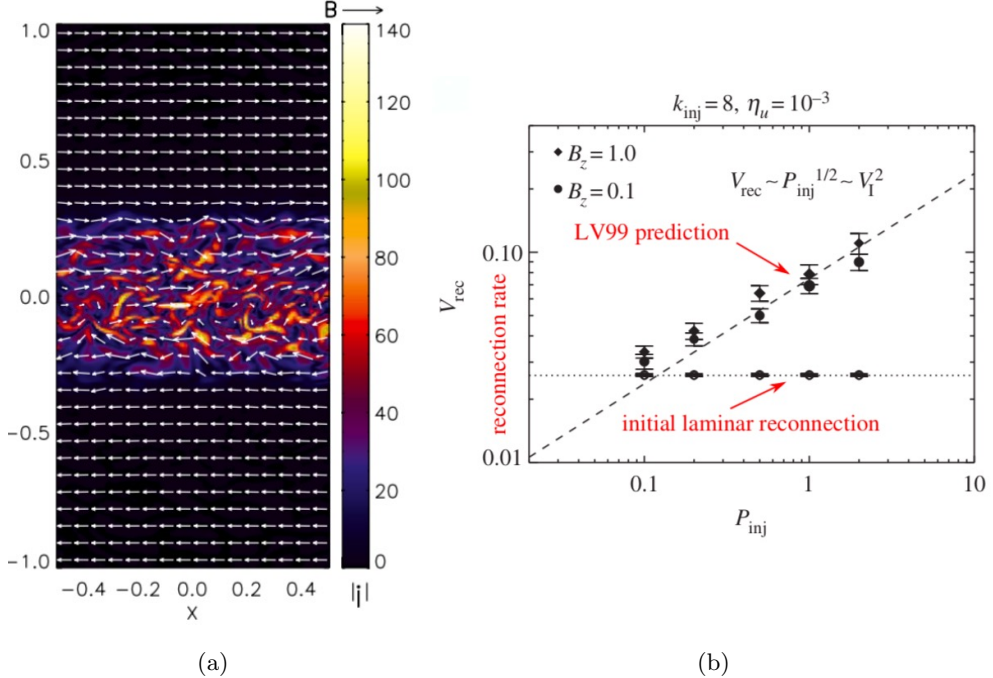


FIGURE 51. Simulations of stochastic reconnection by Kowal *et al.* (2009): (a) arrows are magnetic fields, colour shows (turbulent) currents; (b) reconnection rate V_{rec} vs. injected power P_{inj} , which, in my notation, are u_x and ε , respectively—this plot, taken from Lazarian *et al.* (2015), shows $u_x \propto \varepsilon^{1/2}$, in accordance with (D 111).

Most of their simulations, however, seem to be in the second regime considered by LV99, one in which $L_\perp \lesssim \delta$.

Since the turbulence that they are injecting into the sheet is still weak, and its scale is smaller than the width of the sheet, the expression for the turbulent diffusion coefficient used in (D 98) no longer applies (unless the sheet manages to generate its own turbulence, which, in their simulations, it does not appear to do—perhaps because it is quite short?). Instead, we have

$$\frac{d\Delta r^2}{dt} \sim D(L_\perp) \sim \frac{\delta u_{L_\perp}^2}{\tau_c \omega_A^2} \sim \frac{\varepsilon}{\omega_A^2}, \quad (\text{D 109})$$

where $\omega_A \sim v_A/L_\parallel$ is the Alfvén frequency and τ_c is the correlation time of WT [it is given by (4.5), but we do not need to know this to get to the last expression]. An easy way to understand why these two characteristic time scales appear in (D 109) in the way they do is as follows. The turbulent diffusion coefficient is just the time integral of the two-time correlation function of the velocity field, and we can calculate it by assuming a simple functional form for this correlation function characteristic of a slowly decorrelating but fast-oscillating wave field:

$$D \sim \int_0^\infty d\tau \langle \mathbf{u}_\perp(t) \cdot \mathbf{u}_\perp(t - \tau) \rangle \sim \delta u_{L_\perp}^2 \int_0^\infty d\tau e^{-\tau/\tau_c} \cos(\omega_A \tau) = \frac{\delta u_{L_\perp}^2}{\tau_c(\omega_A^2 + 1/\tau_c^2)}. \quad (\text{D 110})$$

In the absence of waves, or in CB ($\omega_A \sim \tau_c^{-1}$), one recovers the usual formula $D \sim \delta u_{L_\perp}^2 \tau_c$, analogous to (D 98), whereas for $\omega_A \gg \tau_c^{-1}$, one gets (D 109).

Thus, adopting (D 109), we get, in the same way as we did in (D 100),

$$\Delta r(t) \sim \frac{(\varepsilon t)^{1/2}}{\omega_A} \Rightarrow \delta \sim \left(\frac{\varepsilon \ell}{u_y} \right)^{1/2} \frac{L_{\parallel}}{v_A}, \quad u_x \sim \left(\frac{\varepsilon u_y}{\ell} \right)^{1/2} \frac{L_{\parallel}}{v_A}. \quad (\text{D 111})$$

With the aid of (D 102), the reconnection rate in terms of M_A becomes

$$\frac{u_x}{v_{Ay}} \sim M_A^2 \frac{v_{Ay} L_{\parallel}}{v_A L_{\perp}} \left(\frac{L_{\parallel} u_y}{\ell v_A} \right)^{1/2} \sim M_A^2 \left(\frac{L}{\ell} \right)^{1/2}, \quad (\text{D 112})$$

the last expression being for an isotropic forcing and Alfvénic outflows, as in (D 105). This prediction too appears in LV99, although derived by a slightly different route. Yet again, $u_x \propto \varepsilon^{1/2} \propto M_A^2$, which is what Kowal *et al.* (2009) confirmed (figure 51).

Note that in (D 109), the L_{\perp} dependence disappeared from the expression for turbulent diffusivity. This means that actually the above calculation remains valid also for $L_{\perp} \gg \delta$ —as long as $\delta \gg \lambda_{CB}$, i.e., as long as the turbulence is weak at the scale δ . In this case, one must replace L_{\perp} with $\Delta r(t)$ in (D 109), but the result is the same because, as we have just seen, $D(\Delta r)$ is independent of Δr for WT—the divergence of Lagrangian trajectories in WT is always just diffusive, Richardson superdiffusion (D 99) being a distinctive property of strong turbulence. Therefore, (D 112) only breaks down and transitions into (D 105) when λ_{CB} becomes comparable to δ , i.e., when (D 104) becomes true. In summary,

$$\frac{u_x}{v_{Ay}} \sim M_A^2 \frac{v_{Ay} L_{\parallel}}{v_A L_{\perp}} \min \left\{ \left(\frac{\ell v_A}{L_{\parallel} u_y} \right)^{1/2}, \left(\frac{L_{\parallel} u_y}{\ell v_A} \right)^{1/2} \right\}, \quad (\text{D 113})$$

the LV99 magic formula for the rate of stochastic reconnection, generalised to the case of anisotropic driving.

D.7.3. Stochastic Reconnection in GS95 Turbulence

Let us now apply (D 100) to a typical turbulent structure in which $\ell = \xi$ and $u_y \sim \delta u_{\xi} \sim (\varepsilon \xi)^{1/3}$. This instantly implies

$$\delta \sim \xi, \quad u_x \sim \delta u_{\xi}. \quad (\text{D 114})$$

For GS95 turbulence ($\xi \sim \lambda$), this means that reconnection of field lines within each “eddy” occurs on the same time scale as the “eddy” turns over—this is, I think, what Lazarian *et al.* (2015) mean when they say that stochastic reconnection makes GS95 turbulence “self-consistent”.

D.7.4. Stochastic Reconnection in Aligned Turbulence

What if the turbulence is aligned? According to my argument above, in view of (6.31), it might seem that (D 114) remains valid. This is worrisome: indeed this tells us that the width of the layer over which stochastic reconnection would be happening is larger than the width of the aligned structure: $\delta \sim \xi \gg \lambda$! If this were true, writing this review would have been a waste of time: aligned structures would be quickly broken up by stochastic reconnection, so there would be no aligned cascade. This would invalidate all of § 6 and, consequently, obviate any consideration of tearing-mediated turbulence in § 7—the cascade would just be GS95 all the way to the dissipation scale. Lazarian *et al.* (2015) (and their previous papers referenced therein) might then be excused for (politely) ignoring all the newfangled turbulence theory postdating GS95, and Beresnyak (2011, 2012a, 2014b, 2019) would be vindicated much more completely than I could offer to do

in § 7.2.2. I cannot prove formally that this does not or cannot happen (cf. § 8.2), but I can show that aligned turbulence is, in fact, not ruled out by stochastic reconnection.

Let us imagine that an aligned structure has emerged with transverse (to fluctuating fields) scale λ and longitudinal (fluctuation-direction) scale $\xi \gg \lambda$. In order for stochastic reconnection to destroy it quickly, there must be turbulent structures within the layer of width λ whose longitudinal scales are as large as $\sim \lambda$. But within this layer, there is an intense shear $\sim \delta u_\lambda / \lambda$, which should suppress any turbulent motions whose typical nonlinear time scales are longer than the inverse of this shear. For small enough structures, the nonlinear times will be short and eventually overcome the shear. Let us find the longitudinal scale ξ' of the largest possible such motions: their nonlinear decorrelation rate is

$$\frac{\delta u_{\xi'}}{\xi'} \sim \frac{\delta u_\lambda}{\lambda} \Rightarrow \frac{\xi'}{\lambda} \sim \left(\frac{\lambda}{\xi}\right)^{1/2} \sim \left(\frac{\lambda}{\lambda_{CB}}\right)^{1/8} \ll 1, \quad (\text{D } 115)$$

where I have used (6.31) for $\delta u_{\xi'} \sim (\varepsilon \xi')^{1/3}$ and $\delta u_\lambda = \delta u_\xi \sim (\varepsilon \xi)^{1/3}$.¹⁰⁹ If these motions are aligned in the usual way, with transverse scale λ' , then, using (6.31) again, $\lambda'/\lambda \sim (\lambda/\lambda_{CB})^{1/2}$.

Going back to (D 98), one must now integrate this equation up to time $t_{\text{out}} \sim \xi/\delta u_\xi \sim \varepsilon^{-1/3} \xi^{2/3}$, which is longer than the nonlinear time $\xi'/\delta u_{\xi'} \sim \varepsilon^{-1/3} \xi'^{2/3}$ of the largest turbulent structures within our layer. This gives conventional turbulent diffusion:

$$\delta \sim \Delta r(t_{\text{out}}) \sim \left(\varepsilon^{1/3} \xi'^{4/3} t_{\text{out}}\right)^{1/2} \sim \xi'^{2/3} \xi^{1/3} \sim \lambda, \quad (\text{D } 116)$$

where the last step follows from (D 115). Just like in (D 114), the width of the stochastically reconnecting layer is the same as the width of the (now aligned) structure, so the magnetic fields in the aligned cascade reconnect just as fast as the turbulent structures decorrelate. Thus, the aligned cascade is consistent with stochastic reconnection.

The same is going to be true of the tearing-mediated cascade of § 7.2 because, in the argument leading to (D 116), all I needed was the Kolmogorov scaling of the turbulent velocities in the fluctuation direction, which is always preserved (§ 7.2.3). The competition between the nonlinear decorrelation rate and the tearing rate that leads to disruption (§ 7.1) is unaffected by all this because disruption happens precisely at the scale where tearing becomes “ideal”. Any smaller-scale turbulence, ambient or created by the tearing, can presumably be viewed as providing seed perturbations for the instability.

The overall conclusion appears to be that stochastic reconnection, while a useful notion in the treatment of large-scale magnetic-field configurations with externally imposed turbulence, does not undermine (or modify) the existing theory of the aligned or tearing-mediated turbulence, but rather plays an interpretative role: it provides a further insight into the behaviour of tangled magnetic fields in a turbulent environment and reassures us that, whatever topological rearrangements are necessary for the cascade to proceed, they can always occur on the time scales of the cascade.

REFERENCES

- ABEL, I. G., PLUNK, G. G., WANG, E., BARNES, M., COWLEY, S. C., DORLAND, W. & SCHEKOCHIHIHIN, A. A. 2013 Multiscale gyrokinetics for rotating tokamak plasmas: fluctuations, transport and energy flows. *Rep. Prog. Phys.* **76**, 116201.
 ADKINS, T. & SCHEKOCHIHIHIN, A. A. 2018 A solvable model of Vlasov-kinetic plasma turbulence in Fourier-Hermite phase space. *J. Plasma Phys.* **84**, 905840107.

¹⁰⁹NB: ξ is a function of λ ; by δu_ξ , I mean δu_λ expressed in terms of ξ , not δu_λ taken at $\lambda = \xi$.

- ADKINS, T., SCHEKOCHIHIHIN, A. A., IVANOV, P. G. & ROACH, C. M. 2022 Electromagnetic instabilities and plasma turbulence driven by electron-temperature gradient. *J. Plasma Phys.*, in press; *E-print arXiv:2201.05670*.
- ALEXAKIS, A. & BRACHET, M.-E. 2019 On the thermal equilibrium state of large-scale flows. *J. Fluid Mech.* **872**, 594.
- ALFVÉN, H. 1942 Existence of electromagnetic-hydrodynamic waves. *Nature* **150**, 405.
- ALUIE, H. & EYINK, G. L. 2010 Scale locality of magnetohydrodynamic turbulence. *Phys. Rev. Lett.* **104**, 081101.
- AVSARKISOV, V. 2020 On the buoyancy subrange in stratified turbulence. *Atmosphere* **11**, 659.
- BAÑÓN NAVARRO, A., TEACA, B., TOLD, D., GROŠELJ, D., CRANDALL, P. & JENKO, F. 2016 Structure of plasma heating in gyrokinetic Alfvénic turbulence. *Phys. Rev. Lett.* **117**, 245101.
- BAGGALEY, A. W., SHUKUROV, A., BARENTHI, C. F. & SUBRAMANIAN, K. 2010 Fluctuation dynamo based on magnetic reconnections. *Astron. Nachr.* **331**, 46.
- BALBUS, S. A. 2004 Viscous shear instability in weakly magnetized, dilute plasmas. *Astrophys. J.* **616**, 857.
- BALKOVSKY, E., FOUXON, A. & LEBEDEV, V. 2001 Turbulence of polymer solutions. *Phys. Rev. E* **64**, 056301.
- BANDYOPADHYAY, R., MATTHAEUS, W. H., OUGHTON, S. & WAN, M. 2019 Evolution of similarity lengths in anisotropic magnetohydrodynamic turbulence. *J. Fluid Mech.* **876**, 5.
- BANERJEE, R. & JEDAMZIK, K. 2004 Evolution of cosmic magnetic fields: From the very early Universe, to recombination, to the present. *Phys. Rev. D* **70**, 123003.
- BARNES, M., PARRA, F. I. & SCHEKOCHIHIHIN, A. A. 2011 Critically balanced ion temperature gradient turbulence in fusion plasmas. *Phys. Rev. Lett.* **107**, 115003.
- BÁRTA, M., BÜCHNER, J., KARLICKÝ, M. & SKÁLA, J. 2011 Spontaneous current-layer fragmentation and cascading reconnection in solar flares. I. Model and analysis. *Astrophys. J.* **737**, 24.
- BÁRTA, M., SKÁLA, J., KARLICKÝ, M. & BÜCHNER, J. 2012 Energy cascades in large-scale solar flare reconnection. In *Multi-scale Dynamical Processes in Space and Astrophysical Plasmas* (ed. M. P. Leubner & Z. Vörös), p. 43. Berlin: Springer.
- BATCHELOR, G. K. 1950 On the spontaneous magnetic field in a conducting liquid in turbulent motion. *Proc. R. Soc. London A* **201**, 405.
- BATCHELOR, G. K. 1953 *The Theory of Homogeneous Turbulence*. Cambridge: Cambridge University Press.
- BATCHELOR, G. K. 1959 Small-scale variation of convected quantities like temperature in turbulent fluid. Part 1. General discussion and the case of small conductivity. *J. Fluid Mech.* **5**, 113.
- BATCHELOR, G. K. & PROUDMAN, I. 1956 The large-scale structure of homogeneous turbulence. *Philos. Trans. R. Soc. London A* **248**, 369.
- BEC, J. & KHANIN, K. 2007 Burgers turbulence. *Phys. Rep.* **447**, 1.
- BERERA, A. & LINKMANN, M. 2014 Magnetic helicity and the evolution of decaying magnetohydrodynamic turbulence. *Phys. Rev. E* **90**, 041003.
- BERESNYAK, A. 2011 The spectral slope and Kolmogorov constant of MHD turbulence. *Phys. Rev. Lett.* **106**, 075001.
- BERESNYAK, A. 2012a Basic properties of magnetohydrodynamic turbulence in the inertial range. *Mon. Not. R. Astron. Soc.* **422**, 3495.
- BERESNYAK, A. 2012b Simulations of nonlinear small-scale dynamo. Unpublished.
- BERESNYAK, A. 2012c Universal nonlinear small-scale dynamo. *Phys. Rev. Lett.* **108**, 035002.
- BERESNYAK, A. 2013 Comment on Perez et al [PRX 2, 041005 (2012), arXiv:1209.2011]. *E-print arXiv:1301.7425*.
- BERESNYAK, A. 2014a Reply to Comment on “Spectra of strong magnetohydrodynamic turbulence from high-resolution simulations”. *E-print arXiv:1410.0957*.
- BERESNYAK, A. 2014b Spectra of strong magnetohydrodynamic turbulence from high-resolution simulations. *Astrophys. J.* **784**, L20.
- BERESNYAK, A. 2015 On the parallel spectrum in magnetohydrodynamic turbulence. *Astrophys. J.* **801**, L9.

- BERESNYAK, A. 2017 Three-dimensional spontaneous magnetic reconnection. *Astrophys. J.* **834**, 47.
- BERESNYAK, A. 2019 MHD turbulence. *Living Rev. Comput. Astrophys.* **5**, 2.
- BERESNYAK, A. & LAZARIAN, A. 2006 Polarization intermittency and its influence on MHD turbulence. *Astrophys. J.* **640**, L175.
- BERESNYAK, A. & LAZARIAN, A. 2008 Strong imbalanced turbulence. *Astrophys. J.* **682**, 1070.
- BERESNYAK, A. & LAZARIAN, A. 2009a Comparison of spectral slopes of magnetohydrodynamic and hydrodynamic turbulence and measurements of alignment effects. *Astrophys. J.* **702**, 1190.
- BERESNYAK, A. & LAZARIAN, A. 2009b Structure of stationary strong imbalanced turbulence. *Astrophys. J.* **702**, 460.
- BERESNYAK, A. & LAZARIAN, A. 2010 Scaling laws and diffuse locality of balanced and imbalanced magnetohydrodynamic turbulence. *Astrophys. J.* **722**, L110.
- BERSHADSKII, A. 2019 Cross-helicity and extended inertial range in MHD turbulence. *E-print arXiv:1909.10992*.
- BHAT, P., ZHOU, M. & LOUREIRO, N. F. 2021 Inverse energy transfer in decaying, three dimensional, nonhelical magnetic turbulence due to magnetic reconnection. *Mon. Not. R. Astron. Soc.* **501**, 3074.
- BHATTACHARJEE, A., HUANG, Y.-M., YANG, H. & ROGERS, B. 2009 Fast reconnection in high-Lundquist-number plasmas due to the plasmoid instability. *Phys. Plasmas* **16**, 112102.
- BHATTACHARJEE, A. & NG, C. S. 2001 Random scattering and anisotropic turbulence of shear Alfvén wave packets. *Astrophys. J.* **548**, 318.
- BIAN, X. & ALUIE, H. 2019 Decoupled cascades of kinetic and magnetic energy in magnetohydrodynamic turbulence. *Phys. Rev. Lett.* **122**, 135101.
- BIERMANN, L. & SCHLÜTER, A. 1951 Cosmic radiation and cosmic magnetic fields. II. Origin of cosmic magnetic fields. *Phys. Rev.* **82**, 863.
- BIGOT, B. & GALTIER, S. 2011 Two-dimensional state in driven magnetohydrodynamic turbulence. *Phys. Rev. E* **83**, 026405.
- BISKAMP, D. 1982 Effect of secondary tearing instability on the coalescence of magnetic islands. *Phys. Lett. A* **87**, 357.
- BISKAMP, D. 1986 Magnetic reconnection via current sheets. *Phys. Fluids* **29**, 1520.
- BISKAMP, D. & BREMER, U. 1994 Dynamics and statistics of inverse cascade processes in 2D magnetohydrodynamic turbulence. *Phys. Rev. Lett.* **72**, 3819.
- BISKAMP, D. & MÜLLER, W.-C. 1999 Decay laws for three-dimensional magnetohydrodynamic turbulence. *Phys. Rev. Lett.* **83**, 2195.
- BISKAMP, D. & MÜLLER, W.-C. 2000 Scaling properties of three-dimensional isotropic magnetohydrodynamic turbulence. *Phys. Plasmas* **7**, 4889.
- BISKAMP, D. & WELTER, H. 1989 Dynamics of decaying two-dimensional magnetohydrodynamic turbulence. *Phys. Fluids B* **1**, 1964.
- BOLDYREV, S. 2002 Kolmogorov-Burgers model for star-forming turbulence. *Astrophys. J.* **569**, 841.
- BOLDYREV, S. 2005 On the spectrum of magnetohydrodynamic turbulence. *Astrophys. J.* **626**, L37.
- BOLDYREV, S. 2006 Spectrum of magnetohydrodynamic turbulence. *Phys. Rev. Lett.* **96**, 115002.
- BOLDYREV, S. & CATTANEO, F. 2004 Magnetic-field generation in Kolmogorov turbulence. *Phys. Rev. Lett.* **92**, 144501.
- BOLDYREV, S., CHEN, C. H. K., XIA, Q. & ZHDANKIN, V. 2015 Spectral breaks of Alfvénic turbulence in a collisionless plasma. *Astrophys. J.* **806**, 238.
- BOLDYREV, S., HORAITES, K., XIA, Q. & PEREZ, J. C. 2013 Toward a theory of astrophysical plasma turbulence at subproton scales. *Astrophys. J.* **777**, 41.
- BOLDYREV, S. & LOUREIRO, N. F. 2017 Magnetohydrodynamic turbulence mediated by reconnection. *Astrophys. J.* **844**, 125.
- BOLDYREV, S. & LOUREIRO, N. F. 2018 Calculations in the theory of tearing instability. *J. Phys. Conf. Ser.* **1100**, 012003.
- BOLDYREV, S. & LOUREIRO, N. F. 2019 Role of reconnection in inertial kinetic-Alfvén turbulence. *Phys. Rev. Res.* **1**, 012006(R).

- BOLDYREV, S. & LOUREIRO, N. F. 2020 Tearing instability in Alfvén and kinetic-Alfvén turbulence. *J. Geophys. Res.* **125**, A28185.
- BOLDYREV, S., MASON, J. & CATTANEO, F. 2009 Dynamic alignment and exact scaling laws in magnetohydrodynamic turbulence. *Astrophys. J.* **699**, L39.
- BOLDYREV, S., NORDLUND, Å. & PADOAN, P. 2002 Supersonic turbulence and structure of interstellar molecular clouds. *Phys. Rev. Lett.* **89**, 031102.
- BOLDYREV, S. & PEREZ, J. C. 2009 Spectrum of weak magnetohydrodynamic turbulence. *Phys. Rev. Lett.* **103**, 225001.
- BOLDYREV, S. & PEREZ, J. C. 2012 Spectrum of kinetic-Alfvén turbulence. *Astrophys. J.* **758**, L44.
- BOLDYREV, S., PEREZ, J. C., BOROVSKY, J. E. & PODESTA, J. J. 2011 Spectral scaling laws in magnetohydrodynamic turbulence simulations and in the solar wind. *Astrophys. J.* **741**, L19.
- BOLDYREV, S., PEREZ, J. C. & ZHDANKIN, V. 2012 Residual energy in MHD turbulence and in the solar wind. *AIP Conf. Proc.* **1436**, 18.
- BOOZER, A. H. 2021 Magnetic reconnection and thermal equilibration. *Phys. Plasmas* **28**, 032102.
- BOOZER, A. H. & ELDER, T. 2021 Example of exponentially enhanced magnetic reconnection driven by a spatially bounded and laminar ideal flow. *Phys. Plasmas* **28**, 062303.
- BOTT, A. F. A., ARZAMASSKIY, L., KUNZ, M. W., QUATAERT, E. & SQUIRE, J. 2021a Adaptive critical balance and firehose instability in an expanding, turbulent, collisionless plasma. *Astrophys. J.* **922**, L35.
- BOTT, A. F. A., CHEN, L., TZEFERACOS, P., PALMER, C. A. J., BELL, A. R., BINGHAM, R., BIRKEL, A., FROUZA, D. H., KATZ, J., KUNZ, M. W., LI, C.-K., PARK, H.-S., PETRASSO, R., ROSS, J. S., REVILLE, B., RYU, D., SÉGUIN, F. H., WHITE, T. G., SCHEKOCHIHIN, A. A., LAMB, D. Q. & GREGORI, G. 2022 Insensitivity of a turbulent laser-plasma dynamo to initial conditions. *Matter Radiat. Extremes* **7**, 046901.
- BOTT, A. F. A., TZEFERACOS, P., CHEN, L., PALMER, C. A. J., RIGBY, A., BELL, A. R., BINGHAM, R., BIRKEL, A., GRAZIANI, C., FROUZA, D. H., KATZ, J., KOENIG, M., KUNZ, M. W., LI, C., MEINECKE, J., MINIATI, F., PETRASSO, R., PARK, H.-S., REMINGTON, B. A., REVILLE, B., ROSS, J. S., RYU, D., RYUTOV, D., SÉGUIN, F. H., WHITE, T. G., SCHEKOCHIHIN, A. A., LAMB, D. Q. & GREGORI, G. 2021b Time-resolved turbulent dynamo in a laser plasma. *Proc. Nat. Acad. Sci.* **118**, 2015729118.
- BOWEN, T. A., BADMAN, S. T., BALE, S. D., DUDOK DE WIT, T., HORBURY, T. S., KLEIN, K. G., LARSON, D., MALLET, A., MATTEINI, L., McMANUS, M. D. & SQUIRE, J. 2021 Nonlinear interactions in spherically polarized Alfvénic turbulence. *E-print arXiv:2110.11454*.
- BOWEN, T. A., MALLET, A., BONNELL, J. W. & BALE, S. D. 2018 Impact of residual energy on solar wind turbulent spectra. *Astrophys. J.* **865**, 45.
- BRAGINSKII, S. I. 1965 Transport processes in a plasma. *Rev. Plasma Phys.* **1**, 205.
- BRANDENBURG, A. 2001 The inverse cascade and nonlinear alpha-effect in simulations of isotropic helical hydromagnetic turbulence. *Astrophys. J.* **550**, 824.
- BRANDENBURG, A. 2011 Nonlinear small-scale dynamos at low magnetic Prandtl numbers. *Astrophys. J.* **741**, 92.
- BRANDENBURG, A. 2014 Magnetic Prandtl number dependence of the kinetic-to-magnetic dissipation ratio. *Astrophys. J.* **791**, 12.
- BRANDENBURG, A., HAUGEN, N. E. L., LI, X.-Y. & SUBRAMANIAN, K. 2018 Varying the forcing scale in low Prandtl number dynamos. *Mon. Not. R. Astron. Soc.* **479**, 2827.
- BRANDENBURG, A. & KAHNIASHVILI, T. 2017 Classes of hydrodynamic and magnetohydrodynamic turbulent decay. *Phys. Rev. Lett.* **118**, 055102.
- BRANDENBURG, A., KAHNIASHVILI, T., MANDAL, S., POL, A. R., TEVZADZE, A. G. & VACHASPATI, T. 2019 Dynamo effect in decaying helical turbulence. *Phys. Rev. Fluids* **4**, 024608.
- BRANDENBURG, A., KAHNIASHVILI, T. & TEVZADZE, A. G. 2015 Nonhelical inverse transfer of a decaying turbulent magnetic field. *Phys. Rev. Lett.* **114**, 075001.
- BRANDENBURG, A. & REMPEL, M. 2019 Reversed dynamo at small scales and large magnetic Prandtl number. *Astrophys. J.* **879**, 57.

- BRANDENBURG, A. & SUBRAMANIAN, K. 2005 Astrophysical magnetic fields and nonlinear dynamo theory. *Phys. Rep.* **417**, 1.
- BRUNO, R. & CARBONE, V. 2013 The solar wind as a turbulence laboratory. *Living Rev. Solar Phys.* **10**, 2.
- BULANOV, S. V., SAKAI, J. & SYROVATSKII, S. I. 1979 Tearing-mode instability in approximately steady MHD configurations. *Sov. J. Plasma Phys.* **5**, 280.
- BULANOV, S. V., SYROVATSKII, S. I. & SAKAI, J. 1978 Stabilizing influence of plasma flow on dissipative tearing instability. *Sov. Phys.-JETP Lett.* **28**, 177.
- BUSSE, A., MÜLLER, W.-C., HOMANN, H. & GRAUER, R. 2007 Statistics of passive tracers in three-dimensional magnetohydrodynamic turbulence. *Phys. Plasmas* **14**, 122303.
- CAMPANELLI, L. 2004 Scaling laws in magnetohydrodynamic turbulence. *Phys. Rev. D* **70**, 083009.
- CARBONE, V., VELTRI, P. & MANGENEY, A. 1990 Coherent structure formation and magnetic field line reconnection in magnetohydrodynamic turbulence. *Phys. Fluids A* **2**, 1487.
- CASSAK, P. A. & DRAKE, J. F. 2009 The impact of microscopic magnetic reconnection on pre-flare energy storage. *Astrophys. J.* **707**, L158.
- CASSAK, P. A., SHAY, M. A. & DRAKE, J. F. 2009 Scaling of Sweet-Parker reconnection with secondary islands. *Phys. Plasmas* **16**, 120702.
- CATTANEO, F., HUGHES, D. W. & KIM, E.-J. 1996 Suppression of chaos in a simplified nonlinear dynamo model. *Phys. Rev. Lett.* **76**, 2057.
- CATTANEO, F. & TOBIAS, S. M. 2009 Dynamo properties of the turbulent velocity field of a saturated dynamo. *J. Fluid Mech.* **621**, 205.
- CERRI, S. S. & CALIFANO, F. 2017 Reconnection and small-scale fields in 2D-3V hybrid-kinetic driven turbulence simulations. *New J. Phys.* **19**, 025007.
- CERRI, S. S., KUNZ, M. W. & CALIFANO, F. 2018 Dual phase-space cascades in 3D hybrid-Vlasov-Maxwell turbulence. *Astrophys. J.* **856**, L13.
- CHANDRAN, B. D. G. 1997 *Ph. D. Thesis*. Princeton University.
- CHANDRAN, B. D. G. 2008 Strong anisotropic MHD turbulence with cross helicity. *Astrophys. J.* **685**, 646.
- CHANDRAN, B. D. G., LI, B., ROGERS, B. N., QUATAERT, E. & GERMASCHEWSKI, K. 2010 Perpendicular ion heating by low-frequency Alfvén-wave turbulence in the solar wind. *Astrophys. J.* **720**, 503.
- CHANDRAN, B. D. G. & PEREZ, J. C. 2019 Reflection-driven magnetohydrodynamic turbulence in the solar atmosphere and solar wind. *J. Plasma Phys.* **85**, 905850409.
- CHANDRAN, B. D. G., SCHEKOCHIHIN, A. A. & MALLET, A. 2015 Intermittency and alignment in strong RMHD turbulence. *Astrophys. J.* **807**, 39.
- CHAPMAN, S. & KENDALL, P. C. 1963 Liquid instability and energy transformation near a magnetic neutral line: a soluble non-linear hydromagnetic problem. *Proc. R. Soc. London A* **271**, 435.
- CHAVANIS, P.-H. 2021 Kinetic theory of collisionless relaxation for systems with long-range interactions. *E-print arXiv:2112.13664*.
- CHEN, C. H. K. 2016 Recent progress in astrophysical plasma turbulence from solar wind observations. *J. Plasma Phys.* **82**, 535820602.
- CHEN, C. H. K., BALE, S. D., BONNELL, J. W., BOROVIKOV, D., BOWEN, T. A., BURGESS, D., CASE, A. W., CHANDRAN, B. D. G., DUDOK DE WIT, T., GOETZ, K., HARVEY, P. R., KASPER, J. C., KLEIN, K. G., KORRECK, K. E., LARSON, D., LIVI, R., MACDOWALL, R. J., MALASPINA, D. M., MALLET, A., McMANUS, M. D., MONCUQUET, M., PULUPA, M., STEVENS, M. L. & WHITTLESEY, P. 2020 The evolution and role of solar wind turbulence in the inner heliosphere. *Astrophys. J. Suppl.* **246**, 53.
- CHEN, C. H. K., BALE, S. D., SALEM, C. S. & MARUCA, B. A. 2013 Residual energy spectrum of solar wind turbulence. *Astrophys. J.* **770**, 125.
- CHEN, C. H. K. & BOLDYREV, S. 2017 Nature of kinetic scale turbulence in the Earth's magnetosheath. *Astrophys. J.* **842**, 122.
- CHEN, C. H. K., KLEIN, K. G. & HOWES, G. G. 2019 Evidence for electron Landau damping in space plasma turbulence. *Nature Comm.* **10**, 740.
- CHEN, C. H. K., LEUNG, L., BOLDYREV, S., MARUCA, B. A. & BALE, S. D. 2014a Ion-scale

- spectral break of solar wind turbulence at high and low beta. *Geophys. Res. Lett.* **41**, 8081.
- CHEN, C. H. K., MALLET, A., SCHEKOCHIHIN, A. A., HORBURY, T. S., WICKS, R. T. & BALE, S. D. 2012 Three-dimensional structure of solar wind turbulence. *Astrophys. J.* **758**, 120.
- CHEN, C. H. K., MALLET, A., YOUSEF, T. A., SCHEKOCHIHIN, A. A. & HORBURY, T. S. 2011 Anisotropy of Alfvénic turbulence in the solar wind and numerical simulations. *Mon. Not. R. Astron. Soc.* **415**, 3219.
- CHEN, C. H. K., SORRISO-VALVO, L., ŠAFRÁNKOVÁ, J. & NĚMEČEK, Z. 2014b Intermittency of solar wind density fluctuations from ion to electron scales. *Astrophys. J.* **789**, L8.
- CHEN, X. L. & MORRISON, P. J. 1990 Resistive tearing instability with equilibrium shear flow. *Phys. Fluids B* **2**, 495.
- CHERNOGLAZOV, A., RIPPERDA, B. & PHILIPPOV, A. 2021 Dynamic alignment and plasmoid formation in relativistic magnetohydrodynamic turbulence. *Astrophys. J.* **923**, L13.
- CHO, J. 2011 Magnetic helicity conservation and inverse energy cascade in electron magnetohydrodynamic wave packets. *Phys. Rev. Lett.* **106**, 191104.
- CHO, J. & KIM, H. 2016 Spectral evolution of helical electron magnetohydrodynamic turbulence. *J. Geophys. Res. A* **121**, 6157.
- CHO, J. & LAZARIAN, A. 2002 Compressible sub-Alfvénic MHD turbulence in low- β plasmas. *Phys. Rev. Lett.* **88**, 245001.
- CHO, J. & LAZARIAN, A. 2003 Compressible magnetohydrodynamic turbulence: mode coupling, scaling relations, anisotropy, viscosity-damped regime and astrophysical implications. *Mon. Not. R. Astron. Soc.* **345**, 325.
- CHO, J. & LAZARIAN, A. 2004 The anisotropy of electron magnetohydrodynamic turbulence. *Astrophys. J.* **615**, L41.
- CHO, J., LAZARIAN, A. & VISHNIAC, E. T. 2002a New regime of magnetohydrodynamic turbulence: Cascade below the viscous cutoff. *Astrophys. J.* **566**, L49.
- CHO, J., LAZARIAN, A. & VISHNIAC, E. T. 2002b Simulations of magnetohydrodynamic turbulence in a strongly magnetized medium. *Astrophys. J.* **564**, 291.
- CHO, J., LAZARIAN, A. & VISHNIAC, E. T. 2003 Ordinary and viscosity-damped magnetohydrodynamic turbulence. *Astrophys. J.* **595**, 812.
- CHO, J. & RYU, D. 2009 Characteristic lengths of magnetic field in magnetohydrodynamic turbulence. *Astrophys. J.* **705**, L90.
- CHO, J. & VISHNIAC, E. T. 2000 The anisotropy of magnetohydrodynamic Alfvénic turbulence. *Astrophys. J.* **539**, 273.
- CHO, J., VISHNIAC, E. T., BERESNYAK, A., LAZARIAN, A. & RYU, D. 2009 Growth of magnetic fields induced by turbulent motions. *Astrophys. J.* **693**, 1449.
- CHRISTENSSON, M., HINDMARSH, M. & BRANDENBURG, A. 2001 Inverse cascade in decaying three-dimensional magnetohydrodynamic turbulence. *Phys. Rev. E* **64**, 056405.
- CHRISTENSSON, M., HINDMARSH, M. & BRANDENBURG, A. 2005 Scaling laws in decaying helical hydromagnetic turbulence. *Astron. Nachr.* **326**, 393.
- COMISSO, L. & GRASSO, D. 2016 Visco-resistive plasmoid instability. *Phys. Plasmas* **23**, 032111.
- COMISSO, L., HUANG, Y.-M., LINGAM, M., HIRVIJOKI, E. & BHATTACHARJEE, A. 2018 Magnetohydrodynamic turbulence in the plasmoid-mediated regime. *Astrophys. J.* **854**, 103.
- COMISSO, L., LINGAM, M., HUANG, Y.-M. & BHATTACHARJEE, A. 2016 General theory of the plasmoid instability. *Phys. Plasmas* **23**, 100702.
- COMISSO, L., LINGAM, M., HUANG, Y.-M. & BHATTACHARJEE, A. 2017 Plasmoid instability in forming current sheets. *Astrophys. J.* **850**, 142.
- COMISSO, L. & SIRONI, L. 2018 Particle acceleration in relativistic plasma turbulence. *Phys. Rev. Lett.* **121**, 255101.
- COMISSO, L. & SIRONI, L. 2021 Pitch-angle anisotropy controls particle acceleration and cooling in radiative relativistic plasma turbulence. *Phys. Rev. Lett.* **127**, 255102.
- COPPI, B., GALVÃO, R., PELLAT, R., ROSENBLUTH, M. & RUTHERFORD, P. 1976 Resistive internal kink modes. *Sov. J. Plasma Phys.* **2**, 961.
- CORRSIN, S. 1963 Estimates of the relations between Eulerian and Lagrangian scales in large Reynolds number turbulence. *J. Atmos. Sci.* **20**, 115.

- DAHLBURG, R. B., ZANG, T. A. & MONTGOMERY, D. 1986 Unstable transition properties of the driven magnetohydrodynamic sheet pinch. *J. Fluid Mech.* **169**, 71.
- DALDORFF, L. K. S., LEAKE, J. E. & KLIMCHUK, J. A. 2022 Impact of 3D structure on magnetic reconnection. *Astrophys. J.* **927**, 196.
- DALLAS, V. & ALEXAKIS, A. 2013a Origins of the k^{-2} spectrum in decaying Taylor-Green magnetohydrodynamic turbulent flows. *Phys. Rev. E* **88**, 053014.
- DALLAS, V. & ALEXAKIS, A. 2013b Symmetry breaking of decaying magnetohydrodynamic Taylor-Green flows and consequences for universality. *Phys. Rev. E* **88**, 063017.
- DALLAS, V. & ALEXAKIS, A. 2014 The signature of initial conditions on magnetohydrodynamic turbulence. *Astrophys. J.* **788**, L36.
- DAUGHTON, W., ROYTERSHTEYN, V., ALBRIGHT, B. J., KARIMABADI, H., YIN, L. & BOWERS, K. J. 2009a Influence of Coulomb collisions on the structure of reconnection layers. *Phys. Plasmas* **16**, 072117.
- DAUGHTON, W., ROYTERSHTEYN, V., ALBRIGHT, B. J., KARIMABADI, H., YIN, L. & BOWERS, K. J. 2009b Transition from collisional to kinetic regimes in large-scale reconnection layers. *Phys. Rev. Lett.* **103**, 065004.
- DAVIDSON, P. A. 2013 *Turbulence in Rotating, Stratified and Electrically Conducting Fluids*. Cambridge: Cambridge University Press.
- DAVIDSON, P. A. 2015 *Turbulence: An Introduction for Scientists and Engineers*. Oxford: Oxford University Press.
- DEL SARTO, D. & OTTAVIANI, M. 2017 Secondary fast reconnecting instability in the sawtooth crash. *Phys. Plasmas* **24**, 012102.
- DEL ZANNA, L., LANDI, S., PAPINI, E., PUCCI, F. & VELLI, M. 2016 The ideal tearing mode: theory and resistive MHD simulations. *J. Phys. Conf. Ser.* **719**, 012016.
- DOBROWOLNY, M., MANGENEY, A. & VELTRI, P. 1980 Fully developed anisotropic hydromagnetic turbulence in interplanetary space. *Phys. Rev. Lett.* **45**, 144.
- DOBROWOLNY, M., VELTRI, P. & MANGENEY, A. 1983 Dissipative instabilities of magnetic neutral layers with velocity shear. *J. Plasma Phys.* **29**, 393.
- DONG, C., WANG, L., COMISSO, L., HUANG, Y.-M. & BHATTACHARJEE, A. 2021 MHD turbulence mediated by the plasmoid instability. 63rd Annual Meeting of the APS Division of Plasma Physics, Pittsburgh, 8–12 November 2021, Abstract J09.00005.
- DONG, C., WANG, L., HUANG, Y.-M., COMISSO, L. & BHATTACHARJEE, A. 2018 Role of the plasmoid instability in magnetohydrodynamic turbulence. *Phys. Rev. Lett.* **121**, 165101.
- DUBRULLE, B. 1994 Intermittency in fully developed turbulence: Log-Poisson statistics and generalized scale covariance. *Phys. Rev. Lett.* **73**, 959.
- DUPREE, T. H. 1972 Theory of phase space density granulation in plasma. *Phys. Fluids* **15**, 334.
- EGEDAL, J., LE, A. & DAUGHTON, W. 2013 A review of pressure anisotropy caused by electron trapping in collisionless plasma, and its implications for magnetic reconnection. *Phys. Plasmas* **20**, 061201.
- EINAUDI, G. & RUBINI, F. 1986 Resistive instabilities in a flowing plasma. I. Inviscid case. *Phys. Fluids* **29**, 2563.
- EINAUDI, G. & RUBINI, F. 1989 Resistive instabilities in a flowing plasma. II. Effects of viscosity. *Phys. Fluids B* **1**, 2224.
- ELSASSER, W. M. 1950 The hydromagnetic equations. *Phys. Rev.* **79**, 183.
- EVENT HORIZON TELESCOPE COLLABORATION 2019 First M87 Event Horizon Telescope results. V. Physical origin of the asymmetric ring. *Astrophys. J.* **875**, L5.
- EWART, R. J., BROWN, A., ADKINS, T. & SCHEKOCHIHIN, A. A. 2022 Collisionless relaxation of a Lynden-Bell plasma. *E-print arXiv:2201.03376*.
- EYINK, G., VISHNIAC, E., LALESCU, C., ALUIE, H., KANOV, K., BÜRGER, K., BURNS, R., MENEVEAU, C. & SZALAY, A. 2013 Flux-freezing breakdown in high-conductivity magnetohydrodynamic turbulence. *Nature* **497**, 466.
- EYINK, G. L. 2009 Stochastic line motion and stochastic flux conservation for nonideal hydromagnetic models. *J. Math. Phys.* **50**, 083102.
- EYINK, G. L. 2011 Stochastic flux freezing and magnetic dynamo. *Phys. Rev. E* **83**, 056405.
- EYINK, G. L. 2015 Turbulent general magnetic reconnection. *Astrophys. J.* **807**, 137.

- EYINK, G. L. 2018 Cascades and dissipative anomalies in nearly collisionless plasma turbulence. *Phys. Rev. X* **8**, 041020.
- EYINK, G. L., LAZARIAN, A. & VISHNIAC, E. T. 2011 Fast magnetic reconnection and spontaneous stochasticity. *Astrophys. J.* **743**, 51.
- FAN, Q.-L., FENG, X.-S. & XIANG, C.-Q. 2004 Magnetohydrodynamic simulations of turbulent magnetic reconnection. *Phys. Plasmas* **11**, 5605.
- FATHALI, M. & KHOEI, S. 2019 Spectral energy transfer in a viscoelastic homogeneous isotropic turbulence. *Phys. Fluids* **31**, 095105.
- FOUXON, A. & LEBEDEV, V. 2003 Spectra of turbulence in dilute polymer solutions. *Phys. Fluids* **15**, 2060.
- FOWLER, T. K. 1968 Thermodynamics of unstable plasmas. *Adv. Plasma Phys.* **1**, 201.
- FRANCI, L., CERRI, S. S., CALIFANO, F., LANDI, S., PAPINI, E., VERDINI, A., MATTEINI, L., JENKO, F. & HELLINGER, P. 2017 Magnetic reconnection as a driver for a sub-ion-scale cascade in plasma turbulence. *Astrophys. J.* **850**, L16.
- FRANCI, L., LANDI, S., VERDINI, A., MATTEINI, L. & HELLINGER, P. 2018 Solar wind turbulent cascade from MHD to sub-ion scales: large-size 3D hybrid particle-in-cell simulations. *Astrophys. J.* **853**, 26.
- FRENKEL, A. & LEVICH, E. 1983 “Statistical helicity invariant” and decay of inertial turbulence. *Phys. Lett. A* **98**, 25.
- FRICK, P. & STEPANOV, R. 2010 Long-term free decay of MHD turbulence. *Europhys. Lett.* **92**, 34007.
- FRISCH, U. 1995 *Turbulence: The Legacy of A. N. Kolmogorov*. Cambridge: Cambridge University Press.
- FURTH, H. P., KILLEEN, J. & ROSENBLUTH, M. N. 1963 Finite-resistivity instabilities of a sheet pinch. *Phys. Fluids* **6**, 459.
- GALISHNIKOVA, A. K., KUNZ, M. W. & SCHEKOCHIHIN, A. A. 2022 Tearing instability and current-sheet disruption in the turbulent dynamo. *E-print arXiv:2201.07757*.
- GALTIER, S., NAZARENKO, S. V., NEWELL, A. C. & POUQUET, A. 2000 A weak turbulence theory for incompressible magnetohydrodynamics. *J. Plasma Phys.* **63**, 447.
- GOGOBERIDZE, G., CHAPMAN, S. C. & HNAT, B. 2012 Generation of residual energy in the turbulent solar wind. *Phys. Plasmas* **19**, 102310.
- GOLDREICH, P. & SRIDHAR, S. 1995 Toward a theory of interstellar turbulence. 2: Strong Alfvénic turbulence. *Astrophys. J.* **438**, 763.
- GOLDREICH, P. & SRIDHAR, S. 1997 Magnetohydrodynamic turbulence revisited. *Astrophys. J.* **485**, 680.
- GRAPPIN, R., FRISCH, U., POUQUET, A. & LEORAT, J. 1982 Alfvénic fluctuations as asymptotic states of MHD turbulence. *Astron. Astrophys.* **105**, 6.
- GRAPPIN, R., LEORAT, J. & POUQUET, A. 1983 Dependence of MHD turbulence spectra on the velocity field-magnetic field correlation. *Astron. Astrophys.* **126**, 51.
- GRAPPIN, R., MÜLLER, W.-C. & VERDINI, A. 2016 Alfvén-dynamo balance and magnetic excess in magnetohydrodynamic turbulence. *Astron. Astrophys.* **589**, A131.
- GRAUER, R., KRUG, J. & MARLIANI, C. 1994 Scaling of high-order structure functions in magnetohydrodynamic turbulence. *Phys. Lett. A* **195**, 335.
- GRECO, A., PERRI, S., SERVIDIO, S., YORDANOVA, E. & VELTRI, P. 2016 The complex structure of magnetic field discontinuities in the turbulent solar wind. *Astrophys. J.* **823**, L39.
- GRETE, P., O’SHEA, B. W. & BECKWITH, K. 2021 As a matter of tension: kinetic energy spectra in MHD turbulence. *Astrophys. J.* **909**, 148.
- GRETE, P., O’SHEA, B. W., BECKWITH, K., SCHMIDT, W. & CHRISTLIEB, A. 2017 Energy transfer in compressible magnetohydrodynamic turbulence. *Phys. Plasmas* **24**, 092311.
- GROŠELJ, D., CHEN, C. H. K., MALLET, A., SAMTANEY, R., SCHNEIDER, K. & JENKO, F. 2019 Kinetic turbulence in astrophysical plasmas: waves and/or structures? *Phys. Rev. X* **9**, 031037.
- GRUZINOV, A. V. & DIAMOND, P. H. 1996 Nonlinear mean field electrodynamics of turbulent dynamos. *Phys. Plasmas* **3**, 1853.
- HANKLA, A. M., ZHDANKIN, V., WERNER, G. R., UZDENSKY, D. A. & BEGELMAN, M. C.

- 2022 Kinetic simulations of imbalanced turbulence in a relativistic plasma: net flow and particle acceleration. *Mon. Not. R. Astron. Soc.* **509**, 3826.
- HARE, J. D., LEBEDEV, S. V., SUTTLE, L. G., LOUREIRO, N. F., CIARDI, A., BURDIAK, G. C., CHITTENDEN, J. P., CLAYSON, T., EARDLEY, S. J., GARCIA, C., HALLIDAY, J. W. D., NIASSE, N., ROBINSON, T., SMITH, R. A., STUART, N., SUZUKI-VIDAL, F., SWADLING, G. F., MA, J. & WU, J. 2017a Formation and structure of a current sheet in pulsed-power driven magnetic reconnection experiments. *Phys. Plasmas* **24**, 102703.
- HARE, J. D., SUTTLE, L., LEBEDEV, S. V., LOUREIRO, N. F., CIARDI, A., BURDIAK, G. C., CHITTENDEN, J. P., CLAYSON, T., GARCIA, C., NIASSE, N., ROBINSON, T., SMITH, R. A., STUART, N., SUZUKI-VIDAL, F., SWADLING, G. F., MA, J., WU, J. & YANG, Q. 2017b Anomalous heating and plasmoid formation in a driven magnetic reconnection experiment. *Phys. Rev. Lett.* **118**, 085001.
- HARE, J. D., SUTTLE, L. G., LEBEDEV, S. V., LOUREIRO, N. F., CIARDI, A., CHITTENDEN, J. P., CLAYSON, T., EARDLEY, S. J., GARCIA, C., HALLIDAY, J. W. D., ROBINSON, T., SMITH, R. A., STUART, N., SUZUKI-VIDAL, F. & TUBMAN, E. R. 2018 An experimental platform for pulsed-power driven magnetic reconnection. *Phys. Plasmas* **25**, 055703.
- HARRIS, E. G. 1962 On a plasma sheath separating regions of oppositely directed magnetic field. *Nuovo Cimento* **23**, 115.
- HATORI, T. 1984 Kolmogorov-style argument for the decaying homogeneous MHD turbulence. *J. Phys. Soc. Japan* **53**, 2539.
- HAUGEN, N. E., BRANDENBURG, A. & DOBLER, W. 2004 Simulations of nonhelical hydromagnetic turbulence. *Phys. Rev. E* **70**, 016308.
- HAUGEN, N. E. L., BRANDENBURG, A. & DOBLER, W. 2003 Is nonhelical hydromagnetic turbulence peaked at small scales? *Astrophys. J.* **597**, L141.
- HEINEMANN, T., McWILLIAMS, J. C. & SCHEKOCHIHIN, A. A. 2011 Large-scale magnetic field generation by randomly forced shearing waves. *Phys. Rev. Lett.* **107**, 255004.
- HIGDON, J. C. 1984 Density fluctuations in the interstellar medium: evidence for anisotropic magnetogasdynamic turbulence. I — Model and astrophysical sites. *Astrophys. J.* **285**, 109.
- HOFMAN, I. 1975 Resistive tearing modes in a sheet pinch with shear flow. *Plasma Phys.* **17**, 143.
- HORBURY, T. S., FORMAN, M. & OUGHTON, S. 2008 Anisotropic scaling of magnetohydrodynamic turbulence. *Phys. Rev. Lett.* **101**, 175005.
- HOSKING, D. N. & SCHEKOCHIHIN, A. A. 2021 Reconnection-controlled decay of magnetohydrodynamic turbulence and the role of invariants. *Phys. Rev. X* **11**, 041005.
- HOSKING, D. N. & SCHEKOCHIHIN, A. A. 2022a Cosmic-void observations reconciled with primordial magnetogenesis. *E-print* arXiv:2203.03573.
- HOSKING, D. N. & SCHEKOCHIHIN, A. A. 2022b Emergence of long-range correlations and thermal spectra in forced turbulence. *E-print* arXiv:2202.00462.
- HOSKING, D. N., SCHEKOCHIHIN, A. A. & BALBUS, S. A. 2020 Elasticity of tangled magnetic fields. *J. Plasma Phys.* **86**, 905860511.
- HOSSAIN, M., GRAY, P. C., PONTIUS, JR., D. H., MATTHAEUS, W. H. & OUGHTON, S. 1995 Phenomenology for the decay of energy-containing eddies in homogeneous MHD turbulence. *Phys. Fluids* **7**, 2886.
- HOWES, G. G. 2016 The dynamical generation of current sheets in astrophysical plasma turbulence. *Astrophys. J.* **827**, L28.
- HOWES, G. G., COWLEY, S. C., DORLAND, W., HAMMETT, G. W., QUATAERT, E. & SCHEKOCHIHIN, A. A. 2006 Astrophysical gyrokinetics: basic equations and linear theory. *Astrophys. J.* **651**, 590.
- HUANG, Y.-M. & BHATTACHARJEE, A. 2010 Scaling laws of resistive magnetohydrodynamic reconnection in the high-Lundquist-number, plasmoid-unstable regime. *Phys. Plasmas* **17**, 062104.
- HUANG, Y.-M. & BHATTACHARJEE, A. 2012 Distribution of plasmoids in high-Lundquist-number magnetic reconnection. *Phys. Rev. Lett.* **109**, 265002.
- HUANG, Y.-M. & BHATTACHARJEE, A. 2013 Plasmoid instability in high-Lundquist-number magnetic reconnection. *Phys. Plasmas* **20**, 055702.

- HUANG, Y.-M. & BHATTACHARJEE, A. 2016 Turbulent magnetohydrodynamic reconnection mediated by the plasmoid instability. *Astrophys. J.* **818**, 20.
- HUANG, Y.-M., COMISSO, L. & BHATTACHARJEE, A. 2017 Plasmoid instability in evolving current sheets and onset of fast reconnection. *Astrophys. J.* **849**, 75.
- HUANG, Y.-M., COMISSO, L. & BHATTACHARJEE, A. 2019 Scalings pertaining to current sheet disruption mediated by the plasmoid instability. *Phys. Plasmas* **26**, 092112.
- IROSHNIKOV, R. S. 1963 Turbulence of a conducting fluid in a strong magnetic field. *Astron. Zh.* **40**, 742.
- ISKAKOV, A. B. & SCHEKOCHIHIHIN, A. A. 2008 Saturated small-scale turbulent dynamo revisited. Unpublished.
- ISKAKOV, A. B., SCHEKOCHIHIHIN, A. A., COWLEY, S. C., MCWILLIAMS, J. C. & PROCTOR, M. R. E. 2007 Numerical demonstration of fluctuation dynamo at low magnetic Prandtl numbers. *Phys. Rev. Lett.* **98**, 208501.
- JARA-ALMONTE, J., JI, H., YAMADA, M., YOO, J. & FOX, W. 2016 Laboratory observation of resistive electron tearing in a two-fluid reconnecting current sheet. *Phys. Rev. Lett.* **117**, 095001.
- JEMELLA, B. D., DRAKE, J. F. & SHAY, M. A. 2004 Singular structure of magnetic islands resulting from reconnection. *Phys. Plasmas* **11**, 5668.
- JEMELLA, B. D., SHAY, M. A., DRAKE, J. F. & ROGERS, B. N. 2003 Impact of frustrated singularities on magnetic island evolution. *Phys. Rev. Lett.* **91**, 125002.
- JI, H., YAMADA, M., HSU, S. & KULSRUD, R. 1998 Experimental test of the Sweet-Parker model of magnetic reconnection. *Phys. Rev. Lett.* **80**, 3256.
- JI, H., YAMADA, M., HSU, S., KULSRUD, R., CARTER, T. & ZAHARIA, S. 1999 Magnetic reconnection with Sweet-Parker characteristics in two-dimensional laboratory plasmas. *Phys. Plasmas* **6**, 1743.
- JINGADE, N., SINGH, N. K. & SRIDHAR, S. 2018 Generation of large-scale magnetic fields due to fluctuating α in shearing systems. *J. Plasma Phys.* **84**, 735840601.
- KADOMTSEV, B. B. & POGUTSE, O. P. 1970 Collisionless relaxation in systems with Coulomb interactions. *Phys. Rev. Lett.* **25**, 1155.
- KADOMTSEV, B. B. & POGUTSE, O. P. 1974 Nonlinear helical perturbations of a plasma in the tokamak. *Soviet Phys. JETP* **38**, 283.
- KAWAZURA, Y., BARNES, M. & SCHEKOCHIHIHIN, A. A. 2019 Thermal disequilibration of ions and electrons by collisionless plasma turbulence. *Proc. Nat. Acad. Sci.* **116**, 771.
- KAZANTSEV, A. P. 1968 Enhancement of a magnetic field by a conducting fluid. *Sov. Phys.-JETP* **26**, 1031.
- KIDA, S., YANASE, S. & MIZUSHIMA, J. 1991 Statistical properties of MHD turbulence and turbulent dynamo. *Phys. Fluids A* **3**, 457.
- KIM, E.-J. 1999 Nonlinear dynamo in a simplified statistical model. *Phys. Lett. A* **259**, 232.
- KIM, H. & CHO, J. 2015 Inverse cascade in imbalanced electron magnetohydrodynamic turbulence. *Astrophys. J.* **801**, 75.
- KINNEY, R. M., CHANDRAN, B., COWLEY, S. & MCWILLIAMS, J. C. 2000 Magnetic field growth and saturation in plasmas with large magnetic Prandtl number. I. The two-dimensional case. *Astrophys. J.* **545**, 907.
- KIYANI, K. H., CHAPMAN, S. C., KHOTYAITSEV, Y. V., DUNLOP, M. W. & SAHRAOUI, F. 2009 Global scale-invariant dissipation in collisionless plasma turbulence. *Phys. Rev. Lett.* **103**, 075006.
- KOBAYASHI, S., SAHRAOUI, F., PASSOT, T., LAVEDER, D., SULEM, P. L., HUANG, S. Y., HENRI, P. & SMETS, R. 2017 Three-dimensional simulations and spacecraft observations of sub-ion scale turbulence in the solar wind: influence of Landau damping. *Astrophys. J.* **839**, 122.
- KOLMOGOROV, A. N. 1941a Dissipation of energy in the locally isotropic turbulence. *Dokl. Acad. Nauk SSSR* **32**, 19.
- KOLMOGOROV, A. N. 1941b Local structure of turbulence in incompressible viscous fluid at very large Reynolds numbers. *Dokl. Acad. Nauk SSSR* **30**, 299.
- KOLMOGOROV, A. N. 1941c On the degeneration of isotropic turbulence in an incompressible viscous fluid. *Dokl. Acad. Nauk SSSR* **31**, 538.
- KOLMOGOROV, A. N. 1962 A refinement of previous hypotheses concerning the local structure

- of turbulence in a viscous incompressible fluid at high Reynolds number. *J. Fluid Mech.* **13**, 82.
- KOWAL, G., FALCETA-GONÇALVES, D. A., LAZARIAN, A. & VISHNIAC, E. T. 2017 Statistics of reconnection-driven turbulence. *Astrophys. J.* **838**, 91.
- KOWAL, G., FALCETA-GONÇALVES, D. A., LAZARIAN, A. & VISHNIAC, E. T. 2020 Kelvin-Helmholtz versus tearing instability: What drives turbulence in stochastic reconnection? *Astrophys. J.* **892**, 50.
- KOWAL, G. & LAZARIAN, A. 2010 Velocity field of compressible magnetohydrodynamic turbulence: wavelet decomposition and mode scalings. *Astrophys. J.* **720**, 742.
- KOWAL, G., LAZARIAN, A., VISHNIAC, E. T. & OTMIANOWSKA-MAZUR, K. 2009 Numerical tests of fast reconnection in weakly stochastic magnetic fields. *Astrophys. J.* **700**, 63.
- KOWAL, G., LAZARIAN, A., VISHNIAC, E. T. & OTMIANOWSKA-MAZUR, K. 2012 Reconnection studies under different types of turbulence driving. *Nonlin. Proc. Geophys.* **19**, 297.
- KRAICHNAN, R. H. 1965 Inertial-range spectrum of hydromagnetic turbulence. *Phys. Fluids* **8**, 1385.
- KUHN, T. S. 1962 *The Structure of Scientific Revolutions*. Chicago: University of Chicago Press.
- KULPA-DYBEL, K., KOWAL, G., OTMIANOWSKA-MAZUR, K., LAZARIAN, A. & VISHNIAC, E. 2010 Reconnection in weakly stochastic B-fields in 2D. *Astron. Astrophys.* **514**, A26.
- KULSRUD, R. M. 2005 *Plasma Physics for Astrophysics*. Princeton: Princeton University Press.
- KULSRUD, R. M. & ANDERSON, S. W. 1992 The spectrum of random magnetic fields in the mean field dynamo theory of the Galactic magnetic field. *Astrophys. J.* **396**, 606.
- KUNZ, M. W., ABEL, I. G., KLEIN, K. G. & SCHEKOCHIHIHIN, A. A. 2018 Astrophysical gyrokinetics: turbulence in pressure-anisotropic plasmas at ion scales and beyond. *J. Plasma Phys.* **84**, 715840201.
- KUNZ, M. W., SCHEKOCHIHIHIN, A. A., CHEN, C. H. K., ABEL, I. G. & COWLEY, S. C. 2015 Inertial-range kinetic turbulence in pressure-anisotropic astrophysical plasmas. *J. Plasma Phys.* **81**, 325810501.
- KUNZ, M. W., SCHEKOCHIHIHIN, A. A. & STONE, J. M. 2014 Firehose and mirror instabilities in a collisionless shearing plasma. *Phys. Rev. Lett.* **112**, 205003.
- KUNZ, M. W., SQUIRE, J., SCHEKOCHIHIHIN, A. A. & QUATAERT, E. 2020 Self-sustaining sound in collisionless, high- β plasma. *J. Plasma Phys.* **86**, 905860603.
- KUNZ, M. W., STONE, J. M. & QUATAERT, E. 2016 Magnetorotational turbulence and dynamo in a collisionless plasma. *Phys. Rev. Lett.* **117**, 235101.
- LAESCU, C. C., SHI, Y.-K., EYINK, G. L., DRIVAS, T. D., VISHNIAC, E. T. & LAZARIAN, A. 2015 Inertial-range reconnection in magnetohydrodynamic turbulence and in the solar wind. *Phys. Rev. Lett.* **115**, 025001.
- LANDAU, L. 1946 On the vibration of the electronic plasma. *Zh. Eksp. Teor. Fiz.* **16**, 574.
- LANDAU, L. D. & LIFSHITZ, E. M. 1987 *Fluid Mechanics*. Oxford: Pergamon Press.
- LANDI, S., DEL ZANNA, L., PAPINI, E., PUCCI, F. & VELLI, M. 2015 Resistive magnetohydrodynamics simulations of the ideal tearing mode. *Astrophys. J.* **806**, 131.
- LAPENTA, G. 2008 Self-feeding turbulent magnetic reconnection on macroscopic scales. *Phys. Rev. Lett.* **100**, 235001.
- LAZARIAN, A., EYINK, G., VISHNIAC, E. & KOWAL, G. 2015 Turbulent reconnection and its implications. *Philos. Trans. R. Soc. London A* **373**, 20140144.
- LAZARIAN, A., EYINK, G. L., JAFARI, A., KOWAL, G., LI, H., XU, S. & VISHNIAC, E. T. 2020 3D turbulent reconnection: theory, tests and astrophysical implications. *Phys. Plasmas* **27**, 012305.
- LAZARIAN, A. & VISHNIAC, E. T. 1999 Reconnection in a weakly stochastic field. *Astrophys. J.* **517**, 700.
- LAZARIAN, A., VISHNIAC, E. T. & CHO, J. 2004 Magnetic field structure and stochastic reconnection in a partially ionized gas. *Astrophys. J.* **603**, 180.
- LEE, E., BRACHET, M. E., POUQUET, A., MININNI, P. D. & ROSENBERG, D. 2010 Lack of universality in decaying magnetohydrodynamic turbulence. *Phys. Rev. E* **81**, 016318.
- LEE, L. C. & FU, Z. F. 1986 Multiple X line reconnection. I. A criterion for the transition from a single X line to a multiple X line reconnection. *J. Geophys. Res.* **91**, 6807.
- LEVICH, E. 2009 Coherence in turbulence: new perspective. *Old and New Concepts of Physics* **6**, 239.

- LEVICH, E., SHTILMAN, L. & TUR, A. V. 1991 The origin of coherence in hydrodynamical turbulence. *Physica A* **176**, 241.
- LEVICH, E. & TSINOBER, A. 1983 On the role of helical structures in three-dimensional turbulent flow. *Phys. Lett. A* **93**, 293.
- LITHWICK, Y. & GOLDRICH, P. 2003 Imbalanced weak magnetohydrodynamic turbulence. *Astrophys. J.* **582**, 1220.
- LITHWICK, Y., GOLDRICH, P. & SRIDHAR, S. 2007 Imbalanced strong MHD turbulence. *Astrophys. J.* **655**, 269.
- LOMONOSOV, M. V. 1748 Letter to L. Euler, 5 July 1748. Source: <http://lomonosov.niv.ru/lomonosov/pisma/letter-12.htm>.
- LOUREIRO, N. F. 2016 Unpublished.
- LOUREIRO, N. F. & BOLDYREV, S. 2017a Collisionless reconnection in magnetohydrodynamic and kinetic turbulence. *Astrophys. J.* **850**, 182.
- LOUREIRO, N. F. & BOLDYREV, S. 2017b Role of magnetic reconnection in magnetohydrodynamic turbulence. *Phys. Rev. Lett.* **118**, 245101.
- LOUREIRO, N. F. & BOLDYREV, S. 2018 Turbulence in magnetized pair plasmas. *Astrophys. J.* **866**, L14.
- LOUREIRO, N. F. & BOLDYREV, S. 2020 Nonlinear reconnection in magnetized turbulence. *Astrophys. J.* **890**, 55.
- LOUREIRO, N. F., COWLEY, S. C., DORLAND, W. D., HAINES, M. G. & SCHEKOCHIHIN, A. A. 2005 X-point collapse and saturation in the nonlinear tearing mode reconnection. *Phys. Rev. Lett.* **95**, 235003.
- LOUREIRO, N. F., SAMTANEY, R., SCHEKOCHIHIN, A. A. & UZDENSKY, D. A. 2012 Magnetic reconnection and stochastic plasmoid chains in high-Lundquist-number plasmas. *Phys. Plasmas* **19**, 042303.
- LOUREIRO, N. F., SCHEKOCHIHIN, A. A. & COWLEY, S. C. 2007 Instability of current sheets and formation of plasmoid chains. *Phys. Plasmas* **14**, 100703.
- LOUREIRO, N. F., SCHEKOCHIHIN, A. A. & UZDENSKY, D. A. 2013a Plasmoid and Kelvin-Helmholtz instabilities in Sweet-Parker current sheets. *Phys. Rev. E* **87**, 013102.
- LOUREIRO, N. F., SCHEKOCHIHIN, A. A. & ZOCCHI, A. 2013b Fast collisionless reconnection and electron heating in strongly magnetized plasmas. *Phys. Rev. Lett.* **111**, 025002.
- LOUREIRO, N. F., UZDENSKY, D. A., SCHEKOCHIHIN, A. A., COWLEY, S. C. & YOUSEF, T. A. 2009 Turbulent magnetic reconnection in two dimensions. *Mon. Not. R. Astron. Soc.* **399**, L146.
- LUGONES, R., DMITRUK, P., MININNI, P. D., POUQUET, A. & MATTHAEUS, W. H. 2019 Spatio-temporal behavior of magnetohydrodynamic fluctuations with cross-helicity and background magnetic field. *Phys. Plasmas* **26**, 122301.
- LUGONES, R., DMITRUK, P., MININNI, P. D., WAN, M. & MATTHAEUS, W. H. 2016 On the spatio-temporal behavior of magnetohydrodynamic turbulence in a magnetized plasma. *Phys. Plasmas* **23**, 112304.
- LUMLEY, J. L. 1969 Drag reduction by additives. *Annu. Rev. Fluid Mech.* **1**, 367.
- LUO, Q. Y. & WU, D. J. 2010 Observations of anisotropic scaling of solar wind turbulence. *Astrophys. J.* **714**, L138.
- MAC LOW, M.-M., KLESSEN, R. S., BURKERT, A. & SMITH, M. D. 1998 Kinetic energy decay rates of supersonic and super-Alfvénic turbulence in star-forming clouds. *Phys. Rev. Lett.* **80**, 2754.
- MALARIA, F., VELTRI, P. & CARBONE, V. 1992 Competition among nonlinear effects in tearing instability saturation. *Phys. Fluids B* **4**, 3070.
- MALLET, A. 2020 The onset of electron-only reconnection. *J. Plasma Phys.* **86**, 905860301.
- MALLET, A., KLEIN, K. G., CHANDRAN, B. D. G., GROŠELJ, D., HOPPOCK, I. W., BOWEN, T. A., SALEM, C. S. & BALE, S. D. 2019 Interplay between intermittency and dissipation in collisionless plasma turbulence. *J. Plasma Phys.* **85**, 175850302.
- MALLET, A. & SCHEKOCHIHIN, A. A. 2011 Simulations of imbalanced RMHD turbulence. Unpublished.
- MALLET, A. & SCHEKOCHIHIN, A. A. 2017 A statistical model of three-dimensional anisotropy and intermittency in strong Alfvénic turbulence. *Mon. Not. R. Astron. Soc.* **466**, 3918.

- MALLET, A., SCHEKOCHIHIN, A. A. & CHANDRAN, B. D. G. 2015 Refined critical balance in strong Alfvénic turbulence. *Mon. Not. R. Astron. Soc.* **449**, L77.
- MALLET, A., SCHEKOCHIHIN, A. A. & CHANDRAN, B. D. G. 2017a Disruption of Alfvénic turbulence by magnetic reconnection in a collisionless plasma. *J. Plasma Phys.* **83**, 905830609.
- MALLET, A., SCHEKOCHIHIN, A. A. & CHANDRAN, B. D. G. 2017b Disruption of sheetlike structures in Alfvénic turbulence by magnetic reconnection. *Mon. Not. R. Astron. Soc.* **468**, 4862.
- MALLET, A., SCHEKOCHIHIN, A. A., CHANDRAN, B. D. G., CHEN, C. H. K., HORBURY, T. S., WICKS, R. T. & GREENAN, C. C. 2016 Measures of three-dimensional anisotropy and intermittency in strong Alfvénic turbulence. *Mon. Not. R. Astron. Soc.* **459**, 2130.
- MARON, J., COWLEY, S. & MCWILLIAMS, J. 2004 The nonlinear magnetic cascade. *Astrophys. J.* **603**, 569.
- MARON, J. & GOLDRICH, P. 2001 Simulations of incompressible magnetohydrodynamic turbulence. *Astrophys. J.* **554**, 1175.
- MARSCH, E. 2006 Kinetic physics of the solar corona and solar wind. *Living Rev. Solar Phys.* **3**, 1.
- MARSCH, E. 2018 Solar wind and kinetic heliophysics. *Ann. Geophys.* **36**, 1607.
- MARTINOVÍC, M. M., KLEIN, K. G., KASPER, J. C., CASE, A. W., KORRECK, K. E., LARSON, D., LIVI, R., STEVENS, M., WHITTLESEY, P., CHANDRAN, B. D. G., ALTERMAN, B. L., HUANG, J., CHEN, C. H. K., BALE, S. D., PULUPA, M., MALASPINA, D. M., BONNELL, J. W., HARVEY, P. R., GOETZ, K., DUDOK DE WIT, T. & MACDOWALL, R. J. 2020 The enhancement of proton stochastic heating in the near-Sun solar wind. *Astrophys. J. Suppl.* **246**, 30.
- MASON, J., CATTANEO, F. & BOLDYREV, S. 2006 Dynamic alignment in driven magnetohydrodynamic turbulence. *Phys. Rev. Lett.* **97**, 255002.
- MASON, J., CATTANEO, F. & BOLDYREV, S. 2008 Numerical measurements of the spectrum in magnetohydrodynamic turbulence. *Phys. Rev. E* **77**, 036403.
- MASON, J., PEREZ, J. C., BOLDYREV, S. & CATTANEO, F. 2012 Numerical simulations of strong incompressible magnetohydrodynamic turbulence. *Phys. Plasmas* **19**, 055902.
- MASON, J., PEREZ, J. C., CATTANEO, F. & BOLDYREV, S. 2011 Extended scaling laws in numerical simulations of magnetohydrodynamic turbulence. *Astrophys. J.* **735**, L26.
- MATTHAEUS, W. H., GHOSH, S., OUGHTON, S. & ROBERTS, D. A. 1996 Anisotropic three-dimensional MHD turbulence. *J. Geophys. Res.* **101**, 7619.
- MATTHAEUS, W. H. & GOLDSTEIN, M. L. 1982 Measurement of the rugged invariants of magnetohydrodynamic turbulence in the solar wind. *J. Geophys. Res.* **87**, 6011.
- MATTHAEUS, W. H. & LAMKIN, S. L. 1985 Rapid magnetic reconnection caused by finite amplitude fluctuations. *Phys. Fluids* **28**, 303.
- MATTHAEUS, W. H. & LAMKIN, S. L. 1986 Turbulent magnetic reconnection. *Phys. Fluids* **29**, 2513.
- MATTHAEUS, W. H. & MONTGOMERY, D. 1980 Selective decay hypothesis at high mechanical and magnetic Reynolds numbers. *Ann. N. Y. Acad. Sci.* **357**, 203.
- MATTHAEUS, W. H., MONTGOMERY, D. C. & GOLDSTEIN, M. L. 1983 Turbulent generation of outward-traveling interplanetary Alfvénic fluctuations. *Phys. Rev. Lett.* **51**, 1484.
- MATTHAEUS, W. H., POUQUET, A., MININNI, P. D., DMITRU, P. & BREECH, B. 2008 Rapid alignment of velocity and magnetic field in magnetohydrodynamic turbulence. *Phys. Rev. Lett.* **100**, 085003.
- MATTHAEUS, W. H., SERVIDIO, S., DMITRU, P., CARBONE, V., OUGHTON, S., WAN, M. & OSMAN, K. T. 2012 Local anisotropy, higher order statistics, and turbulence spectra. *Astrophys. J.* **750**, 103.
- MATTHAEUS, W. H., WAN, M., SERVIDIO, S., GRECO, A., OSMAN, K. T., OUGHTON, S. & DMITRU, P. 2015 Intermittency, nonlinear dynamics and dissipation in the solar wind and astrophysical plasmas. *Philos. Trans. R. Soc. London A* **373**, 20140154.
- MATTHAEUS, W. H., YANG, Y., WAN, M., PARASHAR, T. N., BANDYOPADHYAY, R., CHASAPIS, A., PEZZI, O. & VALENTINI, F. 2020 Pathways to dissipation in weakly collisional plasmas. *Astrophys. J.* **891**, 101.
- MCKAY, M. E., BERERA, A. & HO, R. D. J. G. 2019 Fully resolved array of simulations

- investigating the influence of the magnetic Prandtl number on magnetohydrodynamic turbulence. *Phys. Rev. E* **99**, 013101.
- MELVILLE, S., SCHEKOCHIHIN, A. A. & KUNZ, M. W. 2016 Pressure-anisotropy-driven microturbulence and magnetic-field evolution in shearing, collisionless plasma. *Mon. Not. R. Astron. Soc.* **459**, 2701.
- MENEGUZZI, M., FRISCH, U. & POUQUET, A. 1981 Helical and nonhelical turbulent dynamos. *Phys. Rev. Lett.* **47**, 1060.
- MEYRAND, R., GALTIER, S. & KIYANI, K. H. 2016 Direct evidence of the transition from weak to strong magnetohydrodynamic turbulence. *Phys. Rev. Lett.* **116**, 105002.
- MEYRAND, R., KANEKAR, A., DORLAND, W. & SCHEKOCHIHIN, A. A. 2019 Fluidization of collisionless plasma turbulence. *Proc. Nat. Acad. Sci.* **116**, 1185.
- MEYRAND, R., KIYANI, K. H. & GALTIER, S. 2015 Weak magnetohydrodynamic turbulence and intermittency. *J. Fluid Mech.* **770**, R1.
- MEYRAND, R. & SQUIRE, J. 2020 private communication.
- MEYRAND, R., SQUIRE, J., SCHEKOCHIHIN, A. A. & DORLAND, W. 2021 On the violation of the zeroth law of turbulence in space plasmas. *J. Plasma Phys.* **87**, 535870301.
- MILANESE, L. M., LOUREIRO, N. F., DASCHNER, M. & BOLDYREV, S. 2020 Dynamic phase alignment in inertial Alfvén turbulence. *Phys. Rev. Lett.* **125**, 265101.
- MILANO, L. J., MATTHAEUS, W. H., DMITRUK, P. & MONTGOMERY, D. C. 2001 Local anisotropy in incompressible magnetohydrodynamic turbulence. *Phys. Plasmas* **8**, 2673.
- MILITELLO, F., ROMANELLI, M., HASTIE, R. J. & LOUREIRO, N. F. 2009 Effect of current corrugations on the stability of the tearing mode. *Phys. Plasmas* **16**, 032101.
- MILOSHEVICH, G., LAVEDER, D., PASSOT, T. & SULEM, P.-L. 2021 Inverse cascade and magnetic vortices in kinetic Alfvén-wave turbulence. *J. Plasma Phys.* **87**, 905870201.
- MININNI, P. D., POUQUET, A. G. & MONTGOMERY, D. C. 2006 Small-scale structures in three-dimensional magnetohydrodynamic turbulence. *Phys. Rev. Lett.* **97**, 244503.
- MOFFATT, H. K. 1986 Magnetostatic equilibria and analogous Euler flows of arbitrarily complex topology. Part 2. Stability considerations. *J. Fluid Mech.* **166**, 359.
- MONTGOMERY, D. & TURNER, L. 1981 Anisotropic magnetohydrodynamic turbulence in a strong external magnetic field. *Phys. Fluids* **24**, 825.
- MONTGOMERY, D., TURNER, L. & VAHALA, G. 1978 Three-dimensional magnetohydrodynamic turbulence in cylindrical geometry. *Phys. Fluids* **21**, 757.
- MONTGOMERY, D., TURNER, L. & VAHALA, G. 1979 Most probable states in magnetohydrodynamics. *J. Plasma Phys.* **21**, 239.
- MÜLLER, W.-C. & BISKAMP, D. 2000 Scaling properties of three-dimensional magnetohydrodynamic turbulence. *Phys. Rev. Lett.* **84**, 475.
- MÜLLER, W.-C., BISKAMP, D. & GRAPPIN, R. 2003 Statistical anisotropy of magnetohydrodynamic turbulence. *Phys. Rev. E* **67**, 066302.
- MÜLLER, W.-C. & GRAPPIN, R. 2005 Spectral energy dynamics in magnetohydrodynamic turbulence. *Phys. Rev. Lett.* **95**, 114502.
- MÜLLER, W.-C., MALAPAKA, S. K. & BUSSE, A. 2012 Inverse cascade of magnetic helicity in magnetohydrodynamic turbulence. *Phys. Rev. E* **85**, 015302.
- NÄTTILÄ, J. & BELOBORODOV, A. M. 2022 Heating of magnetically dominated plasma by Alfvén wave turbulence. *Phys. Rev. Lett.* **128**, 075101.
- NAZARENKO, S. 2007 2D enslaving of MHD turbulence. *New J. Phys.* **9**, 307.
- NAZARENKO, S. 2011 *Wave Turbulence*. Berlin: Springer.
- NAZARENKO, S. V. & SCHEKOCHIHIN, A. A. 2011 Critical balance in magnetohydrodynamic, rotating and stratified turbulence: towards a universal scaling conjecture. *J. Fluid Mech.* **677**, 134.
- NG, C. S. & BHATTACHARJEE, A. 1996 Interaction of shear-Alfvén wave packets: implication for weak magnetohydrodynamic turbulence in astrophysical plasmas. *Astrophys. J.* **465**, 845.
- NG, C. S. & BHATTACHARJEE, A. 1997 Scaling of anisotropic spectra due to the weak interaction of shear-Alfvén wave packets. *Phys. Plasmas* **4**, 605.
- NI, L., GERMASCHEWSKI, K., HUANG, Y.-M., SULLIVAN, B. P., YANG, H. & BHATTACHARJEE, A. 2010 Linear plasmoid instability of thin current sheets with shear flow. *Phys. Plasmas* **17**, 052109.

- OGILVIE, G. I. & PROCTOR, M. R. E. 2003 On the relation between viscoelastic and magnetohydrodynamic flows and their instabilities. *J. Fluid Mech.* **476**, 389.
- OISHI, J. S., MAC LOW, M.-M., COLLINS, D. C. & TAMURA, M. 2015 Self-generated turbulence in magnetic reconnection. *Astrophys. J.* **806**, L12.
- OLESEN, P. 1997 Inverse cascades and primordial magnetic fields. *Phys. Lett. B* **398**, 321.
- OLESEN, P. 2015 Dimensional reduction in freely decaying turbulent non-helical magnetic fields. *E-print arXiv:1511.05007*.
- OSMAN, K. T., MATTHAEUS, W. H., GOSLING, J. T., GRECO, A., SERVIDIO, S., HNAT, B., CHAPMAN, S. C. & PHAN, T. D. 2014 Magnetic reconnection and intermittent turbulence in the solar wind. *Phys. Rev. Lett.* **112**, 215002.
- OSMAN, K. T., WAN, M., MATTHAEUS, W. H., BREECH, B. & OUGHTON, S. 2011 Directional alignment and non-Gaussian statistics in solar wind turbulence. *Astrophys. J.* **741**, 75.
- OTTAVIANI, M. & PORCELLI, F. 1993 Nonlinear collisionless magnetic reconnection. *Phys. Rev. Lett.* **71**, 3802.
- OUGHTON, S., MATTHAEUS, W. H. & DMITRUK, P. 2017 Reduced MHD in astrophysical applications: two-dimensional or three-dimensional? *Astrophys. J.* **839**, 2.
- OUGHTON, S., PRIEST, E. R. & MATTHAEUS, W. H. 1994 The influence of a mean magnetic field on three-dimensional magnetohydrodynamic turbulence. *J. Fluid Mech.* **280**, 95.
- PARIS, R. B. & SY, W. N.-C. 1983 Influence of equilibrium shear flow along the magnetic field on the resistive tearing instability. *Phys. Fluids* **26**, 2966.
- PARK, K. 2017 On the inverse transfer of (non-)helical magnetic energy in a decaying magnetohydrodynamic turbulence. *Mon. Not. R. Astron. Soc.* **472**, 1628.
- PARK, W., MONTICELLO, D. A. & WHITE, R. B. 1984 Reconnection rates of magnetic fields including the effects of viscosity. *Phys. Fluids* **27**, 137.
- PARKER, E. N. 1957 Sweet's mechanism for merging magnetic fields in conducting fluids. *J. Geophys. Res.* **62**, 509.
- PARKER, J. T., HIGHCOCK, E. G., SCHEKOCCHIHIH, A. A. & DELLAR, P. J. 2016 Suppression of phase mixing in drift-kinetic plasma turbulence. *Phys. Plasmas* **23**, 070703.
- PASSOT, T., SULEM, P. L. & TASSI, E. 2017 Electron-scale reduced fluid models with gyroviscous effects. *J. Plasma Phys.* **83**, 715830402.
- PEREZ, J. C. & BOLDYREV, S. 2008 On weak and strong magnetohydrodynamic turbulence. *Astrophys. J.* **672**, L61.
- PEREZ, J. C. & BOLDYREV, S. 2009 Role of cross-helicity in magnetohydrodynamic turbulence. *Phys. Rev. Lett.* **102**, 025003.
- PEREZ, J. C. & BOLDYREV, S. 2010a Numerical simulations of imbalanced strong magnetohydrodynamic turbulence. *Astrophys. J.* **710**, L63.
- PEREZ, J. C. & BOLDYREV, S. 2010b Strong magnetohydrodynamic turbulence with cross helicity. *Phys. Plasmas* **17**, 055903.
- PEREZ, J. C. & CHANDRAN, B. D. G. 2013 Direct numerical simulations of reflection-driven, reduced magnetohydrodynamic turbulence from the Sun to the Alfvén critical point. *Astrophys. J.* **776**, 124.
- PEREZ, J. C., MASON, J., BOLDYREV, S. & CATTANEO, F. 2012 On the energy spectrum of strong magnetohydrodynamic turbulence. *Phys. Rev. X* **2**, 041005.
- PEREZ, J. C., MASON, J., BOLDYREV, S. & CATTANEO, F. 2014a Comment on the numerical measurements of the magnetohydrodynamic turbulence spectrum by A. Beresnyak (Phys. Rev. Lett. 106 (2011) 075001; MNRAS 422 (2012) 3495; ApJ 784 (2014) L20). *E-print arXiv:1409.8106*.
- PEREZ, J. C., MASON, J., BOLDYREV, S. & CATTANEO, F. 2014b Scaling properties of small-scale fluctuations in magnetohydrodynamic turbulence. *Astrophys. J.* **793**, L13.
- PETERSON, E. E., ENDRIZZI, D. A., BEIDLER, M., BUNKERS, K. J., CLARK, M., EGEDAL, J., FLANAGAN, K., MCCOLLAM, K. J., MILHONE, J., OLSON, J., SOVINEC, C. R., WALEFFE, R., WALLACE, J. & FOREST, C. B. 2019 A laboratory model for the Parker spiral and magnetized stellar winds. *Nature Phys.* **15**, 1095.
- PEZZI, O., SERVIDIO, S., PERRONE, D., VALENTINI, F., SORRISO-VALVO, L., GRECO, A., MATTHAEUS, W. H. & VELTRI, P. 2018 Velocity-space cascade in magnetized plasmas: numerical simulations. *Phys. Plasmas* **25**, 060704.

- PLUNK, G. G., COWLEY, S. C., SCHEKOCHIHIHIN, A. A. & TATSUNO, T. 2010 Two-dimensional gyrokinetic turbulence. *J. Fluid Mech.* **664**, 407.
- PODESTA, J. J. 2009 Dependence of solar-wind power spectra on the direction of the local mean magnetic field. *Astrophys. J.* **698**, 986.
- PODESTA, J. J. 2011 On the cross-helicity dependence of the energy spectrum in magnetohydrodynamic turbulence. *Phys. Plasmas* **18**, 012907.
- PODESTA, J. J. & BHATTACHARJEE, A. 2010 Theory of incompressible magnetohydrodynamic turbulence with scale-dependent alignment and cross-helicity. *Astrophys. J.* **718**, 1151.
- PODESTA, J. J. & BOROVSKY, J. E. 2010 Scale invariance of normalized cross-helicity throughout the inertial range of solar wind turbulence. *Phys. Plasmas* **17**, 112905.
- PODESTA, J. J., CHANDRAN, B. D. G., BHATTACHARJEE, A., ROBERTS, D. A. & GOLDSTEIN, M. L. 2009 Scale-dependent angle of alignment between velocity and magnetic field fluctuations in solar wind turbulence. *J. Geophys. Res.* **114**, A131107.
- POLITANO, H. & POUQUET, A. 1998a Dynamical length scales for turbulent magnetized flows. *Geophys. Res. Lett.* **25**, 273.
- POLITANO, H. & POUQUET, A. 1998b von Kármán-Howarth equation for magnetohydrodynamics and its consequences on third-order longitudinal structure and correlation functions. *Phys. Rev. E* **57**, R21.
- POLITANO, H., POUQUET, A. & SULEM, P. L. 1989 Inertial ranges and resistive instabilities in two-dimensional magnetohydrodynamic turbulence. *Phys. Fluids B* **1**, 2330.
- PORCELLI, F. 1987 Viscous resistive magnetic reconnection. *Phys. Fluids* **30**, 1734.
- PORCELLI, F., BORGOGNO, D., CALIFANO, F., GRASSO, D., OTTAVIANI, M. & PEGORARO, F. 2002 Recent advances in collisionless magnetic reconnection. *Plasma Phys. Control. Fusion* **44**, B389.
- PORTER, D. H., JONES, T. W. & RYU, D. 2015 Vorticity, shocks, and magnetic fields in subsonic, ICM-like turbulence. *Astrophys. J.* **810**, 93.
- POUQUET, A., FRISCH, U. & LEORAT, J. 1976 Strong MHD helical turbulence and the nonlinear dynamo effect. *J. Fluid Mech.* **77**, 321.
- POUQUET, A., FRISCH, U. & MENEGUZZI, M. 1986 Growth of correlations in magnetohydrodynamic turbulence. *Phys. Rev. A* **33**, 4266.
- POUQUET, A., SULEM, P. L. & MENEGUZZI, M. 1988 Influence of velocity-magnetic field correlations on decaying magnetohydrodynamic turbulence with neutral X points. *Phys. Fluids* **31**, 2635.
- PUCCI, F. & VELLI, M. 2014 Reconnection of quasi-singular current sheets: the “ideal” tearing mode. *Astrophys. J.* **780**, L19.
- PUCCI, F., VELLI, M., TENERANI, A. & DEL SARTO, D. 2018 Onset of fast “ideal” tearing in thin current sheets: dependence on the equilibrium current profile. *Phys. Plasmas* **25**, 032113.
- PUCCI, F., VIVIANI, M., VALENTINI, F., LAPENTA, G., MATTHAEUS, W. H. & SERVIDIO, S. 2021 Turbulent magnetogenesis in a collisionless plasma. *Astrophys. J.* **922**, L18.
- PUSZTAI, I., JUNO, J., BRANDENBURG, A., TENBARGE, J. M., HAKIM, A., FRANCISQUEZ, M. & SUNDSTRÖM, A. 2020 Dynamo in weakly collisional nonmagnetized plasmas impeded by Landau damping of magnetic fields. *Phys. Rev. Lett.* **124**, 255102.
- QUATAERT, E. & GRUZINOV, A. 1999 Turbulence and particle heating in advection-dominated accretion flows. *Astrophys. J.* **520**, 248.
- REMPEL, E. L., CHIAN, A. C.-L., BRANDENBURG, A., MUÑOZ, P. R. & SHADDEN, S. C. 2013 Coherent structures and the saturation of a nonlinear dynamo. *J. Fluid Mech.* **729**, 309.
- REPPIN, J. & BANERJEE, R. 2017 Nonhelical turbulence and the inverse transfer of energy: a parameter study. *Phys. Rev. E* **96**, 053105.
- RETINÒ, A., SUNDKVIST, D., VAIVADS, A., MOZER, F., ANDRÉ, M. & OWEN, C. J. 2007 In situ evidence of magnetic reconnection in turbulent plasma. *Nature Phys.* **3**, 236.
- RICHARDSON, L. F. 1926 Atmospheric diffusion shown on a distance-neighbour graph. *Proc. R. Soc. London A* **110**, 709.
- RINCON, F. 2019 Dynamo theories. *J. Plasma Phys.* **85**, 205850401.
- RINCON, F., CALIFANO, F., SCHEKOCHIHIHIN, A. A. & VALENTINI, F. 2016 Turbulent dynamo in a collisionless plasma. *Proc. Nat. Acad. Sci.* **113**, 3950.
- ROBERTS, D. A., GOLDSTEIN, M. L., KLEIN, L. W. & MATTHAEUS, W. H. 1987 Origin and

- evolution of fluctuations in the solar wind—HELIOS observations and Helios-Voyager comparisons. *J. Geophys. Res.* **92**, 12023.
- ROBINSON, D. C. & RUSBRIDGE, M. G. 1971 Structure of turbulence in the Zeta plasma. *Phys. Fluids* **14**, 2499.
- ROH, S., RYU, D., KANG, H., HA, S. & JANG, H. 2019 Turbulence dynamo in the stratified medium of galaxy clusters. *Astrophys. J.* **883**, 138.
- ROVELLI, C. 2015 Aristotle's physics: a physicist's look. *J. Amer. Philos. Assoc.* **1**, 23.
- RUTHERFORD, P. H. 1973 Nonlinear growth of the tearing mode. *Phys. Fluids* **16**, 1903.
- SAFFMAN, P. G. 1967 The large-scale structure of homogeneous turbulence. *J. Fluid Mech.* **27**, 581.
- SAHOO, G., PERLEKAR, P. & PANDIT, R. 2011 Systematics of the magnetic-Prandtl-number dependence of homogeneous, isotropic magnetohydrodynamic turbulence. *New J. Phys.* **13**, 013036.
- SAMTANEY, R., LOUREIRO, N. F., UZDENSKY, D. A., SCHEKOCHIHIHIN, A. A. & COWLEY, S. C. 2009 Formation of plasmoid chains in magnetic reconnection. *Phys. Rev. Lett.* **103**, 105004.
- SCHEKOCHIHIHIN, A. A. 2022 *Lectures on Kinetic Theory and Magnetohydrodynamics of Plasmas*. Lecture Notes for the Oxford MMathPhys programme; URL: <http://www-thphys.physics.ox.ac.uk/people/AlexanderSchekochihih/KT/2015/KTLectureNotes.pdf>.
- SCHEKOCHIHIHIN, A. A. & COWLEY, S. C. 2006 Turbulence, magnetic fields, and plasma physics in clusters of galaxies. *Phys. Plasmas* **13**, 056501.
- SCHEKOCHIHIHIN, A. A. & COWLEY, S. C. 2007 Turbulence and magnetic fields in astrophysical plasmas. In *Magnetohydrodynamics: Historical Evolution and Trends* (ed. Molokov, S., Moreau, R., and Moffatt, H. K.), p. 85. Berlin: Springer.
- SCHEKOCHIHIHIN, A. A., COWLEY, S. C., DORLAND, W., HAMMETT, G. W., HOWES, G. G., PLUNK, G. G., QUATAERT, E. & TATSUNO, T. 2008 Gyrokinetic turbulence: a nonlinear route to dissipation through phase space. *Plasma Phys. Control. Fusion* **50**, 124024.
- SCHEKOCHIHIHIN, A. A., COWLEY, S. C., DORLAND, W., HAMMETT, G. W., HOWES, G. G., QUATAERT, E. & TATSUNO, T. 2009 Astrophysical gyrokinetics: kinetic and fluid turbulent cascades in magnetized weakly collisional plasmas. *Astrophys. J. Suppl.* **182**, 310.
- SCHEKOCHIHIHIN, A. A., COWLEY, S. C., HAMMETT, G. W., MARON, J. L. & MCWILLIAMS, J. C. 2002 A model of nonlinear evolution and saturation of the turbulent MHD dynamo. *New J. Phys.* **4**, 84.
- SCHEKOCHIHIHIN, A. A., COWLEY, S. C., RINCON, F. & ROSIN, M. S. 2010 Magnetofluid dynamics of magnetized cosmic plasma: firehose and gyrothermal instabilities. *Mon. Not. R. Astron. Soc.* **405**, 291.
- SCHEKOCHIHIHIN, A. A., COWLEY, S. C., TAYLOR, S. F., HAMMETT, G. W., MARON, J. L. & MCWILLIAMS, J. C. 2004a Saturated state of the nonlinear small-scale dynamo. *Phys. Rev. Lett.* **92**, 084504.
- SCHEKOCHIHIHIN, A. A., COWLEY, S. C., TAYLOR, S. F., MARON, J. L. & MCWILLIAMS, J. C. 2004b Simulations of the small-scale turbulent dynamo. *Astrophys. J.* **612**, 276.
- SCHEKOCHIHIHIN, A. A., ISKAKOV, A. B., COWLEY, S. C., MCWILLIAMS, J. C., PROCTOR, M. R. E. & YOUSEF, T. A. 2007 Fluctuation dynamo and turbulent induction at low magnetic Prandtl numbers. *New J. Phys.* **9**, 300.
- SCHEKOCHIHIHIN, A. A., KAWAZURA, Y. & BARNES, M. A. 2019 Constraints on ion versus electron heating by plasma turbulence at low beta. *J. Plasma Phys.* **85**, 905850303.
- SCHEKOCHIHIHIN, A. A., NAZARENKO, S. V. & YOUSEF, T. A. 2012 Weak Alfvén-wave turbulence revisited. *Phys. Rev. E* **85**, 036406.
- SCHEKOCHIHIHIN, A. A., PARKER, J. T., HIGHCOCK, E. G., DELLAR, P. J., DORLAND, W. & HAMMETT, G. W. 2016 Phase mixing versus nonlinear advection in drift-kinetic plasma turbulence. *J. Plasma Phys.* **82**, 905820212.
- SCHOBER, J., SCHLEICHER, D. R. G., FEDERRATH, C., BOVINO, S. & KLESSEN, R. S. 2015 Saturation of the turbulent dynamo. *Phys. Rev. E* **92**, 023010.
- SEELY, H. 2003 *The Poetry of D. H. Rumsfeld*. URL: <https://slate.com/news-and-politics/2003/04/the-poetry-of-donald-rumsfeld.html>.
- SERVIDIO, S., CHASAPIS, A., MATTHAEUS, W. H., PERRONE, D., VALENTINI, F., PARASHAR,

- T. N., VELTRI, P., GERSHMAN, D., RUSSELL, C. T., GILES, B., FUSELIER, S. A., PHAN, T. D. & BURCH, J. 2017 Magnetospheric Multiscale (MMS) observation of plasma velocity-space cascade: Hermite representation and theory. *Phys. Rev. Lett.* **119**, 205101.
- SERVIDIO, S., DMITRUK, P., GRECO, A., WAN, M., DONATO, S., CASSAK, P. A., SHAY, M. A., CARBONE, V. & MATTHAEUS, W. H. 2011a Magnetic reconnection as an element of turbulence. *Nonlin. Proc. Geophys.* **18**, 675.
- SERVIDIO, S., GRECO, A., MATTHAEUS, W. H., OSMAN, K. T. & DMITRUK, P. 2011b Statistical association of discontinuities and reconnection in magnetohydrodynamic turbulence. *J. Geophys. Res.* **116**, A09102.
- SERVIDIO, S., MATTHAEUS, W. H. & DMITRUK, P. 2008 Depression of nonlinearity in decaying isotropic MHD turbulence. *Phys. Rev. Lett.* **100**, 095005.
- SERVIDIO, S., MATTHAEUS, W. H., SHAY, M. A., CASSAK, P. A. & DMITRUK, P. 2009 Magnetic reconnection in two-dimensional magnetohydrodynamic turbulence. *Phys. Rev. Lett.* **102**, 115003.
- SERVIDIO, S., MATTHAEUS, W. H., SHAY, M. A., DMITRUK, P., CASSAK, P. A. & WAN, M. 2010 Statistics of magnetic reconnection in two-dimensional magnetohydrodynamic turbulence. *Phys. Plasmas* **17**, 032315.
- SETA, A., BUSHBY, P. J., SHUKUROV, A. & WOOD, T. S. 2020 Saturation mechanism of the fluctuation dynamo at $\text{Pr}_M \geq 1$. *Phys. Rev. Fluids* **5**, 043702.
- SHE, Z.-S. & LEVEQUE, E. 1994 Universal scaling laws in fully developed turbulence. *Phys. Rev. Lett.* **72**, 336.
- SHE, Z.-S. & WAYMIRE, E. C. 1995 Quantized energy cascade and log-Poisson statistics in fully developed turbulence. *Phys. Rev. Lett.* **74**, 262.
- SHEBALIN, J. V., MATTHAEUS, W. H. & MONTGOMERY, D. 1983 Anisotropy in MHD turbulence due to a mean magnetic field. *J. Plasma Phys.* **29**, 525.
- SHEN, C., LIN, J., MURPHY, N. A. & RAYMOND, J. C. 2013 Statistical and spectral properties of magnetic islands in reconnecting current sheets during two-ribbon flares. *Phys. Plasmas* **20**, 072114.
- SHI, C., VELLI, M. & TENERANI, A. 2018 Marginal stability of Sweet–Parker type current sheets at low Lundquist numbers. *Astrophys. J.* **859**, 83.
- SHIBATA, K. & TANUMA, S. 2001 Plasmoid-induced-reconnection and fractal reconnection. *Earth, Planets, and Space* **53**, 473.
- SINGH, A., PUCCI, F., TENERANI, A., SHIBATA, K., HILLIER, A. & VELLI, M. 2019 Dynamic evolution of current sheets, ideal tearing, plasmoid formation and generalized fractal reconnection scaling relations. *Astrophys. J.* **881**, 52.
- SKOUTNEV, V. A. 2022 Critical balance and scaling of stably stratified turbulence at low Prandtl number. *E-print* arXiv:2205.01540.
- SMITH, C. W., STAWARZ, J. E., VASQUEZ, B. J., FORMAN, M. A. & MACBRIDE, B. T. 2009 Turbulent cascade at 1 AU in high cross-helicity flows. *Phys. Rev. Lett.* **103**, 201101.
- SON, D. T. 1999 Magnetohydrodynamics of the early Universe and the evolution of primordial magnetic fields. *Phys. Rev. D* **59**, 063008.
- SOUTHWOOD, D. J. & KIVELSON, M. G. 1993 Mirror instability: 1. Physical mechanism of linear instability. *J. Geophys. Res. A* **98**, 9181.
- SQUIRE, J. & BHATTACHARJEE, A. 2015 Generation of large-scale magnetic fields by small-scale dynamo in shear flows. *Phys. Rev. Lett.* **115**, 175003.
- SQUIRE, J. & BHATTACHARJEE, A. 2016 The magnetic shear-current effect: generation of large-scale magnetic fields by the small-scale dynamo. *J. Plasma Phys.* **82**, 535820201.
- SQUIRE, J., CHANDRAN, B. D. G. & MEYRAND, R. 2020 In-situ switchback formation in the expanding solar wind. *Astrophys. J.* **891**, L2.
- SQUIRE, J., KUNZ, M. W., QUATAERT, E. & SCHEKOCHIHIN, A. A. 2017a Kinetic simulations of the interruption of large-amplitude shear-Alfvén waves in a high- β plasma. *Phys. Rev. Lett.* **119**, 155101.
- SQUIRE, J., MEYRAND, R., KUNZ, M. W., ARZAMASSKIY, L., SCHEKOCHIHIN, A. A. & QUATAERT, E. 2022 High-frequency heating of the solar wind triggered by low-frequency turbulence. *Nature Astron.* **6**, 715.
- SQUIRE, J., QUATAERT, E. & SCHEKOCHIHIN, A. A. 2016 A stringent limit on the amplitude of Alfvénic perturbations in high-beta low-collisionality plasmas. *Astrophys. J.* **830**, L25.

- SQUIRE, J., SCHEKOCHIHIHIN, A. A. & QUATAERT, E. 2017*b* Amplitude limits and nonlinear damping of shear-Alfvén waves in high-beta low-collisionality plasmas. *New J. Phys.* **19**, 055005.
- SQUIRE, J., SCHEKOCHIHIHIN, A. A., QUATAERT, E. & KUNZ, M. W. 2019 Magneto-immutable turbulence in weakly collisional plasmas. *J. Plasma Phys.* **85**, 905850114.
- SRIDHAR, S. & GOLDREICH, P. 1994 Toward a theory of interstellar turbulence. 1: Weak Alfvénic turbulence. *Astrophys. J.* **432**, 612.
- ST-ONGE, D. A. & KUNZ, M. W. 2018 Fluctuation dynamo in a collisionless, weakly magnetized plasma. *Astrophys. J.* **863**, L25.
- ST-ONGE, D. A., KUNZ, M. W., SQUIRE, J. & SCHEKOCHIHIHIN, A. A. 2020 Fluctuation dynamo in a weakly collisional plasma. *J. Plasma Phys.* **86**, 905860503.
- STANIER, A., DAUGHTON, W., LE, A., LI, X. & BIRD, R. 2019 Influence of 3D plasmoid dynamics on the transition from collisional to kinetic reconnection. *Phys. Plasmas* **26**, 072121.
- STEINOLFSOHN, R. S. & VAN HOVEN, G. 1984 Nonlinear evolution of the resistive tearing mode. *Phys. Fluids* **27**, 1207.
- STRAUSS, H. R. 1976 Nonlinear, three-dimensional magnetohydrodynamics of noncircular tokamaks. *Phys. Fluids* **19**, 134.
- STRIBLING, T. & MATTHAEUS, W. H. 1991 Relaxation processes in a low-order three-dimensional magnetohydrodynamics model. *Phys. Fluids B* **3**, 1848.
- SUBRAMANIAN, K. 1999 Unified treatment of small- and large-scale dynamos in helical turbulence. *Phys. Rev. Lett.* **83**, 2957.
- SUBRAMANIAN, K. 2003 Hyperdiffusion in nonlinear large- and small-scale turbulent dynamos. *Phys. Rev. Lett.* **90**, 245003.
- SUN, H., YANG, Y., LU, Q., LU, S., WAN, M. & WANG, R. 2022 Physical regimes of two-dimensional MHD turbulent reconnection in different Lundquist numbers. *Astrophys. J.* **926**, 97.
- SUNDKVIST, D., RETINÒ, A., VAIVADS, A. & BALE, S. D. 2007 Dissipation in turbulent plasma due to reconnection in thin current sheets. *Phys. Rev. Lett.* **99**, 025004.
- SWEET, P. A. 1958 The neutral point theory of solar flares. In *Electromagnetic Phenomena in Cosmical Physics* (ed. B. Lehnert), *IAU Symposium*, vol. 6, p. 123.
- SYROVATSKIĬ, S. I. 1971 Formation of current sheets in a plasma with a frozen-in strong magnetic field. *Sov. Phys.–JETP* **33**, 933.
- TAJIMA, T. & SHIBATA, K. 1997 *Plasma Astrophysics*. Reading, MA: Addison-Wesley.
- TATSUNO, T., DORLAND, W., SCHEKOCHIHIHIN, A. A., PLUNK, G. G., BARNES, M., COWLEY, S. C. & HOWES, G. G. 2009 Nonlinear phase mixing and phase-space cascade of entropy in gyrokinetic plasma turbulence. *Phys. Rev. Lett.* **103**, 015003.
- TAYLOR, J. B. 1974 Relaxation of toroidal plasma and generation of reverse magnetic fields. *Phys. Rev. Lett.* **33**, 1139.
- TAYLOR, J. B. & NEWTON, S. L. 2015 Special topics in plasma confinement. *J. Plasma Phys.* **81**, 205810501.
- TEACA, B., LALESCU, C. C., KNAEPEN, B. & CARATI, D. 2011 Controlling the level of the ideal invariant fluxes for MHD turbulence using TURBO spectral solver. *E-print arXiv:1108.2640*.
- TENBARGE, J. M. & HOWES, G. G. 2013 Current sheets and collisionless damping in kinetic plasma turbulence. *Astrophys. J.* **771**, L27.
- TENERANI, A., RAPPAZZO, A. F., VELLI, M. & PUCCI, F. 2015*a* The tearing mode instability of thin current sheets: the transition to fast reconnection in the presence of viscosity. *Astrophys. J.* **801**, 145.
- TENERANI, A. & VELLI, M. 2018 Nonlinear firehose relaxation and constant-B field fluctuations. *Astrophys. J.* **867**, L26.
- TENERANI, A. & VELLI, M. 2020*a* Alfvénic fluctuations in the solar wind: nonlinearities and pressure anisotropy effects. *Plasma Phys. Control. Fusion* **62**, 014001.
- TENERANI, A. & VELLI, M. 2020*b* Spectral signatures of recursive magnetic field reconnection. *Mon. Not. R. Astron. Soc.* **491**, 4267.
- TENERANI, A., VELLI, M. & HELLINGER, P. 2017 The parametric instability of Alfvén waves: effects of temperature anisotropy. *Astrophys. J.* **851**, 99.

- TENERANI, A., VELLI, M., PUCCI, F., LANDI, S. & RAPPAZZO, A. F. 2016 “Ideally” unstable current sheets and the triggering of fast magnetic reconnection. *J. Plasma Phys.* **82**, 535820501.
- TENERANI, A., VELLI, M., RAPPAZZO, A. F. & PUCCI, F. 2015b Magnetic reconnection: recursive current sheet collapse triggered by ideal tearing. *Astrophys. J.* **813**, L32.
- TING, A. C., MONTGOMERY, D. & MATTHAEUS, W. H. 1986 Turbulent relaxation processes in magnetohydrodynamics. *Phys. Fluids* **29**, 3261.
- TOLMAN, E. A., LOUREIRO, N. F. & UZDENSKY, D. A. 2018 Development of tearing instability in a current sheet forming by sheared incompressible flow. *J. Plasma Phys.* **84**, 905840115.
- TZEFERACOS, P., RIGBY, A., BOTT, A. F. A., BELL, A. R., BINGHAM, R., CASNER, A., CATTANEO, F., CHURAZOV, E. M., EMIG, J., FIUZA, F., FOREST, C. B., FOSTER, J., GRAZIANI, C., KATZ, J., KOENIG, M., LI, C.-K., MEINECKE, J., PETRASSO, R., PARK, H.-S., REMINGTON, B. A., ROSS, J. S., RYU, D., RYUTOV, D., WHITE, T. G., REVILLE, B., MINIATI, F., SCHEKOCHIHIN, A. A., LAMB, D. Q., FROULA, D. H. & GREGORI, G. 2018 Laboratory evidence of dynamo amplification of magnetic fields in a turbulent plasma. *Nature Comm.* **9**, 591.
- UZDENSKY, D. A. 2022 Relativistic non-thermal particle acceleration in two-dimensional collisionless magnetic reconnection. *J. Plasma Phys.* **88**, 905880114.
- UZDENSKY, D. A. & BOLDYREV, S. A. 2006 Unpublished.
- UZDENSKY, D. A. & KULSRUD, R. M. 2000 Two-dimensional numerical simulation of the resistive reconnection layer. *Phys. Plasmas* **7**, 4018.
- UZDENSKY, D. A., KULSRUD, R. M. & YAMADA, M. 1996 Theoretical analysis of driven magnetic reconnection experiments. *Phys. Plasmas* **3**, 1220.
- UZDENSKY, D. A. & LOUREIRO, N. F. 2016 Magnetic reconnection onset via disruption of a forming current sheet by the tearing instability. *Phys. Rev. Lett.* **116**, 105003.
- UZDENSKY, D. A., LOUREIRO, N. F. & SCHEKOCHIHIN, A. A. 2010 Fast magnetic reconnection in the plasmoid-dominated regime. *Phys. Rev. Lett.* **105**, 235002.
- VACCA, V., MURGIA, M., GOVONI, F., ENSSLIN, T., OPPERMANN, N., FERETTI, L., GIOVANNINI, G. & LOI, F. 2018 Magnetic fields in galaxy clusters and in the large-scale structure of the Universe. *Galaxies* **6**, 142.
- VALENTE, P. C., DA SILVA, C. B. & PINHO, F. T. 2016 Energy spectra in elasto-inertial turbulence. *Phys. Fluids* **28**, 075108.
- VARSHNEY, A. & STEINBERG, V. 2019 Elastic Alfvén waves in elastic turbulence. *Nature Comm.* **10**, 652.
- VAZZA, F., LOCATELLI, N., RAJPUROHIT, K., BANFI, S., DOMÍNGUEZ-FERNÁNDEZ, P., WITTOR, D., ANGELINELLI, M., INCHINGOLO, G., BRIENZA, M., HACKSTEIN, S., DALLACASA, D., GHELLER, C., BRÜGGGEN, M., BRUNETTI, G., BONAFEDE, A., ETTORI, S., STUARDI, C., PAOLETTI, D. & FINELLI, F. 2021 Magnetogenesis and the cosmic web: a joint challenge for radio observations and numerical simulations. *Galaxies* **9**, 109.
- VECH, D. & CHEN, C. H. K. 2016 Testing the effects of expansion on solar wind turbulence. *Astrophys. J.* **832**, L16.
- VECH, D., MALLET, A., KLEIN, K. G. & KASPER, J. C. 2018 Magnetic reconnection may control the ion-scale spectral break of solar wind turbulence. *Astrophys. J.* **855**, L27.
- VEGA, C., BOLDYREV, S. & ROYTERSHTEYN, V. 2022a Spectra of magnetic turbulence in a relativistic plasma. *Astrophys. J.* **931**, L10.
- VEGA, C., BOLDYREV, S., ROYTERSHTEYN, V. & MEDVEDEV, M. 2022b Turbulence and particle acceleration in a relativistic plasma. *Astrophys. J.* **924**, L19.
- VERDINI, A. & GRAPPIN, R. 2015 Imprints of expansion on the local anisotropy of solar wind turbulence. *Astrophys. J.* **808**, L34.
- VERDINI, A., GRAPPIN, R., ALEXANDROVA, O., FRONCI, L., LANDI, S., MATTEINI, L. & PAPINI, E. 2019 Three-dimensional local anisotropy of velocity fluctuations in the solar wind. *Mon. Not. R. Astron. Soc.* **486**, 3006.
- VERDINI, A., GRAPPIN, R., ALEXANDROVA, O. & LION, S. 2018 3D anisotropy of solar wind turbulence: tubes or ribbons? *Astrophys. J.* **853**, 85 [erratum: *Astrophys. J.* **867**, 168 (2018)].
- VERMA, M. K., ROBERTS, D. A., GOLDSTEIN, M. L., GHOSH, S. & STRIBLING, W. T. 1996 A

- numerical study of the nonlinear cascade of energy in magnetohydrodynamic turbulence. *J. Geophys. Res.* **101**, 21619.
- VERSCHAREN, D., CHEN, C. H. K. & WICKS, R. T. 2017 On kinetic slow modes, fluid slow modes, and pressure-balanced structures in the solar wind. *Astrophys. J.* **840**, 106.
- WAELBROECK, F. L. 1993 Onset of the sawtooth crash. *Phys. Rev. Lett.* **70**, 3259.
- WALKER, J., BOLDYREV, S. & LOUREIRO, N. 2018 Influence of tearing instability on magnetohydrodynamic turbulence. *Phys. Rev. E* **98**, 033209.
- WAN, M., OUGHTON, S., SERVIDIO, S. & MATTHAEUS, W. H. 2012 von Kármán self-preservation hypothesis for magnetohydrodynamic turbulence and its consequences for universality. *J. Fluid Mech.* **697**, 296.
- WAN, M., RAPPAZZO, A. F., MATTHAEUS, W. H., SERVIDIO, S. & OUGHTON, S. 2014 Dissipation and reconnection in boundary-driven reduced magnetohydrodynamics. *Astrophys. J.* **797**, 63.
- WANG, Y., BOLDYREV, S. & PEREZ, J. C. 2011 Residual energy in magnetohydrodynamic turbulence. *Astrophys. J.* **740**, L36.
- WICKS, R. T., HORBURY, T. S., CHEN, C. H. K. & SCHEKOCHIHIHIN, A. A. 2010 Power and spectral index anisotropy of the entire inertial range of turbulence in the fast solar wind. *Mon. Not. R. Astron. Soc.* **407**, L31.
- WICKS, R. T., HORBURY, T. S., CHEN, C. H. K. & SCHEKOCHIHIHIN, A. A. 2011 Anisotropy of imbalanced Alfvénic turbulence in fast solar wind. *Phys. Rev. Lett.* **106**, 045001.
- WICKS, R. T., MALLET, A., HORBURY, T. S., CHEN, C. H. K., SCHEKOCHIHIHIN, A. A. & MITCHELL, J. J. 2013a Alignment and scaling of large-scale fluctuations in the solar wind. *Phys. Rev. Lett.* **110**, 025003.
- WICKS, R. T., ROBERTS, D. A., MALLET, A., SCHEKOCHIHIHIN, A. A., HORBURY, T. S. & CHEN, C. H. K. 2013b Correlations at large scales and the onset of turbulence in the fast solar wind. *Astrophys. J.* **778**, 177 [erratum: *Astrophys. J.* **782**, 118 (2014)].
- WONG, K., ZHDANKIN, V., UZDENSKY, D., WERNER, G. & BEGELMAN, M. 2020 First-principles demonstration of diffusive-advective particle acceleration in kinetic simulations of relativistic plasma turbulence. *Astrophys. J.* **893**, L7.
- XU, S. & LAZARIAN, A. 2016 Turbulent dynamo in a conducting fluid and a partially ionized gas. *Astrophys. J.* **833**, 215.
- XU, S. & LAZARIAN, A. 2017 Magnetohydrodynamic turbulence and turbulent dynamo in partially ionized plasma. *New J. Phys.* **19**, 065005.
- YAGLOM, A. N. 1949 Local structure of temperature field in a turbulent flow. *Dokl. Acad. Nauk SSSR* **69**, 743.
- YAMADA, M., JI, H., HSU, S., CARTER, T., KULSRUD, R., BRETZ, N., JOBES, F., ONO, Y. & PERKINS, F. 1997 Study of driven magnetic reconnection in a laboratory plasma. *Phys. Plasmas* **4**, 1936.
- YANG, L., LI, H., GUO, F., LI, X., LI, S., HE, J., ZHANG, L. & FENG, X. 2020 Fast magnetic reconnection with turbulence in high Lundquist number limit. *Astrophys. J.* **901**, L22.
- YOUSEF, T. A., HEINEMANN, T., RINCON, F., SCHEKOCHIHIHIN, A. A., KLEEORIN, N., ROGACHEVSKII, I., COWLEY, S. C. & McWILLIAMS, J. C. 2008a Numerical experiments on dynamo action in sheared and rotating turbulence. *Astron. Nachr.* **329**, 737.
- YOUSEF, T. A., HEINEMANN, T., SCHEKOCHIHIHIN, A. A., KLEEORIN, N., ROGACHEVSKII, I., ISKAKOV, A. B., COWLEY, S. C. & McWILLIAMS, J. C. 2008b Generation of magnetic field by combined action of turbulence and shear. *Phys. Rev. Lett.* **100**, 184501.
- YOUSEF, T. A., RINCON, F. & SCHEKOCHIHIHIN, A. A. 2007 Exact scaling laws and the local structure of isotropic magnetohydrodynamic turbulence. *J. Fluid Mech.* **575**, 111.
- YOUSEF, T. A. & SCHEKOCHIHIHIN, A. A. 2009 Simulations of weak RMHD turbulence. Unpublished.
- ZAKHAROV, V. E., L'VOV, V. S. & FALKOVICH, G. 1992 *Kolmogorov Spectra of Turbulence I: Wave Turbulence*. Berlin: Springer.
- ZAKHAROV, V. E. & SAGDEEV, R. Z. 1970 Spectrum of acoustic turbulence. *Sov. Phys. Doklady* **15**, 439.
- ZELDOVICH, Y. B. 1956 The magnetic field in the two-dimensional motion of a conducting turbulent liquid. *Zh. Eksp. Teor. Fiz.* **31**, 154, English translation: *Sov. Phys. JETP* **4**, 460 (1957).

- ZHANG, Y.-B., BODENSCHATZ, E., XU, H. & XI, H.-D. 2021 Experimental observation of the elastic range scaling in turbulent flow with polymer additives. *Science Adv.* **7**, eabd3525.
- ZHDANKIN, V. 2022a Generalized entropy production in collisionless plasma flows and turbulence. *Phys. Rev. X* **12**, 031011.
- ZHDANKIN, V. 2022b Nonthermal particle acceleration from maximum entropy in collisionless plasmas. *J. Plasma Phys.* **88**, 175880303.
- ZHDANKIN, V., BOLDYREV, S. & CHEN, C. H. K. 2016a Intermittency of energy dissipation in Alfvénic turbulence. *Mon. Not. R. Astron. Soc.* **457**, L69.
- ZHDANKIN, V., BOLDYREV, S., PEREZ, J. C. & TOBIAS, S. M. 2014 Energy dissipation in magnetohydrodynamic turbulence: coherent structures or “nanoflares”? *Astrophys. J.* **795**, 127.
- ZHDANKIN, V., BOLDYREV, S. & UZDENSKY, D. A. 2016b Scalings of intermittent structures in magnetohydrodynamic turbulence. *Phys. Plasmas* **23**, 055705.
- ZHDANKIN, V., UZDENSKY, D. A. & BOLDYREV, S. 2015 Temporal analysis of dissipative structures in magnetohydrodynamic turbulence. *Astrophys. J.* **811**, 6.
- ZHDANKIN, V., UZDENSKY, D. A. & KUNZ, M. W. 2021 Production and persistence of extreme two-temperature plasmas in radiative relativistic turbulence. *Astrophys. J.* **908**, 71.
- ZHDANKIN, V., UZDENSKY, D. A., PEREZ, J. C. & BOLDYREV, S. 2013 Statistical analysis of current sheets in three-dimensional magnetohydrodynamic turbulence. *Astrophys. J.* **771**, 124.
- ZHDANKIN, V., WERNER, G. R., UZDENSKY, D. A. & BEGELMAN, M. C. 2017 Kinetic turbulence in relativistic plasma: from thermal bath to nonthermal continuum. *Phys. Rev. Lett.* **118**, 055103.
- ZHOU, M., BHAT, P., LOUREIRO, N. F. & UZDENSKY, D. A. 2019 Magnetic island merger as a mechanism for inverse magnetic energy transfer. *Phys. Rev. Res.* **1**, 012004(R).
- ZHOU, M., LOUREIRO, N. F. & UZDENSKY, D. A. 2020 Multi-scale dynamics of magnetic flux tubes and inverse magnetic energy transfer. *J. Plasma Phys.* **86**, 535860401.
- ZHOU, M., WU, D. H., LOUREIRO, N. F. & UZDENSKY, D. A. 2021 Statistical description of coalescing magnetic islands via magnetic reconnection. *J. Plasma Phys.* **87**, 905870620.
- ZHOU, M., ZHDANKIN, V., KUNZ, M. W., LOUREIRO, N. F. & UZDENSKY, D. A. 2022 Spontaneous magnetization of collisionless plasma. *Proc. Nat. Acad. Sci.* **119**, e2119831119.
- ZIENICKE, E., POLITANO, H. & POUQUET, A. 1998 Variable intensity of Lagrangian chaos in the nonlinear dynamo problem. *Phys. Rev. Lett.* **81**, 4640.
- ZOCCHI, A. & SCHEKOCHIHIN, A. A. 2011 Reduced fluid-kinetic equations for low-frequency dynamics, magnetic reconnection, and electron heating in low-beta plasmas. *Phys. Plasmas* **18**, 102309.
- ZRAKE, J. 2014 Inverse cascade of nonhelical magnetic turbulence in a relativistic fluid. *Astrophys. J.* **794**, L26.